EXPLORATION OF STRUCTURAL FEATURES OF SOME NEWLY SYNTHESIZED TRANSITION METAL COORDINATION COMPLEXES

THESIS SUBMITTED FOR THE DEGREE OF

DOCTOR OF PHILOSOPHY (SCIENCE)

OF

JADAVPUR UNIVERSITY

PAMPI PAL, M. Sc

DEPARTMENT OF CHEMISTRY

JADAVPUR UNIVERSITY

KOLKATA 700032

INDIA

2022

যাদবপুর বিশ্ববিদ্যালয়
কলকাতা-৭০০ ০৩২, ভারত

*JADAVPUR UNIVERSITY
KOLKATA-700032, INDIA

FACULTY OF SCIENCE : DEPARTMENT OF CHEMISTRY : INORGANIC CHEMISTRY SECTION

CERTIFICATE FROM THE SUPERVISORS

This is to certify that the thesis entitled **"Exploration of structural features of some newly synthesized transition metal coordination complexes"** submitted by Pampi Pal who got her name registered on 19.11.2015 for the award of Ph. D. (Science) degree of Jadavpur University, is absolutely based upon her own work under the joint supervision of Dr. Subrata Mukhopadhyay, Professor, Department of Chemistry, Jadavpur University, Kolkata 700032 and Dr. Kinsuk Das, Assistant Professor, Department of Chemistry, Chandernagore College, Chandannagar, Hooghly, 712136. It is also mentioning that neither this thesis nor any part of it has been submitted for either any degree/ diploma or any other academic award anywhere before.

Subrata Mukhopadhyay
7/6/2022

Dr. Subrata Mukhopadhyay
Professor,
Department of Chemistry
Jadavpur University

Dr. Subrata Mukhopadhyay
Professor of Chemistry
Jadavpur University
Kolkata – 700032

Kinsuk Das
07.06.2022

Dr. Kinsuk Das
Assistant Professor,
Department of Chemistry
Chandernagore College

Dr. Kinsuk Das
Assistant Professor, W.B.E.S. (Gr.A)
Department of Chemistry
Chandernagore College
Govt. of West Bengal

Signature of the Supervisors and date with official seal

To

My Beloved Parents
and My Son

ACKNOWLEDGEMENTS

Today is the day I have been eagerly waiting for to express my deep sense of gratitude & indebtedness to a number of people who helped me in completing the research work and some deserve special mention.

I would like to thank my esteemed supervisors Professor Subrata Mukhopadhyay of the Department of Chemistry, Jadavpur University, Kolkata 700032 and Dr. Kinsuk Das of Department of Chemistry, Chandernagore Collage, Hooghly 712136 for their invaluable supervision, continuous support & tutelage during this course. Their immense knowledge and plentiful experience have given me a lot of confidence to proceed smoothly with my work. Words can only inadequately express my gratitude to my supervisors for patiently helping me to think clearly and consistently by discussing every point.

I would like to extend my sincere thank to my collaborators from India and abroad; Professor Antonio Frontera, Antonio Bauzá and Rosa M. Gomila of Universitat de Illes Balears, Spain and Mohamed Salah El Fallah of Universitat de Barcelona, Spain, for DFT calculations, theoretical studies and magnetic measurements.

My Heartfelt thanks to all my senior, contemporary and junior lab mates, Dr. Monojit Mitra, Dr. Abdullah Al Masum, Dr. Anowar Hossain, Dr. Tripti Mondal, Dr. Nurunnesa Siddiqui and Samit Pramanik for the stimulating discussions, kind cooperation and for all the fun we have had in the last few years. In addition, I also thank Dr. Saugata Konar, Dr. Sudipta Pathak and Dr. Sumanta Jana for their support and valuable suggestions.

Very special thanks to the Jadavpur University for giving me the opportunity to carry out my doctoral research. I would like to make a special note of thank to all Faculty members and research scholars of the Department of Chemistry, Jadavpur University for their overall cooperation. I wish to express my sincere thanks to the technical and office staffs who have helped me always spontaneously.

I cordially convey my gratitude to the Head Mistress, Assistant Head Mistress and all my colleagues, office staffs and non-teaching staffs of Ghoshpara Nischinda Balika Vidyapith, where I am serving as an Assistant Teacher in Chemistry, for their encouragement and cooperation to complete the work.

I am grateful to all my teachers who inspired me at various stages of my career. I am very grateful to all those who given me their friendship, put up with my odd hours and provided me lifts and practical help.

Finally, I acknowledge the people who mean a lot to me, my parents, 'Ma' and 'Baba'. I am truly blessed to have such wonderful parents. Everything I have and everything I am, I owe it all to them. I salute them for helping me to shape my life with positivity and passion, for showing faith in me and giving me liberty to chose what I desire. Without them I would never been the person I am today. I cherished the sweet childhood memory with my dear brother and thank him for giving me a broader outlook. I also thank sister-in-law and my nephew Soumya for their love and support. I would like to recognise my uncle, aunt and cousin brother for their warm companion and good wishes. With profound respect I also remember my grandparents and really miss their blessings at this joyful moment.

My regard goes to father-in-law and mother-in-law for their love and concern. Thanks to my sister-in-law for her support and generous care throughout the research tenure.

Now, I thank to a very special person, my husband, for his support, understanding, constant encouragement and unfailing love. Without him my pursuit of Ph. D degree was not possible. He was always around there when I thought it was impossible to continue, helped me to keep things in perspective. I deeply appreciate his contribution and belief in me. I appreciate my baby, my little son, Diptarka for making me stronger and better, for abiding my ignorance and showing patience during my thesis writing. I am the luckiest person in the world to have such an affectionate and caring husband and loving son who are my constant source of inspiration.

Many individuals who influenced me at various stages of my life could not be mentioned here. I wish fulfilment in life for them and everybody around me.

Date:
Department of Chemistry
Jadavpur University
Kolkata 7000032
INDIA

PAMPI PAL

Contents

FOREWARD i – iii

CHAPTER: 1 1 - 44

A brief introduction of Crystal Engineering and Supramolecular Chemistry: Emphasis on Coordination complexes of heterocyclic ligands

1.1. General Introduction 2
1.2. A brief introduction of heterocyclic ligands used in Coordination Chemistry 3
1.3. A brief introduction of Supramolecular Chemistry and Crystal Engineering 7
1.3.1. Supramolecular Synthon 9
1.3.2. Host – Guest Chemistry 11
1.3.3. Molecular Recognition 13
1.4. A brief introduction of Non - Covalent interactions 14
1.4.1. Hydrogen Bonding Interaction 16
1.4.1.1. Types of Hydrogen bonding 18
1.4.1.2. Role of hydrogen bonding in bio-chemical system 19
1.4.2. $\pi\cdots\pi$ stacking interaction 22
1.4.3. $C-H\cdots\pi$ interaction 25
1.4.4. Cation$\cdots\pi$ interaction 26
1.4.5. Anion$\cdots\pi$ interaction 29
1.5. Density Functional Theory (DFT) 31
1.5.1. Molecular Electrostatic Potential (MEP) 32
1.5.2. Atoms in Molecule (AIM) 33
1.5.3. Non – covalent Interaction Plot (NCI plot) 34
References 36

CHAPTER: 2 44 - 69

Construction of a novel two dimensional Co(II) polymer from a one dimensional Co(II) polymer: Theoretical elucidation on the role of non-covalent carbon-bonding interaction

2.1. Introduction 46
2.2. Experimental Section 48
2.2.1. Materials and Physical measurements 48
2.2.2. Synthesis 49
2.2.2.1. Synthesis of 3,5-dimethyl-1-(2'-pyridyl) pyrazole (pypz) 49
2.2.2.2. Synthesis of $[Co(dca)_2(DMF)_2]_n$ (1) 50
2.2.2.3. Synthesis of $[Co(dca)_2(pypz)]_n$ (2) 50
2.2.3. X-ray Crystallographic Analysis 51
2.3. Theoretical Methods 53
2.4. Results and Discussion 53
2.4.1. Structural description of Complex 1 53
2.4.2. Structural description of Complex 2 57
2.4.3. Thermal Analysis 59
2.4.4. Theoretical Study 60
2.5. Conclusion 65
References 66

CHAPTER: 3 70 – 95

One mononuclear and one oxalate bridged 1-D polymeric copper(II) complex derived from pyrazole based heterocyclic ligand: Synthesis, crystallographic characterization and DFT calculations

3.1. Introduction 71
3.2. Experimental Section 73
3.2.1. Materials and Physical measurements 73
3.2.2. Synthesis 73
3.2.2.1. Synthesis of 3,5-dimethyl-1-(2'-pyridyl) pyrazole (pypz) 73
3.2.2.2. Synthesis of $[Cu(L)(NO_3)_2]$ (Complex 1) 73
3.2.2.3. Synthesis of $[Cu(L)(Ox)_2(H_2O)]_n$ (Complex 2) 74
3.2.3. X-ray Crystallographic Analysis 75
3.3. Theoretical Methods 77
3.4. Results and Discussion 77
3.4.1. Structural description of Complex 1 77
3.4.2. Structural description of Complex 2 79
3.4.3. Magnetic Properties 82
3.4.4. Magneto-structural Comparison 84
3.4.5. Theoretical Study 86
3.5. Conclusion 92
References 93

CHAPTER: 4 96 – 122

Formation of supramolecular associations involving C–H···Cl and π···π interactions in M^{II} - 2,2':6',2''-terpyridine complexes (M: Ni, Cu): Synthetic and theoretical perspective

4.1. Introduction 95
4.2. Experimental Section 99
4.2.1. Materials and Physical measurements 99
4.2.2. Synthesis 100
4.2.2.1. Synthesis of $[Ni(L)Cl(H_2O)_2]Cl$ (Complex 1) 100
4.2.2.2. Synthesis of $[Cu(L)Cl_2]$ (Complex 2) 101
4.2.3. X-ray Crystallographic Analysis 102
4.3. Theoretical Methods 103
4.4. Results and Discussion 104
4.4.1. Structural description of Complex 1 105
4.4.2. Structural description of Complex 2 108
4.4.3. Thermal analysis 114
4.4.4. Theoretical Study 115
4.5. Conclusion 119
References 120

CHAPTER: 5 *123 – 151*

On the importance of orchestrated interplay between anion···π, π···π and hydrogen bonding interactions in simultaneous binding of Nickel (II) cation and chloride anion by 2,4,6 tris-(2-pyridyl)-1,3,5 triazine: Synthetic, supramolecular and theoretical aspects

5.1. Introduction *124*
5.2. Experimental Section *126*
5.2.1. Materials and Physical measurements *126*
5.2.2. Synthesis *127*
5.2.2.1. Synthesis of protonated ligand ($Htptz^+$) *127*
5.2.2.2. Synthesis of $[Ni(Htptz^+)Cl(H_2O)_2]$ $2Cl.$ $2H_2O$ (Complex 1) *127*
5.2.3. X-ray Crystallographic Analysis *129*
5.3. Theoretical Methods *129*
5.4. Results and Discussion *129*
5.4.1. Structural description of Complex 1 *131*
5.4.2. Thermal analysis *137*
5.4.3. Theoretical Study *138*
5.5. A brief comparative account on anion···π interactions of some related 2,4,6 tris-(2-pyridyl)-1,3,5 triazine based Ni(II) complexes: *142*
5.6. Conclusion *147*
References *148*

APPENDIX: LIST OF PUBLICATIONS *a - b*

FOREWORD

Supramolecular chemistry is an interdisciplinary field of science involving physical, chemical, material and biological features of molecular assemblies having a greater complexity than the individual molecule themselves. Henceforth, it can be considered as the study of the structures and functions of the supermolecules which results from the intermolecular binding interactions of two or more chemical entities in an organized manner. It elucidates the weaker and reversible non-covalent interactions between the molecules, while the traditional chemistry deals with covalent bonds. Supramolecular interactions span a wide range of binding energies and encompasses electrostatic interaction, such as, hydrogen bonding, ion-dipole, dipole-dipole and hydrophobic interaction, such as van der Waals, π···π and dispersion interaction. Jean Marie Lehn aptly described supramolecular chemistry as 'Chemistry beyond the molecule' and 'an information science'. Nature have provided the most versatile examples of supramolecular chemistry: enzyme-substrate complex, DNA structure, protein-protein interactions etc. Supramolecular assemblies demonstrate cooperativity that affects both the stability of the cluster and the mechanism of its formation and rearrangement. Detailed mechanistic and theoretical studies of supramolecular assemblies are important not only for understanding the self-assembly process but also for designing assemblies for specific applications. For the synthetic chemists, self-assembly represents a powerful synthetic methodology in the creation of large, discrete, ordered structures from relatively simple synthons. Acquiring a growing knowledge about the supramolecular synthons available in the database new strategies have been constructed to synthesize new molecules with desired functionality incorporating several non-covalent interactions, namely hydrogen bonding, halogen bonding, chalcogen bonding, pnictogen, cation···π, anion···π, C–H···π, π···π, chelate ring···π, salt bridge···π, lone-pair···π, C–H···anion interactions along with hydrophobic interactions.

In this dissertation, a detailed investigation and exploration of various non-covalent interactions those play a significant role in forming the supramolecular architectures of the newly synthesized transition metal complexes have been described. The synthesis was carried out either by mixing the M(II) salts [M(II): Co(II), Ni(II) and Cu(II)] with heterocyclic substituted pyridine ligands (as primary ligands) and dicyanamide, dimethylformamide, oxalate (as ancillary or bridging ligands) or taking one metal complex as a precursor for

synthesis of another complex. The structures of all complexes were analyzed critically by single crystal X-ray crystallography and other available physico-chemical techniques. Advanced level theoretical studies have been used to characterize the different non-covalent interactions present in the solid state of the newly synthesized complexes.

Chapter: 1

This chapter illustrates the background of the work presented in the thesis. This introductory chapter briefly describes about synthesis of coordination complexes, X-ray crystallographic characterization from non-covalent supramolecular interactions point of view. It also includes salient features of crystal engineering, self-assembly, host-guest chemistry, supramolecular synthons, molecular recognition and theoretical (DFT) studies.

Chapter: 2

This chapter describes two newly synthesized cobalt (II) coordination polymers where one Co(II) polymer was utilized as a precursor of another Co(II) coordination polymer that forms a macrocyclic chain along the crystallographic 'c' axis having 'sql' (Shubnikov notation) net topology with a 4-connected uninodal node having point symbol $\{4^4.6^2\}$. Here $\mu_{1,5}$ dicyanamide (dca) has been chosen as a linker in both coordination polymers. The thermal stability of polymers has been characterized by thermogravimetric analysis. The remarkable non-covalent carbon bonding contacts detected in the crystal structure of precursor Co(II) polymer and has been characterized by density functional theory calculation and electron charge density (atoms in molecule).

Chapter: 3

In this chapter the synthesis, crystal structure and magnetic interactions of an uncommon oxalate containing Cu(II) chain of formula $[Cu(L)(ox)_2(H_2O)]_n$ (where 'L': 3,5 dimethyl-1-(2′-pyridyl)-pyrazole) and a mononuclear Cu(II) complex $[Cu(L)(NO_3)_2]$ have been incorporated. Variable-temperature magnetic susceptibility measurements show the occurrence of a weak ferromagnetic [J = +1.95 ±0.08 cm^{-1}] interaction through the bridging oxalate moiety in axial-equatorial fashion. DFT calculations have been supported to rationalize

several aspects including the magnetic coupling mechanism and the interesting non-covalent interactions observed in the solid-state architecture of both complexes.

Chapter: 4

This chapter elucidates the synthesis and structural characterization of two new complexes [one Ni(II) and one Cu(II)] derived from 2,2′:6′,2″ terpyridine ligand. The noncovalent interactions and supramolecular assemblies observed in the crystal packing of both complexes have been described focusing on 'non-traditional' C–H···Cl and 'traditional' O–H···Cl hydrogen bonding interactions along with π···π interactions. A DFT study has been carried out to analyse the π···π, hydrogen bonding interactions with their rationalization and characterization using molecular electrostatic potential (MEP) surfaces and NCI plot computational tools.

Chapter: 5

This chapter consists a new octahedral Ni(II) complex with a protonated ligand 2,4,6-tris(2-pyridyl)-1,3,5-triazine). Here the protonated ligand simultaneously chelates the Ni(II) and interacts with two non-coordinated chloride ions via anion···π and hydrogen bonding interactions. The role of the protonated ligand and ancillary chloride ions in stabilizing the structural assemblies have been demonstrated. Besides π···π interactions, theoretical investigations provide significant insight about the interplay between anion···π and hydrogen bonding interactions that in turn conclusively confirm the decisive role of protonation as well as metal coordination [here Ni(II)]. The different contributions to the complexation energies have been evaluated by using several theoretical models.

CHAPTER 1

A brief introduction of Crystal Engineering and Supramolecular Chemistry: Emphasis on Coordination complexes of heterocyclic ligands

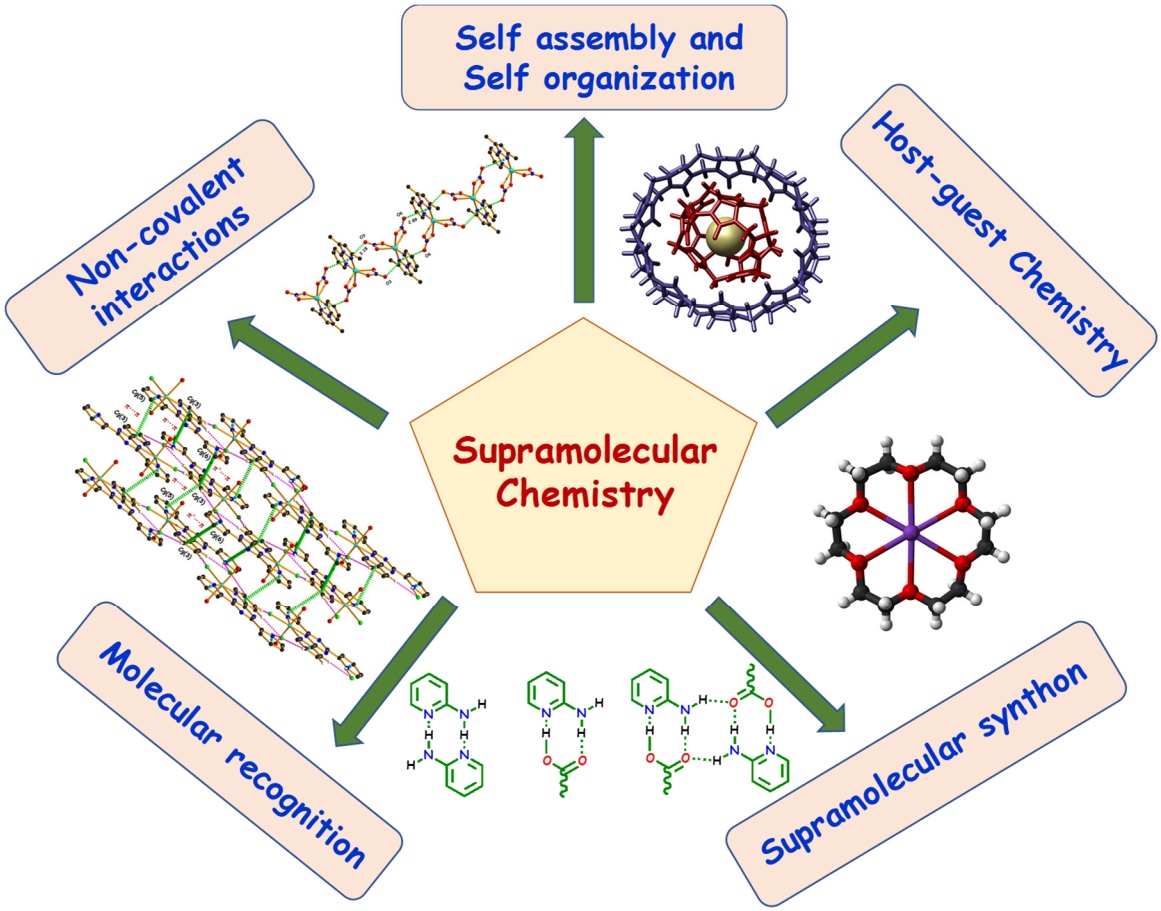

A brief introduction of Crystal Engineering and Supramolecular Chemistry: Emphasis on Coordination complexes of heterocyclic ligands

1.1. GENERAL INTRODUCTION

After the exceptional proposal of **Alfred Werner [1866-1919: The Swiss Chemist, won Nobel prize in 1913]** regarding bonding and structural features of coordination compounds, chemists found enormous excitement and interest in synthesizing variety of complexes worldwide. In this synthetic journey, scientists revealed that the transition metal ions are the most potential candidates for complex formation. In the coordination sphere, if only one type of ligand excluding the solvent molecule is present, the complex is described as a binary or **homoleptic complex** and if different types of ligands excluding the solvent molecule within the coordination sphere, then it is described as a mixed ligand complex or **heteroleptic complex**. Henceforth, the judicious choice of metal ion, ligand, ancillary ligand, counter ions, solvent, temperature, pH etc., play a crucial role in synthesizing the complex. Generally, the metal-ligand complexes can be synthesized in two broad ways:

Way 1: The ligands are synthesized directly from desired chemical components and then characterized using carbon, hydrogen, nitrogen (CHN) analysis, IR spectroscopy, mass spectroscopy, ^{1}HNMR and ^{13}CNMR spectroscopy etc. Now it was utilized for complex formation by choosing suitable metal salts.

Way 2: Some polydentate ligands, especially macrocyclic ligands require the presence of certain metal ions. Formation of such ligands passes through the multistep reactions in which the metal ions on being coordinated to the partially formed ligand direct the course of the reaction. Sometimes the metal coordination can stabilize the polydentate ligand and the influence of metal ions is described as **template effect** and two basic types, namely, thermodynamic and kinetic template effects are involved either singly or simultaneously.

In the last few decades, there has been a phenomenal growth in ‘coordination chemistry’ due to their broad multidisciplinary applications, e.g., pure, applied, analytical and in particular material and biological fields. The chemistry of heterocyclic bases with at least one heteroatom like nitrogen, oxygen, sulfur etc., arrest significant attention not only for their

physiological and medicinal importance, but also for their potent role as ligands for complex formation with several transition metal ions. In all the complexes of heterocycle ligands, the lone pair of electrons on the heteroatoms participate in forming metal-ligand bonds effectively. Before going into the discussion on the subject matter of the present thesis entitled "***EXPLORATION OF STRUCTURAL FEATURES OF SOME NEWLY SYNTHESIZED TRANSITION METAL COORDINATION COMPLEXES***" it is a convention to depict a concise review of the work done so far on the synthetic and structural illumination of coordination compounds from supramolecular point of view.

1.2. A BRIEF INTRODUCTION OF HETEROCYCLIC LIGANDS USED IN COORDINATION CHEMISTRY

Organometallic chemistry is the study of interaction between metal cations and ligands. Ligands often play a crucial role in tuning metal cation reactivity [1]. Often, some ‘‘prestigious" ligand frameworks could be crucial and provide a strong impact that can lead to the paradigm shift for coordination chemistry research [2-5]. With inherent lone pair electrons, nitrogen can coordinate with various transition metal cations. Thus, N-containing ligands are a significant component in coordination chemistry [6-8]. These heterocyclic compounds are well recognized as a main structural components of several bioactive natural products like vitamin, glycosides, hormones, antibiotic alkaloids and many naturally occurring drugs, e.g., quinine, morphine, codeine, theophylline etc. Hence the synthesis of nitrogen containing heterocycles has been encouraged worldwide for their ever-growing applications. Generally used heterocyclic ligands (containing either one or more nitrogen atoms as hetero-atom) are pyrazole, pyridine, pyrimidine, imidazole, triazole, triazine, bipyridine, 1,10 ortho-phenanthroline etc., (either unsubstituted or substituted manner) [Fig. 1.1].

Pyridine is the simplest and supreme prevalent among N-containing heterocycles has been appointed for many years as a unique ligand towards metal ions and the coordination chemistry of pyridine and substituted pyridines are now well established. Pyridine ring containing compounds used as anti-convulsant, anti-microbial, anti-cancers, anti-inflammatory, antibacterial activities and cover a broad bio-spectrum. Pyridine derivatives having a 2-pyridone core signify a diverse group of intriguing organic compounds because of

their capability to be used as anti-malarial, anti-tumoral, analgesic and anti-HIV agents. Pyrazole (Fig. 1.1) is one of the most versatile molecules used in synthetic inorganic chemistry and many review works on the coordination and organometallic chemistry of pyrazole reported [9-11]. The N–H proton is acidic and the lone pair housed on sp^2 hybridised 'N' is basic and able to coordinate to the metal ions. As five membered hetero cycles are π-excessive, they act as better π donor (hard donor centre) compared to six membered heterocycles. A significant pyrazole chemistry has been developed by Meyer and co-workers [12-16], who have studied the coordination potentiality of the 3,5-disubstituted pyrazole ligands with chelating side arms, mainly with N-donor atoms. These ligands differ in the chain lengths of the chelating side arms and the number of donor sites.

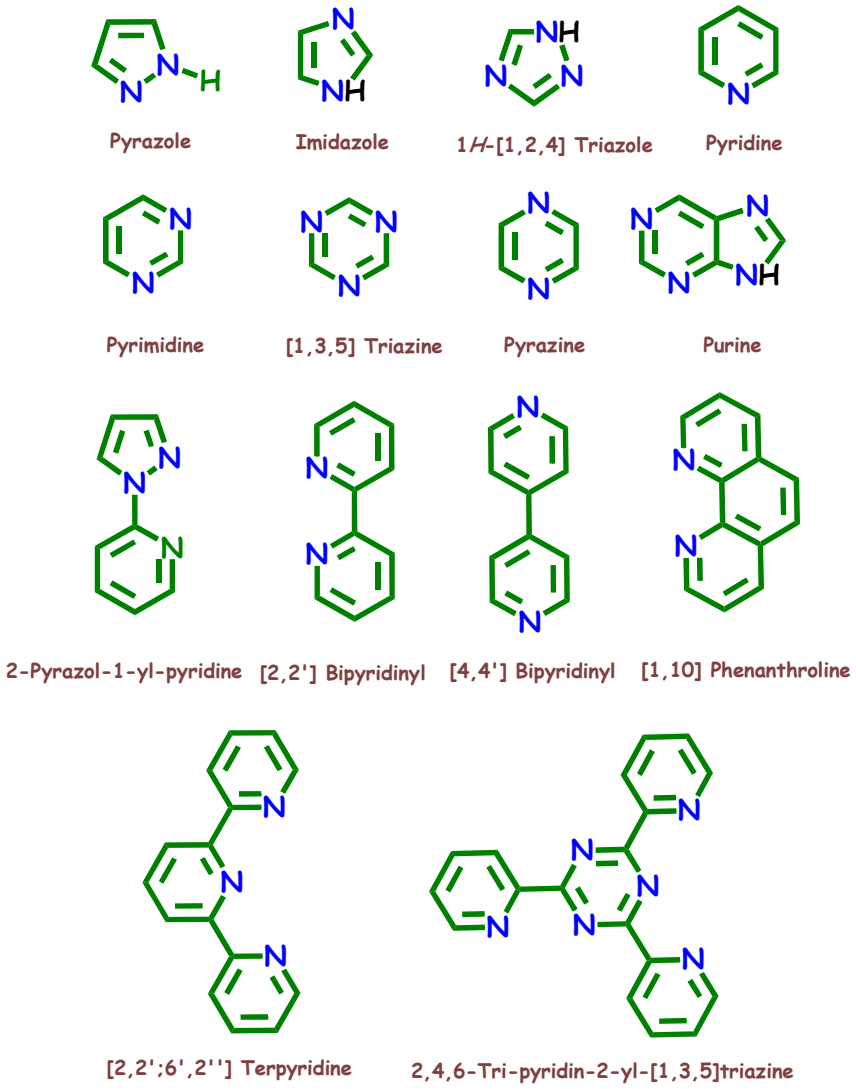

Fig. 1.1: Some representative heterocyclic ligands (containing either one or more nitrogen atoms as heteroatom)

The ease of synthesis of diversely substituted pyrazoles is the most interesting feature in the incorporation of pyrazole groups in the strategy of new ligands and hence bargains the opportunity of both electronic and steric control of the properties of the metal complexes. An interesting situation arises when a six-membered heterocycle such as pyridine and a five-membered heterocycle such as pyrazole are linked directly in a single ligand system. In fact, the complexes of such ligands give rise to significantly different electronic properties.2-Pyridylpyrazole derivatives (Fig. 1.2) have been proven to be good ligands for obtaining different assemblies, such as metallo-helicates [17, 18] or clusters [19-21].

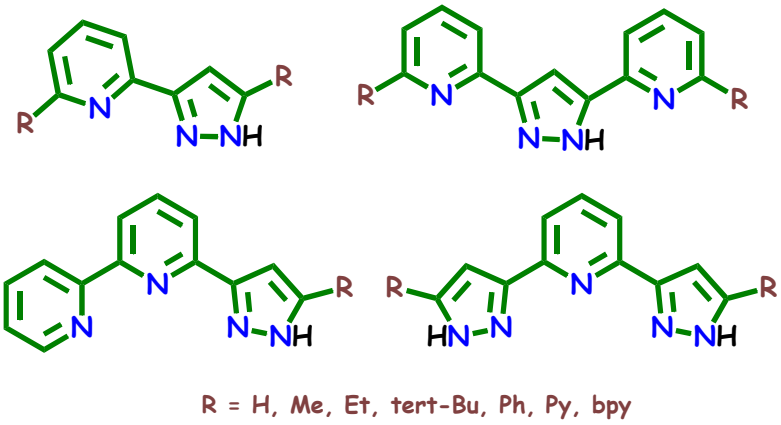

Fig. 1.2: Pyrazole-based ligand with N-donor pyridine substituents

A seminal review published in 2000, Hosseini et. al., described the archetypal polypyridyl ligand, 2,2′-bipyridine (bpy), as the ‘‘most widely used ligand” [22]. The strong metal–ligand interactions associated with bpy and other polypyridyl ligands are driven by the cooperativity of the nitrogen-based σ-donation into the metal orbitals and the π-accepting character of the aromatic heterocycles that idealised five-membered chelating rings that they form with the metal ions [23]. Naturally, these effects are enhanced when employing flexidentate ligands, such as 2,2′;6,2″-terpyridine (terpy), that necessarily form multiple rings chelates and hence have higher binding capabilities with metal ions than their bidentate counterparts [24, 25]. Before the metal coordination, nitrogen on 2-pyridine present a trans–trans geometry to avoid lone-pair electron repulsion. Upon coordination, a cis–cis geometry (Fig. 1.3) will be formed through metal chelation [26]. As a result, three pyridines adopt perfect coplanar conformation, allowing a good conjugation between the aromatic rings and metal cation. 2,2′;6,2″-terpyridine or their derivatives are well known oligopyridine metal-

binding motifs and used as a renowned building block in metallo-supramolecular chemistry. This feature makes 'terpy' a potential 'non-innocent' ligand, with the capability to stabilize the low valency metal, including nickel [27-31], iron [32, 33], cobalt [34-37] and manganese [38] etc.

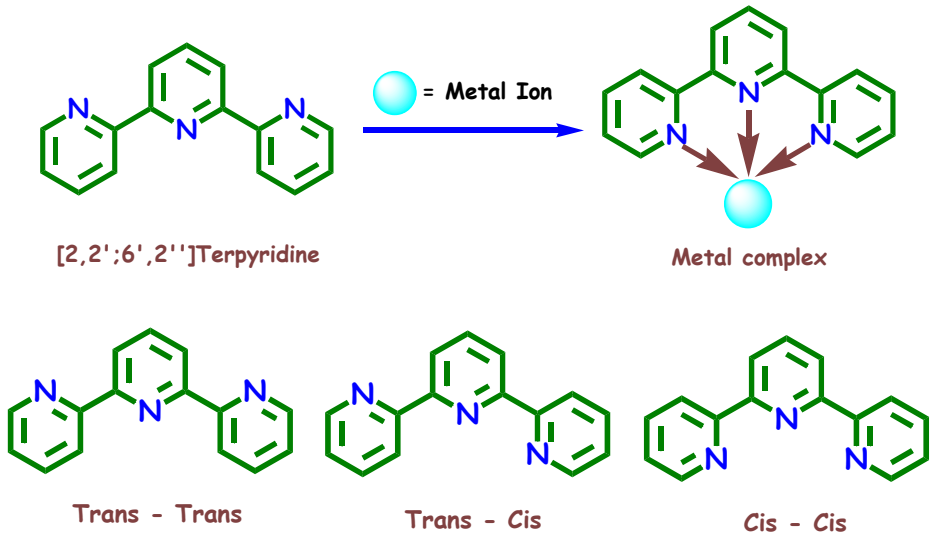

Fig. 1.3: Schematic representation free ligand and metal-ligand complex

2,4,6-tris(2-pyridyl)-1,3,5-triazine (tptz) or their structural analogues are well known metal binding sites that can arrest an immense attention in the field of contemporary metallo-supramolecular chemistry [39, 40]. As a flexidentate coordinating ligand tptz shows several coordination modes with the metal centres (Fig. 1.4).

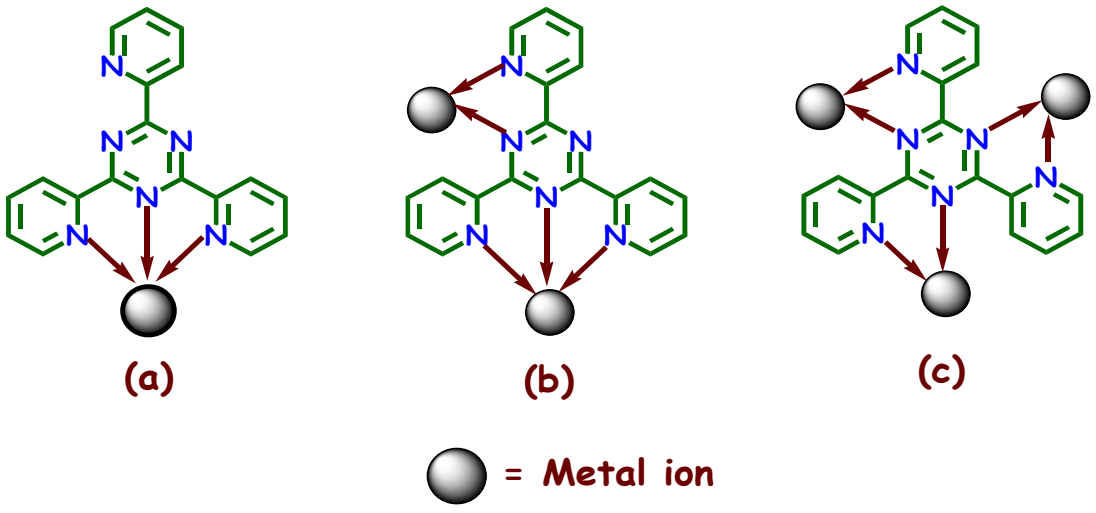

Fig. 1.4: Schematic representation of the possible coordination modes of the ligand '**tptz**'

The predominant coordination mode of 'tptz' is tridentate terpyridine like (Fig. 1.4a). Moreover, it is also able to coordinate two metal centres in one terpyridine and one bipyridine like coordination modes (Fig. 1.4b) and to bind three metal centres via all bipyridine-like coordination, although this binding mode is quite rare (Fig. 1.4c).

From crystal engineering point of view N-based heterocycles have been chosen due to their ability to construct π···π, C–H···π, cation···π, cation···π^+, anion···π, lone pair···π interactions. The potentiality of such interactions is based on interaction between electron rich and electron deficient moieties that in turn generates the self-assembly of small molecules into supramolecular architecture and are also accountable in enhancement of both directionality and dimensionality in the solid state of transition metal complexes.

Here, judiciously and strategically π-rich ligand systems have been chosen for metal coordination and the role of ancillary ligands and counterions have been investigated from crystal engineering point of view. The metal salts of cobalt, nickel and copper have been chosen due to their adaptability in forming several coordination geometries.

1.3. A BRIEF INTRODUCTION OF SUPRAMOLECULAR CHEMISTRY AND CRYSTAL ENGINEERING

Supramolecular chemistry, also known as "chemistry beyond the molecule", emphases on the study of molecular recognition and high-order assemblies formed by noncovalent interactions. **In 1987, the Nobel Prize in Chemistry** was awarded jointly to **Donald J. Cram, Jean-Marie Lehn, and Charles J. Pedersen** "***for their development and use of molecules with structure-specific interactions of high selectivity***". Following the definition of supramolecular chemistry by Jean-Marie Lehn as ''***chemistry beyond the molecule, bearing on the organized entities of higher complexity that results from the association of two or more chemical species held together by intermolecular forces***'' (Fig. 1.5) the review [41] will focus on specific examples of host–guest complexes determined through single crystal X-ray crystallography.

This established supramolecular chemistry as a well-accepted chemical discipline because supramolecular systems are made from building blocks that are linked together by noncovalent interactions and can show stimuli-responsive behavior [42]. The review deals

with selected clathrate and container molecule systems where the guest is bound inside the cavity of the host or pores, channels or cavities of the crystal structure by weak supramolecular interactions. After only roughly 50 years of the discipline, supramolecular chemistry has put its signature in various areas like: molecular machines, molecular sensors, gas absorption, nanoreactors, chemical catalysis, and drug delivery. Supramolecular chemistry, therefore, is an intersection topic of organic, physical, coordination, polymer chemistry, materials science, biological science, and so on.

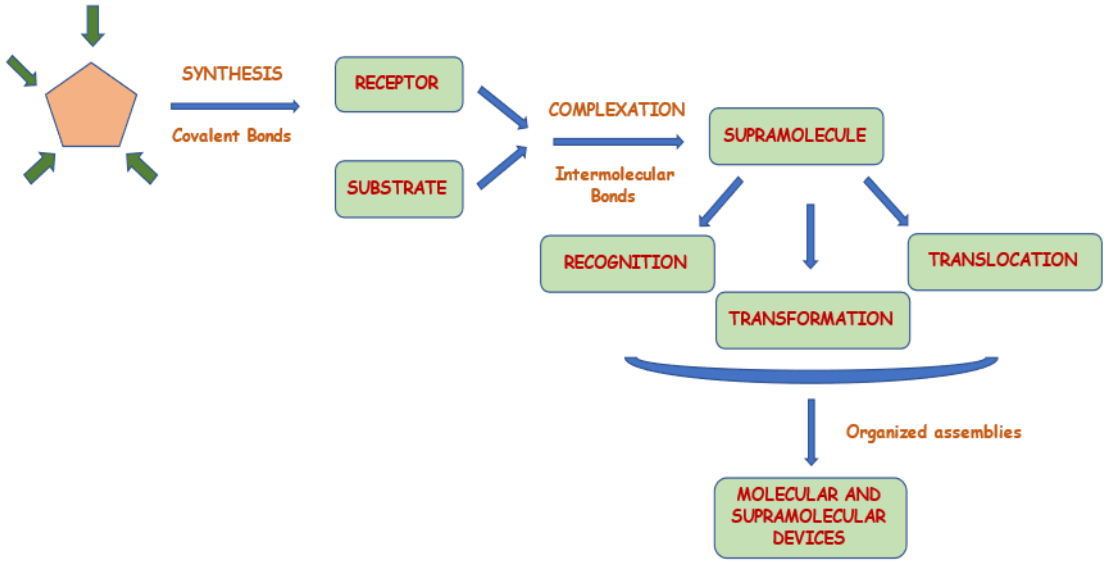

Fig. 1.5: From molecular to supramolecular chemistry, according to Lehn [41]

X-ray crystallography is the most influential tool for the detailed structural analysis of intermolecular interactions in crystalline complexes and only if a good enough quality single crystal of the target metallo-organic complex is available. A crystal is in fact a supramolecular entity where the molecules that constitute it interacts implicitly among themselves during crystallization. Sometimes to ensure the presence of such weak interactions in the solid state of the complex can be corroborated with powder X-ray crystallography (as it is a bulk property in comparison to a single crystal X-ray crystallography).The development of the concept of supramolecular interactions within crystals has been merged in the 1980's and 1990's by prominent crystallographers like G. R. Desiraju and M. Zaworotko to a new research area called crystal engineering, which is now considered to be a topic of interest [43-46]. The term ''**crystal engineering**'' appears first in

the proceedings of the American Physical Society Meeting (as abstract) in 1955 and it became generally accepted as general term after being used by G. M. J. Schmidt in 1971 [47]. This field has arrest widespread interest over last few decades as a natural interplay between chemistry and crystallography. Basically, it is the study of intermolecular interactions in the light of crystal packing and the extension of this idea in designing novel solids with desired physical and chemical properties. Crystal engineering has extensive applications in the domain of material science, molecular biology and pharmaceutical science.

1.3.1. Supramolecular synthon

The term 'supramolecular synthon' has been clarified by Desiraju as "*supramolecular synthons are structural units within supermolecules which can be formed and/ or assembled by known or conceivable synthetic operations involving intermolecular interactions*". These are the smallest unit in which the entire information regarding the mutual recognition of molecules to generate solid-state supramolecules is encoded. The crystal seems to be an organization of different types of supramolecular interactions. The concept of introduction of supramolecular synthons (Fig. 1.6) was an extremely important step for the understanding of the organization of molecular crystals.

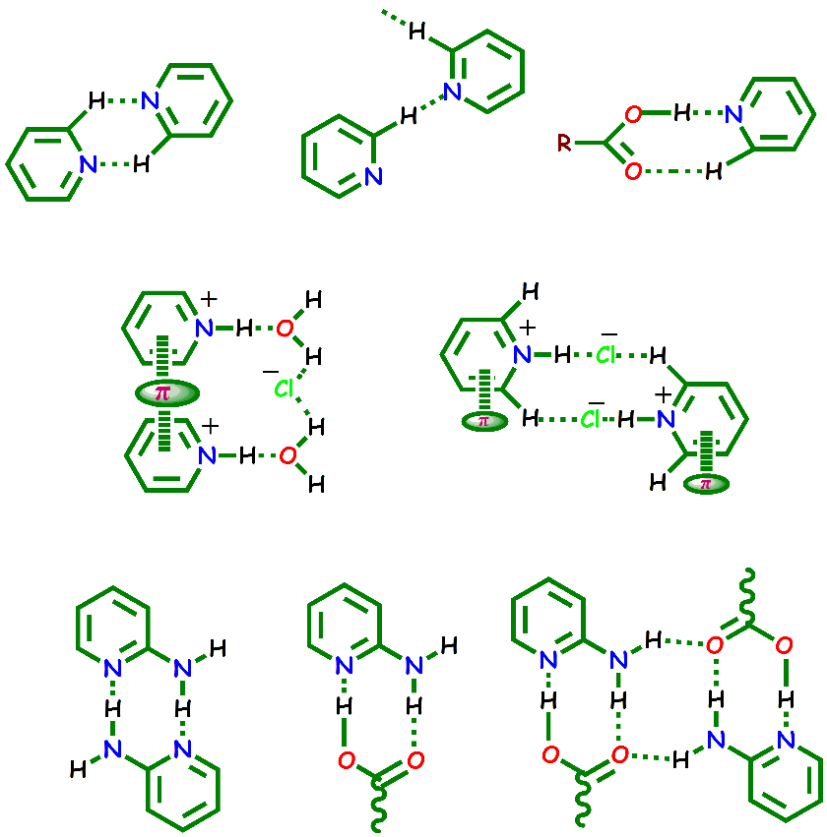

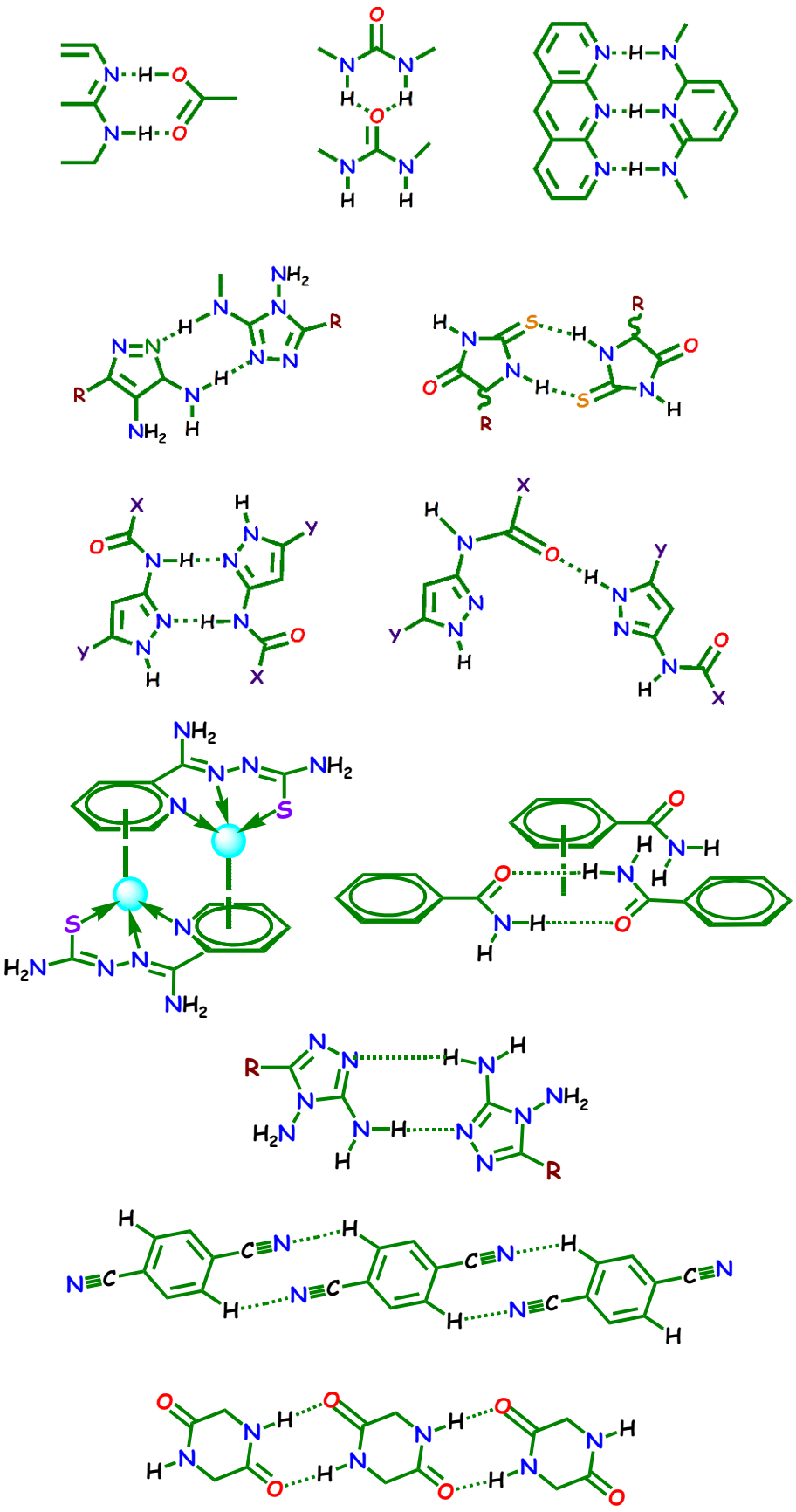

Fig. 1.6: Some representative supramolecular synthons

The main objective of crystal engineering is designing of periodic structures with a desired supramolecular organization which makes it feasible to achieve or modify a desired property in the synthesized material. An empirical knowledge of the non-covalent forces mediates the formation of supramolecular synthons which is nothing but a retrosynthetic approach to supramolecular chemistry where one can fragment the crystal structures into supramolecular synthons (small repetitive unit), and based on their relative abundance available in the data- base, new synthetic strategies can be constructed. Therefore, when one starts with a crystal structure and deconstructs it into the smallest non-reducible unit, i.e., the synthon, both geometrical and chemical factors get deconstructed, and it is here where synthons score over individual molecules (or functional groups) in terms of consistency and robustness [48]. This shaped an opportunity for the synthesis of new complexes with targeted patterns of binding between molecules similar to the synthesis of organic molecules using molecular building blocks or synthons [49]. By these concepts of synthon and their stabilizing motif (with quantifying their energy at least theoretically) one can utilize them in crystal engineering and may create or form a strategy to form new synthons.

1.3.2. Host-guest Chemistry

Host-guest chemistry is a branch of supramolecular chemistry that is concerned with the formation of structural aggregates and their properties. The complex is held by one or a combination of forces including: hydrogen bonding, ion-dipole, ion-ion, π···π, van der Waals and hydrophobic interactions. The host generally possesses binding sites, that converge in the complex. Guests may be ionic or neutral, and can include metal ions, ammonium ions, carboxylic acids, amino acid derivatives, and many others. According to D. Cram *"The host component is defined as an organic molecule or ion whose binding sites converge in the complex……. the guest component is any molecule or ion whose binding sites diverge in the complex"*. Conventionally the larger molecule is termed as 'host' and the smaller one is its 'guest'. The 'host' can wrap around the 'guest' and act as an envelope around the 'guest'. Probably the earliest and most common examples of "host-guest" chemistry are enzyme-substrate interactions where the substrate fits into the enzyme's active site with complete specificity (Fig. 1.7 and 1.8).

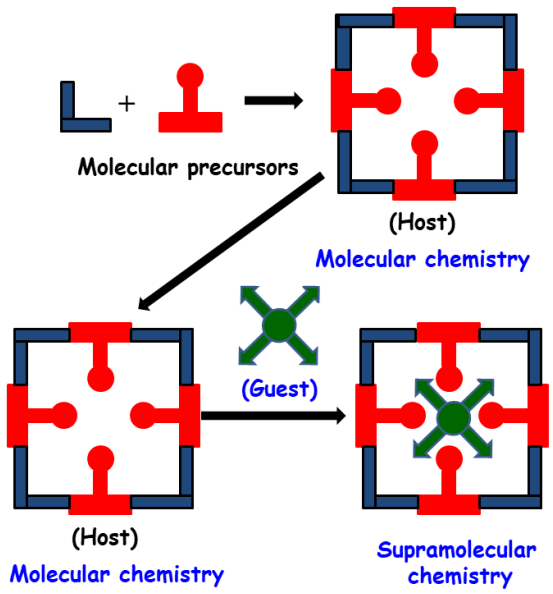

Fig. 1.7: Schematic representation of host-guest complex and comparison between the scopes of molecular and supramolecular chemistry

In 1894, Emil Fischer proposed the now ubiquitous 'Lock and Key' principle for the active site and the substrate, where the 'lock' represents the host and the 'key' the guest. In 1967, the discovery of crown ethers directs to the phenomenal growth of this field and new type of molecules like cryptands, calixarenes, cavitands, carcerands, spherands, crypta-spherands etc., have been synthesized. This major class of complexes also show importance in biological arena and act as an information storage and transfer, replication and catalysis in living organisms. Sensing systems based on host-guest systems have been synthesized for various anion recognition.

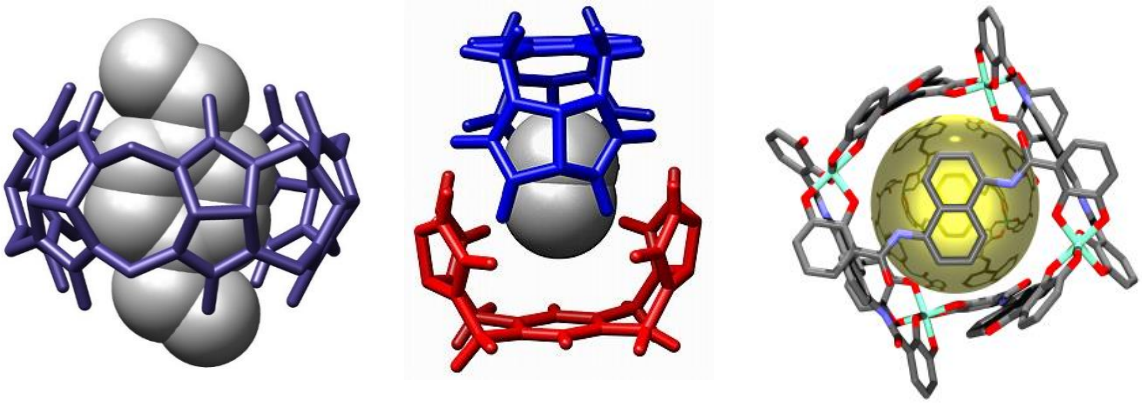

Fig. 1.8: Some representative molecular view of host-guest complexes [54, 55]

Self-assembly differs from host-guest chemistry from the fact that where there is no major difference in size and no species is acting as a host for another, the involvement of two or more species through noncovalent interactions is termed as self-assembly. Strictly, self-assembly is equilibrium among two or more molecular components that produces an aggregate with a structure depend only on the information contained within the chemical building blocks.

1.3.3. Molecular Recognition

In molecular recognition, a molecule selectively recognizes its counterpart through various molecular interactions that are mostly non-covalent in nature. The basis of molecular recognition is the appropriate molecular interactions between the host and the guest. During recognition hydrogen bonding (both classical and non-classical) plays a significant role in adapting proper geometry. Coordinate bonding is another type of direction-specific interaction that also helps in recognition process. The van der Waals interaction is weaker and less specific in nature but it is undoubtedly essential because this interaction generally applies to all kinds of molecules. This type of interaction is generally driven by the interactions of dipoles which are generated by instantaneous unbalance of electronic distributions in neutral molecules. The individual interactions are generally weak but collective cooperative contributions from numerous van der Waals interactions make considerable impact to molecular recognition. As van der Waals interaction depends on the surface area and shapes of the molecules, interacting molecules having surfaces with complementary shapes, as in the lock and key concept, the van der Waals interaction becomes more effective. This interaction is particularly important when the host molecule recognizes the shape of the guest molecule [50]. Various type of π···π, C–H···π, etc. interactions also provide important contributions to molecular recognition [51]. Molecular recognition plays central role in different areas of science and technology, such as bio-chemical processes [52], catalysis [53], host-guest systems [54], design of sensor materials [55], surface patterning [56], nano-scale assembly [57] and soon. Self-assembly of molecular building blocks through molecular recognition has led the way in the design and preparation of various functional materials, both of organic as well as of hybrid organic-inorganic type [58]. It is generally assumed that identical recognition patterns exist both in solution and in the crystalline solid state; in many cases, this has been unequivocally established [59]. The rational synthesis of desired supramolecular materials has reached a state of the art where one

relies on the most commonly observed recognition pattern between a set of molecular building blocks (Fig.1.9). However, sometimes various unforeseen factors such as the participation of solvent molecules or the pH of the solution play an important role in the self-assembly process.

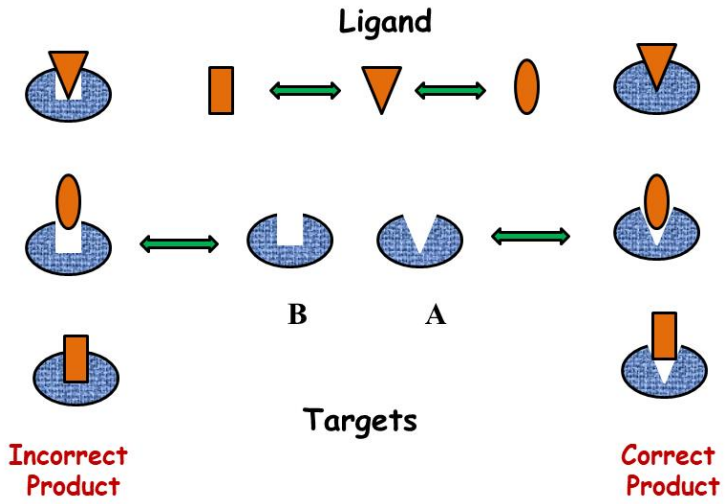

Fig. 1.9: Representative view of molecular recognition by lock & key mechanism

1.4. A BRIEF INTRODUCTION OF NON-COVALENT INTERACTIONS

In supramolecular systems, the molecular components are held together through the non-covalent intermolecular forces. Thus, molecular chemistry deals with covalent interactions while the supramolecular chemistry describes the chemistry of molecular assemblies held together through non-covalent interactions. A very large number and variety of intermolecular interactions have been used in crystal engineering namely hydrogen bonding, halogen bonding, chalcogen bonding, pnictogen, cation···π, anion···π, C–H···π, π···π, chelate ring···π, salt bridge···π, lone pair···π, C–H···anion interactions and the hydrophobic interactions (Fig.1.10).

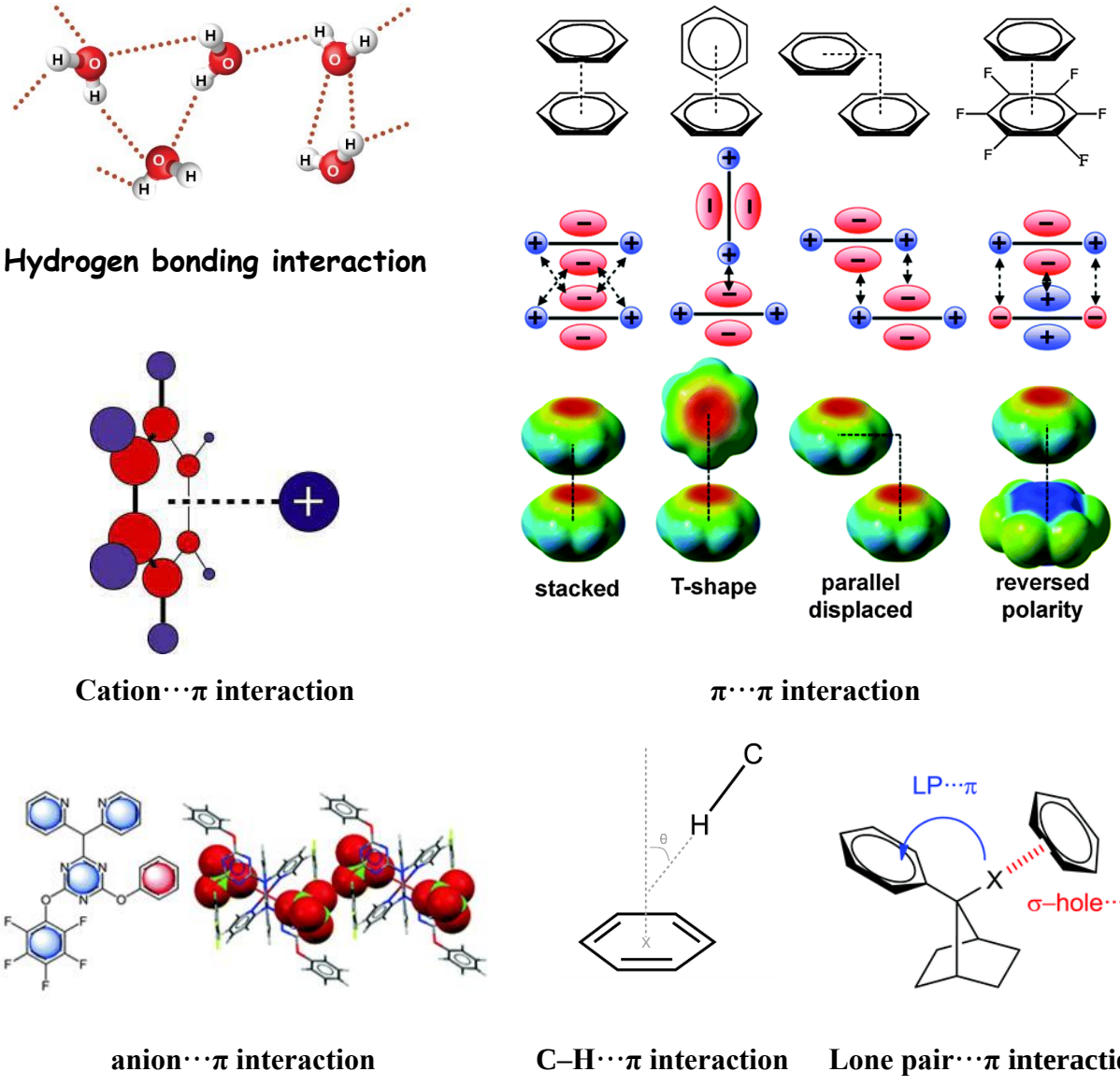

Fig. 1.10: Some representative non-covalent interactions

Most notable among such interactions are hydrogen bonds that arise from the polar region of molecules and a herringbone and stacking interactions which arise from the non-polar regions of aromatic molecules and hydrophobic interaction that arise from aliphatic regions. At present, these types of non-covalent interactions play a crucial role in modern chemical research and considered as skeleton of supramolecular chemistry, materials science and even biochemistry. Such interactions have involved in crystal packing and generating multi-dimensionality of coordination complexes, large molecules like nucleic acids and proteins. In biological processes several large molecules bind one another in a specified way

by exploiting these variety of non-covalent interactions. Approximate supramolecular interaction energeias have been summarized in table 1.1 [60].

Table 1.1: Approximate chemical interaction energeias (in kJ mol^{-1})

Interaction type	**Directionality**	**Bond Energy (kJ mol^{-1})**	**Example**
Ion – ion	Omnidirectional	200 – 300	Tetrabutylammonium chloride
Coordination bonds	Directional	100 – 300	Metal - pyridine
Ion – dipole	Nondirectional	50 – 200	$[Na\ (15\text{-crown } 5)]^{+}$
Closed-shell metal – metal bond	Nondirectional	5 – 60	Argentophilic (Ag⋯Ag) Aurophilic (Au⋯Au)
Hydrogen bonds	Directional	4 – 120	Carboxylic acid dimer
Halogen bonds	Directional	10 – 50	Sulphur – iodine complex
cation⋯π/ anion⋯π	Directional	5 – 80	K^{+}⋯benzine
π⋯π interactions	Directional	2 – 50	Benzene dimer
Dipole – induced dipole interaction	Directional	2 – 10	HCl⋯Cl_2
van der Waals	Directional	<5	Argon

1.4.1. Hydrogen bonding interaction

Hydrogen bonding has been extremely well studied and recognized as the most important of all noncovalent interactions [61. 62] and is basically an electrostatic interaction which may increase the degree of association among the molecular species. The hydrogen bond is especially important because it is both strong and directional [63]. Therefore, it is a very effective design component in crystal engineering. Hydrogen bonding is generally represented as A⋯H–D denotes the interaction between the donor species (HD) and the acceptor species (A) through the hydrogen end (Fig. 1.11). This hydrogen bonding is extremely significant and well elucidated in biological systems to explain the stability of numerous biomolecules such as DNA, proteins etc. (Fig. 1.12).

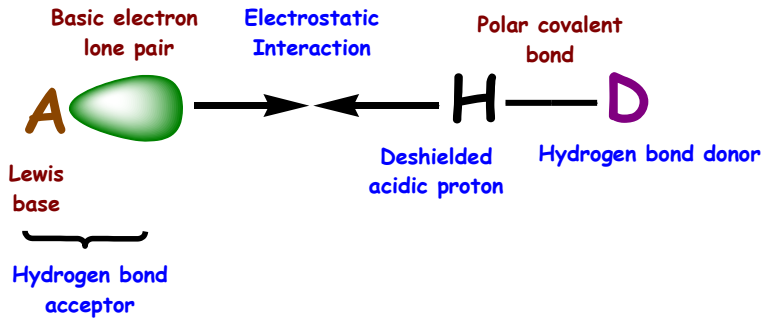

Fig. 1.11: General representation of hydrogen bonding interaction

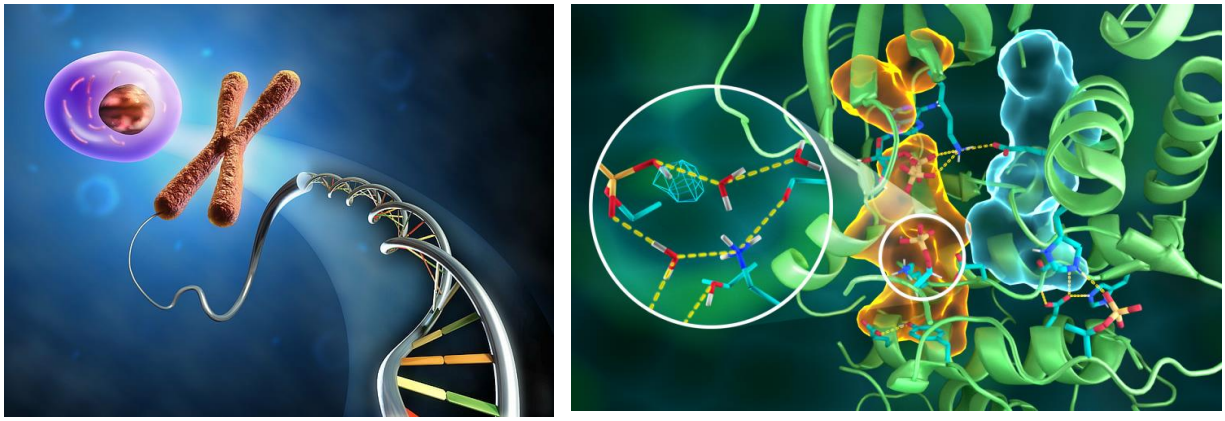

Fig. 1.12: Hydrogen bonding in DNA and protein molecules

In classical definition of the hydrogen bond the strongly polar hydrogen bond donor groups D–H (D = O, N, or halogen) on one side and hydrogen bond acceptor atoms A (A = O, N, halogen, etc.) are usually considered on the other. Beside this a weak 'non-classical' hydrogen bond of type C–H···X arrest recent interests in the fields of host–guest chemistry and anion recognition. In addition to relatively abundant C–H···N/ O hydrogen bonding the existence of C–H···Cl hydrogen bonding is much less frequent but well appreciated in current research [64, 65]. If the heterocyclic ring is associated with a donor atom which is capable to reduce the electron density in the ring concomitantly increases the protic character of the ring C–H groups and enable to produce C–H···Cl hydrogen bonding interaction [66]. The C–H···Cl distances reported in this context should be less than the sum of the van der Waals radii for the hydrogen and the neutral chlorine atom (2.95Å) The strength of hydrogen bonds can differ from very feeble (1 to 2 $kJmol^{-1}$) to extremely strong (161.5 $kJmol^{-1}$in the bifluoride ion) [67]. According to the investigation, O–H···O is the strongest among all types

of hydrogen bonds [68]. C–H···O is considered as a model as well as the oldest weak hydrogen bonding interaction [69]. According to Jeffrey's categorization based on donor-acceptor distances of hydrogen bond, donor-acceptor distance 2.2 to 2.5Å may be considered as strong, 2.5 to 3.2Å is to be considered as moderate and 3.2 to 4.0Å is to be considered as weak [68]. Table 1.2 bears a brief collection of some typical values of distance and energies.

Table 1.2: Approximate interaction energeias& distances of various H-bonding interactions

Interaction	**Energy (kcal mol^{-1})**	**H···A (Å)**	**D – A (Å)**
O–H···O	3.8	1.51	2.78
O–H···C	1.79	2.66	3.30
O–H···S	4.0	2.49	3.25
N–H···O	6.0	1.80	2.81
N–H···C	3.0	2.61	3.30
N–H···N	6.0	1.92	2.83
N–H···S	3.0	2.60	3.12
C–H···O	2.0	2.6	3.50
C–H···N	2.0	2.51	3.41
C–H···S	1.5	2.7	3.66
C–H···C	0.33	2.74	3.59

1.4.1.1. Types of Hydrogen bonding

Based on the geometry, hydrogen bonds can be classified in different categories as shown in figure 1.13. The simplest and prototype arrangement of a hydrogen bond is D–H···A model, where the angle is ~180°, (Fig. 1.13a). In the 2nd type the angle shows a deviation from 180° in D–H···A model (Fig. 1.13b). Fig. 1.13c depicts that one hydrogen atom interacts with two acceptor atoms generating a centre of three atoms known as bifurcated arrangement. Similarly, Fig. 1.13d provides a multifurcated hydrogen bond, a donor creates hydrogen bonds with more than two acceptors simultaneously. Multifurcated hydrogen bonding needs a large concentration of acceptors, at least locally [69].

Multifurcated hydrogen bonds are present in protein molecules in large numbers. However, bond directions have been shown by rigorous theoretical calculation for both components for a number of bifurcated bonds [70].

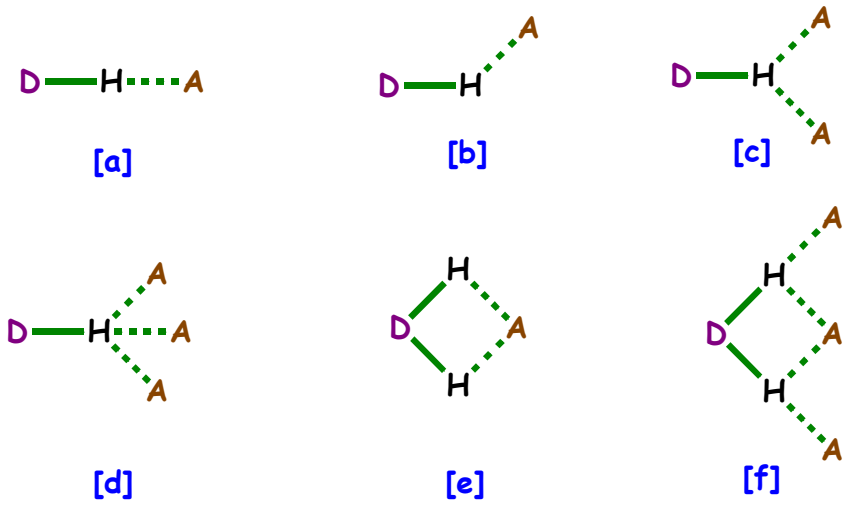

Fig. 1.13: Different kinds of hydrogen bonding geometries: (a) linear; (b) bent; (c) donating bifurcated; (d) trifurcated; (e) accepting bifurcated; (f) three-centre bifurcated

1.4.1.2. Role of Hydrogen bonding in bio-chemical system

The formation of hydrogen bonds is highly important in biological systems because the bonds stabilize and determine the structure and shape of large macromolecules such as nucleic acids and proteins. This type of bonding occurs in biological structures, such as DNA and RNA. This bond is very significant in water because this is the force that exists between water molecules to hold them together.

Both as a liquid and as solid ice, the hydrogen bond formation between the water molecules provides the attractive force to hold the molecular mass together. Intermolecular hydrogen bonding is responsible for the high boiling point of water because it increases the amount of energy required to break the bonds before boiling can begin. Hydrogen bonding forces water molecules to form crystals when it freezes. Since the positive and negative ends of the water molecules must orient themselves in an array that allows the positive ends to attract the negative ends of the molecules, the lattice or framework of the ice crystal isn't as tightly meshed as the liquid form and allows ice to float in water (Fig. 1.14).

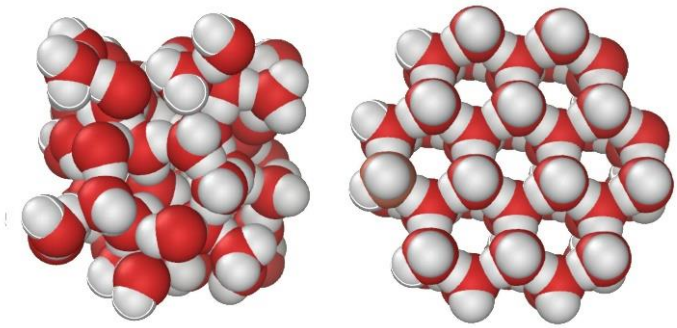

Fig. 1.14: Hydrogen bonding in water and ice

The 3-D structure of proteins is very important in biological reactions such as those involving enzymes where the shape of one or more proteins must fit into openings in enzymes much as a lock and key mechanism (Fig. 1.9). Hydrogen bonding allows these proteins to bend, fold and fit into various shapes as necessary which determines the protein's biological activity. This is very important in DNA because the formation of numerous hydrogen bonds allows the molecule to assume its double helix formation (Fig. 1.15).

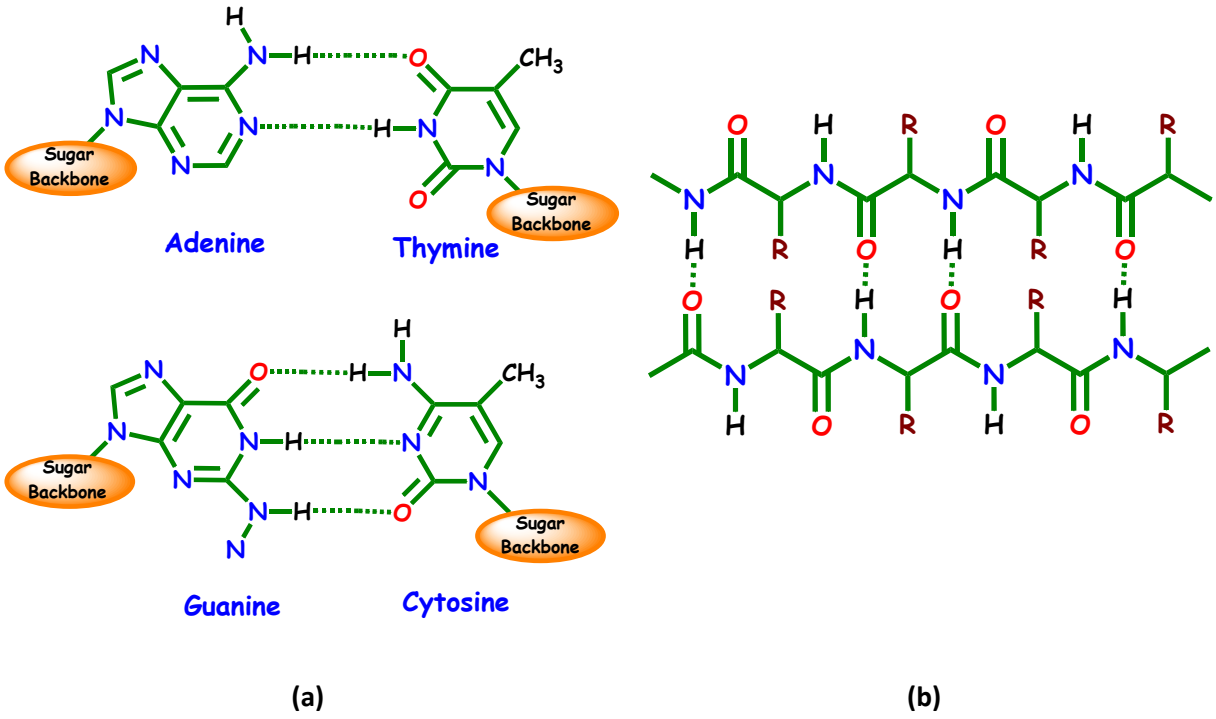

Fig. 1.15: Hydrogen bonding in (a) DNA and (b) protein chain

Antibodies are folded protein structures that precisely target and fit a specific antigen. Once the antibody is produced and attains its three-dimensional shape (aided by hydrogen bonding), the antibody will conform like a key in a lock to its specific antigen. The antibody will lock onto the antigen through a series of interactions including hydrogen bonds. The human body has the capacity to produce over ten billion different types of antibodies in an immunity reaction (Fig. 1.16).

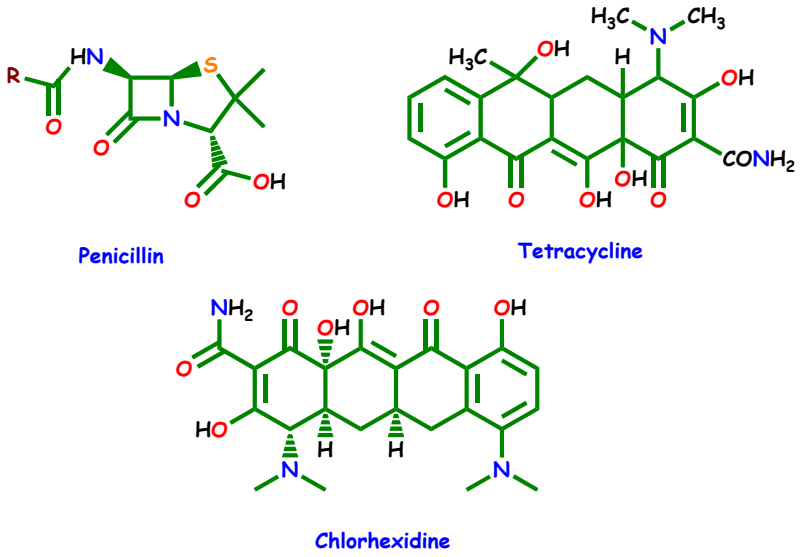

Fig. 1.16: Molecular representation of some antibiotics

While individual hydrogen bonds are not very strong, a series of hydrogen bonds is very secure. When one molecule hydrogen bonds through two or more sites with another molecule, a ring structure known as a chelate is formed (Fig. 1.17). Chelating compounds are useful for removing or mobilizing molecules and atoms such as metals.

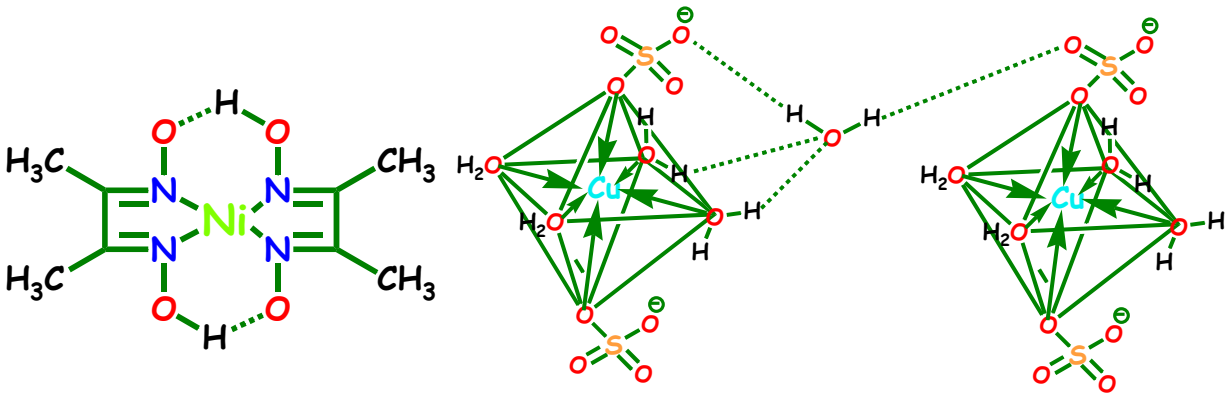

Fig. 1.17: Hydrogen bonding in some metal complexes

1.4.2. π···π stacking interaction

The arene-arene interaction is the most extensively observed noncovalent π-interaction and it is therefore considered as the fundamental interaction. As a consequence, a broad scientific community has been involved in investigating the π-stacking ability of aromatic rings. These types of interactions are extensively ubiquitous in organic crystals, clusters, nanomaterials and biomolecules [71, 72]. It also plays a crucial role during intercalation of drugs into the DNA channels and have been utilized in several host-guest systems [73]. These π···π staking interactions also have the potentiality of being used for various applications such as immobilization, specific recognition and the material construction as long as the materials contain aromatic moieties. Furthermore, these facial, reversible and non-destructive π···π interaction is promising in material engineering particularly [74]. The most common typical of an arene-arene interaction is the benzene dimer which can be considered as a model system for π···π interactions. Because of its immense significance extensive research ranging from early gas phase studies to more recent computational studies are going on [75]. This huge amount of research helps the scientific community to acquire useful knowledge and perception about the fundamental properties of π···π interactions. The theoretical basis for π···π interactions depends essentially on quadrupole moment arising in interacting aromatic systems. This is quite similar to the dipole moment which describes the molecular charge distribution in an aromatic system. Ritchie *et al.* calculated the quadrupole moment of various aromatic systems using electric field-gradient birefringence [76]. The binding energy for benzene dimer is obtained 1.6 kcal mol^{-1} experimentally [77]. Generally, it is assumed that π-stacking interactions do not exist as a discrete intermolecular interaction between closed-shell molecules [78]. A detail investigation of various crystal structures and high level of computational analysis indicates that for a successful interaction the preferred alignment of aromatic π-systems shows a "noticeable lack of predominant face centred stacking and, therefore, no preference for interacting π clouds among associated aromatic molecules normally encountered in synthetic and biological systems" [78]. π-stacking interaction should be reflected as a geometric descriptor without implications for a distinct π-stacking interaction. As a consequence, three geometries of the benzene dimer have been modelled after high level of theoretical calculation with preferences for T-shaped and parallel displaced geometries. These geometries are: parallel-displaced, T-shaped edge-to-face, and eclipsed face-to-face (Fig. 1.18A-C) and all of them are found to be attractive in nature. It is well observed fact that

there is a competition for T-shaped versus parallel orientations in case of π-stacking interactions [79]. In fact, for large aromatic sheet like molecules (such as coronene and circulene) parallel orientations are the predominant one over T-shaped orientation though parallel displaced geometry is preferred over perfectly overlapping face-to-face "sandwich" geometry by several kcalmol^{-1} [80, 81].

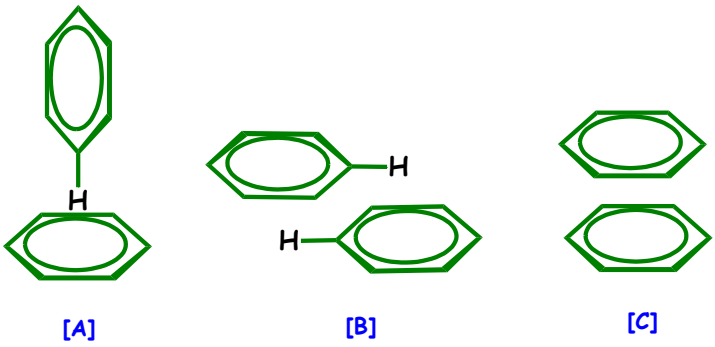

Fig. 1.18: The geometry of the π···π interactions in benzene molecules: (A) edge-to-face, (B) offset, and (C) face-to-face [81].

To understand and explore the aromatic–aromatic interactions qualitatively Hunter and Sanders have devised a set of rules based on a simple model of the charge distribution in a π system. They separated the σ framework and the π electrons and assumed that π···π interactions are the result of π···σ attractions that overcome π···πrepulsions [78]. These "Hunter-Sanders" rules state for non-polarized π-systems [82, 83]:

- Rule 1: π···π repulsion dominates in a face-to-face π- stacked geometry.
- Rule 2: π···σ attraction dominates in an edge on or T-shaped geometry.
- Rule 3: π···σ attraction dominates in an offset π-stacked geometry. For polarized π systems there are an additional three rules, which are stated here in the form of a requirement for face-to-face π stacking.
- Rule 4: For interaction between highly charged atoms, charge–charge interaction dominates.
- Rule 5: A favourable (face-to-face) interaction with a neutral or weakly polarized site requires as a π polarization a π-deficient atom (in the aromatic ring).
- Rule 6: A favourable (face-to-face) interaction with a neutral or weakly polarized site requires as an σ polarization a positively charged atom (in the aromatic ring).

Experimental findings portrayed that electron withdrawing substituents or heteroatoms enhance the strength of π···π interaction. This electron withdrawing by substituents or heteroatoms causes decrease in electron density of the π-system and consequently the π-electron repulsion. Eventually, the stability of face-to-face π-stacked aromatic moieties increases when both the participating aromatic molecules are electron poor, whereas electron donating substituents disfavoured π···π interaction. Electron donating substituents increases the electron density of aromatic systems and thus results an increase in repulsion between interacting aromatic moieties [82]. The order of stability in the interaction of two π systems is π-deficient···π-deficient > π-deficient····π-rich > π-rich···π-rich [82, 83]. Stoddart *et al.* [84] and Foster [85] have elegantly exploited the π···π stacking interactions between π-donor and π-accepting ring systems in the self-assembly (Fig. 1.19).Aromatic nitrogen heterocycles, being electron deficient, should in principle be well suited for π···π interactions and hence heterocyclic nitrogen increases the tendency to stack [78].Though π···π interactions are weak in nature they found to play significant role in the folding [86] and the thermal stability of proteins [82, 87]. However, their weak and non-directional nature makes it difficult to develop a general structural and energetic model for their description [88]. The pioneering work of Burley and Petsko described that the protein side chains i.e., amino acid residues are the main determining factors for interactions between them during protein-folding processes [89]. They investigated 34 proteins and came to the ultimate conclusion that around 60% of the aromatic side chains (Phe, Trp, Tyr) are involved in π···π interactions and in most of the cases the predominant geometry was found to be the T-shaped edge-to-face structure (Fig. 1.18A). McGaughey *et al*. extended the analysis with greater number of sample of proteins and proposed that the parallel-displaced geometry was a preferred orientation [90]. Curiously, none of these studies described the face-to-face geometry (Fig. 1.18C) as preferred orientation.

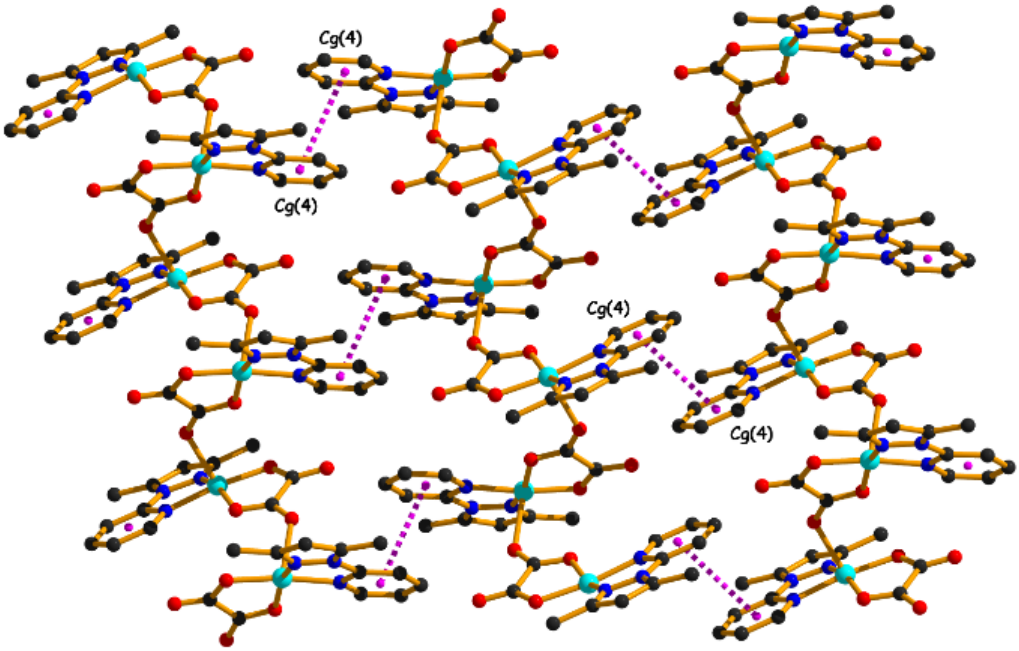

Fig. 1.19: Representation of the π···π interactions in molecular crystals

1.4.3. C–H···π interaction

Being different from classical hydrogen-bonding interactions, C–H···π interactions have been known to be the weakest non-classical hydrogen bond contributing significantly indifferent fields of chemistry like self-assembly, chiral recognition, stabilization of structures of proteins and nucleic acids and many more [91-94]. C–H···π interaction has been recognized as the attractive interaction working between a non-polar or feebly polar C–H bond and an aromatic π-system [95]. Despite of the recognition in several fields of chemistry, the character of the C–H···π interaction is still controversial. C–H···π has different characteristic from classical hydrogen bonding because electrostatic interactions are mainly responsible for the attraction in conventional hydrogen bonds whereas, C–H···π have similar nature with the trivial van der Waals attractive force. Again, the hydrogen bonds generally have strong directionality whereas, the C–H···π interactions mostly take place between soft acids and bases comprise electron correlation energy or dispersion energy through the electrostatic interactions can have a trivial contribution (ca. 20%) in few cases [96]. Thus, it is considered as the weakest nonclassical hydrogen bond [97]. The attractive nature of CHs and π-systems was first predicted by M. Tamres through his thermochemical observations

[98]. Later, it was supported by spectroscopic evidence and theoretical calculations [99, 100]. The significance of C–H···π interaction in supramolecular chemistry was first suggested by Andreetti and his co-workers based on crystallographic data of a range of calix-[4]-arene complexes with toluene [101, 102]. Various evidence for the C–H···π interactions (Fig. 1.20) was obtained afterward from the study of different crystal structures and supramolecular systems [103, 104]. The T-form conformation of benzene dimer gives rise to C–H···π interaction. According to the theoretical calculations, stabilization of the C–H···π bond basically appears from the dispersion force. The nature of the hydrogen bonds in C–H···π interactions was confirmed by AIM (atoms in molecule) analyses and by relative MO studies of intramolecular systems [105, 106]. Nakagawa and Nikki reported the importance of interaction between the C–H dipole and the quadrupole of aromatic moieties [107]. The stronger is the protonic nature of the CH, the stronger is the stabilizing effect and thus the arrangement for C–H···π interaction become as sp-CH···π > sp^2-CH···π > sp^3-CH···π. Interactions concerning aromatic CHs are stronger than the aliphatic ones. A recent theoretical study (2015) proposed that C–H···π stacking interactions between monomeric units can also be utilized for intending novel single-chain magnets [108].

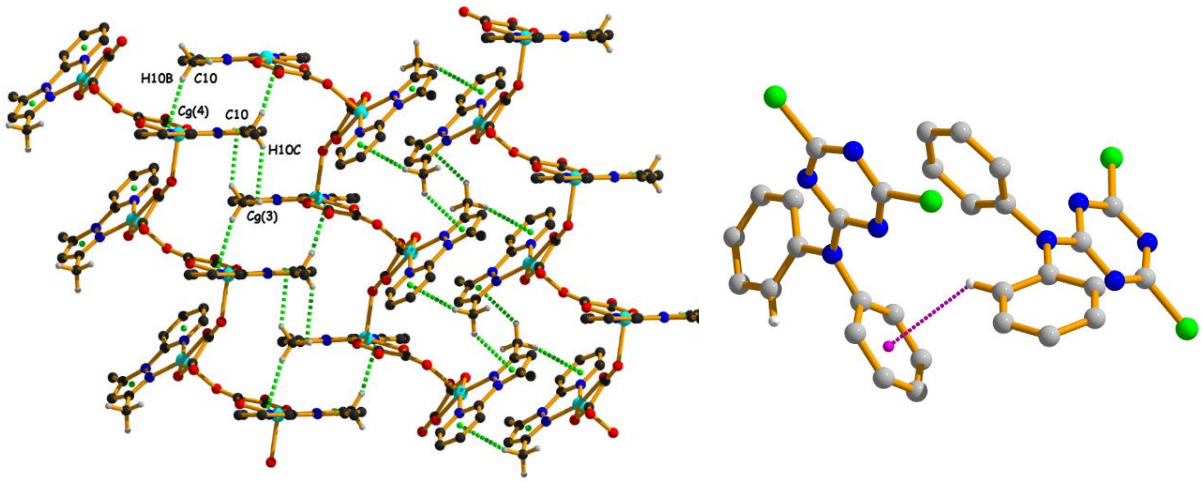

Figure 1.20: Representation of the C-H···π interactions in molecular crystals [103]

1.4.4. Cation···π interaction

The cation···π interaction is an attractive noncovalent force based on interaction between an electron-rich π-system (e.g., benzene, ethylene, acetylene) and a cation (e.g., Na^+,

NBu_4^+; Fig. 1.21) [109, 110]. Usually, staking interactions are weaker than hydrogen bonding interactions however cation···π interactions tend to be stronger [111]. Such interactions are pervasive and are of principal importance in several fields of contemporary interest, such as chemistry, biology, material science, and allied areas [112-114]. Cation···πinteractions were observed almost four-decade ago but their consequences and relative importance has been firmly elucidated in recent year. Also, this cation···π interaction, being sufficiently strong, are likely to have a profound impact in controlling the neighbouring structural environment. Though this interaction is generally sufficiently strong, under certain circumstances cation···π interactions may also be moderately weak depending on the nature of cation, whether it is co-ordinately saturated or not and also on the nature of the π-system and hence the range that is spanned by them is quite vast [109]. Therefore, the modern scientific interest focusing on understanding of the nature, range and significance of cation···π interaction which is of great importance in designing molecules and materials [115].

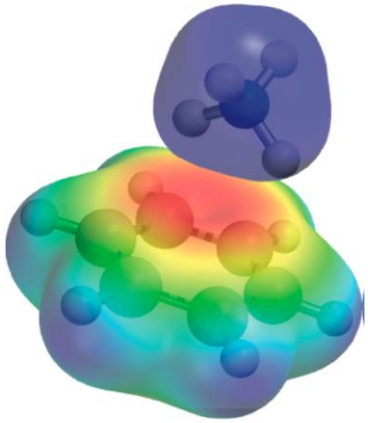

Fig. 1.21: Cation···π interaction [110]

An interaction between neutral molecule and ion tends to be favourable electrostatically and the interaction energy becomes greater than that between two neutral molecules, especially when the neutral molecule is easily polarizable [116, 117]. A noncovalent cation···π interaction is resulted when a closed shell cation come close enough and interacts with a neutral π-system [115]. Since its discovery in the 1980s [118], a detail experimental, synthetic and computational investigation have been carried out to quantify and further understanding of the basis for and the extent of this interaction in both gas and condensed phases [119, 120]. The thermodynamic factors responsible for this attractive

interaction have also been studied in solution [121-127]. Generally, in solution phase the strength of cation···π interactions are weakened compare to that in the gas phase though their strength is almost comparable to other critically important, strong non-covalent interactions, including ion pairs and hydrogen bonds [128]. The major reason accountable for this substantial binding energy is predominantly due to the electrostatic attraction of a cation to an electron-rich π-aromatic system [129], while charge-transfer and dispersion forces have also play significant contributing roles [130-134]. Moreover, the cation···πinteraction shows a high degree of directionality, where the cation has a prominent energetic tendency for placing themselves directly over the centroid of the π-system. This results in maximization of charge and orbital interactions [135, 136]. A detail study regarding the geometrical orientation of the cation with respect to the π-system was also done to observe the variation of cation···π interaction energy. The strength of cation···π interaction is described by considering the factors: *R*, θ and ϕ (Fig. 1.22). It was well concluded that this interaction is best when the cation is placed just over the centroid of the arene system and the cation···π interaction energy decreases on shifting the cation from centroid [137]. Moreover, solvation and more generally environment effects may have a vital influence on the stability of cation···π complexes given the charged nature of the cation [138].

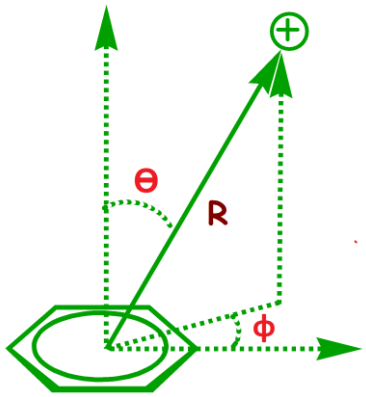

Fig. 1.22: Geometries for cation···π systems

Cation···π interaction was first experimentally proved by Kebarle and co-workers. They calculated the interaction enthalpy between benzene and K^+ ion, and it was found to be significant and comparable to the interaction of K^+ with either methanol or water. Latter Castleman *et al.* studied similar interactions with Na^+ using mass spectroscopy [139]. It was found that the enthalpies of interaction between Na^+ and benzene is greater than that for K^+

and benzene as Na^+ has more charge density than K^+. Additional computational and mass spectrometric evidences were reported by Lisy *et al.* on the basis of their investigation on alkali metal-arene cation···π interactions [140, 141].

Host guest complexes, bearing artificial/ synthetic receptors and guest molecules mediated by cation···π interactions, are exceptionally useful in studying molecular recognition [142-145]. Dougherty *et al.* reported in their pioneer investigation regarding the design, synthesis and characterization of a large number of derivatives of cyclophane hosts which impart insights into host-guest binding both in aqueous and in organic solvents [121, 146-148]. Several cage-like structures have been probed and display great ability to hold cations in their cavities or clefts [149-151]. Tran *et al.* reported the synthesis of zorbarene, which has a calixarene-like structure, and illustrate how the tetramethylammonium cation has moderately strong association constants suggesting stronger cation···π mediated interactions with these hosts [149]. Rathore and co-workers report the design and synthesis of a hexa aryl benzene-based receptor that contains a bipolar receptor site, that allows efficient binding of a single potassium cation by way of a synergistic interaction with a polar ethereal fence and with the central benzene ring through a cation···π interaction [152, 153]. The fundamental studies on the thermodynamics of the cation···π interaction and its expanding importance in biological systems assisted the scientist to frame the prospective for its application as a design element in synthetic chemistry [154]. Again, complementary nature and directionality of cation···π interaction can drive the association of small molecule into controlled assemblies. As a fact, this interaction is extremely important for molecular recognition [155, 156], crystal engineering [157], and materials design [158]. The cation···π interaction has, of course, also found imperative applications in the area of supramolecular chemistry. Supramolecular aggregates like catenanes [159], molecular tweezers, rotaxanes [160], dendrimers [161] have been associated through the involvement of cation···π interactions [162-165].

1.4.5. Anion···π interaction

Anion···π interactions, i.e., the attraction between anions and electron deficient π system, have witnessed a significant recognition and their pivotal role in many chemical and biological processes is being appreciated increasingly. Such interactions largely depend not only on the nature and shape of the anions but also the position of the π lobes offered by heterocyclic aromatic moieties. The design and quantification of highly selective anion···π

interactions arrests recent interests in the nascent field of supramolecular chemistry [166-168]. In 2002, almost simultaneous pioneering theoretical studies by Alkorta et. al, [169] Deya et. al, [170] and Mascal et. al, [171] confirmed the presence of favorable non-covalent interactions between electron deficient aromatic rings and anion. Its binding energy are almost comparable to hydrogen bonds (20-50 $kJmol^{-1}$).

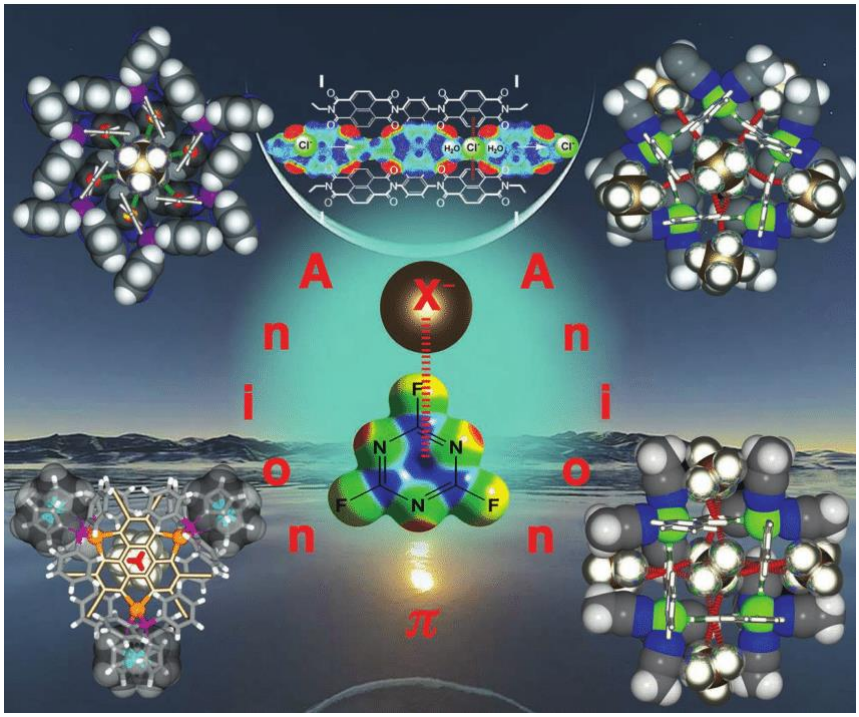

Fig. 1.23: Anion···π interaction [168]

The term anion···π was first coined by Deya et. al to describe such interactions [170]. Mascal et. al, [171] first pointed out about the effect of substitution by electron withdrawing groups in the aromatic ring. They provide a theoretical justification that the central triazine ring of trifluoro 1,3,5-triazine has a greater positive potential than 1,3,5-triazine due to the presence of electron withdrawing fluoride groups [168] and hence are more susceptible to ensure anion···π interactions (Fig. 1.23).

The first X-ray crystal structures with recognized and unambiguous anion···π interactions were independently reported by Meyer et. al, [172] and Reedijik et. al, [173] in 2004 using electron deficient ligand hexakis-(pyridine-2-yl)-[1,3,5]-triazine-2,4,6-triamine. In their report the anion···π distance is 3.11Å and the angle of contact is 88° both of which

are close to theoretically as predicted by Deya [170]and Mascal [171]. Both crystallographic database and theoretical elucidation proved that the strength of this anion···π interaction is dependent on anion···π non-covalent interaction distance and as well as on the angle (θ) that is defined as the angle of the $[X]^-$···aryl centroid axis and the line connecting the ring centroid with a ring atom.

Meyer's work [172] inspired chemists to use a substituted triazine ring for inducing an anion···π interaction employing several anions like fluoride, chloride, bromide, nitrate, perchlorate etc.

Giese et. al, [174, 175] performed a series of studies in order to investigate the role of anions in anion···π interactions and are able to prove the centroid to anion distances increases in the order chloride < bromide < iodide.

From crystallographic database it was evident that the interplay between anion···π and π···π or anion···π and hydrogen bonding interactions play a significant role in a synergistic manner to stabilize the crystal structure in solid state. But the challenging task is to ensure both anion···π and π···π interactions simultaneously because for the former electron deficient π system and for the later electron rich π systems are required. When the heterocycle ring is coordinated to the metal centre, the ring became electron deficient, but not to such extent so that it can be utilized to ensure a strong anion···π interaction but this interaction became a significant one if the aromatic ring moiety is protonated [176].

1.5. DENSITY FUNCTIONAL THEORY (DFT)

Density Functional Theory (DFT) is a computational tool generally used in physics, materials science and chemistry to elucidate the electronic structure of many body systems, in particular atoms, molecules and clusters. DFT has found importance in solid state physics since 1970's. However, it was not considered as a significant tool till 1990's as DFT was not considered accurate enough for calculations in quantum chemistry. After 1990's, when the approximations used in the theory were greatly refined to better model for the exchange and correlation interaction.

Electronic structure calculation has a crucial importance in the multi-scale modelling scheme of materials: not only do they enable one to accurately determine physical and chemical properties of materials, they also provide data for the adjustment of parameters (or potentials) in higher scale methods such as classical molecular dynamics, cluster dynamics, kinetic Monte Carlo etc. Most of the properties of a solid depend on the behavior of its electrons, and in order to model or predict them it is necessary to have an accurate method to compute the electronic structure. DFT is basically based on quantum theory and does not make use of any adjustable or empirical parameter: the only input data are the atomic number of the constituent atoms and some initial basic structural information. The complicated many-body problem of interacting electrons is replaced by an equivalent single electron problem, in which each electron is moving in an effective potential. This theory has been applied successfully to the determination of structural and dynamical properties (lattice structure, charge density, magnetization etc.) of a wide variety of solids [177-182]. The efficiency and enormous prospect of this computational method was acknowledged by Nobel committee in 1998 and the prize was divided equally to Walter Kohn [for his development of the density functional theory] and John A. Pople [for his development of computational methods in quantum chemistry] for their significant contributions in chemistry.

In this Density Functional Theory, several models have been chosen (almost comparable to the molecular structure found in single crystal X-ray crystallography) to fit them using different softwires and the energy values are calculated. For better understanding and visualization of inherent electronic structure of solids, Molecular Electrostatic Potential (MEP), Atoms in Molecule (AIM), Non-covalent Interaction plots (NCI Plot) with specific isosurfaces have been used.

1.5.1. Molecular Electrostatic Potential (MEP)

Electrostatic potential correlates with dipole moment, electronegativity, and partial charges. It provides an easy visual method to understand the relative polarity of a molecule [183-186]. The molecular electrostatic potential (MEP) is the potential energy of a proton at a particular location near a molecule. Negative electrostatic potential corresponds to an attraction of the proton by the concentrated electron density in the molecules (from lone pairs, pi-bonds, etc.) (**coloured in shades of red**). Positive electrostatic potential corresponds to repulsion of the proton by the atomic nuclei in regions where low electron density exists and the nuclear charge is incompletely shielded (**coloured in shades of blue**) (Fig. 1.24).

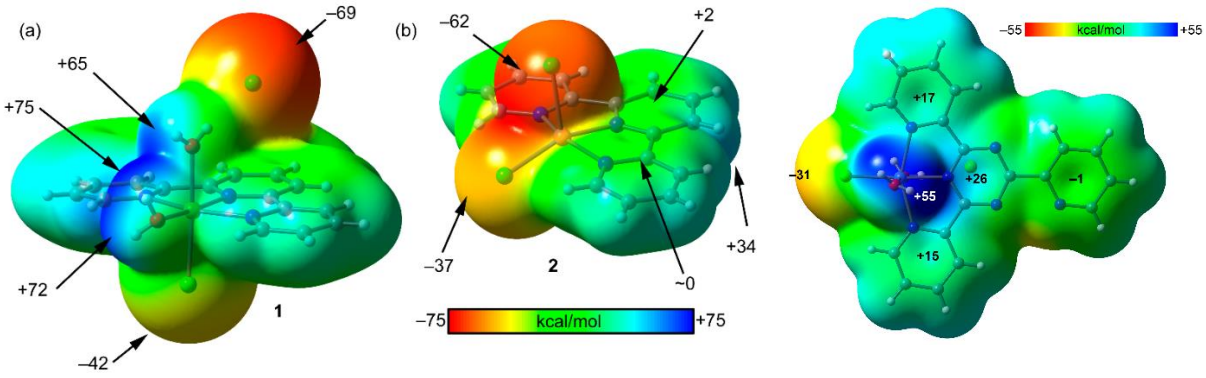

Fig. 1.24: Some representative figures of Molecular Electrostatic Potentials (MEP)

The calculated partial charges represented as spheres (**yellow is negative, red is positive**) show how the molecule would interact with approaching protons or positive charges. When a unit of positive charge (proton) approaches a positive region of the molecule, the repulsive interaction results in an increasing positive potential energy (**coloured in shades of blue**). As a proton approaches a negative region an attractive interaction results in negative potential energy (**coloured in shades of red**). The electron density isosurface is a surface on which the molecule's electron density has a particular value and that encloses a specified fraction of the molecule's electron probability density. The electrostatic potential at different points on the electron density isosurface is shown by colouring the isosurface with contours. The more red/ blue differences, the more polar the molecule. If the surface is largely white or lighter colour shades, the molecule is mostly non-polar.

1.5.2. Atoms in molecule

It is now possible to define the structure of molecules quantum mechanically [187] with the help of Bader's Quantum Theory of Atoms in Molecules (QTAIM) [188]. This theory has been widely applied to unravel atom-atom interactions in covalent and non-covalent interactions in molecules [189], molecular clusters [190], small molecular crystals [191], proteins [192], DNA base pairing and stacking [193]. Bader's group has made several seminal contributions to the development of the QTAIM theory and its applications to unravel chemical bonding [194, 195]. Popelier and co-workers have employed the QTAIM to address several issues in chemistry (Fig. 1.25) [196, 197]. Particularly, they have

demonstrated the possibility of developing structure-activity-relationship to predict various physico-chemical properties [197]. Several groups have applied the QTAIM for unravelling the non-covalent interactions such as weak van der Waals, π···π, X-H···π, conventional hydrogen bonding, cation···π interactions, halogen bonds, etc. and also other applications in chemistry. All these interactions have been vividly characterized with the help of theory of QTAIM [198-201].

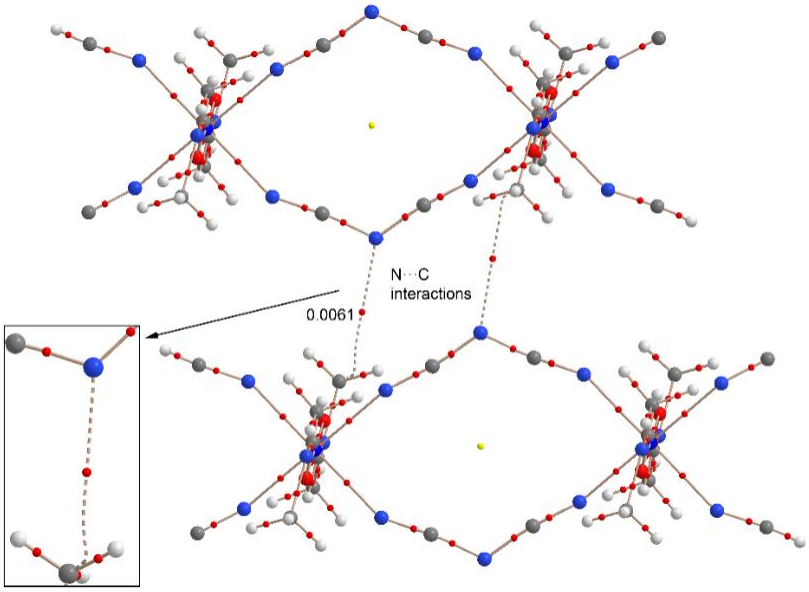

Fig.1.25: Perspective view of Atoms in Molecule

1.5.3. Non-covalent Interaction plot (NCI Plot)

Non-covalent interactions hold the key for understanding many chemicals, biological and technological problems. Describing these non-covalent interactions accurately, including their positions in real space, constitutes a first step in the process of decoupling the complex balance of forces that define non-covalent interactions. Because of the size of the macromolecules, the most common approach has been to assign van der Waals interactions (vdW), steric clashes and hydrogen bonds based on pair wise distances between atoms according to their vdW radii. Recently an alternative perspective, derived from the electron density, the non-covalent interactions (NCI) index that has the dual advantages of being generally transferable to diverse chemical applications and being very fast to compute as it can be calculated from promolecular densities. Thus, NCI analysis is applicable to large

systems, including proteins and DNA, where analysis of non-covalent interactions is of great potential value. Hence, NCI computation algorithm has been used to analyze and visualize the weak interactions using both self-consistent fully quantum mechanical as well as promolecular densities [202-204].

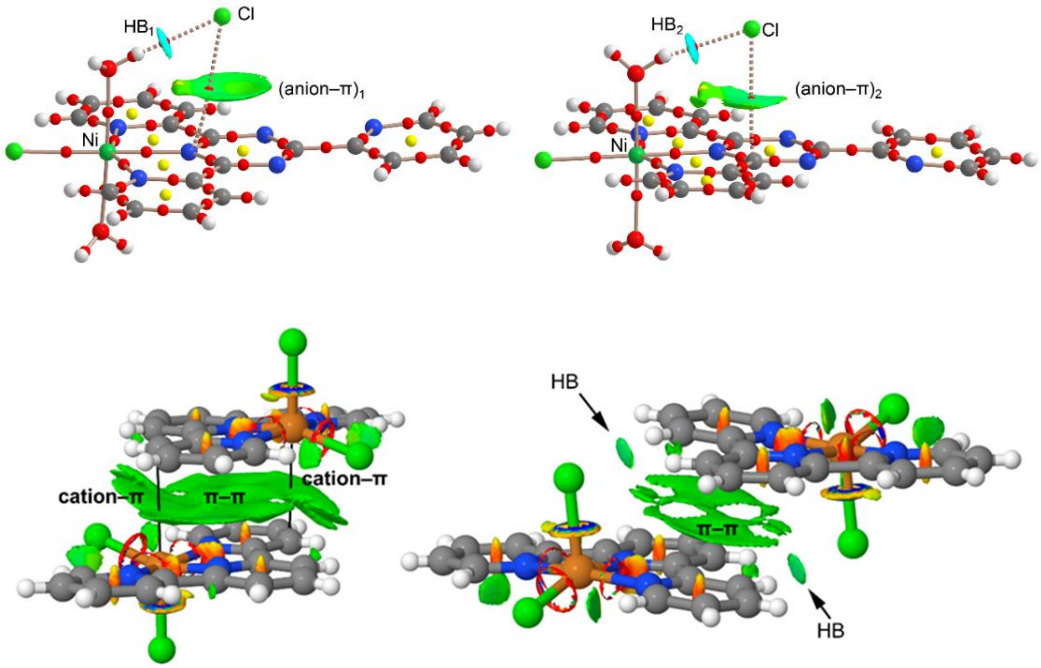

Fig. 1.26: Representative figure for NCI isosurfaces to visualize the non-covalent interactions

A RGB (red-green-blue) colouring scheme is chosen to rank interactions, where red is used for destabilizing interactions, blue for stabilizing interactions and green for delocalized weak interactions. The intensity of these colours (i.e., the deepness of the colour) is associated with a higher local density and therefore to a stronger interaction (Fig. 1.26).

REFERENCES

1. J. F. Hartwig, *Organo-transition Metal Chemistry: From Bonding to Catalysis*, University Science Books, 2010.
2. Z. Liu, P. J. Sadler, *Acc. Chem. Res.*, 2014, **47**,1174-1185.
3. O. R. Luca, R. H. Crabtree, *Chem. Soc. Rev*., 2013, **42**, 1440-1459.
4. E. Peris, R. H. Crabtree, *Coord. Chem. Rev*., 2004, **248**, 2239-2246.
5. G. C. Vougioukalakis, R. H. Grubbs, *Chem. Rev.*, 2010, **110**, 1746-1787.
6. Y. Chi, P. T. Chou, *Chem. Soc. Rev.*, 2010, **39**, 638-655.
7. A. Deiters, S. F. Martin, *Chem. Rev.*, 2004, **104**, 2199-2238.
8. F. Fache, E. Schulz, M. L. Tommasino, M. Lemaire, *Chem. Rev.*, 2000, **100**, 2159-2231.
9. S. Trofimenko, *Chem. Rev.*, 1993, **93**, 943-980.
10. R. Mukherjee, *Coord. Chem. Rev., 2000,* **203**, 151-218.
11. M. A. Halcrow, *Coord. Chem. Rev.*, 2005, **249**, 2880-2908.
12. S. Demeshko, G. Leibeling, S. Dechert, F. Meyer, *Dalton Trans.*, 2006, 3458-3465.
13. S. Demeshko, G. Leibeling, S. Dechert, S. Fuchs, T. Pruschke, F. Meyer, *Chem. Phys. Chem.*, 2007, **8**, 405-417.
14. A. Prokofieva, A. I. Prikhod'ko, E. A. Enyedy, E. Farkas, W. Maringgele, S. Demeshko, S. Dechert, F. Meyer, *Inorg. Chem.*, 2007, **46**, 4298-4307.
15. M. Stollenz, C. Gross, F. Meyer, *Chem. Commun.*, 2008, 1744-1746.
16. M. Stollenz, M. John, H. Gehring, S. Dechert, C. Grosse, F. Meyer, *Inorg. Chem.*, 2009, **48**, 10049-10059.
17. K. Yoneda, K. Adachi, K. Nishio, M. Yamasaki, A. Fuyuhiro, M. Katada, S. Kaizaki, S. Kawata, *Angew. Chem. Int. Ed.*, 2006, **45**, 5459-5461.
18. J. Z. Hou, M. Li, Z. Li, S. Z. Zhan, X. C. Huang, D. Li, *Angew. Chem. Int. Ed.*, 2008, **47**, 1711.
19. T. L. Hu, J. R. Li, C. S. Liu, X. S. Shi, J. N. Zhou, X. H. Bu, J. Ribas, *Inorg. Chem.*, 2006, **45**, 162-173.
20. A. L. Gavrilova, B. Bosnich, *Chem. Rev.*, 2004, **104**, 349-383.
21. J. I. van der Vlugt, S. Demeshko, S. Dechert, F. Meyer, *Inorg. Chem.*, 2008, **47**, 1576-1585.
22. C. Kaes, A. Katz, M.W. Hosseini, *Chem. Rev.*, 2000, **100**, 3553-3590.
23. J. A. G. Williams, *Chem Soc. Rev.*, 2009, **38**, 1783-1801.

24. H. Hofmeier, U.S. Schubert, *Chem. Soc. Rev.*, 2004, **33**, 373-399.
25. A. F. Henwood, I. N. Hegarty, E. P. McCarney, J. I. Lovitt, S. Donohoe, T. Gunnlaugsson, *Coord. Chem. Rev.*, 2021, **449**, 214206.
26. E.C. Constable, *Chem. Soc. Rev.*, 2007, **36**, 246-253.
27. L. An, C. Xu, X.G. Zhang, *Nature Comm.*, 2017, **8**.
28. L. Hie, E.L. Baker, S.M. Anthony, J.N. Desrosiers, C. Senanayake, N.K. Garg, *Angew. Chem. Int. Ed.*, 2016, **55**, 15129-15132.
29. K. M. M. Huihui, R. Shrestha, D. J. Weixs, *Org. Lett.*, 2017, **19**, 340-343.
30. S. Y. Ni, W. Z. Zhang, H. B. Mei, J. L. Han, Y. Pan, *Org. Lett.*, 2017, **19**, 2536-2539.
31. K. C. Shekhar, P. Basnet, S. Thapa, B. Shrestha, R. Giri, *J. Org. Chem.*, 2018, **83**, 2920-2936.
32. K. Kamata, A. Suzuki, Y. Nakai, H. Nakazawa, *Organometallics*, 2012, **31**, 3825-3828.
33. A. M. Tondreau, C. C. H. Atienza, J. M. Darmon, C. Milsmann, H. M. Hoyt, K. J. Weller, S. A. Nye, K. M. Lewis, J. Boyer, J. G. P. Delis, E. Lobkovsky, P. J. Chirik, *Organometallics*, 2012, **31**, 4886-4893.
34. H. A. Duong, W. Q. Wu, Y. Y. Teo, *Organometallics*, 2017, **36**, 4363-4366.
35. N. G. Leonard, M. J. Bezdek, P. J. Chirik, *Organometallics*, 2017, **36**, 142-150.
36. W. N. Palmer, T. N. Diao, I. Pappas, P. J. Chirik, *ACS Catal.*, 2015, **5**, 622-626.
37. J. Wu, H. S. Zeng, J. Cheng, S. P. Zheng, J. A. Golen, D. R. Manke, G. Q. Zhang, *J. Org. Chem.*, 2018, **83**, 9442-9448.
38. G. Q. Zhang, H. S. Zeng, J. Wu, Z. W. Yin, S. P. Zheng, J. C. Fettinger, *Angew. Chem. Int. Ed.*, 2016, **55**, 14369-14372.
39. M. G. Alexandru, D. Visinescu, B. B. Cula, F. Lloret, M. Julve, *Eur. J. Inorg. Chem.*, 2018, **3-4**, 349-359.
40. H. Hadadzadeh, M. Maghami, J. Simpson, A. D. Khalaji, K. Abdi, *J. Chem. Crystallogr*. 2012, **42**, 656-667.
41. J.-M. Lehn, Supramolecular Chemistry: Concepts and Perspectives, VCH, Weinheim, 1995.
42. J.-M. Lehn, *Pure Appl. Chem*., 1978, **50**, 871–892.
43. E. R. T. Tiekink, J. J. Vittal and M. Zaworotko, *Organic Crystal Engineering: Frontiers in Crystal Engineering*, ed. Wiley VCH, 2010.
44. E. R. T. Tiekink and J. Zukerman-Schpector, *The Importance of π-Interactions in Crystal Engineering: Frontiers in Crystal Engineering*, (Ed). 2nd Edn, Wiley, 2012.

45. G. R Desiraju, J. J Vittal and A. Ramanan, *Crystal Engineering, A Text book*, World Scientific, 2011.
46. G. R. Desiraju, *J. Am. Chem. Soc*., 2013, **135**, 9952.
47. G. M. J. Schmidt, *Pure Appl. Chem*., 1971, **27**, 647-678.
48. A. Mukherjee, *Cryst. Growth Des*., 2015, **15**, 3076-3085.
49. O. V. Shishkin, R. I. Zubatyuk, S. V. Shishkina, V. V. Dyakonenko and V. V. Medviediev, *Phys. Chem. Chem. Phys*., 2014, **16**, 6773–6786.
50. K. Ariga, T. Kunitake, *Supramolecular Chemistry−Fundamentals and Applications*, Springer, Germany, 2006.
51. Y. Zhang, M. Z. Yang, F. Yuan, H. W. Gu, P. Gao, B. Xu, *J. Am. Chem. Soc*., 2004, **126**, 15028-15029.
52. M. J. Hannon, *Chem. Soc. Rev*., 2007, **36**, 280-295.
53. B. Cornils, W. A. Hermann, R. Scholgl, C.-H. Wong, Catalysis from A to Z: A Concise Encylopedia, John Wiley & Sons, New York, 2000.
54. C. Valdes, L. M. Toledo, U. Spitz, J. Rebek Jr, *Chem. Eur. J*., 1996, **2**, 989-991.
55. W. A. Freeman, *Acta Cryst*. 1984, **B. 40**, 382-387.
56. L. M. A. Perdigão, N. R. Champness, P. H. Beton, *Chem. Commun*., 2006, 538-540.
57. A. Mulder, J. Huskens, D. N. Reinhoudt, *Org. Biomol. Chem*., 2004, **2**, 3409-3424.
58. C. J. Kepert, *Chem. Commun*., 2006, 695-700.
59. S. Parveen, R. J. Davey, G. Dent, R. G. Pritchard, *Chem. Commun*., 2005, 1531-1533.
60. J. W. Steed, D. R. Turner, K. J. Wallace, *Core concepts in supramolecular chemistry and nano-chemistry*, John Wiley & sons. Ltd., 2007.
61. H. Schneider, *Angew. Chem., Int. Ed*., 2009, **48**, 3924-3977.
62. A. M. Maharramov, K. T. Mahmudov, M. N. Kopylovich and A. J. L. Pombeiro, (Edn) *Non-covalent interaction in the synthesis and design of new compounds*, John Wiley & Sons. Inc., Hoboken, NJ, 2016.
63. G. R. Desiraju and T. Steiner, *The weak hydrogen bond in structural chemistry and biology*, Oxford University Press Inc, New York, 1999.
64. L. M. Eytel, H. A. Fargher, M. M. Haley and D. W. Johnson, *Chem. Comm*., 2019, **55**, 5195-5206.
65. Y. Liu, W. Zhao, C. H. Chen and A. H. Flood, *Science*, 2019, **365**, 159-161.
66. V. Balamurugen, M. S. Hundal and R. Mukherjee, *Chem. Eur. J*., 2004, **10**, 1683-1690.
67. J. M. Larson, T. B. McMahon, *Inorg. Chem*., 1984, **23**, 2029-2033.

68. A. George Jeffrey, *An introduction to Hydrogen bonding*, Oxford University Press, New York, 1997.
69. R. C. Johnston, P. H. Y. Cheong, *Org. Biomol. Chem*., 2013, **11**, 5057-5064.
70. I. Rozas, I. Alkorta, J. Elguero, *J. Phys. Chem. A*, 1998, **102**, 9925-9932.
71. R. Preibner, U. Egner, W. Saenger, *FEBS Lett*., 1991, **288**, 192-196.
72. K. S. Kim, P. Tarakeshwar, J.Y. Lee, *Chem. Rev*., 2000, **100**, 4145-4186.
73. C. G. Claessens, J. F. Stoddart, *J. Phys. Org. Chem*., 1997, **10**, 254-272.
74. M. Cao, A. Fu, Z. Wang, J. Liu, N. Kong, X. Zong, H. Liu, J. J. Gooding, *J. Phys. Chem. C*, 2014, **118**, 2650-2659.
75. M. O. Sinnokrot, C. D. Sherrill, *J. Phys. Chem. A*, 2006, **110**, 10656-10668.
76. J. Pawliszyn, M. M. Szczesniak, S. Scheiner, *J. Phys. Chem*., 1984, **88**, 1726-1730.
77. C. A. Hunter, *Chem. Soc. Rev*., 1994, **23**, 101-109.
78. C. Janiak, *J. Chem. Soc. Dalton Trans*., 2000, 3885-3896.
79. T. Janowski, P. Pulay, *Chem. Phys. Lett*., 2007, **447**, 27-32.
80. T. Janowski, P. Pulay, *Theor. Chem. Acc*., 2011, **130**, 419-427.
81. M. Kertesz, *Chem. Eur. J*., 2019, **25**, 400-416.
82. C. A. Hunter, *Angew. Chem., Int. Ed*., 1993, **32**, 1584-1586.
83. C. A. Hunter, J. K. M. Sanders, *J. Am. Chem. Soc*., 1990, **112**, 5525-5534.
84. D. B. Amabilino, J. F. Stoddart, *Chem. Rev*., 1995, **95**, 2725-2828.
85. R. Foster, *J. Phys. Chem*., 1980, **84**, 2135-2141.
86. P. Hobza, H. L. Selzle, E. W. Schlag, *J. Phys. Chem*., 1993, **97**, 3937-3938.
87. F. Cozzi, M. Cinquini, R. Annuziata, J. S. Siegel, *J. Am. Chem. Soc*., 1993, **115**, 5330-5331.
88. J. P. Glusker, *Directional Aspects of Intermolecular Interactions: In Design of Organic Solids*. Springer, Berlin, Heidelberg, 1998.
89. S. K. Burley, G. A. Petsko, *Adv. Protein Chem*., 1988, **39**, 125-189.
90. G. B. McGaughey, M. Gagné, A. K. Rappé, *J. Biol. Chem*., 1998, **273**, 15458-15463.
91. M. Akazome, Y. Ueno, H. Ooiso, K. Ogura, *J. Org. Chem*., 2000, **65**, 68-76.
92. Y. Umezawa, M. Nishio, *Bioorg. Med. Chem*., 2000, **8**, 2643-2650.
93. A. Arduini, G. Giorgi, A. Pochini, A. Secchi, F. Ugozzoli, *Tetrahedron* 2001, **57**, 2411-2417.
94. M. Muraki, K. Harata, N. Sugita, K. I. Sato, *Biochemistry*, 2000, **39**, 292-299.
95. M. Nishio, M.Hirota, Y. Umezawa, *The C–H···π interaction: evidence, nature and consequences*; John Wiley & Sons, 1998.

96. H. Suezawa, T. Yoshida, Y. Umezawa, S. Tsuboyama, M. Nishio, *Eur. J. Inorg. Chem*., 2002, 3148-3155.
97. D. Sadhukhan, M. Maiti, G. Pilet, A. Bauzá, A.Frontera, S. Mitra, *Eur. J. Inorg. Chem*., 2015, 1958-1972.
98. M. Tamres, *J. Am. Chem. Soc*., 1952, **74**, 3375-3378.
99. T. Aoyama, O. Matsuoka, N. Nakagawa, *Chem. Phys. Lett*., 1979, **67**, 508-510.
100. T. Takagi, A. Tanaka, S. Matsuo, H. Maezaki, M. Tani, H. Fujiwara, Y. Sasaki, *J. Chem. Soc., Perkin Trans*., 1987, **2**, 1015-1018.
101. G. D. Andreetti, A. Pochini, R. Ungaro, *J. Chem. Soc., Perkin Trans*., 1983, **2**, 1773-1779.
102. R. Ungaro, A. Pochini, G. D. Andreetti, V. Sangermano, *J. Chem. Soc. Perkin Trans*., 1984, **2**, 1979-1985.
103. Z. Lu, P. Gamez, I. Mutikainen, U. Turpeinen, J. Reedijk, *Cryst. Growth Des*., 2007, **7**, 1669-1671.
104. S. K. Singh, A. Das, *Phys. Chem. Chem. Phys*., 2015, **17**, 9596-9612.
105. O. Takahashi, Y. Kohno, K. Saito, *Chem. Phys. Lett*., 2003, **378**, 509-515.
106. M. Hirota, K. Sakakibara, H. Suezawa, T. Yuzuri, E. Ankai, M. Nishio, *J. Phys. Org. Chem*., 2000, **13**, 620-623.
107. N. Nakagawa, K. Nikki, Y. Takeuchi, I. Kumagai, *Chem. Lett*., 1972, **1**, 1239-1242.
108. M. K. Singh, G. Rajaraman, *Chem.: Eur. J*., 2015, **21**, 980-983.
109. J. C. Ma, D. A. Dougherty, *Chem. Rev*., 1997, **97**, 1303-1324.
110. D. A. Dougherty, *Acc. Chem. Res*., 2013, **46**, 885-893.
111. M. O. Sinnokrot, E. F. Valeev, C. D. Sherrill, *J. Am. Chem. Soc*., 2002, **124**, 10887-10893.
112. D. A. Dougherty, *J. Nutr*., 2007, **137**, 1504S-1508S.
113. M. M. Torrice, K. S. Bower, H. A. Lester, D. A.; Dougherty, *Proc. Natl. Acad. Sci. U. S. A*., 2009, **106**, 11919-11924.
114. E. T. Kool, M. L. Waters, *Nat. Chem. Biol*., 2007, **3**, 70-73.
115. A. S. Mahadevi, G. N. Sastry, *Chem. Rev*., 2013, **113**, 2100-2138.
116. K. Morokuma, *Acc. Chem. Res*., 1977, **10**, 294-300.
117. R. D. Bowen, *Acc. Chem. Res*., 1991, **24**, 364-371.
118. M. Meot-Ner, C. A. Deakyne, *J. Am. Chem. Soc*., 1985, **107**, 474-479.

119. R. K. Raju, J. W. G. Bloom, Y. An, S. E. Wheeler, *Chem. Phys. Chem*., 2011, **12**, 3116-3130.
120. S. L. Cockroft, C. A. Hunter, *Chem. Soc. Rev*., 2007, **36**, 172-188.
121. T. J. Shepodd, M. A. Petti, D. A. Dougherty, *J. Am. Chem. Soc*., 1988, **110**, 1983-1985.
122. H. -J. Schneider, *Angew. Chem. Int. Ed. Engl*., 1991, **30**, 1417-1436;
123. J. Canceill, L. Lacombe, A. Collet, *J. Chem. Soc. Chem. Commun*., 1987, 219-221.
124. A. W. Schwabacher, S. Zhang, W. Davy, *J. Am. Chem. Soc*., 1993, **115**, 6995-6996.
125. J. M. Harrowfield, M. I. Ogden, W. R. Richmond, B. W. Skelton, A. H. White, *J. Chem. Soc. Perkin Trans*., 1993, **2**, 2183-2190.
126. B. Odell, M. V. Reddington, A. M. Z. Slawin, N. Spencer, J. F. Stoddart, D. J. Williams, *Angew. Chem. Int. Ed. Engl*., 1988, **27**, 1547-1550.
127. A. Cattani, A. Dalla-Cort, L. Mandolini, *J. Org. Chem*., 1995, **60**, 8313-8314.
128. J. P. Gallivan, D. A. Dougherty, *J. Am. Chem. Soc*., 2000, **122**, 870-874.
129. E. Jiménez-Moreno, A. M. Gómez, A. Bastida, F. Corzana, G. Jiménez-Oses, J. Jiménez-Barbero, J. L. Asensio, *Angew. Chem. Int. Ed*., 2015, **54**, 4344-4348.
130. A. McCurdy, L. Jimenez, D. A. Stauffer, D. A. Dougherty, *J. Am. Chem. Soc*., 1992, **114**, 10314-10321.
131. S. Tsuzuki, M. Mikami, S. Yamada, *J. Am. Chem. Soc*., 2007, **129**, 8656-8662.
132. D. Vijay, G. N. Sastry, *Phys. Chem. Chem. Phys*., 2008, **10**, 582-590.
133. J. Hwang, B. E. Dial, P. Li, M. E. Kozik, M. D. Smith, K. D. Shimizu, *Chem. Sci*., 2015, **6**, 4358-4364.
134. J. W. Caldwell, P. A. Kollman, *J. Am. Chem. Soc*., 1995, **117**, 4177-4178.
135. B. P. Hay, R. Custelcean, *Cryst. Growth Des*., 2009, **9**, 2539-2545.
136. C. Estarellas, A. Bauzá, A. Frontera, D. QuiÇonero, P. M. Deyà, *Phys. Chem. Chem. Phys*., 2011, **13**, 5696-5702.
137. M. S. Marshall, R. P. Steele, K. S. Thanthiriwatte, C. D. Sherrill, *J. Phys. Chem. A*, 2009, **113**, 13628-13632.
138. B. U. Emenike, S. N. Bey, R. A. Spinelle, J. T. Jones, B. Yoo, M. Zeller, *Phys. Chem. Chem. Phys*., 2016, **18**, 30940-30945.
139. B. C. Guo, J. W. Purnell, Jr. A. W. Castleman Jr. *Chem. Phys. Lett*., 1990, **168**, 155-160.
140. O. M. Cabarcos, C. J. Weinheimer, J. M. Lisy, *J. Chem. Phys*., 1999, **110**, 8429-8435.
141. O. M. Cabarcos, C. J. Weinheimer, J. M. Lisy, *J. Chem. Phys*., 1998, **108**, 5151-5154.

142. R. Faraoni, R. K. Castellano, V. Gramlich, F. Diederich, *Chem. Commun*., 2004, 370-371.
143. V. Dvornikovs, D. V. Smithrud, *J. Org. Chem*., 2002, **67**, 2160-2167.
144. M. O. Vysotsky, A. Pop, F. Broda, I. Thondorf, V. Böhmer, *Chem. Eur. J*., 2001, **7**, 4403-4410.
145. A. L. Whiting, F. Hof, *Org. Biomol. Chem*., 2012, **10**, 6885-6892.
146. P. C. Kearney, L. S. Mizoue, R. A. Kumpf, J. E. Forman, A. McCurdy, D. A. Dougherty, *J. Am. Chem. Soc*., 1993, **115**, 9907-9919.
147. J. E. Forman, Jr. R. E.; Barrans, D. A. Dougherty, *J. Am. Chem. Soc*., 1995, **117**, 9213-9228.
148. M. A. Petti, T. J. Shepodd, R. E. Barrans, D. A. Dougherty, *J. Am. Chem. Soc*., 1988, **110**, 6825-6840.
149. A. H. Tran, D. O. Miller, P. E. Georghiou, *J. Org. Chem*., 2005, **70**, 1115-1121.
150. J. Kim, Y. K. Kim, N. Park, J. H. Hahn, K. H. Ahn, *J. Org. Chem*., 2005, **70**, 7087-7092.
151. P. Cheng, P. Huang, W. Li, S. Ueng, W. Hung, Y. Liu, C. Lai, Y. Wang, S. Peng, I. Chao, S. Chiu, S. *J. Org. Chem*., 2006, **71**, 2373-2383.
152. R. Shukla, S. V. Lindeman, R. Rathore, *J. Am. Chem. Soc*., 2006, **128**, 5328-5329.
153. R. Shukla, S. V. Lindeman, R. Rathore, *Chem. Commun*., 2009, 5600-5602.
154. L. M. Salonen, M. Ellermann, F. Diederich, *Angew. Chem. Int. Ed*., 2011, 4808-4842.
155. J. M. Lehn, R. Meric, J. -P. Vigneron, M. Cesario, J. Guilhem, C. Pascard, Z. Asfari, J. Vicens, *J. Supramol. Chem*., 1995, **5**, 97-103.
156. R. A. Bissell, E. Cordova, A. E. Kaifer, J. F. Stoddart, *Nature* 1994, **369**, 133-137.
157. E. R. Tiekink, J. Zukerman-Schpector, *The importance of π -interactions in crystal engineering. Frontiers in Crystal Engineering*. Chichester: Wiley, 2012.
158. B. H. Hong, S. C. Bae, C. W. Lee, S. Jeong, K. S. Kim, *Science* 2001, **294**, 348-351.
159. J. Frey, T. Kraus, V. Heitz, J. -P. Sauvage, *Chem. Commun*., 2005, **53**, 5310-5312.
160. F. G. Gatti, D. A. Leigh, S. A. Nepogodiev, A. M. Z. Slawin, S. J. Teat, J. K. Y. Wong, *J. Am. Chem. Soc*., 2001, **123**, 5983-5989.
161. R. E. Bauer, V. Enkelmann, U. M. Wiesler, A. J. Berresheim, K. Müllen, *Chem. Eur. J*., 2002, **8**, 3858-3864.
162. H. Masu, M. Sakai, K. Kishikawa, M. Yamamoto, K. Yama-guchi, S. Kohmoto, *J. Org. Chem.*, 2005, **70**, 1423-1431.

163. X. Bao, I. Isaacsohn, A. F. Drew, D. B. Smithrud, *J. Org. Chem*., 2007, **72**, 3988-4000.
164. J. M. Heemstra, J. S. Moore, *Chem. Commun*., 2004, 1480-1481.
165. R. Ruloff, U. P. Seelbach, A. E. Merbach, F. G. Klarner, *J. Phys. Org. Chem*., 2002, **15**, 189-196.
166. Y. Li, Z. Yang, M. Zhou, Y. Li, J. He, X. Wang, Z. Lin, *RSC Adv*., 2017, **7**, 41527-41539.
167. I. A. Rather, S. A. Wagay, R. Ali, *Coord. Chem. Rev*., 2020, **415**, 213327.
168. B. L. Schottel, H. T. Chifotides, K. R. Dunber, *Chem. Soc. Rev*., 2008, **37**, 68-83.
169. I. Alkorta, I. Rozas, J. Elguero, *J. Am. Chem. Soc*., 2002, **124**, 8593-8598.
170. D. Quinonero, C. Garau, C. Rotger, A. Frontera, P. Ballester, A. Costa, P. M. Deya, *Angew. Chem. Int. Ed*., 2002, **41**, 3389-3392.
171. M. Mascal, A. Armstrong, M. D. Bartberger, *J. Am. Chem. Soc*., 2002, **124**, 6274-6276.
172. S. Demeshko, S. Dechert, F. Meyer, *J. Am. Chem. Soc*., 2004, **126**, 4508-4509.
173. P. de Hoog, P. Gamez, I. Mutikainen, U. Turpeinen, J. Reedijik, *Angew. Chem. Int. Ed*., 2004, **43**, 5815-5817.
174. M. Giese, M. Albrecht, G. Ivanova, A. Valkonen, K. Rissanen, *Supramol. Chem*., 2012, **24**, 48-55.
175. M. Giese, M. Albrecht, A. Valkonen, K. Rissanen, *Eur. J. Org. Chem*., 2013, **16**, 3247-3253.
176. C. Biswas, M. G. B. Drew, D. Escudero, A. Frontera, A. Ghosh, *Eur. J. Inorg. Chem*., 2009, 2238-2246.
177. W. Kohn, L. J. Sham, *Physical Review*,1965, **140**, A1133.
178. L. Petit, A. Svane, Z. Szotek, W. M. Temmerman, G. M. Stocks, *Physical Review B*, 2009, **80**, 045124.
179. B. Dorado, G. Jomrad, M. Freyss, M. Bertolus, *Physical Review B*, 2010, **82**, 035114.
180. L. Petit, A. Svane, Z. Szotek, W. M. Temmerman, G. M. Stocks, *Physical Review B*, 2010, **81**, 045108.
181. J. P. Crocombette, D. Torumba, A. Chartier, *Physical Review B*, 2011, **83**, 184107.
182. X. Ren, P. Rinke, C. Joas, M. Scheffler, *Journal of Materials Science*, 2012, **47**, 7447-7471.
183. E. E. Hodgkin, W. G. Richards, *Quantum Chemistry*, 1987, **32**, 105-110.
184. G. G. Hall, K. Tsujinaga, *Theoretica Chimica Acta*, 1986, **69**, 425-436.

185. D. L. Wang, H. T. Shen, H. M. Gu, Y. C. Zhai, *J. Mol. Struct: Theochem*, 2006, **776**, 47-51.
186. R. Rahmani, N. Boukabcha, A. Chouaih, F. Hamzaoui, S. G. Said, *J. Mol. Strucrt*, 2018, **1155**, 484-495.
187. J. H. Bohórquez, J. R. Boyd, F. C. Matta, *J. Phys. Chem. A*, 2011, **115**, 12991-12997.
188. R. F. W. Bader, *In Atoms in Molecules: A Quantum Theory* Oxford: Clarendon Press, 1990.
189. S. J. Grabowski, *Chem. Rev*., 2011, **111**, 2597-2625.
190. R. Parthasarthi, V. Subramanian, N. Sathyamurthy, *J. Phys. Chem. A*, 2005, **109**, 843-850.
191. M. S. Pavan, R. Pal, K. Nagarajan, T. N. G. Row, *Cryst. Growth Des*. 2014, **14**, 5477-5485.
192. Y. Hirano, K. Takeda, K. Miki, *Nature*, 2016, **534**, 281-284.
193. R. Parthasarthi, V. Subramanian, *Struct. Chem*., 2005, **16**, 243-255.
194. E. C. Brown, R. F. W. Bader, N. H. Werstiuk, *J. Phys. Chem. A*, 2009, **113**, 3254-3265.
195. R. F. W. Bader, P. J. MacDougall, *J. Am. Chem. Soc*., 1985, **107**, 6788-6795.
196. U. A. Chaudry, P. L. A. Popelier, *J. Org. Chem*., 2004, **69**, 233-241.
197. M. Z. Griffiths, P. L. A. Popelier, *J. Chem. Inf. Model*. 2013, **53**, 1714-1725.
198. F. C. Guzman, R. F. W. Bader, *Coord. Chem. Rev*., 2005, **249**, 633-662.
199. C. F. Nejad, S. Shahbazian, R. Marek, *Chem. Eur. J*, 2014, **20**, 10140-10152.
200. C. R. Wick, T. Clark, *Journal of Molecular Modelling*, 2018, **24**, 142.
201. L. Reuter, A. Luchow, *Phys. Chem. Chem. Phys*., 2020, **22**, 25892-25903.
202. J. C. Garcia, E. R. Johnson, S. Keinan, R. Chaudret, J. P. Piguemal, D. N. Beraton, W. Yang, *J. Chem. Theo. Comput*., 2011, **7**, 625-632.
203. J. C. Garcia, E. R. Johnson, W. Yang, *J. Phys. Chem. A*, 2011, **115**, 12983-12990.
204. E. R. Johnson, A. O. Roza, *J. Chem. Theo. Comput*., 2012, **8**, 5124-5131.

CHAPTER 2

Construction of a novel two dimensional Co(II) polymer from a one dimensional Co(II) polymer: Theoretical elucidation on the role of non-covalent carbon-bonding interaction

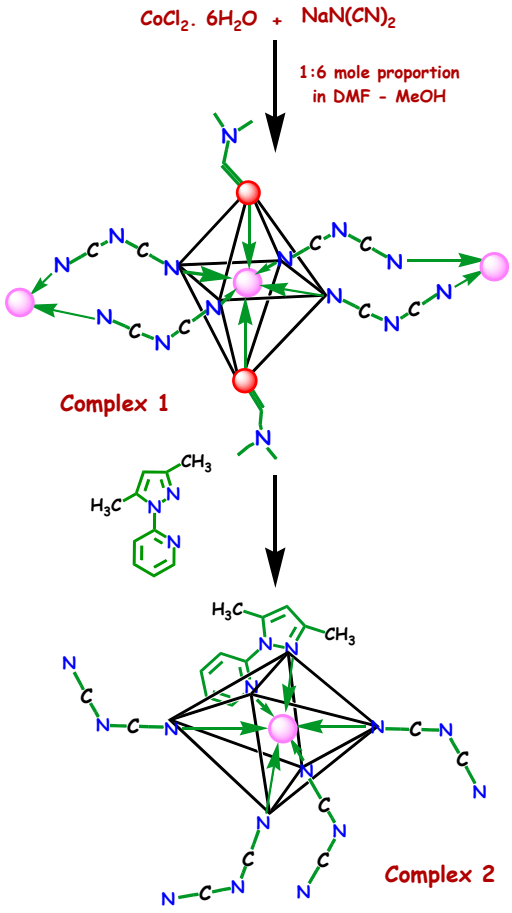

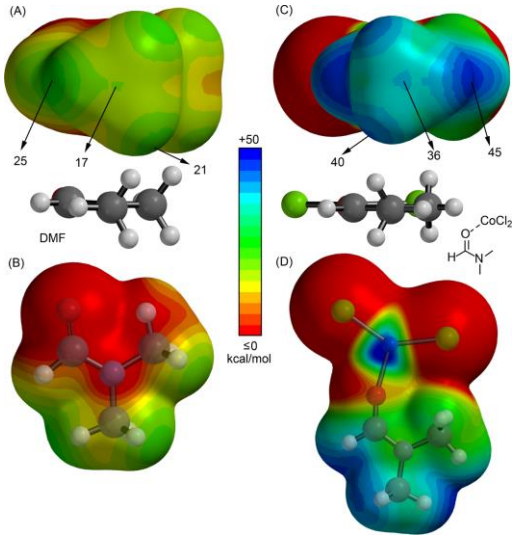

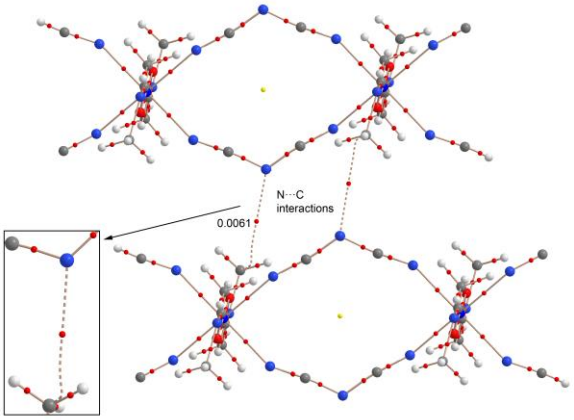

Published in Journal of Physical Chemistry B, 2016, 120, 6803-6811

Construction of a novel two dimensional Co(II) polymer from a one dimensional Co(II) polymer: Theoretical elucidation on the role of non-covalent carbon-bonding interaction

2.1. INTRODUCTION

In current years there have been an extensive growth in organic and inorganic materials chemistry propelled by the supramolecular interactions that play a pivotal role in the syntheses of crystalline substances. The metal−ligand compounds are designated as coordination polymers, especially categorized as metal−organic coordination networks (MOCN), and they extend "infinitely" into multi dimensionalities via metal−ligand bonding [1-3]. The primary objective of crystal engineering in coordination polymers is to achieve the desired structural topology which obviously needs careful choice of specific ligands and metal precursors [4-8]. Generally, the combination of transition metals and adequate "spacers" are responsible in generating the structure and topology of a coordination polymer that needs the proper selection of metal centers, ligands, experimental conditions, nature of spacers, and so forth [9, 10]. Either the main ligand or ancillary ligands must have at least one bridging site that produce extended dimension to facilitate the metal atoms to be bridged only by this ligand. The coordination polymers derived from the well-known bridging ligand dicyanamide (dca) with a captivating architectural framework have drawn much attention in coordination chemistry in the recent past due to their versatile coordinating ability [11-21] (Scheme 2.1).

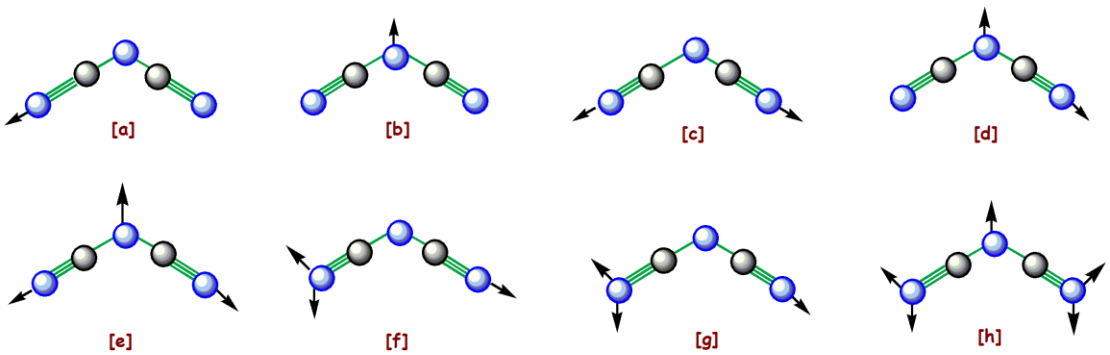

Scheme 2.1: Known coordination modes of dicyanamide **[a**: μ_1 , **b**: μ_3, **c**: $\mu_{1,5}$, **d**: $\mu_{1,3}$, **e**: $\mu_{1,3,5}$, **f**: $\mu_{1,1,5}$, **g**: $\mu_{1,1,3,5}$, **h**: $\mu_{1,1,3,5,5}$].

The coordination properties of the central metal ions (flexibility and signature) enable the generation of different architectures [22-25]. These architectures include one-dimensional (1D) linear chains [26], nanotube-like structures [27], two-dimensional (2D) (4,4) nets [28], and triangular [29] and herringbone-like lattices [30]. Hence, the overall framework of the coordination polymers created in the self-assembly process mostly depends upon the specialty of the bridging linker, and one such extraordinary bridging ligand is dca. In this work, a $\mu_{1,5}$ dicyanamido-bridged 1D linear Co(II) polymer (**1**) with two apically coordinated N,N′-dimethylformamide (DMF) molecules is synthesized. Moreover, polymer **1** is used to synthesize a new Co(II) coordination polymer (**2**) derived from $\mu_{1,5}$ dca with a strongly coordinated bidentate 3,5-dimethyl-1-(2′- pyridyl)pyrazole (pypz) as an ancillary ligand (Scheme 2.2).

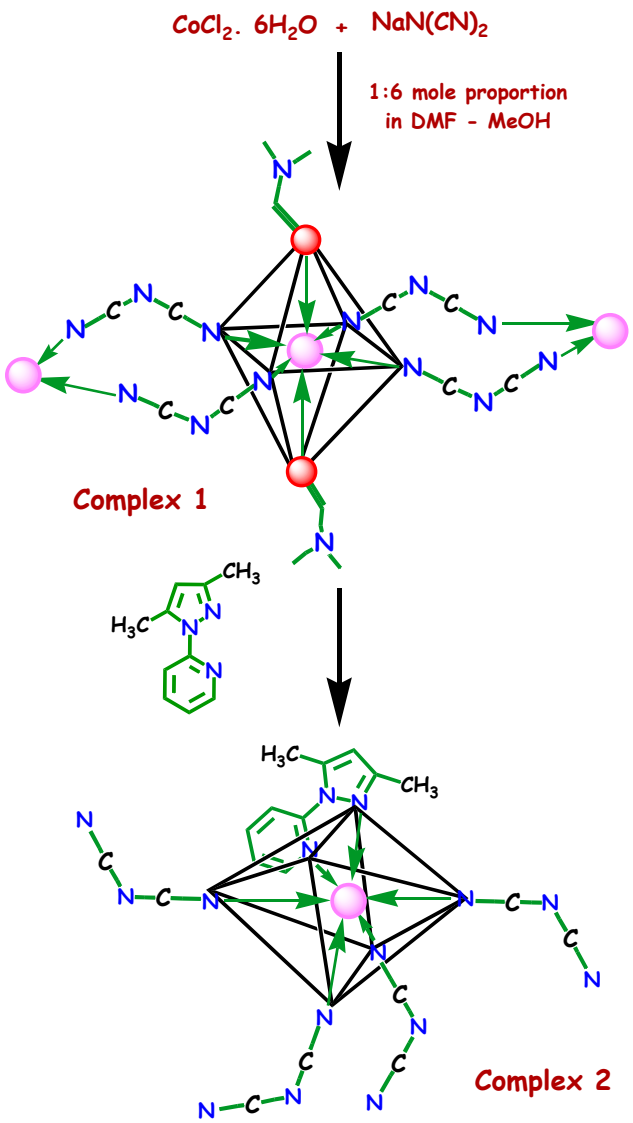

Scheme 2.2: Schematic representation of synthesis of complex **1** and **2**

During the entire process, complex **1** (an 1D coordination polymer) was metamorphosed to complex **2** with increased dimensionality (2D) and generating a macrocyclic chain that runs along the crystallographic 'c' axis with a 4-connected uninodal system representing a 'sql' (Shubnikov notation) net topology with point symbol $\{4^4.6^2\}$. Thermal analysis of the polymers reveals that complex **2** is thermally more stable than complex **1**. Moreover, the relevant role of noncovalent carbon-bonding interactions in complex **1** has also been analyzed and explored in solid state, in particular, the $-CH_3$ group of the end-to-end (**EE**) doubly bridging dca. Exhaustive theoretical calculations have shown that sp^3-hybridized carbon and silicon atoms are able to form noncovalent complexes with electron rich entities [31-53]. Furthermore, important proof of carbon···oxygen/ carbon noncovalent interactions in complexes of carbon monoxide with haloalkanes has been described very recently [54] and referred to as carbon and dicarbon bonds. In addition, carbon-bonding interactions with hydride donors have been reported by Li et. al., [55]. Finally, carbon-bonding interactions involving π-holes instead of σ-holes have been recently described in XCN derivatives (X = halogen atom) [56]. Experimental works confirming these theoretical predictions are scarcely found in the literature [57]. Recently, evidence of carbon-bonding interactions in sarcosine salts has been reported by means of solid nuclear magnetic resonance spectroscopy [58]. In this article, the existence of noncovalent carbon-bonding interactions in complex **1** have been demonstrated using charge-density analysis and other computational tools. To best of my knowledge, this is the first experimental evidence of noncovalent carbon bonding interaction using nitrogen as an electron donor (RCH_3···N motif).

2.2. EXPERIMENTAL SECTION

2.2.1. Materials and Physical Measurements

All chemicals were of reagent grade, purchased from commercial sources and used without further purification. 2-chloro pyridine, acetyl acetone and hydrazine hydrate (Aldrich) were used without further purification.

Elemental analyses (carbon, hydrogen and nitrogen) of the ligand and the metal complexes were determined with a Perkin–Elmer CHN analyzer 2400 at the Indian Association for the Cultivation of Science, Kolkata. IR spectra (KBr pellet, 300-4000 cm^{-1})

were recorded on a Perkin-Elmer model 883 infrared spectrophotometer. Thermogravimetric analysis (TGA) of both **1** and **2** were performed with an SDT 2960 thermoanalyzer under nitrogen (50^{o}C – 800^{o}C) at a heating rate of 10^{o}C/ minute.

2.2.2. Synthesis

2.2.2.1. Synthesis of 3,5-dimethyl-1-(2´-pyridyl) pyrazole (pypz)

2-chloro pyridine (34g) was boiled with hydrazine hydrate (140g, density: 1.03g/ cc) for 4 hours on a sand bath. At hot condition it is yellow in colour but after cooling it turns red and if it is heated further, then the yellow colour turns into black. After cooling the whole red coloured solution was extracted with ether and the distilled product was dried over Na_2SO_4 overnight. Then the ether is removed from it and the mass was fractionated under roteryevaporator. The residue (pyridine-2-yl-hydrazine) is cooled in an ice bath and it becomes solid of light yellow colour [59]. Now, pyridine-2-yl-hydrazine (10.9g, 0.1mol) was condensed with and acetyl acetone (10g, 0.1mol) in methanol (100 mL) under refluxing condition for three hours (Scheme. 2.3).

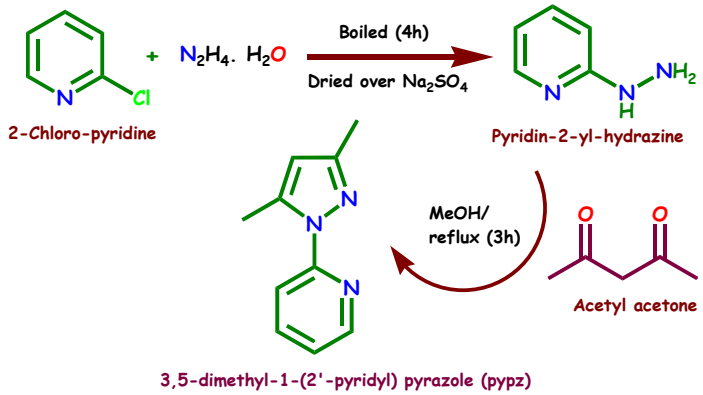

Scheme. 2.3: Schematic representation of synthesis of ligand

The solvent was then removed by evaporation. The resulting dark brown red liquid was then dried over silica gel overnight. The dried liquid was finally distilled under reduced pressure. A yellow fraction was separated at 74^{o} C under a pressure of 0.4 mm of Hg.

2.2.2.2. Synthesis of complex $[Co(dca)_2(DMF)_2]_n$ (1)

An aqueous solution (10 mL) of sodium dicyanamide (0.534g, 6 mmol) was added drop wise to a methanolic solution (10 mL) of $CoCl_2$, $6H_2O$ (0.238g, 1 mmol) with constant stirring which continued for 2 hours. The separated reddish coloured powder compound was dissolved in minimum volume of DMF and excess methanol (1:20) by continuous stirring. Then the solution was left for slow evaporation. After one week a blue colored X-ray quality crystals of **1** were isolated. (Yield: 0.231g, 46%). Anal. Calc. for $C_{10}H_{14}CoN_8O_2$: C,35.61; H,4.15; N,33.23. Found: C,35.58; H,4.13; N,33.21. IR (KBr; ν/cm-1): 2310 (s), 2244 (m), 2159 (s) [Fig. 2.1].

2.2.2.3. Synthesis of complex $[Co(dca)_2(pypz)]_n$ (2)

The solid crystals of complex **1** (0.337g, 1mmol) was added to the methanolic solution of the ligand pypz (0.173 g, 1 mmol). The heterogeneous mixture was kept undisturbed for 10 hrs and filtered. The filtrate was kept for slow evaporation. After one-week dark blue X-ray quality crystals of **2** were obtained. (Yield: 0.421g, 39.5%). Anal. Calc. for $C_{14}H_{11}CoN_9$: C, 46.15; H, 3.02; N, 34.61. Found: C, 46.11; H, 3.00; N, 34.58. IR (KBr; ν/cm^{-1}): 2310 (s), 2244 (m), 2159 (s) [Fig. 2.2].

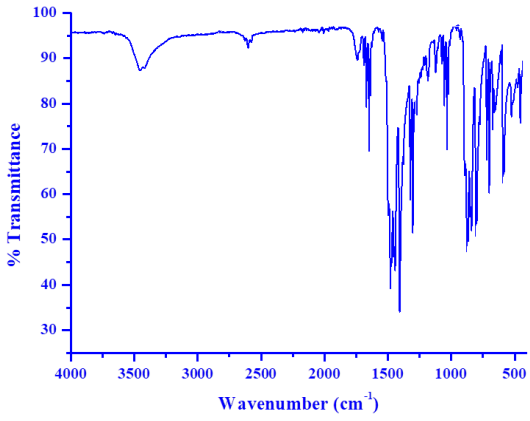

Fig. 2.1: IR spectrum for Complex **1**

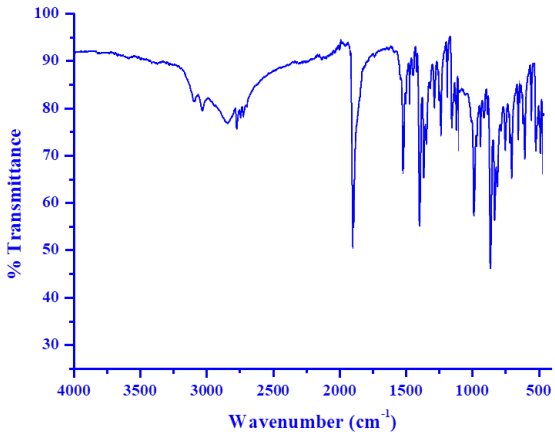

Fig. 2.2: IR spectrum for Complex **2**

2.2.3. X-ray crystallographic analysis

Selected crystal data for **1** and **2** are given in Table 2.1 and selected metrical parameters of the complexes are given in Table 2.2. For both complexes **1** and **2** data collections were made using Bruker SMART APEX II CCD area detector equipped with graphite monochromated Mo Kα radiation (λ = 0.71073 Å) source in φ and ω scan mode at 293(2) K and 296(2) K respectively.

Table 2.1: Experimental data for crystallographic analyses of **1** and **2**

Compound	**1** CCDC: 877582	**2** CCDC: 877583
Empirical formula	$[C_{10}H_{14}CoN_8O_2]_n$	$[C_{14}H_{11}CoN_9]_n$
Formula weight	337.22	364.25
Temperature (K)	293	296
Wavelength (Å)	0.71073	0.71073
Crystal system	Triclinic	Monoclinic
Space group	$P\bar{1}$	$P2_1/c$
Unit cell dimensions		
a (Å)	6.4415(5)	13.9366(10)
b (Å)	7.3787(6)	8.8995(6)
c (Å)	8.5998(8)	14.6385(10)
α (˚)	105.661(4)	90
β (˚)	107.985(3)	117.760(2)
γ (˚)	96.254(3)	90
Volume ($Å^3$)	366.00(5)	1606.63(19)
z	1	4
$Density_{cal}$ (Mg m^{-3})	1.530	1.506
Absorption coefficient (mm^{-1})	1.190	1.084
F(000)	173	741
θ Range (˚) for data collection	2.6-26.2	1.6-27.2
Index ranges	$-7 \le h \le 7$	$-16 \le h \le 17$
	$-9 \le k \le 8$	$-11 \le k \le 11$
	$-10 \le l \le 10$	$-18 \le l \le 18$
Goodness-of-fit on F^2	1.13	1.28
Independent reflections [R_{int}]	1403	3542
Absorption correction	Empirical	Empirical
Refinement method	Full-matrix least squares on F^2	Full-matrix least squares on F^2
Data/restraints/parameters	1403/0/97	3542/0/219
Reflections collected	1463	19169
Final R indices [I > 2σ (I)]	R=0.0376, wR_2=0.1271	R=0.0398, wR_2=0.1565
Largest difference peak and hole ($eÅ^{-3}$)	-0.44, 0.56	-0.30, 0.38

Table 2.2: Selected bond distances (Å) and angles (°) in **1** and **2**

Selected Bonds	Value (Å)	Selected Angles	(°)
Complex **1**			
Co1–N1	2.122(3)	N2_c–Co1–O1	90.89(11)
Co1–N1_c	2.122(3)	O1–Co1–N1	90.30(11)
Co1–N2	2.102(3)	N1–Co1–N2	91.92(12)
Co1–N2_c	2.102(3)	N2–Co1–O1	89.11(11)
Co1–O1	2.109(2)	N1–Co1–O1	90.30(11)
Co1–O1_c	2.109(2)	N1–Co1–N2_c	88.08(12)
C5–N2	1.153(4)	N1–Co1–N1_c	180.00
C4–N1	1.147(4)	N2–Co1–N2_c	180.00
C5–N3	1.289(4)	O1–Co1–O1_c	180.00
N3–C4_b	1.302(4)	Co1–N1–C4	151.7(3)
		Co1–N2–C5	159.7(3)
Complex **2**			
Co1–N1	2.166(2)	N1–Co1–N4	96.11(10)
Co1–N3	2.130(3)	N9–Co1–N6	90.84(10)
Co1–N4	2.130(2)	N6–Co1–N1	87.71(10)
Co1–N6	2.123(3)	N1–Co1–N3	75.86(11)
Co1–N9	2.107(3)	N3–Co1–N4	85.34(10)
Co1–N8	2.093(3)	N4–Co1–N8	90.38(10)
		N8–Co1–N9	92.72(11)
		N1–Co1–N8	172.18(11)
		N3–Co1–N9	166.83(11)
		N6–Co1–N4	174.08(12)
		N3–Co1–N8	100.41(11)
		N1–Co1–N9	91.23(11)

Translation of Symmetry Code to Equiv. Pos

b = [1565] = x,1+y, z, c = [2555] = -x, -y, -z

Cell parameters refinement and data reduction were carried out using the Bruker SMART and Bruker SAINT softwares [60] for all the complexes. The structure of **1** and **2** were solved by conventional direct methods and refined by full-matrix least square methods using F^2 data. SHELXS-97 and SHELXL-97 programs [61] were used for structure of all the complexes solution and refinement respectively. For both **1** and **2** non hydrogen atoms were refined anisotropically till the convergence is attained.

2.3. THEORETICAL METHODS

The energies of all complexes included in this study were computed at the BP86-D3/def2TZVP level of theory. For the theoretical analysis of the noncovalent interactions present in the solid state the crystallographic coordinates have used. The calculations have been performed by using the program TURBOMOLE version 7.0 [62]. The interaction energies were calculated with correction for the basis set superposition error (BSSE) by using the Boys–Bernardi counterpoise technique [63]. For the calculations the DFT-D functional have used with the latest available correction for dispersion (D3) [64]. The Bader's "Atoms in molecules" theory [65] has been used to study the interactions discussed herein by means of the AIMall calculation package [66].

2.4. RESULTS AND DISCUSSION

2.4.1. Structural description of Complex 1

The asymmetric unit with atom numbering scheme and the polymeric 1D chain of complex **1** are shown in Fig. 2.3 (a) and 2.3 (b) respectively.

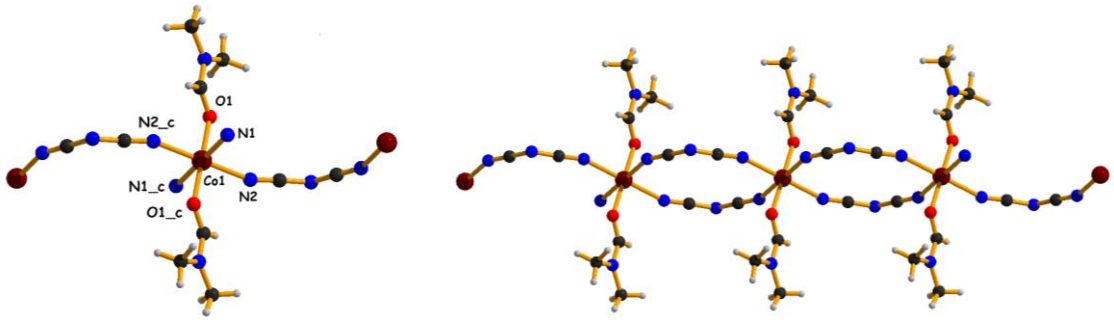

(a) **(b)**

Fig. 2.3: (a) Asymmetric unit of complex **1**. (b) 1D chain running along *a*-axis in **1**. Color code: Co(II), Chocolate brown; O, red; N, Duke blue; C, black; H, light grey.

Crystallographic studies and structural refinement data for **1** are listed in table 2.1 and bond lengths and bond angles are included in table 2.2. The structure of **1** consists of well isolated chain of cobalt atom bridged by double end to end ($\mu_{1,5}$, **EE**) dicyanamide ligands.

Complex **1** crystallizes in *P*ī space group and the asymmetric unit comprised of only one dicyanamide molecule with one DMF and half occupancy Co(II) ion. The geometry around the Co(II) center can be described as a distorted octahedron, with the four nitrogen atoms from four different nitrile groups of dicyanamide in the basal plane (the average deviation is 0.03 Å) with the angle subtended at the Co(II) ion ranging from 88.08 (12)^{o} to 91.92 (12)^{o} while two oxygen atoms of DMF occupying the axial coordination positions with exactly linear O1–Co–O1_c (Translation of Symmetry Code to Equiv. Pos c = [2555] = -x,-y,-z) disposition (180^{o}). The dicyanamide ligand chain propagates in such a manner that each DMF molecule of adjacent chain lies between two DMF molecules (Fig. 2.4).

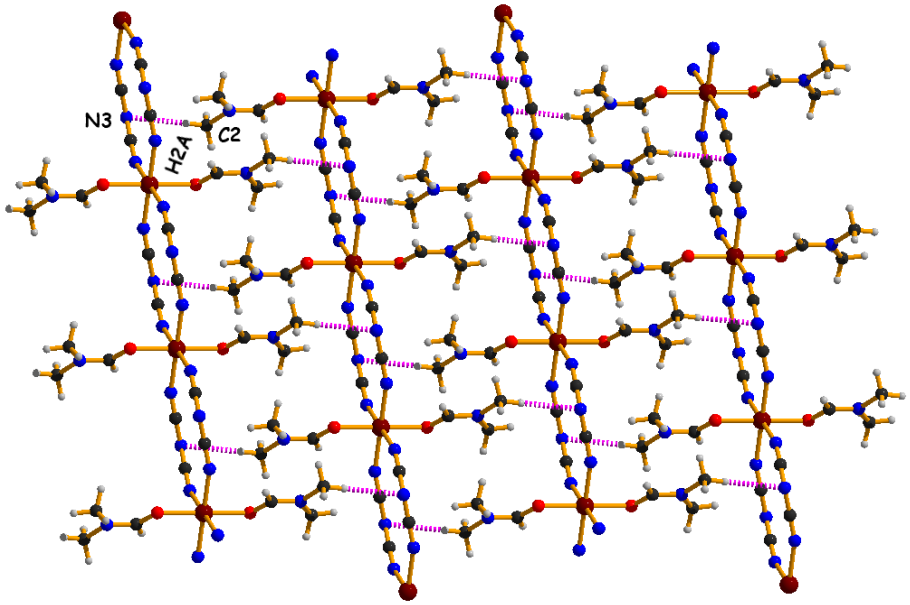

Fig. 2.4: $CH_3\cdots N$ noncovalent interactions in complex **1**

The Co(II) ion is placed exactly in the equatorial plane N2N1N2N1. In complex **1**, dca anions coordinate through nitrile nitrogen atoms and discrete the metals at 7.379(3) Å corresponding to the length of crystallographic '*b*' axis. The bond angles related to the bridging dca ligands are 159.7(3)^{o} and 151.7(3)^{o} for Co1–N2–C5 and Co1–N1–C4 respectively. An approximately C_{2v} symmetry is observed for the dca ligand with C5–N2 and C4–N1 bond distances of 1.153(4) Å and 1.147(4) Å respectively as is typical of the $[N(CN)_2]^-$ anion [17, 33-37]. A small degree of π conjugation results in the longer C–N bond distances [C5–N3: 1.289(4) Å and N3–C4: 1.302(4) Å]. The DMF molecules in compliance with symmetry requirements are trans to each other and adjacent chains are held together by a weak $CH_3\cdots N$ non-covalent interaction (table 2.3).

Table 2.3: Details of Hydrogen bond distances (Å) and angles (°) for **1** and **2**

D – H···A	d (D – H) (Å)	D (H···A) (Å)	D (D···A) (Å)	<DHA (°)
Complex 1				
C2–H2A···N3	0.9600	2.590	3.482(5)	154
Complex 2				
C1–H1···N9	0.9300	2.620	3.162(4)	117
C6–H6A···N6	0.9600	2.610	3.466(7)	149
C10–H10C···N8	0.9600	2.530	3.411(5)	152

The 1D chain in **1** formed by the interaction of coordinated DMF molecules and dicyanamide ligands runs parallel along crystallographic '*b*' axis (Fig. 2.4). The CH_3···N interaction can be viewed as a trifurcated H-bonding interaction (with poor directionality since the C–H···N angle ranges 76° to 100°) or as a noncovalent carbon bonding (C···N interaction). As a matter of fact, all three H···N distances are higher than the sum of their van der Waals radii (ΣR_{vdW}) and, conversely the C···N distance is shorter that ΣR_{vdW} of C and N. The nature of this interaction is further analysed below in the theoretical study section. Moreover, further description of the cobalt environment in **1** with related structures revealed from the Cambridge structural Database (CSD) have been compared in table 2.4.

Table 2.4: Intermetallic distance (Å) and $Co(dca)_2Co$ moiety conformation in 1D $[Co(dca)_2L_2]_n$ polymeric chains

Ligand	M···M (Å)	Conformation	Reference
Pyridine N-oxide	7.318(3)	Twisted	[67]
2-pyrrolidone-O	7.220(3)	Twisted	[68]
Dicyanamide	7.568(1)	Twisted	[69]
Dicyanamide	7.589(1)	Twisted	[70]
H_2O	7.362(1)	Flat	[71]
H_2O	7.411(1)	Flat	[72]
Imidazole	7.395(1)	Bent	[73]
N, N-dimethylformamide	7.379(3)	Bent	This work

The Cambridge Structural Database search allows to retrieve a number of structures containing $Co(dca)_2L_2$ chain with doubly bridging end to end (**EE**) $\mu_{1,5}$ dicyanamide anions. Some of the analogous cobalt complexes with Co···Co separation are reported in table 2.4 together with the different conformations adopted by the Co-(dca)-Co fragment sketched in scheme 2.4. The variation in the observed intermetallic distances is due to the different crystal packing environment (e.g., planar N-ligands) or several non-covalent interactions that occurs between the adjacent chains to stabilize a suitable conformation.

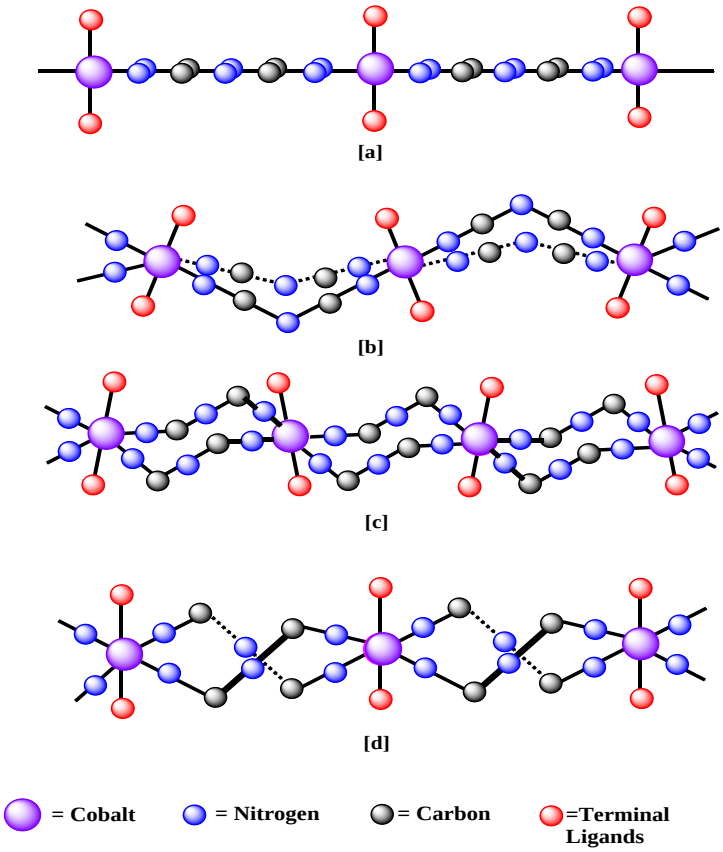

Scheme 2.4: Different conformation of *doubly*-bridging dicyanamide anion (dca) in 1D $Co(dca)_2Co$ polymers and triply bridging (doubly bridging by dca and another by a N, N′ bridging ligand) 1D $[Co(dca)_2L]_n$ (L: a N,N′ bridging ligand) polymers [a] Flat, [b] Bent, [c] Chair and [d] Twisted.

From the table 2.4, it was evident that the Co···Co distances are in the range 7.220-7.411Å [67, 68, 71, 72 and 73] with the exception of two values (7.568Å and 7.589Å) [69, 70] measured in complexes with pendant dca, besides the bridging dca anions.

2.4.2. Structural description of Complex 2

The perspective view of complex **2** with atom numbering scheme is shown in Fig. 2.5. Complex **2** crystallizes in space group $P2_1/c$. Each Co(II) ion is six coordinated with four nitrogen atoms (two nitrile nitrogen atoms from 'dca' and two nitrogen atoms from 'pypz') at equatorial sites and two apical positions are coordinated with nitrile nitrogen atoms N6 and N4 subtend an angle of 174.08(12)^o at the Co(II) center. Four equatorial (two from nitrile nitrogen of 'dca' and other two from pyridyl-pyrazole ligand) Co–N [Co–N1 = 2.166(2) Å, Co–N3 = 2.130(3) Å, Co–N8 = 2.093(3) Å and Co–N9 = 2.107(3) Å] and two apical (both from nitrile nitrogen atoms of 'dca') Co–N [Co–N6 = 2.123(3) Å and Co–N4 = 2.130(2) Å] bond distances in **2** are well tallied with the similar reported complexes. The equatorial angles are [N1–Co–N3 = 75.86(11)^o, N3–Co–N8 = 100.41(11)^o, N1–Co–N9 = 91.23(11)^o and N8–Co–N9 = 92.72(11)^o] more or less in accordance with the cis equatorial angles of octahedron except the angle formed by the bidentate ligand probably due to the steric obligations. Trans Co–N bond distance are consistent with the corresponding reported values for analogous Co(II) systems. The 'dca' ligands adopt the $\mu_{1,5}$ end to end **(EE)** bridging mode and they connect each metal ion to other four neighboring Co(II) centers leading to parallelogram grid sheets (the opposite sides and angles of the geometrical plane created by Co^{II}_4 units are exactly equal) almost parallel to the crystallographic '*bc*' plane.

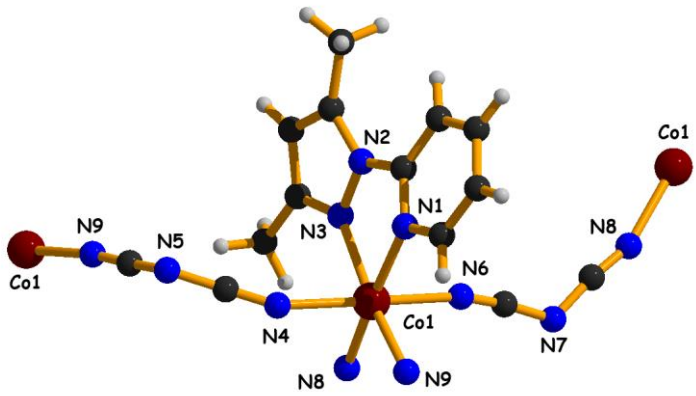

Fig. 2.5: Coordination mode of metal complex in **2**

A topological analysis of this network was performed with the TOPOS 4.0 software [74, 75]. The Co(II) centers create a four connected uninodal net (Fig. 2.6) described by a $\{4^4, 6^2\}$ point symbol that corresponds to the 'sql' topological type.

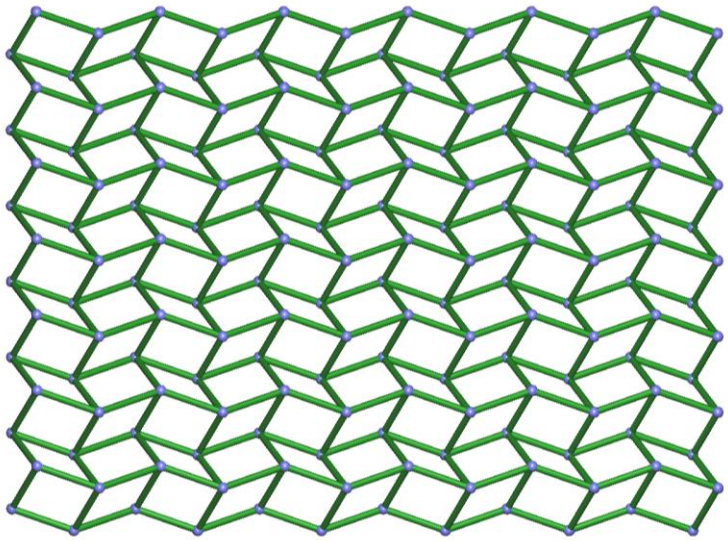

Fig. 2.6: Topological view of **2** having 4-connected sql net with point symbol $\{4^4.6^2\}$.

Keeping the Co^{II}_4 unit in a mean plane two $\mu_{1,5}$ dca linkers are above the plane (distance of the amide nitrogen of the bridging 'dca' from the mean Co^{II}_4 plane is 1.202 and 1.704 Å respectively) and other two $\mu_{1,5}$ dca linkers are below the same plane by the same measurement finally constitute a 24 membered chair arrangement (Fig. 2.7).

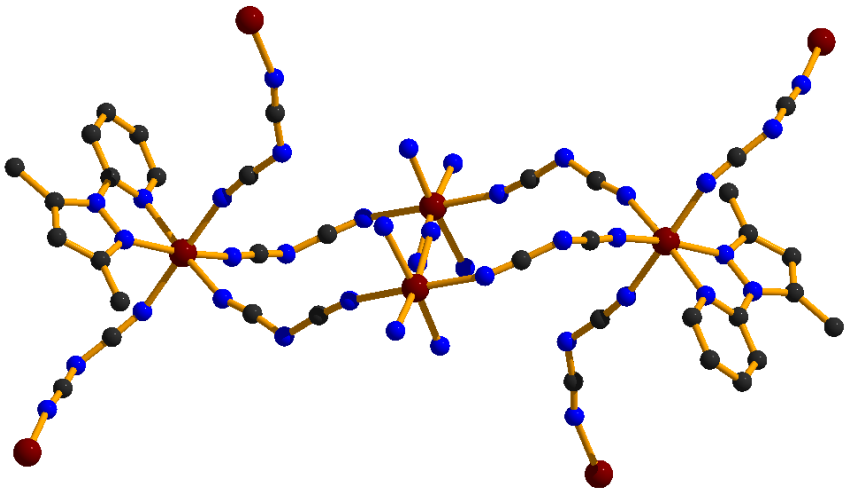

Fig. 2.7: Chair arrangement of complex **2**. Color code: Co(II), Chocolate brown; N, Duke blue; C, black; H, light grey.

In this chair like conformation, each Co(II) centers of Co^{II}_4 unit correspond to hexacoordinated $[Co^{II}(pypz)(dca)_4]$ unit. Each Co(II) center on an arm of chair is coordinated with a strongly bidentated NN donor ligand and four dca anions act as linkers between this Co(II) centers. The intralayer Co···Co separation through the 'dca' bridge is 8.899 Å, whereas the Co···Co distance through the diagonals is different (7.851 Å and 13.802 Å respectively) indicating the neutral center in the Co^{II}_4 units adopt a parallelogram arrangement rather than a rhombus or square disposition.

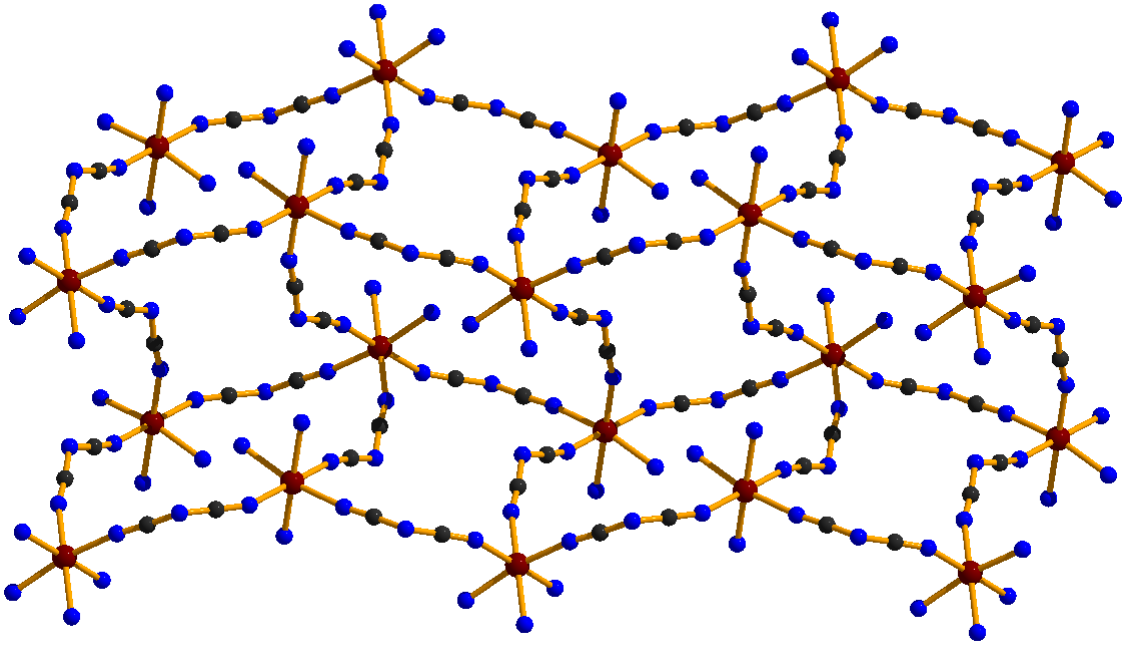

Fig. 2.8: Diagram showing the stacking of macrocyclic chains along '*b*' axis in **2**.

The network forming macrocyclic chains in **2** that stack in 2D layers along the '*b*' axis is shown in Fig. 2.8 exhibiting the uninodal four connected net. The hydrogen bonding interactions that contribute to the further stabilization of the neutral layers is given in table 2.3. Here it is worth noting that, the hydrogen bonding interactions of the type C–H···N are generally considered as non-traditional hydrogen bonding.

2.4.3. Thermal Analysis

Solid state thermal analysis has been carried out in order to (i) understand the thermal decomposition patterns of the complex, (ii) to verify the molecular composition of the complexes, and (iii) to synthesize the thermally stable end products. The TGA curve obtained

for **1** (Fig. 2.9) displays clearly two stages of decomposition. The first weight loss (43.9%) occurs in the range of 180°C to 240°C corresponds to the loss of DMF molecule (Calc. 43.29). Then the compound shows thermal stability up to 300°C. The second step (found 40.1%, calc. 39.14%) of decomposition was found in the region 300° to 460°C indicates the loss of the two dca molecule. TGA curve for **2** (Fig. 2.10) shows the thermal stability up to 400°C and decomposition starts in the temperature range 400° to 530°C. The weight loss of 51.76% of the total weight taken can be assigned to the decomposition of the ligand pypz (Calc. 47.49) and the collapse of the whole framework occurs in the temperature range 530° to 680°C. In both cases, the residual species was assumed to be CoO (found: 18.17%, Calc: 22.21% for **1** and found: 16.86%, Calc: 20.56% for **2**). Overall, the thermal analysis reveals that complex **2** is thermally more stable than complex **1**.

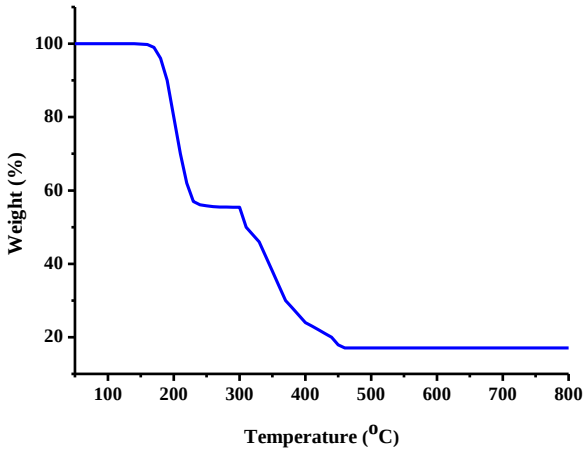

Fig. 2.9: TGA of Complex **1**

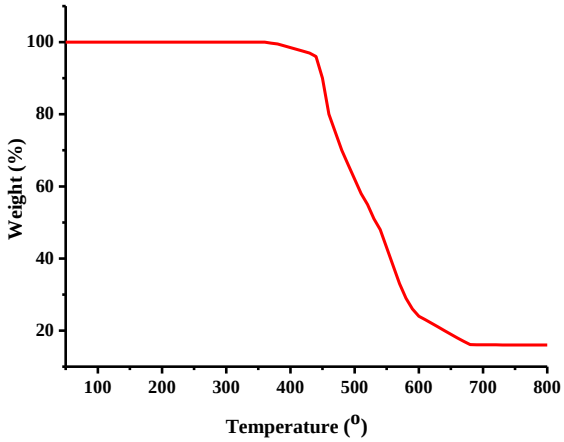

Fig. 2.10: TGA of Complex **2**

2.4.4. Theoretical study

As mentioned above, the theoretical study is devoted to the study of the $CH_3\cdots N$ carbon-bonding interaction observed in **1** that interconnects the 1D polymeric chains [Fig. 2.3 (b)]. First, the molecular electrostatic potential (MEP) surface in DMF have been computed to investigate the existence of a σ-hole in the carbon atom. Moreover, the MEP surface in DMF coordinated to $CoCl_2$ to explore the effect of the coordination of the CO group to a metal on the MEP values have also computed. The MEP surfaces are plotted in Fig. 2.11 in two different orientations.

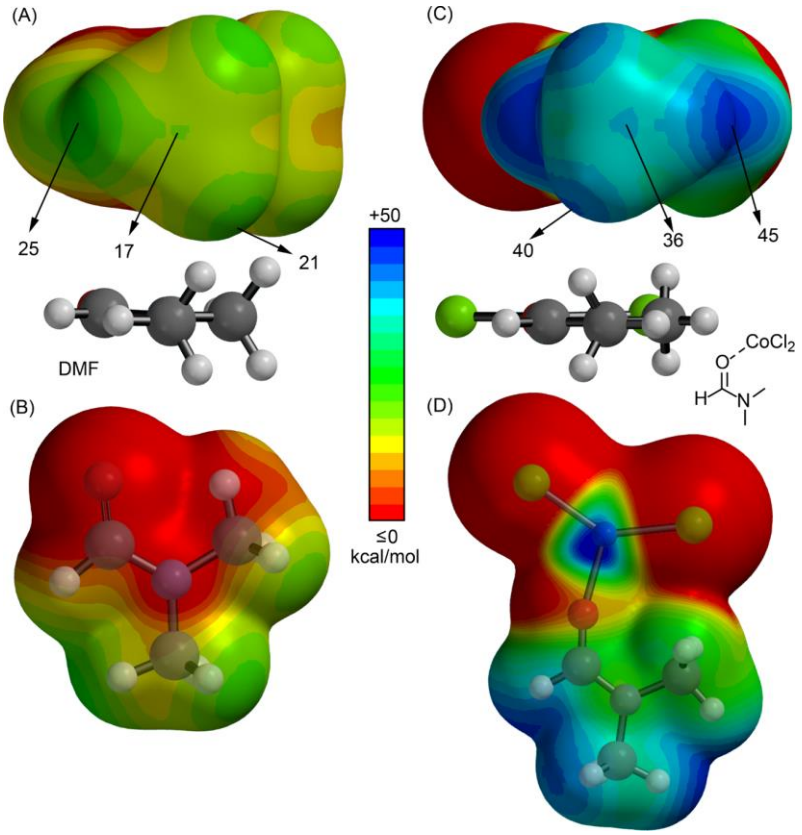

Fig. 2.11: MEP surfaces of DMF (A), on-top view of DMF (B), DMF O-coordinated to $CoCl_2$ (C) and on-top view of coordinated DMF (D). The electrostatic potential values at some points of the surface are shown.

MEP analysis indicates that DMF has several green isocontours in the methyl group and a positive electrostatic potential value at the carbon atom (+17 kcal/mol; [Fig. 2.11 (A, B)]. For the coordinated DMF [Fig. 2.11 (C, D)], the shape of the MEP is very similar; however, the MEP values are significantly more positive. In fact, the MEP at the C atom increases from 17 to 36 kcal/mol. In general, the MEP values measured at the hydrogen atoms of the methyl group are more positive than those measured at the σ-hole of the carbon atom.

Consequently, both coordinated and uncoordinated DMF molecules are better suited to form hydrogen-bonding rather than carbon-bonding interactions in terms of electrostatic effects. A theoretical model of complex **1** has been used in the crystallographic coordinates (Fig. 2.12) to evaluate the carbon (or trifurcated H-bonding) interactions energetically. To use a neutral fragment of the X-ray structure [Fig. 2.12 (A)], a model of polymeric chains have used, where some dca ligands have been substituted by either CN^- or hyperpolarization-

activated cyclic nucleotide-modulated (HCN) ligands at the ends of the chain. In the theoretical model, two discrete polymeric chains including three Co ions have used in each chain. Using this model, the octahedral coordination environment of the central Co of each chain is maintained with respect to the real one present in the crystal structure. In this dimer, four concurrent N···C interactions are established, and the computed interaction energy is significant (ΔE_1 = −17.2 kcal/mol). As other long-range dispersion interactions may also be present between the chains, another model have computed, in which the CH_3 groups are substituted by H-atoms [arrows in Fig. 2.12 (B)]. Using this frozen model, the contribution of long range dispersion interactions have been estimated roughly as they operate in the model in Fig. 2.12 (A).

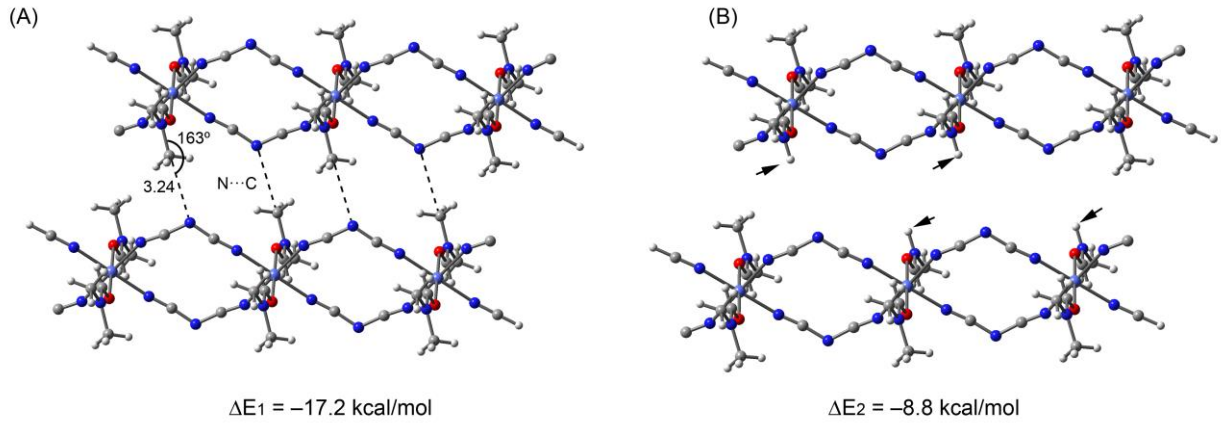

Fig. 2.12: Theoretical models used to evaluate the carbon bonding interactions in **1**.

The resulting interaction energy decreases to ΔE_2 = −8.8 kcal/mol; therefore, the carbon-bonding interaction can be estimated by calculating the difference, that is, $\Delta E_1 - \Delta E_2$ = −8.4 kcal/mol. The characterization of the noncovalent interaction in complex **1** has been performed by means of charge-density analysis and distribution of critical points (CPs). The existence of a bond path linking two atoms and the concomitant bond CP provide strong evidence of interaction. The allocation of CPs and bond paths computed for a reduced model of compound **1** is shown in Fig. 2.13.

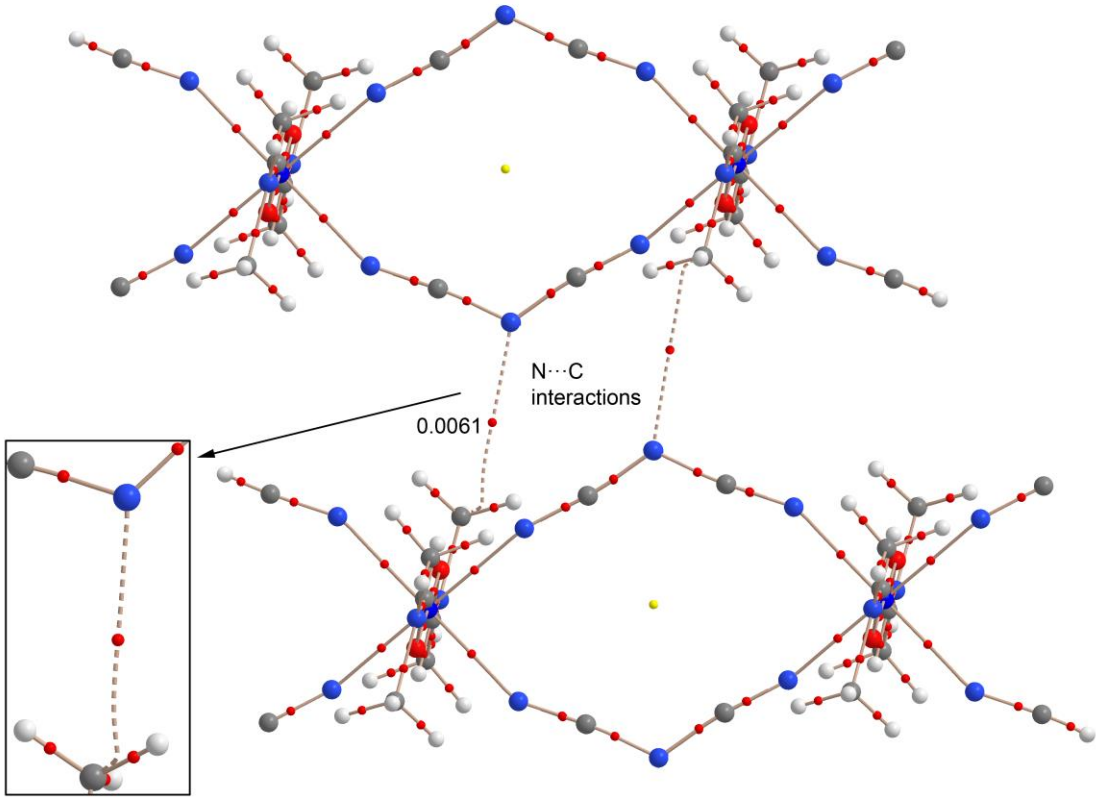

Fig. 2.13: Distribution of critical points (red spheres) and bond paths for the model of complex **1** at the BP86-D3/def2-TZVP level of theory. The value of the charge density (ρ) at the bond critical points that emerge upon complexation is indicated in a.u.

The carbon-bonding N···C interaction is characterized by the existence of a bond CP that links the N atom with the carbon atom, consequently validating the C-bonding nature of this contact. The value of ρ(r) at the bond CP is comparable to that previously reported for O···C interactions [40, 47]. It should be emphasized that the analysis of **1** exhibited a bond path starting from the N atom and ending at the $-CH_3$ carbon atom and, more importantly, there exist no other bond paths connecting the N atom to the H atoms of the methyl group. Therefore, the motif observed in the solid state certainly represents a C···N noncovalent carbon-bonded motif. The value at the Laplacian of ρ supports the closed-shell nature of the interaction. Finally, it can be inferred that the coordination of DMF to Co(II) communicates a charge depletion effect to the carbon atom, thus supporting the carbon-bonding interaction. Moreover, with the purpose of examining the N···C interaction from an orbital perspective, natural bond orbital (NBO) analysis have carried out for the model in Fig. 2.13 [76]. Interestingly, second-order perturbation analysis shows electron donation from the lone pair

of the central N atom of the dca ligand to the C−N antibonding orbital (BD*) of the coordinated DMF with an associated stabilization energy of E(2) = 0.40 kcal/mol for each LP(N) → BD*(CN) interaction. Interestingly, no other donor-acceptor orbital interaction from the ligand to DMF is found in this complex. Therefore, the presence of noncovalent C-bonding instead of hydrogen bonding interactions is confirmed. Finally, the easy transformation of 1D Co(II) polymeric chain **1** to polymer **2** in methanol have also been analyzed theoretically. That is, when pypz is added to the methanolic solution of polymer **1**, the DMF molecules that are axially coordinated in polymer (**1**) are substituted by the bidentate pypz ligand. This substitution likely gives the extra stabilization to **2** through the chelate effect. To give theoretical support to this explanation, the reaction energy associated with the substitution of two DMF molecules in the axial position by bidentate pypz have computed. As the system is polymeric, a monomeric model have used, which is shown in Fig. 2.14 along with the reaction energy.

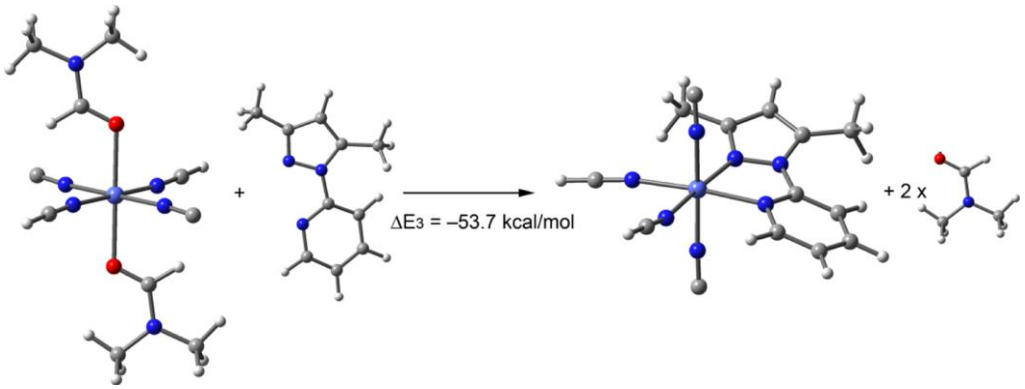

Fig. 2.14: Optimized geometries of the monomeric models and reaction energy to evaluate the chelate effect of the ligand pypz.

In the minimalistic model, each dca ligand has been substituted by either CN− or HCN ligand to use a neutral Co(II) octahedral complex. It can be observed that the substitution of both axial-coordinated DMF molecules by pypz is energetically favored by 53.7 kcal/mol, thus confirming the strong chelate effect of the bidentate ligand. Moreover, it supports the formation of polymer **2** from complex **1** upon addition of the ligand pypz in MeOH.

2.5. CONCLUSION

A novel 2D Co(II) coordination polymer **2** has been synthesized successfully in a stepwise manner from a 1D Co(II) polymer (**1**) by incorporating the ligand pypz (3,5-dimethyl-1-(2′-pyridyl) pyrazole**)** and both complexes were characterized structurally and thermally. From a structural point of view, 2D Co(II) polymer **2** is based on a 24-membered chair like arrangement, which in turn creates a 4-connected uninodal net with sql topology having the point symbol $\{4^4.6^2\}$. Polymer **2** is thermally more stable than polymer **1**, so it may be used as a precursor to design and construct thermally more stable polymeric materials by incorporating ancillary ligands. Remarkably, complex **1** exhibits noncovalent carbon-bonding interactions that involve the N atom of the interconnecting dca ligand and the methyl group of DMF. MEP calculations demonstrate the enhanced ability of coordinated DMF to be involved in noncovalent carbon-bonding interactions compared to that of non-coordinated DMF. AIM analysis of CPs and bond path confirms the existence of C⋯N, not the H-bonding interaction. This investigation may be claimed as a testimony to the importance of nascent interactions in the solid state.

REFERENCES

1. V. A. Blatov, D. M. Proserpio, *In Modern Methods of Crystal Structure Prediction*; A. R. Oganov, Ed.; Wiley-VCH: Weinheim, 2011; Chapter 1.
2. D. Bradshaw, A. Garai, J. Huo, *Chem. Soc. Rev.*, 2012, **41**, 2344-2381.
3. Q.-L. Zhu, Q. Xu, *Chem. Soc. Rev.*, 2014, **43**, 5468-5512.
4. B. F. Hoskins, R. Robson, *J. Am. Chem. Soc.*, 1990, **112**, 1546-1554.
5. M. Singh, A. Ramanan, *Cryst. Growth Des.*, 2011, **11**, 3381-3394.
6. S. R. Batten, R. Robson, *Angew. Chem. Int. Ed.*, 1998, **37**, 1460-1494.
7. N. N. Adarsh, P. Dastidar, *Cryst. Growth Des.*, 2011, **11**, 328-336.
8. A. J. Blake, N. R. Champness, P. Hubberstey, W. S. Li, M. A. Withersby, M. Schroder, *Coord. Chem. Rev.*, 1999, **183**, 117-138.
9. T. K. Maji, K. Uemura, H. C. Chang, R. Matsuda, S. Kitagawa, *Angew. Chem. Int. Ed.*, 2004, **43**, 3269-3272.
10. T. Shiga, H. Okawa, S. Kitagawa, M. Ohba, *J. Am. Chem. Soc.*, 2006, **128**, 16426-16427.
11. I. Potocnak, M. D. Jurco, D. Miklos, M. Kabesova, L. Jager, *Acta Crystallogr., Sect. C* 1995, **51**, 600-602.
12. L. K. Das, A. Ghosh, *Cryst. Eng. Comm.*, 2013, **15**, 9444-9456.
13. B. W. Sun, S. Gao, B. Q. Ma, D. Z. Niu, Z. M. Wang, *J. Chem. Soc. Dalton Trans.*, 2000, 4187-4191.
14. J.-Y. Xu, C.-Z. Xie, F. Xue, L.-F. Hao, Z.-Y. Ma, D.-Z. Liao, S.-P. Yan, *Dalton Trans.*, 2010, **39**, 7159-7166.
15. Z. M. Wang, B. W. Sun, J. Luo, S. Gao, C. S. Liao, C. H. Yan, Y. Li, *Polyhedron*, 2003, **22**, 433-439.
16. P. M. van der Werff, S. R. Batten, P. Jensen, B. Moubaraki, K. S. Murray, *Inorg. Chem.*, 2001, **40**, 1718-1722.
17. S. R. Batten, P. Jensen, B. Moubaraki, K. S. Murray, R. Rubson, *Chem. Commun.*, 1998, 439-440.
18. J. L. Manson, C. R. Kmety, F. Palacio, A. J. Epstein, J. S. Miller, *Chem. Mater.*, 2001, **13**, 1068-1073.
19. J. S. Miller, J. L. Manson, *Acc. Chem. Res.*, 2001, **34**, 563-570.
20. Y. M. Chow, D. Britton, *Acta Crystallogr., Sect. B*, 1975, **31**, 1929-1934.

21. Y. J. Shi, X. T. Chen, Y. Z. Li, Z. L. Xue, X. Z. You, *New J. Chem.*, 2002, **26**, 1711-1713.
22. C. Janiak, *Dalton Trans.*, 2003, 2781-2804.
23. Y. Wei, Y. Yu, R. Sa, Q. Li, K. Wu, *Cryst. Eng. Comm.*, 2009, **11**, 1054-1060.
24. H. L. Sun, Z. M. Wang, S. Gao, *Inorg. Chem.*, 2005, **44**, 2169-2176.
25. S. S. Massoud, S. S.; Louka, F. R.; Mautner, F. A. *Cryst. Eng. Comm*., 2015, **17**, 7604-7617.
26. I. Dasna, S. Golhen, L. Ouahab, O. Pena, J. Guillevic, M. Fettouhi, *J. Chem. Soc., Dalton Trans.*, 2000, 129-132.
27. P. Jensen, S. R. Batten, B. Moubaraki, K. S. Murray, *Chem. Commun.*, 2000, 793-794.
28. J. L. Manson, J. A. Schlueter, U. Geiser, M. B. Stone, D. H. Reich, *Polyhedron*, 2001, **20**, 1423-1429.
29. H. L. Sun, S. Gao, B. Q. Ma, G. Su, *Inorg. Chem.*, 2003, **42**, 5399-5404.
30. J. L. Luo, M. C. Hong, J. B. Weng, Y. J. Zhao, R. Cao, *Inorg. Chim. Acta*, 2002, **329**, 59-65.
31. A. Bauzá, T. J. Mooibroek, A. Frontera, *Chem. Rec.*, 2016, **16**, 473-487.
32. A. Bauzá, T. J. Mooibroek, A. Frontera, *Angew. Chem. Int. Ed.*, 2013, **52**, 12317-12321.
33. P. Politzer, J. S. Murray, T. Clark, *Phys. Chem. Chem. Phys*., 2013, **15**, 11178-11189.
34. J. S. Murray, K. E. Riley, P. Politzer, T. Clark, *Aust. J. Chem.*, 2010, **63**, 1598-1607.
35. T. Clark, *Comput. Mol. Sci.*, 2013, **3**, 13-20.
36. P. Politzer, J. S. Murray, T. Clark, *Phys. Chem. Chem. Phys.*, 2010, **12**, 7748-7757.
37. A. Bundhun, P. Ramasami, J. S. Murray, P. Politzer, *J. Mol. Model*, 2013, **19**, 2739-2746.
38. S. J. Grabowski, *Phys. Chem. Chem. Phys.*, 2014, **16**, 1824-1834.
39. A. Bauzá, T. J. Mooibroek, A. Frontera, *Chem. Eur. J.*, 2014, **20**, 10245-10248.
40. A. Bauzá, T. J. Mooibroek, A. Frontera, *Phys. Chem. Chem. Phys.*, 2016, **18**, 1693-1698.
41. E. C. E. Adán, A. Bauzá, A. Frontera, P. Ballester, *Phys. Chem. Chem. Phys.*, 2015, **16**, 2530-2533.
42. D. Mani, E. Arunan, *Phys. Chem. Chem. Phys.*, 2013, **15**, 14377-14383.
43. S. A. C. McDowell, *Chem. Phys. Lett.*, 2014, **598**, 1-4.
44. Q. Tang, Q. Li, *Comput. Theor. Chem.*, 2014, **1050**, 51-57.

45. X. Guo, Y.-W. Liu, Q.-Z. Li, W.-Z. Li, J. B. Cheng, *Chem. Phys. Lett.*, 2015, **620**, 7-12.
46. M. D. Esrafili, N. Mohammadirad, M. Solimannejad, *Chem. Phys. Lett.*, 2015, **628**, 16-20.
47. M. D. Esrafili, F. Mohammadian-Sabet, *Mol. Phys.*, 2016, **114**, 1528-1538.
48. S. Scheiner, *J. Phys. Chem. A*, 2015, **119**, 9189-9199.
49. M. Marín-Luna, I. Alkorta, J. Elguero, *J. Phys. Chem. A*, 2016, **120**, 648-656.
50. P. Metrangolo, H. Neukirch, T. Pilati, G. Resnati, *Acc. Chem. Res.*, 2005, **38**, 386-395.
51. P. Politzer, J. S. Murray, *Chem. Phys. Chem.*, 2013, **14**, 278-294.
52. A. Bauzá, T. J. Mooibroek, A. Frontera, *Chem. Phys. Chem.*, 2015, **16**, 2496-2517.
53. P. Politzer, J. S. Murray, T. Clark, *Phys. Chem. Chem. Phys.*, 2010, **12**, 7748-7757.
54. P. R. Varadwaj, A. Varadwaj, B.-Y. Jin, *Phys. Chem. Chem. Phys.*, 2014, **16**, 17238-17252.
55. Q.-Z. Li, H.-Y. Zhuo, H.-B. Li, Z.-B. Liu, W.-Z. Li, J.-B. Cheng, *J. Phys. Chem. A*, 2015, **119**, 2217-2224.
56. V. de. P. N. Nziko, S. Scheiner, *Phys. Chem. Chem. Phys.*, 2016, **18**, 3581-3590.
57. S. P. Thomas, M. S. Pavan, T. N. G. Row, *Chem. Commun.*, 2014, **50**, 49-51.
58. S. A. Southern, D. L. Bryce, *J. Phys. Chem. A*, 2015, **119**, 11891-11899.
59. N. Saha, S. K. Kar, *J. Inorg. Nucl. Chem.*, 1977, **39**, 1236-1238.
60. Bruker, SMART, v5.631; Bruker AXS Inc.: Madison, WI, USA, 2001.
61. G. M. Sheldrick, SHELXS-97 and SHELXL-97; University of Göttingen: Germany, 1997.
62. R. Ahlrichs, M. Bär, M. Hacer, H. Horn, C. Kömel, *Chem. Phys. Lett.*, 1989, **162**, 165-169.
63. S. B. Boys, F. Bernardi, *Mol. Phys.*, 1970, **19**, 553-566.
64. S. Grimme, J. Antony, S. Ehrlich, H. Krieg, *J. Chem. Phys.*, 2010, **132**, 154104-154119.
65. R. F. W. Bader, *Atoms in Molecules - A Quantum Theory*, Oxford University Press: Oxford, U.K., 1990.
66. A. Todd, T. K. Keith, AIMA11, version 13.05.06; Gristmill Software: Overland Park, KS, 2013.
67. D. Ghoshal, G. Mostafa, T. K. Maji, E. Zangrando, T. H. Lu, J. Ribas, N. R. Choudhury, *New J. Chem.*, 2004, **28**, 1204-1213.

68. S. W. Ng, *Acta Crystallogr Sect. E, Struct. Rep. online*, 2003, **59**, 530-531.
69. J. N. Racbiger, J. L. Manson, R. D. Soummer, U. Geiser, A. L. Rheingold, J. S. Miller, *Inorg. Chem.*, 2001, **40**, 2578-2581.
70. L. Jager, C. Wagner, M. Korabic, A. Zygmunt, J. Mrozinski, *J. Mol. Str.*, 2001, **570**, 159-164.
71. S. C. Manna, A. K. Ghosh, J. Ribas, M. G. B. Drew, C. N-Lin, E. Zangrando, N. Roy Choudhury, *Inorg. Chim. Acta*, 2006, **359**, 1395-1403.
72. A. M. Kutasi, S. R. Batten, B. Moubaraki, K. S. Murray, *J. Chem. Soc. Dalton Trans.*, 2002, 819-821.
73. A. Das, C. Marschner, J. Cano, J. Baumgartner, J. Ribas, M. S. El. Fallah, S. Mitra, *Polyhedron*, 2009, **28**, 2436-2442.
74. V. A. Blatov, Nanocluster Analysis of Intermetallic Structures with the Program Package TOPOS. *Struct. Chem.*, 2012, **23**, 955-963.
75. M. Li, D. Li, M. O'Keeffe, O. M. Yaghi, *Chem. Rev.*, 2014, **114**, 1343-1370.
76. F. Weinhold, *J. Comput. Chem.*, 2012, **33**, 2363-2379.

CHAPTER 3

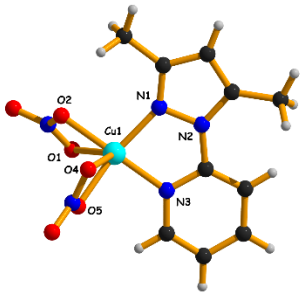

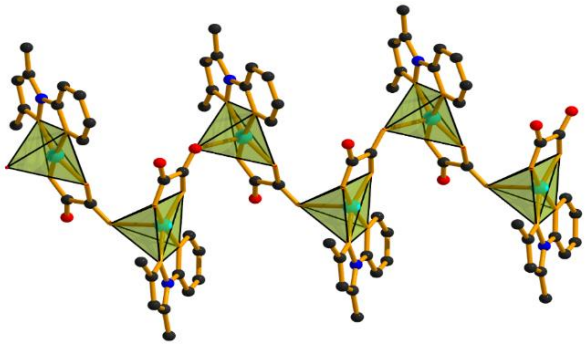

One mononuclear and one oxalate bridged 1-D polymeric copper(II) complex derived from pyrazole based heterocyclic ligand: Synthesis, crystallographic characterization and DFT calculations

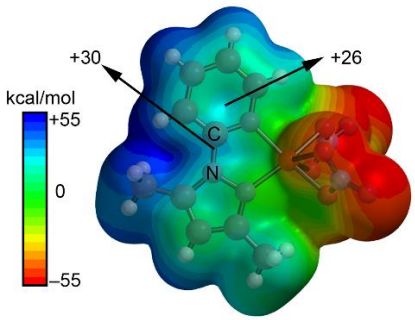

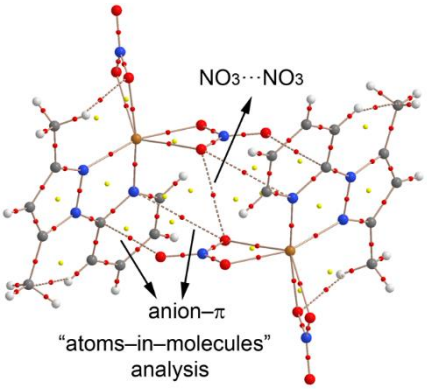

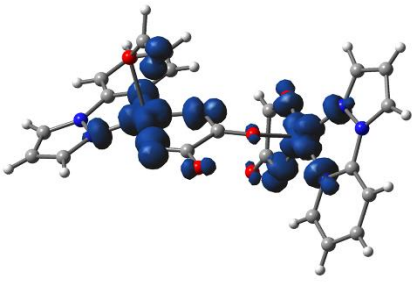

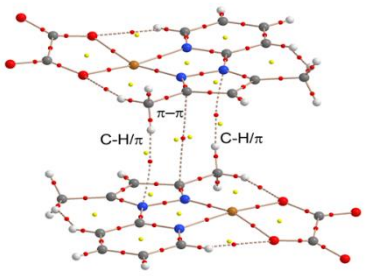

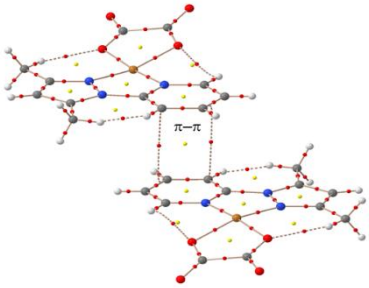

Published in RSC Advances, 2015, 5, 45082-45091

One mononuclear and one oxalate bridged 1-D polymeric copper(II) complex derived from pyrazole based heterocyclic ligand: Synthesis, crystallographic characterization and DFT calculations

3.1. INTRODUCTION

Synthetic inorganic chemists have witnessed an overgrowing interest in synthesizing several coordination complexes derived from heterocyclic base ligands due to their extensive applicability in catalysis, in designing molecular ferromagnets, in biological modeling as liquid crystals and as heterogeneous catalysts [1, 2]. It is well known that the judicious selection of the organic ligands is one of the key factors for synthesizing the coordination compounds with novel structures.

Oxalate ion has been demonstrated as an excellent connector for the construction of organic–inorganic hybrid polymeric compounds. The oxalate group (dianion of the ethanedioic acid, H_2Ox) is a known classical ligand in coordination chemistry and in magneto-structural studies due to versatile coordination modes that it exhibits in its metal complexes [3-6] together with its remarkable ability to mediate strong magnetic interactions between the paramagnetic metal ions when acting as a bis-bidentate bridge, the metal-metal separation being larger than 5.4 Å [6]. In the reported oxalate copper(II) complexes, the $\mu_{1,2,3,4}$-bis-chelating mode is more frequently exhibited, while the number of structurally characterized complexes in which the oxalate group acts as tridentate ligand is scarce [7] which exhibit weak antiferromagnetic interactions between copper(II) ions [8-13]. The ferromagnetic complexes with tridentate coordination mode are very rarely reported. Here, a weak ferromagnetic tridentate oxalato bridged 1D Cu(II) polymeric complex has been reported along with a monomeric Cu(II) complex derived from strongly coordinating bidentate pyridyl-pyrazole (**L**) ligand. Magnetic susceptibility measurements reveal a weak ferromagnetic interaction between the adjacent Cu(II) centers separated by 5.399 Å. There are several oxalato bridged Cu(II) complexes among which some are antiferromagnetic in nature and some other shows ferromagnetic behaviour (*vide infra*). Keeping all these results in mind I extend the present work beyond the monomeric Cu(II) complex (complex **1**) derived from pyridyl-pyrazole (**L**) ligand and finally have synthesized a weak ferromagnetic tridentate oxalato bridged 1D Cu(II) polymeric complex (complex **2**) from the same ligand in two different ways (Scheme 3.1). The first one was synthesized by 1:1 direct condensation

between $K_2[Cu(Ox)_2]$ and the ligand '**L**' in methanol solvent and the second one was synthesized from the condensation of the complex **1** with oxalic acid in aqueous media.

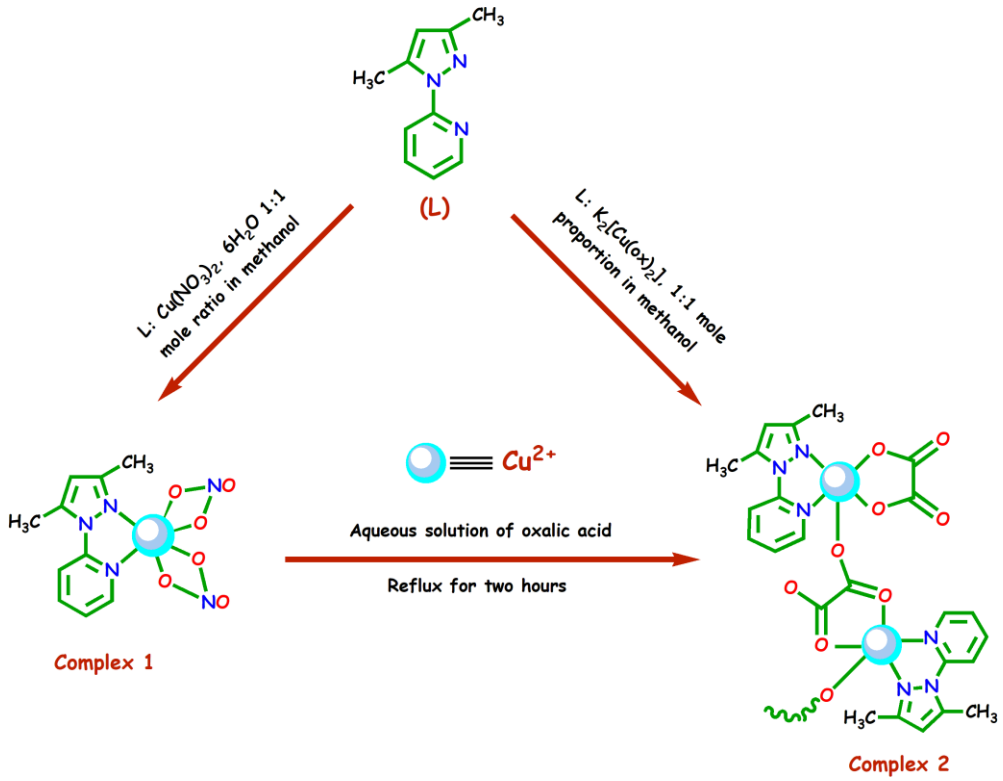

Scheme 3.1: Schematic representation of synthesis of complex **1** and **2**

Even though a great variety of oxalato-bridged polynuclear complexes have been structurally and magnetically characterized (from discrete dimers to three-dimensional systems), to the best of my knowledge only a few weak ferromagnetically one-dimensional $\mu_{1,2,3}$ tridentate oxalato-bridged copper(II) compounds are known [14]. Moreover, complex **2** is the first example of a the tridentate oxalate-bridged ($\mu_{1,2,3}$) copper(II) based on pyridyl pyrazole ligand. Finally, density functional theory (DFT) calculations have been provided in consequence with two interesting aspects of the complexes: first, an interesting π-hole noncovalent interactions have been elucidated involving the coordinated nitro ligands in compound **1**. As a matter of fact, the importance of this particular interaction in supramolecular chemistry has been investigated recently [15] combining a comprehensive analysis of the CSD and theoretical calculations. Second, the magnetic properties of compound **2** have been rationalized using the broken-symmetry approach and analyzing the spin density of a Cu_2 dimeric model of the polymeric chain.

3.2. EXPERIMENTAL SECTION

3.2.1. Materials and Physical Measurements

All chemicals were of reagent grade, purchased from commercial sources and used without further purification. 2-chloro pyridine, acetyl acetone and hydrazine hydrate (Aldrich) were used without further purification. All reactions were carried out in aerobic condition and in methanol-water medium (Scheme 3.1).

Elemental analyses (C, H and N) of the ligand and the metal complexes were determined with a Perkin–Elmer CHN analyzer 2400. Magnetic susceptibility of **2** was measured on a Quantum Design MPMSXL5 (SQUID) magnetometer. Diamagnetic corrections were estimated from Pascal's constants for all constituent atoms. The electronic spectra of the complexes in methanol solution were recorded on a Hitachi model U-3501 spectrophotometer. FT–IR spectra were recorded on a Perkin Elmer; model RX–1(KBr disk, 4000–400 cm^{-1}) spectrometer.

3.2.2. Synthesis

3.2.2.1. *Synthesis of ligand 3, 5 dimethyl-1-(2′-pyridyl) pyrazole (L)*

The ligand **L** (3, 5 dimethyl-1-(2′-pyridyl) pyrazole) was synthesized following the reported method [16].

3.2.2.2. *Synthesis of [Cu(L)(NO_3)$_2$] (Complex 1)*

A methanolic solution (10 mL) of the ligand L (0.173g, 1 mmol) was added drop wise to a solution of $Cu(NO_3)_2$. $6H_2O$ (0.295g, 1 mmol) in the same solvent (10 mL) with constant stirring that continued for 2 h. The separated resulting green compound was filtered and dried over silica gel in desiccator. Then the solution was left for slow evaporation. After one-week deep green X-ray quality crystals of **1** were isolated. (Yield: 62%). Anal. Calc. for $C_{10}H_{11}CuN_5O_6$: C, 33.26; H, 3.05; N, 19.40. Found: C, 33.21; H, 3.01; N, 19.42. μ_{eff} (at 298K) = 1.72 B.M. Main FT-IR absorptions, (KBr pellets): ν = 1429 (s), 1315 (s), 1051 (m) (Fig. 3.1). $\lambda_{max/nm}$ = 287 and 327 (Fig. 3.2).

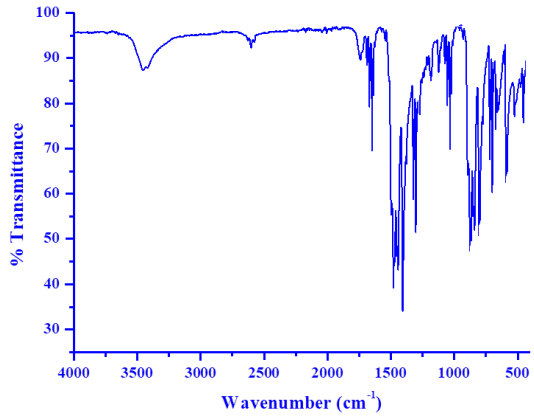

Fig. 3.1: IR spectrum for Complex **1**

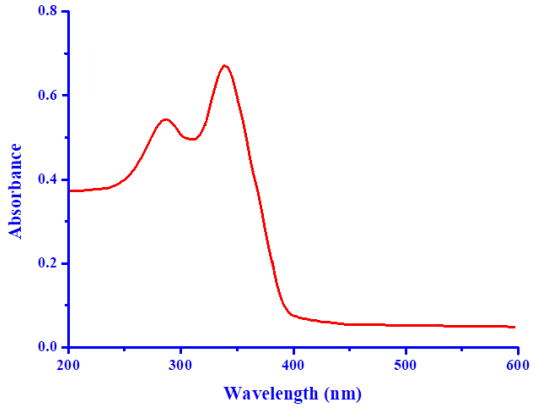

Fig. 3.2: UV-Visible spectrum for Complex **1**

3.2.2.3. *Synthesis of $[Cu(L)(Ox)_2(H_2O)]_n$ (Complex 2)*

The methanolic solution of $K_2[Cu(Ox)_2]$. $2H_2O$ (0.354 g, 1 mmol) was added to an aqueous methanolic solution of the ligand **L** (0.173 g, 1 mmol). The mixture was stirred for 2 h, filtered and kept for slow evaporation. After one-week blue X-ray quality crystals of **2** were obtained. (Yield: 69.5%). Anal. Calc. for $C_{24}H_{24}Cu_2N_6O_9$: C, 43.14; H, 3.59; N, 12.58. Found: C, 43.11; H, 3.57; N, 12.60. FT-IR absorptions, (KBr pellets): ν = 3020 (s), 1992 (s), 1640 (s), 1484 (m), 1341 (s), 1059 (m), 795 (s) (Fig. 3.3). $\lambda_{max/nm}$ = 267, 311 and 489 (Fig. 3.4).

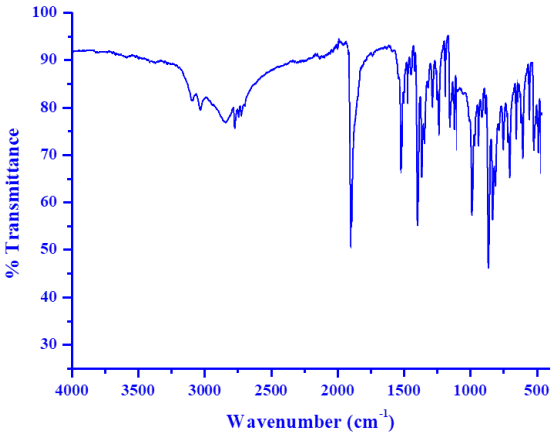

Fig. 3.3: IR spectrum for Complex **2**

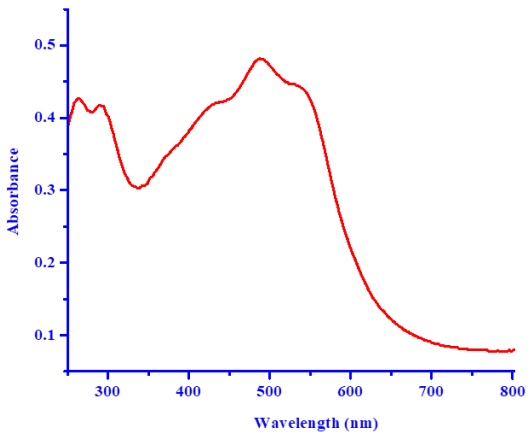

Fig. 3.4: UV-Visible spectrum for Complex **2**

3.2.3. X-ray Crystallographic Analysis

Selected crystal data for **1** and **2** are given in Table 3.1 and selected metrical parameters of the complexes are given in Table 3.2.

Table 3.1: Selected crystallographic features of complex **1** and **2**

Compound	**1** (CCDC: 945288)	**2** (CCDC: 945289)
Empirical formula	$C_{10}H_{11}CuN_5O_6$	$2[C_{12}H_{11}CuN_3O_4].\ H_2O$
Formula weight	360.78	667.59
Temperature (K)	90(2)	150(2)
Wavelength (Å)	0.71073	0.71073
Crystal system	Triclinic	Monoclinic
Space group	P-1	C2/c
Unit cell dimensions		
a (Å)	7.3423(3)	20.402(5)
b (Å)	8.8649(4)	7.233(5)
c (Å)	11.4482(5)	18.215(5)
α (˚)	89.440(4)	90.00
β (˚)	80.271(3)	112.363(5)
γ (˚)	67.287(3)	90.00
Volume ($Å^3$)	676.22(5)	2485.8(19)
z	2	4
$Density_{cal}$ ($Mg\ cm^{-3}$)	1.772	1.784
Absorption coefficient (mm^{-1})	2.681	1.780
F (000)	366	1360
Index ranges	$-8 \le h \le 8$	$-27 \le h \le 27$
	$-8 \le k \le 9$	$-9 \le k \le 4$
	$-13 \le l \le 13$	$-24 \le l \le 24$
Goodness-of-fit on F^2	1.054	1.052
Independent reflections [R_{int}]	2250 [0.032]	3077[0.024]
Absorption correction	multi-scan	multi-scan
Refinement method	Full-matrix least squares on F^2	Full-matrix least squares on F^2
Data/restraints/parameters	2250/0/201	3077/0/191
Reflections collected	4777	7801
Final R indices [$I > 2\sigma(I)$]	R=0.0477 WR_2=0.1260	R=0.0361 WR_2=0.0941
Largest difference peak and hole ($eÅ^{-3}$)	-0.46, 1.01	-0.82, 0.81

Table 3.2: Selected bond distances (Å) and angles (°) in **1** and **2**

Selected Bonds	Value (Å)	Selected Angles	(°)
Complex 1			
Cu1–N1	1.948(4)	O2–Cu1–N3	163.47(16)
Cu1–N3	1.977(4)	N1–Cu1–O5	160.05(14)
Cu1–O1	2.419(3)	N1–Cu1–N3	81.54(17)
Cu1–O2	1.972(3)	O2–Cu1–O1	58.05(11)
Cu1–O5	1.991(3)	O2–Cu1–N1	99.72(15)
Cu1–O4	2.481(3)	N1–Cu1–O1	113.50(13)
		O2–Cu1–O5	91.36(14)
		O5–Cu1–N3	92.54(15)
		O1–Cu1–N3	106.18(14)
Complex 2			
Cu1–O2	1.951(2)	O2–Cu1–O4	85.18(7)
Cu1–O4	1.924(2)	O2–Cu1–N1	93.75(8)
Cu1–N1	1.988(3)	O2–Cu1–N3	160.89(8)
Cu1–N3	1.988(2)	O2–Cu1–O1_a	98.82(6)
Cu1–O1_a	2.284(2)	O4–Cu1–N1	172.05(8)
		O4–Cu1–N3	98.22(8)
		O1_a–Cu1–O4	102.81(2)
		N1–Cu1–N3	80.27(8)

Translation of Symmetry Code to Equiv. Pos

a = [6646.00] = 3/2-x, -1/2+y, 3/2-z

For both complexes **1** and **2** data collections were made using Bruker SMART APEX II CCD area detector equipped with graphite monochromated Cu and Mo Kα radiation (λ = 0.71073 Å) source in φ and ω scan mode at 90(2) K [for complex **1**] and 150(2) K [for complex **2**]. Cell parameters refinement and data reduction were carried out using the Bruker SMART and Bruker SAINT softwares [17] for all the complexes. The structure of both the complexes were solved by conventional direct methods and refined by full-matrix least square methods using F^2 data. SHELXS-97 and SHELXL-97 programs [18] were used for structure of all the complexes solution and refinement respectively and non-hydrogen atoms were refined anisotropically till the convergence is attained.

3.3. THEORETICAL METHODS

The energies of all complexes included in this study were computed at the BP86-D3/def2-TZVP level of theory. The crystallographic coordinates have been used for the theoretical analysis of the non-covalent interactions observed in the solid state. This level of theory has been shown useful and reliable to study noncovalent interactions like those analyzed herein [19] The calculations have been performed by using the program TURBOMOLE version 6.5 [20]. For the calculations the BP86 functional have used with the latest available correction for dispersion (D3) [21]. The Bader's "Atoms in molecules" (AIM) theory has been used to study the interactions discussed herein by means of the AIM all calculation package [22].

The magnetic coupling constants are described using the Heisenberg model. The hybrid *B3LYP* functional [23-25] has been used in all calculations as implemented in Gaussian-09 [26] using the 6-31+G* basis set for all atoms. The approach used to determine the exchange coupling constants for binuclear and trinuclear complexes has been described before in the literature [27-30].

3.4. RESULTS AND DISCUSSION

3.4.1. Structural Description of Complex 1

The perspective view of molecular structure of complex **1** with atom numbering scheme is shown in Fig. 3.5. Complex **1** crystallizes in space group P-1 in which the unit cell is comprised of two molecules.

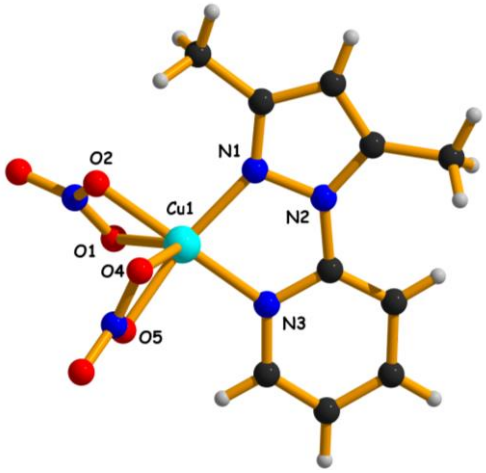

Fig. 3.5: Asymmetric unit of complex **1**

Complex **1** is distorted octahedral where the ligand '**L**', spans the adjacent positions [N1–Cu1–N3=81.54(6)º] as a neutral bidentate NN donor *via* one pyrazolyl nitrogen (N1) and one pyridyl nitrogen (N3). The other four positions of the octahedral geometry are occupied by two oxygen atoms from two different bidentate nitrate anions (O1, O2 and O4, O5). The Cu–N bond distances [Cu1–N1=1.947(18) Å, Cu1–N3=1.977(17) Å] and the copper-oxygen bond lengths [Cu1–O1=2.419(16) Å, Cu1–O2=1.972(16) Å, Cu1–O4=2.481(16) Å and Cu1–O5=1.991(16) Å] are in accord with those values reported previously for similar type of six coordinated octahedral Cu(II) complexes [31-33]. Cu(II) atom sits in the same mean plane constituted by N1N3O5O2 atoms. The three *trans* angles [N1–Cu1–O5 (160.05º), N3–Cu1–O2 (163.47º) and O4–Cu1–O1 (128.69º)] are departed from the ideal trans angle of 180º due to some steric obligations. This is most likely due to the small bite angles [O1–Cu1–O2=58.05(5)º and O4–Cu1–O5=56.74(5)º] of the bidentate nitrate ligand, that may induce a distortion in the geometry of the complex [34]. In this coordination game the pyridyl part is slightly twisted by 9.25º with respect to the pyrazole part. There are two types of anion···π interactions involving the non coordinating atoms O6 and O3 of the nitrate anions that are orientated towards the π-face (Fig. 3.6) of the ligand, pointing to the middle of the N2–C4 bond (the anion···π distances are summarized in Table 3.3).

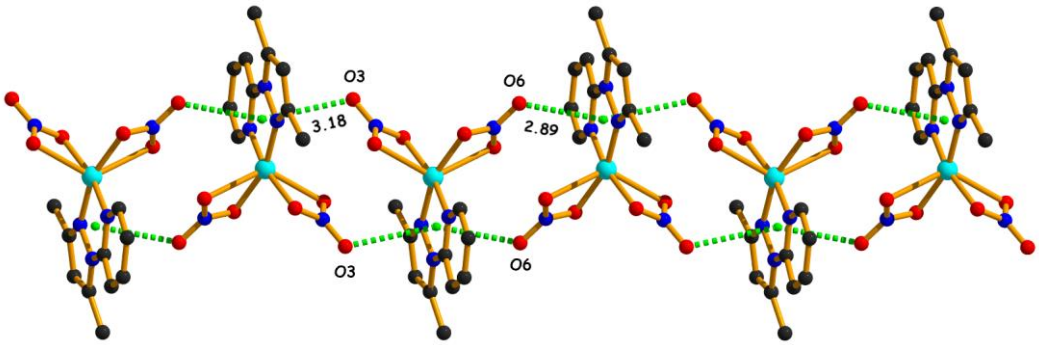

Fig. 3.6: Anion···π interaction along '*a'* axis in **1** to form an infinite 1D chain. Distances to the N–C ring centroid are given in Å. Hydrogen atoms are omitted for clarity. Color code: Cu(II), sky; O, red; N, blue; C, dark grey.

It is remarkably short distance observed for the N5–O6···π contact (< 3.0 Å) that is indicative of a strong interaction. As demonstrated below in the theoretical study by molecular electrostatic potential (MEP) calculations this part of the π-system is the most adequate for interacting with electron rich moieties.

Table 3.3: Geometric features (distances in Å and angles in degrees) of the anion···π interactions observed in complex **1 (**Cg: center of gravity C4–N2 bond)

Interaction	O···N (Å)	O···C (Å)	∠N–O···Cg (º)	∠O···Cg–N (º)
N4–O3···π	3.128(5)	3.387(6)	132.8	79.1
N5–O6···π	2.964(5)	2.974(7)	134.4	89.6

3.4.2. Structural Description of Complex 2

The Perspective view of complex **2** with atom numbering schemes is shown in Fig. 3.7. The complex crystallizes in space group C2/c. The crystal structure of title complex reveals the presence of water molecule of crystallization with the neutral [Cu(Ox)(L)] moiety.

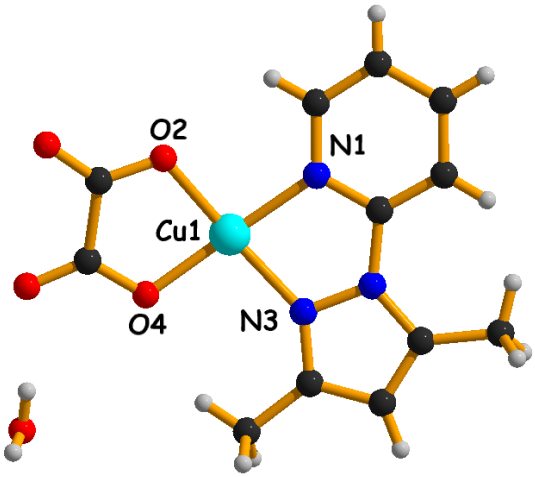

Fig. 3.7: Asymmetric unit of complex **2**

The unit cell of **2** comprises of four molecules. The complex units are stacked in parallel and linked one to other through long Cu-O distances forming a one-dimensional chain along the crystallographic '*a*' axis (Fig. 3.8). As indicated in the structural part of **2**, two oxygen atoms of one bridging oxalate anions (O2 and O4), one oxygen of other bridging oxalate anion (O1) and two cis-coordinated nitrogen atoms [one from pyrazole (N3) and other from pyridine (N1)] of the ligand constitute a slightly distorted tetragonal square pyramid surrounding the Cu(II) ion.

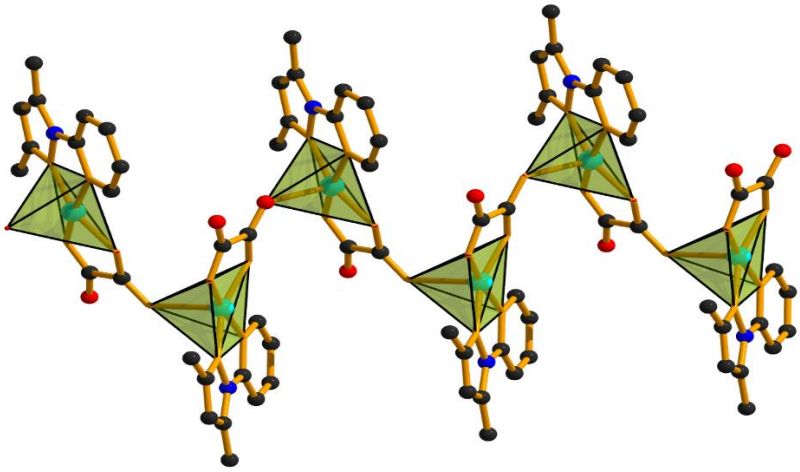

Fig. 3.8: 1D polymeric chain along the crystallographic 'a' axis for **2**

Two copper atoms are indistinguishable crystallographically. The equatorial Cu–O_{basal} [Cu1–O2 (1.951Å) and Cu1–O4 (1.924Å)] and Cu–N [Cu1–N1 (1.988Å) and Cu1–N3 (1.988Å)] bond distances are comparatively shorter than Cu–O_{axial} bond distance (Cu1–O1=2.284Å). The lengthening of the axial bond distance can be explained by the fact that in forming the axial bond less 's' character has been utilized. In this situation the unpaired electron resides in a $d_{x^2-y^2}$ type orbital pointing to the four atoms with short metal–ligand distances (in the basal plane). The overlapping density between σ type orbitals should be rather small, while the '2p' orbitals of the bridging axial oxygen (O1) atom, which is involved in the axial interaction, is approximately orthogonal to the $d_{x^2-y^2}$ orbital of the Cu(II) ion. Cu atom is displaced by 0.226Å from the N_2O_2 least square plane (N1O2O4N3) towards the axial O1 atom. The angles around the copper atom in it are close to ideal angle 90°. The metal- metal separation (Cu–Cu) within the chain of stacked molecules is 5.393Å. These values are more or less comparable to the intramolecular Cu–Cu distance (5.399Å) in the asymmetrical binuclear cation $[(dien)Cu(\mu\text{-}ox)Cu(H_2O)_2\text{-}(tmen)]_2$ (dien = diethylenetriamine and tmen = NNN′N′-tetramethylenediamine) [35], but are somewhat longer than the value of 5.29 Å, reported for the sheet like polymer $[Cu_2(ox)_2(pyz)_3]_n$ (pyz = pyrazine) [36]. Pyrazole part is slightly twisted by an angle 2.31° with respect to the pyridyl ring. The oxalate and pyridyl part are twisted by an angle 17.03° whereas the same with pyrazole part is 17.8°. A two-dimensional supramolecular sheet (Fig. 3.9) is formed in complex **2** by multiple face-to-face π···π stacking interactions between the 1D infinite chains that involve the pyridine rings [Cg(4): N1/C1/C2/C3/C4/C5] of one chain with the symmetry related (1-x,-y,1-z) pyridine rings [Cg(4)] of the neighboring chain (Table 3.4).

Table 3.4: Geometric features (distances in Å and angles in degrees) of the π···π interactions obtained for **2**

Cg(Ring I) – Cg(Ring J)	Cg···Cg (Å)	Cg(I)···Perp (Å)	Cg(J)···Perp (Å)	α (°)	β (°)	γ (°)	Symmetry
Cg(4)···Cg(4)	3.731(3)	3.372	3.372	0.02	25.34	25.34	1-x, -y,1-z

α = Dihedral angle between ring I and ring J (°); β= Cg(I)→Cg(J) or Cg(I)→Me vector and normal to plane I (°); γ = Cg(I) →Cg(J) vector and normal to plane J (°); Cg···Cg: Distance between ring Centroids (Å); Cg(I)···Perp: Perpendicular distance of Cg(I) on ring J (Å); Cg(J)···Perp: Perpendicular distance of Cg(J) on ring I (Å); Cg(4): centre of gravity of ring [N1/C1/C2/C3/C4/C5] for complex **2**.

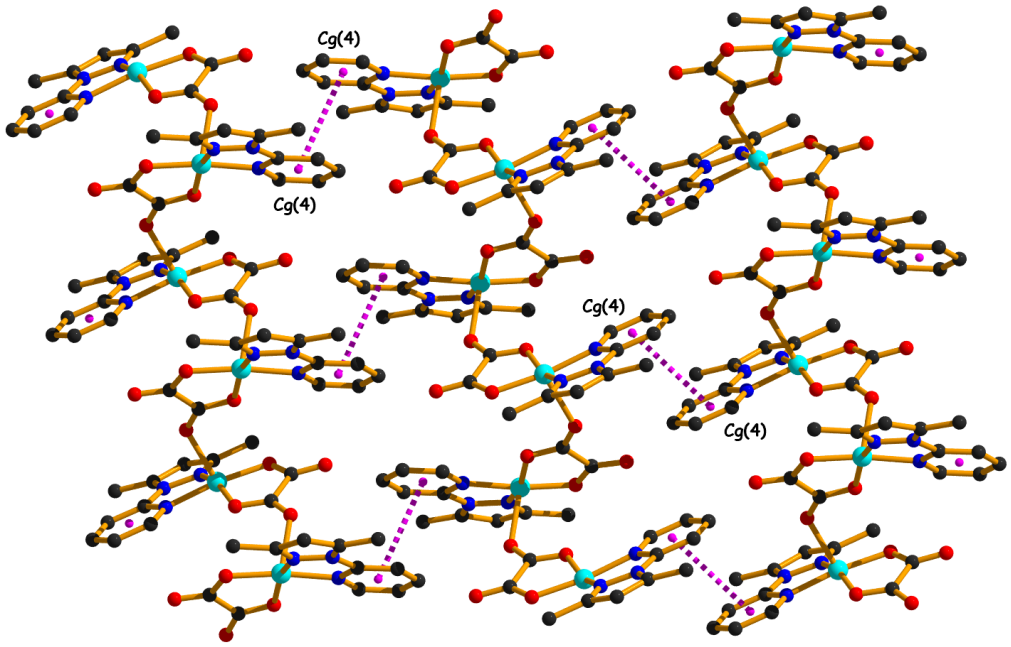

Fig. 3.9: π···π interaction along *c* axis in **2** to form 2D sheet. Hydrogen atoms are omitted for clarity. Color code: Cu(II), sky; O, red; N, blue; C, dark grey.

Each molecule of [Cu(L)(Ox)] is assembled by C–H···π interactions along *c*-axis (Fig. 3.10) involving the one C(methyl)–H group, C(10)–H(10B) donor group of pyrazole ring and another pyridine ring Cg(4) [the ring centroid defined by N1/C1/C2/C3/C4/C5 atoms] of symmetry 3/2-x,1/2-y,1-z and another type involving C(10)–H(10C) donor group of pyrazole ring and aromatic pyrazole ring Cg(3) (the ring centroid defined by N2/N3/C6/C7/C8 atoms) of symmetry 3/2-x,-1/2-y,1-z (Fig. 3.10) (Table 3.5).

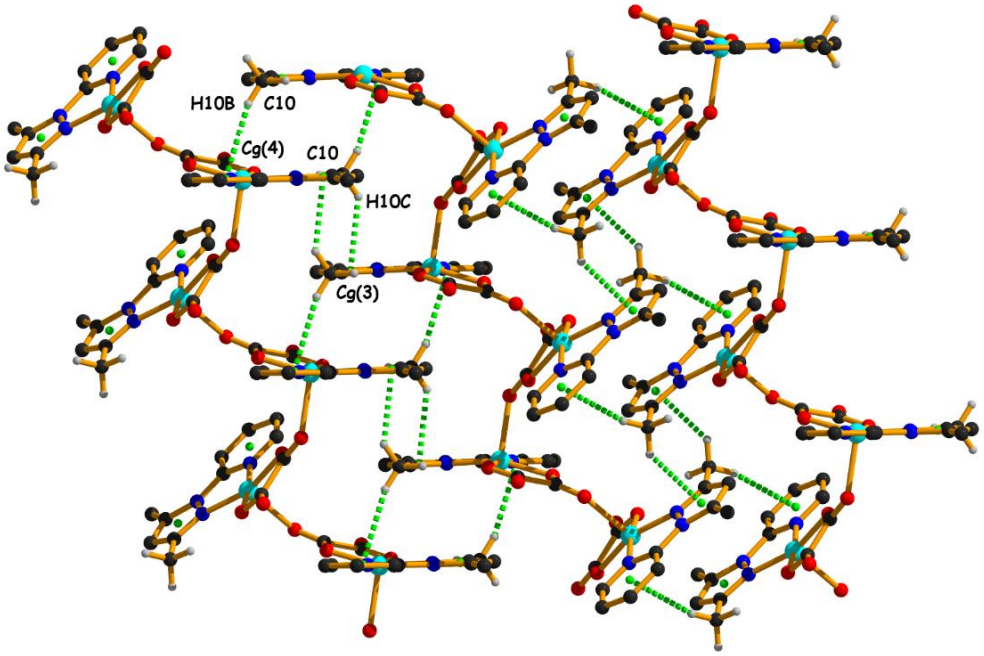

Fig. 3.10: C-H···π along *a* axis to form 2D sheet in **2**. Non related hydrogen atoms are omitted for clarity. Color code: Cu(II), sky; O, red; N, blue; C, grey; H, light green.

Table 3.5: Geometric features (distances in Å and angles in degrees) of the C–H···π interactions obtained for **2**

C–H···Cg (Ring)	H···Cg (Å)	C–H···Cg (°)	C···Cg (Å)	Symmetry
C10–H10B···Cg(4)	2.82	165	3.752(4)	3/2-x, 1/2-y,1-z
C10–H10C···Cg(3)	2.60	138	3.368(3)	3/2-x, -1/2-y,1-z

For complex **2**, Cg(3): center of gravity of ring [N2/N3/C6/C7/C8] and Cg(4): center of gravity of ring [N1/C1/C2/C3/C4/C5].

3.4.3. Magnetic Properties

The magnetic property of complex **2** is shown in Fig. 3.11 as $\chi_M T$ vs. T and $M/N\mu_B$ vs. H (inset) respectively. The values of $\chi_M T$ at 300 K are 0.5 $cm^3mol^{-1}K$ which is as expected for magnetically quasi-isolated spin doublets (g > 2.00). Starting from the room temperature $\chi_M T$ values remain practically constant up to 50 K and below 50 K it increases quickly to 1.1 $cm^3mol^{-1}K$ at 2 K. This global feature is characteristic of very weak ferromagnetic

interactions. The $M/N\mu_B$ value at 5 T is close to 1.1 and the curve practically follows the Brillouin law, assuming g > 2.0, logical for any Cu(II) ion. Complex **2** is, actually, a one-dimensional system in which the copper atoms are linked by oxalato bridging ligands in axial-equatorial fashion.

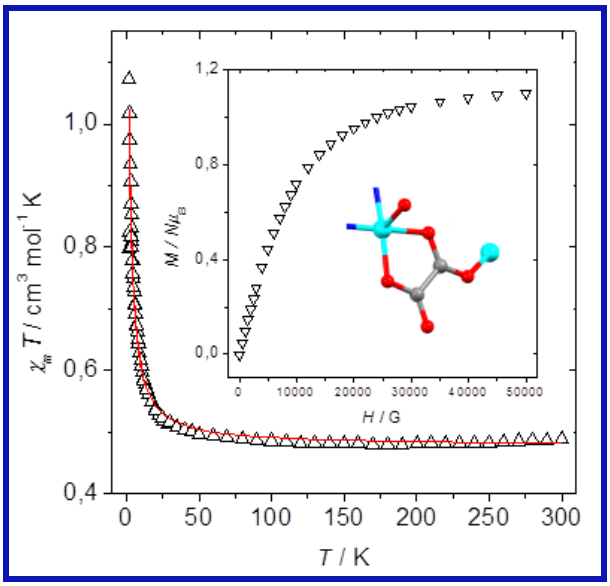

Fig. 3.11: $\chi_M T$ vs. T and $M/N\mu_B$ vs. H (inset) for complex **2**.

This feature gives a uniform S = ½ system (with '*J'* = coupling parameter for the Cu-bridge-Cu pathway). The fit of the magnetic data has been carried out using the formula given by Kahn for this kind of uniform ferromagnetic S = ½ chains [37]. According to Kahn's model [6, 37], the coupling constant '*J*' can be decomposed into two terms, one positive (ferromagnetic, 'J_F') and the other negative (antiferromagnetic, 'J_{AF}'), the expression being 'J'=J_F + J_{AF}. In such a model, the value of the negative term is proportional to the square of the overlap integral (S^2) between the two-metal centered magnetic orbitals. In case of complex **2**, the poor overlap between the two parallel magnetic orbitals through the two OCO oxalate set of atoms would lead to a weak ferro- or antiferromagnetic coupling. The best-fit parameters obtained with this model are 'J' = +1.95 ± 0.08 cm^{-1}, g = 2.21 ± 0.01 and R = 1.1 x 10^{-4}. This result is a signature of the very weak ferromagnetic coupling mediated through the bridging ligands. The small 'J' value can be interpreted as a consequence of the almost nil overlap between the Cu(II) ions through the ligand due to the different character (axial and equatorial), giving quasi-orthogonal magnetic orbitals. The symmetry of the Cu(II) ion is

distorted square-pyramidal (τ parameter = 0.18; '0' for square pyramidal and '1' for trigonal bipyramidal ideally). The major tendency to adopt the square pyramidal geometry avoids the necessary molecular overlap as the electronic density in a square pyramidal is in the d_{x2-y2} orbital. No important density is in the d_{z2} orbital (which corresponds to axial direction). The calculated '*J*' value must be taken with care, because being so small, any interchain coupling will be of the similar order of magnitude (but antiferromagnetic).

3.4.4. Magneto-structural comparison

The versatility in coordination modes of oxalate ion in metal complexes (Scheme. 3.2) constitutes the basis for the development of synthesis and magneto-structural investigation of oxalate bridged complexes [here Cu(II) complex] where the magnetic metal centers are as far away as 5 Å. The magnetic coupling in oxalato complexes ranging from weak ferromagnetic (**6-9**) [37, 38, 40, 41] to weak antiferromagnetic (**3-5**) [38, 39] through the moderate (**10**,**11**) [42, 43] to strong **(12**,**13**) [44, 45] antiferromagnetic are shown in Table 3.6 (our synthesized oxalato bridged copper complex is listed as number **2**). Detailed analysis of oxalate bridged Cu(II) complexes establish that their magnetic exchange interactions are strongly dependent on the geometry around the Cu(II) ion, sensitive to the orientation of the magnetic orbital of each Cu(II) ion relative to the oxalate plane and the bridging mode of the oxalate group.

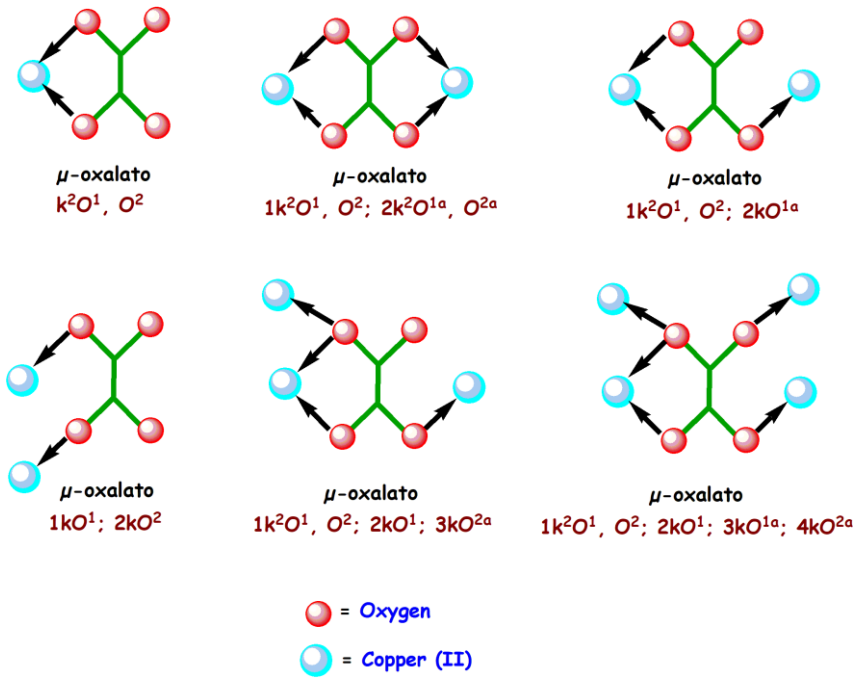

Scheme. 3.2: Selected binding modes of the oxalate dianion in binuclear Cu(II) complexes

Table 3.6: Main structural and magnetic parameters of some previously reported oxalate bridged Cu(II) complexes having Cu…Cu separation more than 5 Å

Compound	$Cu–O_{ax}$ (Å)	Cu–O–C (°)	Cu…Cu (Å)	J (cm^{-1})	Ref.
$[Cu(3\text{-ampy})_2(ox)]_n$ **(3)**	2.170	111.0	5.46	-1.3	[38]
$[Cu(4\text{-ampy})_2(ox)]_n$ **(4)**	2.350	109.7	5.66	-1.1	[38]
$[Cu(en)_2][Cu(ox)_2]$ **(5)**	2.539	148.8	5.87	-1.95	[39]
$[Cu(2\text{-ampy})_2(ox)]_n$ **(6)**	2.380	107.8	5.63	+2.0	[38]
$[Cu(\mu\text{-ox})(isq)_2]_n$ **(7)**	2.003	117.3	5.47	+0.63	[40]
$[Cu_2(bpca)_2(ox)]$ **(8)**	2.260	107.5	5.44	+1.1	[37]
$[Cu_2(bpca)_2(H_2O)_2(ox)].2H_2O$ **(9)**	2.410	106.9	5.63	+1.0	[41]
$\{[Cu_2(L)_2(\mu\text{-ox})_2].\ 2H_2O\}_n$ **(2)**	2.284	126.7	5.39	+1.95	**This work**
$[Cu_2(\mu\text{-ox})_2(ampy)_3]_n$ (**10**)	2.107	112.8	5.51	-22.9	[42]
$[Cu_2(L^1)_2(ox)]$ (**11**)	2.236	116.9	5.40	-12.4	[43]
$[Cu_2(DACO)_2(\mu\text{-ox})Br_2].$ MeOH (**12**)	2.016	111.4	5.24	-121	[44]
$[Cu(dpyam)_2(C_2O_4)(NO_3)_2(Me_2SO)_2]$ (**13**)	1.998	112.2	5.22	-305.1	[45]

Abbreviations used: **3-ampy:** 3-aminopyridine, **4-ampy:** 4-aminopyridine, **en:** ethylene diamine, **2-ampy:** 2-aminopyridine, **isq:** isoquinoline **bpca:** bis(2-pyridylcarbonyl) amidate, **ox:** oxalate, **L:** pyridyl-pyrazole, **ampy**: 2-amino-3-methylpyridine, **L^1:** 2-N-(2'-pyridylimine) benzoic acid, **DACO:** 1,5-diazacyclooctane, **dpyam:** di-2-pyridylamine.

It has been found in oxalato-bridged copper(II) complexes strong antiferromagnetic coupling ('*J*' ranging from -260 to -400 cm^{-1}) results when the short Cu(II)–ligand bonds are coplanar with the bridging ligand (topology 'A' in Fig. 3.12) and the singly occupied molecular orbitals (SOMO's) are built up from metal '*d*' orbitals ($d_{x^2-y^2}$ type orbitals in square pyramidal or elongated octahedral geometry) well oriented to interact with the bridging ligand.

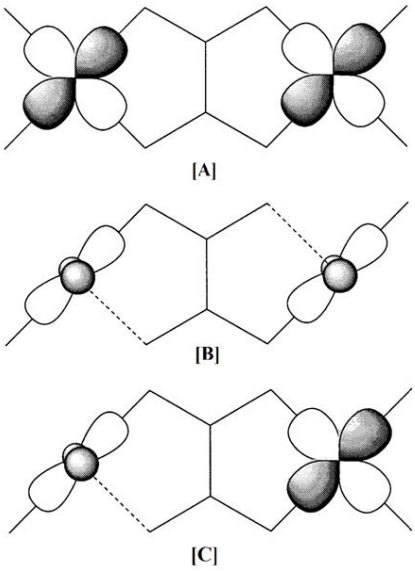

Fig. 3.12: Schematic representation of the orbital topologies in oxalate – copper (II) polymers

When one of the Cu(II)–oxalate bridge distance is long (oxalate bridge is coordinated asymmetrically) the two metal–centered magnetic orbitals are parallel to each other and perpendicular to the bridging oxalate (topology 'B' in Fig. 3.12) and the interaction is poor that results a weak magnetic coupling ('*J*' ranging from +3 to -45 cm^{-1}). An intermediate case is that for which one of the magnetic orbitals is coplanar with the oxalate bridge whereas the other one is perpendicular to it (topology 'C' in Fig. 3.12) [42], as evident in complex **2**.

3.4.5. Theoretical study

The theoretical study has been divided into two parts. Firstly, the noncovalent interactions have analyzed energetically focusing main attention to the C–H···π, anion···π and π···π interactions observed in the solid state of complexes **1** and **2**. In addition, the antiparallel intermolecular NO_3···NO_3 interaction have also examined for complex **1**. Similar interactions have been recently attracted attention due to their increasing interest in supramolecular chemistry and crystal engineering [46, 47]. Secondly, DFT calculations have combined with the broken symmetry approach to gain insight into the qualitative theoretical interpretation on the overall magnetic behavior of the complex. I have focused the theoretical study of complex **1** to the supramolecular 1D chain found in the solid state of **1** that is characterized by the presence of self-complementary anion···π interactions (Fig. 3.6). First of all, the MEP surface of complex **1** have been computed and analyzed which (X-ray asymmetric unit), is shown in Fig. 3.13 (A).

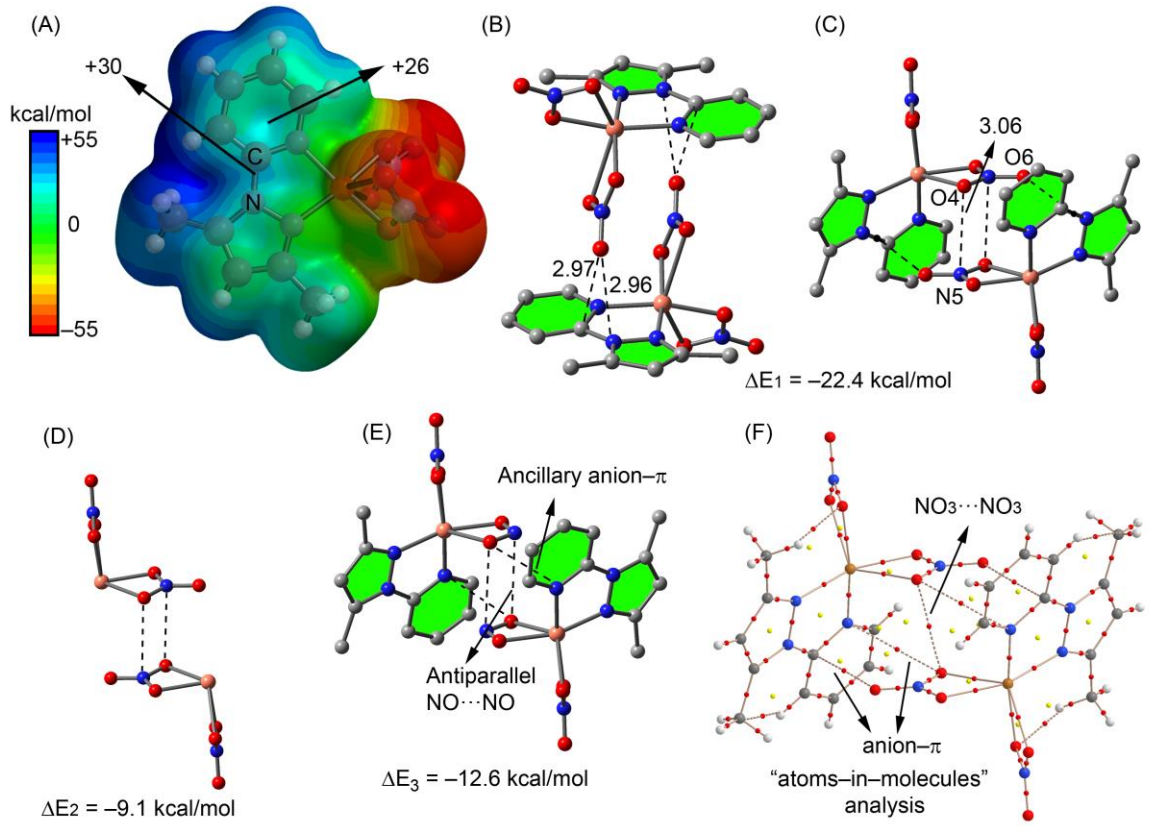

Fig. 3.13: (A) MEP surface computed for **1**. (B) and (C) two views of the self-assembled dimer observed in the solid state of **1**. (D) theoretical model without the organic ligands. (E) theoretical model where the nitrate ligands have been replaced by nitrite ligands. (F) AIM distribution of bond (red sphered) and ring (yellow spheres) critical points. The bond paths are also represented.

It can be observed that the most positive electrostatic potential isovalue is located close to the aromatic hydrogen atoms of the ligand, which that are more acidic than in the free ligand due to the coordination to the Cu(II) ion. The blue (positive electrostatic potential) contours also include the π-system and, remarkably, the contour corresponding to the isovalue = +30 kcal/mol reaches the region of the N2–C4 bond. The electrostatic potential over the center of the pyridine ring is smaller (+26 kcal/mol). This result is helpful to explain the location of the uncoordinated oxygen (O6) atom [Fig. 3.13 (B)] of the nitrate in the X-ray geometry that is pointing to the middle of the C–N bond. The interaction energy of the self-assembled dimer [Fig. 3.13 (B)] have computed, which is large and negative (ΔE_1 = –22.4 kcal/mol). A detailed analysis of this dimeric unit reveals that the coordinated nitrate ligands are also interacting to each other [Fig. 3.13 (C)]. That is, the oxygen atom (O4) of one complex is located at 3.065(5) Å from the nitrogen atom (N5) of the other complex and *vice*

versa (the O4···N5 distance is slightly shorter than the sum of van der Waals radii that is 3.07 Å). This interaction is similar to antiparallel CO···CO interactions described in the literature [48]; however, it should emphasize that in complex **1** the antiparallel NO···NO interaction involves two anionic ligands (even though part of the charge is transfer to the metal center). Therefore, this interaction can be considered as a *pseudo* antielectrostatic interaction that has been recently described for hydrogen bonds [49]. In order to investigate if this NO···NO interaction is energetically favored a theoretical model [Fig. 3.13 (D)] have used where the aromatic ligands have been eliminated and only the NO···NO interaction is evaluated. As a result, the computed interaction energy is ΔE_2 = –9.1 kcal/mol that indicates a favorable contribution of this interaction. It should be mentioned that this is only a rough estimation of the NO···NO interaction energy because the coordination environment of the Cu ion has changed in this reduced model with respect to complex **1**. However, it likely demonstrates (at least qualitatively) that this *pseudo antielectrostatic* interaction is energetically favorable. Moreover, in an effort to evaluate the anion···π interaction, an additional theoretical model has used where the nitrate counterions have been replaced by nitrite ligands [Fig. 3.13 (E)]. This model does not have the contribution of the O6···π interaction that can be then estimated by comparing ΔE_1 and ΔE_3. As a result, the contribution of the anion···π interaction (O6···π) to the formation of the dimer is $\Delta E_1 - \Delta E_3$ = -9.8 kcal/mol. The Bader's "atoms-in-molecules" [50] has been successfully used to describe a great variety of noncovalent interactions to further analyze the interactions. The presence of a bond critical point (CP) and a bond path connecting two atoms is an unambiguous indication of interaction [10.1021/cr00005a013]. The distribution of critical points in the dimer of complex **1** [Fig. 3.13 (F)] reveals the presence of a bond CP that connects the O6 with the carbon atom of the N2–C4 bond confirming the anion···π interaction. Furthermore, the distribution of CPs also reveals the presence of a bond CP connecting the O4 oxygen atom with the nitrogen atom of the pyridine ring [O···N distance is 3.347(5)]. This ancillary anion···π interaction [Fig. 3.13(E)] is likely weak because the O4 oxygen atom is coordinated to the Cu^{II} ion and the long O···N distance. In fact, it can be roughly estimated as the difference between ΔE_3 and ΔE_2, which is –3.5 kcal/mol. Finally, the NO···NO interaction is characterized by the presence of a bond CP that connects both oxygen atoms, confirming the *pseudo antielectrostatic* interaction between the coordinate nitrate anions.

In the polymeric complex **2** the noncovalent interactions have evaluated energetically that are relevant to rationalize the crystal packing described in Fig. 3.9 and 3.10. A repeating structural unit of the polymeric chain of complex **2** have used for the calculations. The theoretical models to analyze the C–H···π and π···π interactions are shown in Fig. 3.14.

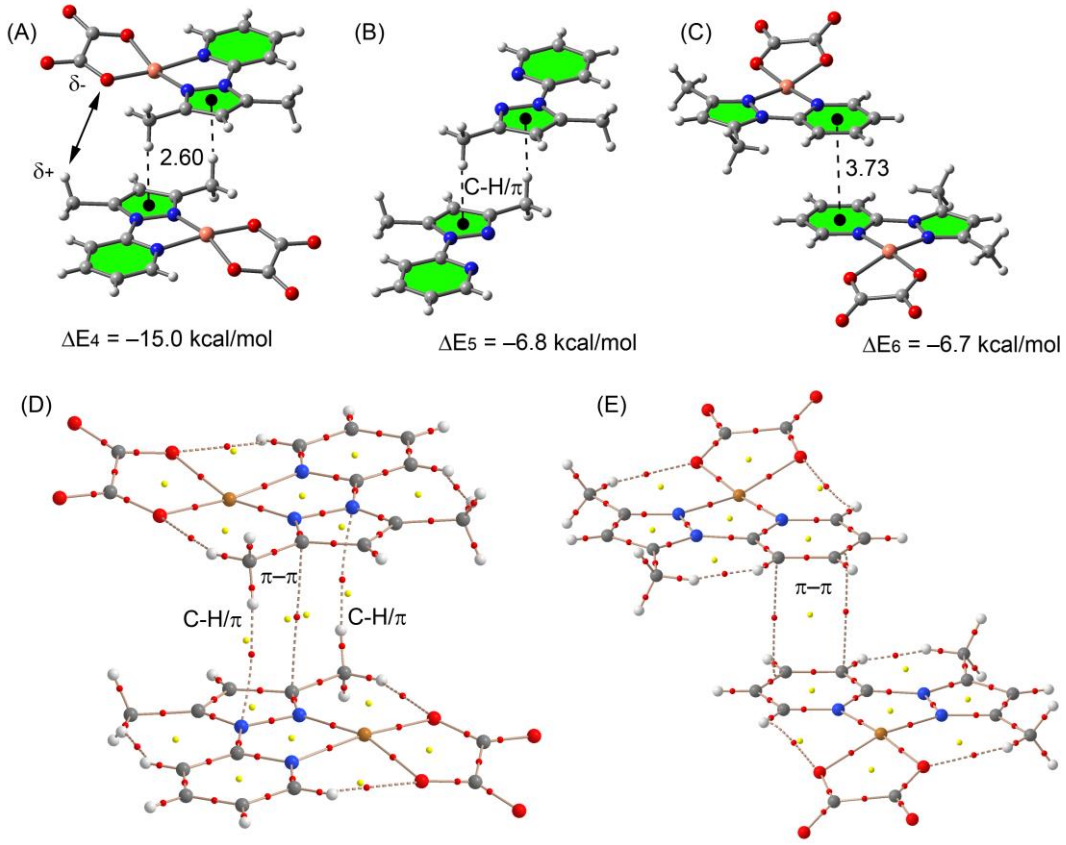

Fig. 3.14: Theoretical models used to evaluate the noncovalent interactions observed in the solid state of **2** (A-C). AIM distribution of bond (red sphered) and ring (yellow spheres) critical points (D-E). The bond paths are also represented.

The interaction energy of the C–H···π self-assembled complex [Fig. 3.14 (A)] is larger in absolute value (ΔE_4 = –15.0 kcal/mol) than expected for this type of interaction [51, 52]. This is likely due to additional electrostatic forces between the anionic oxalate ligands and the hydrogen atoms of the methyl groups that are separated by ~3.8 Å [Fig. 3.14 (A)]. A theoretical model has also computed where only the organic ligands are considered [Fig. 3.14 (B)]. As a result, the interaction energy is reduced to ΔE_5 = –6.8 kcal/mol indicating that each C–H···π interaction contributes in 3.4 kcal/ mol. The π···π interaction mode observed for the coordinated pyridine rings in antiparallel. Previous studies [46] have demonstrated that this

arrangement is energetically favored over the parallel binding model. The interaction energy of the π···π model dimer is ΔE_6 = –6.7 kcal/mol that is almost similar to the previously reported in coordinated pyridine and pyrimidine rings [Fig. 3.14 (C)] [46]. The distribution of critical points of both dimeric complexes have evaluated also [Fig. 3.14 (D, E)]. Interestingly the distribution of critical points in the self-assembled dimer dominated by C–H···π interactions shows that, in addition to the bond CP that connects one hydrogen atom of the methyl group to the N atom of the five membered ring of the ligand, a bond CP connects two carbon atoms of the five membered rings. This additional π···π interaction revealed by the AIM analysis also explains the large interaction energy observed for this dimer (ΔE_4 = –15.0 kcal/mol). The distribution of CPs in the other dimer [Fig. 3.14 (E)] shows that the π···π interaction is characterized by the presence of two bond critical points that connect two carbon atoms of one pyridine ring to two the symmetrically related carbon atoms of the other pyridine ring. The interaction is further characterized by the presence of ring critical point (yellow sphere).

Finally, the magnetic coupling interaction have analyzed theoretically in a binuclear model of complex **2** by computing the spin density distribution. According to the molecular orbital theory, spin delocalization is the result of electron transfer from the magnetic centers to the ligand atoms. A spin-exchange model was generated for theoretical studies using the crystal structure geometry. The theoretical model has been simplified, i.e., hydrogen atoms instead of methyl groups have been used in order to keep the size of the system computationally approachable [Fig. 3.15 (A) and 3.15 (B)]. The calculation of the individual pair-wise exchange constant has been carried out by means of spin-unrestricted DFT calculations using the B3LYP method and employing the 6-31+G* basis set. The theoretical '*J*' value calculation has been performed computing the difference between the energy values of the highest spin state and the broken-symmetry state. Using this methodology and the simplified binuclear model the theoretical '*J*' is 2.4 cm^{-1} that is in good agreement with the experimental value (1.95 cm^{-1}) and confirms the weak ferromagnetic coupling between both metal centers. The Mulliken spin population analysis (Table 3.7) indicates that a significant spin (ca. 0.73 e) is delocalized through the ligands, and the rest (1.27 e) is carried by the copper atoms. The spin density plot is shown in Fig. 3.15 (C) for the high spin state of **2**. The spin density distribution shows a delocalization mechanism in which the copper atoms carry 64 % of net spin and the remaining part is delocalized through coordinating atoms.

Table 3.7: Mulliken spin densities (e) computed for the high spin configuration of the Cu2 dimer model of compound **2**.

Atom Label	Spin density	Atom Label	Spin density
Cu1	0.62	N1	0.07
Cu1′	0.65	N1′	0.10
O1	0.01	N3	0.05
O2	0.10	N3′	0.06
O3	0.03	C11	-0.00
O4	0.15	C12	-0.01

In a square-pyramidal Cu^{II} complex, the d_{x2-y2} orbital contains the unpaired electron; consequently, these orbitals along with the local orbitals of the bridging ligands are involved in the super-exchange pathway, which is confirmed by the spin density plot shown in Fig. 3.15 (C).

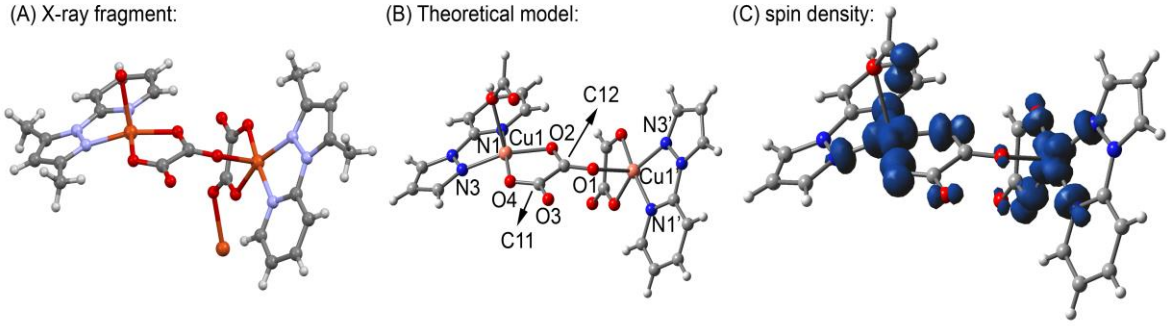

Fig. 3.15: X-ray, theoretical model and spin density plot (isovalue = 0.004 e $Å^{-3}$) of the dinuclear fragment of complex **2**.

The spin density at the O1 is very small (0.01 e) therefore a very weak ferromagnetic coupling is mediated through the bridging ligand communicating the quasi-orthogonal magnetic orbitals. Interestingly, the spin density computed at the carbon atoms of the bridging oxalate group C11 and C12 are negative (-0.003 and −0.010 e, respectively), indicating a spin polarization mechanism that facilitates the ferromagnetic interaction.

3.5. CONCLUSION

A new one-dimensional oxalate-containing copper(II) complex, namely $[Cu(\mathbf{L})(Ox)_2(H_2O)]_n$ (**2**) has been synthesized by condensing the metal salt with the ligand in methanol solvent and then again by condensing the precursor complex $[Cu(\mathbf{L})(NO_3)_2]$ (**1**) with oxalic acid in aqueous media. The geometry around each Cu(II) in **2** is axially elongated square pyramidal with the intrachain copper-copper separation being 5.399 Å. The magnetic studies reveal a weak ferromagnetic interaction through the oxalate bridge, its nature and magnitude being in a good agreement with available magneto-structural data for oxalate-bridged copper(II) complexes where the same out-of-plane exchange pathway is involved. The DFT calculations combined with the broken symmetry approach provide a good estimate of the weak ferromagnetic coupling that is mediated through the tridentate $\mu_{1,2,3}$ oxalate bridging ligand as corroborated by the spin density plot. Moreover, the interesting noncovalent interactions observed in the solid state have been studied by means of DFT calculations assigning discrete energetic values to them. The most important finding is the *pseudo antielectrostatic* interaction between the nitrate ligands that has been characterized both energetically and using the “atoms-in-molecules” methodology.

REFERENCES

1. K. Biradha, M. Sarkar, L. Rajput, *Chem. Commun.*, 2006, 4169-4179.
2. N. Hoshino, *Coord. Chem. Rev.*, 1998, **174**, 77-108.
3. M. H. -Molina, P.A. Lorenzo-Luis, C. Ruiz-Pérez, *Cryst. Eng. Comm.*, 2001, **16**, 1-4.
4. S. Youngme, G.A. van Albada, N. Chaichit, P. Gunnasoot, I. Multikainen, O. Roubeau, J. Reedijk, U. Turpeinen, *Inorg. Chim. Acta*, 2003, **353**, 119-128.
5. G. Marinescu, M. Andruh, F. Lloret, M. Julve, *Coord. Chem. Rev.*, 2011, **255**, 161-185.
6. O. Kahn, *Molecular Magnetism*, Wiley-VCH, New York, 1993, and references therein.
7. H. Núñez, J.-J. Timor, J. Server-Carrió, L. Soto, E. Escrivà, *Inorg. Chim. Acta*, 2001, **318**, 8-14.
8. A. S. Olszewska, B. Matura, J. Mrozinski, B. Kaliuska, R. Kruszynski, M. Penkala, M. *New J. Chem.*, 2014, **38**, 1611-1626.
9. D. Y. Jeter, W. E. Hatfield, *Inorg. Chim. Acta*, 1972, **6**, 523-525.
10. A. Bentana, O. Schott, J. F. Soria, S. E. Stiriba, J. Pasan, C. R. Perez, M. Julve, *Inorg. Chim. Acta*, 2012, **389**, 52-59.
11. U. Geiser, B.L. Ramakrishna, R.D. Wilett, F.B. Hulsbergen, J. Reedijk, *Inorg. Chem.*, 1987, **26**, 3750-3756.
12. A. Gleizes, F. Maury, J. Galy, *Inorg. Chem.*, 1980, **19**, 2074-2078.
13. K. Kadir, T.M. Ahmed, D. Noreus, L. Eriksson, *Acta Crystallogr., Sect. E: Struct. Rep.*, 2006, **62**, 1139-1141.
14. O. Castillo, A. Luque, F. Lloret, M. Julve, P. Roma´n, *Inorg.Chim. Acta*, 2001, **315**, 9-17.
15. A. Bauzá, T. J. Mooibroek, A. Frontera, *Chem. Commun*., 2015, **51**, 1491-1493.
16. N. Saha, S. K. Kar, *J. Inorg. Nucl. Chem.*, 1977, **39**, 1236-1238.
17. Bruker, SMART v5.631, Bruker AXS Inc., Madison, WI, USA, 2001.
18. G.M. Sheldrick, SHELXS-97 and SHELXL-97, University of Göttingen, Germany, 1997.
19. M. Mitra, P. Manna, A. Bauzá, P. Ballester, S. Kumar Seth, S. R. Choudhury, A. Frontera, S. Mukhopadhyay, *J. Phys. Chem. B*, 2014, **118**, 14713-14726.
20. R. Ahlrichs, M. Bär, M. Hacer, H. Horn, C. Kömel, *Chem. Phys. Lett*., 1989, **162**, 165-169.

21. S. Grimme, J. Antony, S. Ehrlich, H. Krieg, *J. Chem. Phys*., 2010, **132**, 154104-154119.
22. AIMAll (Version 13.05.06), Todd A. Keith, TK Gristmill Software, Overland Park KS, USA, 2013.
23. A. D. Becke, *Phys. Rev. A*, 1988, **38**, 3098-3100.
24. C. T. Lee, W. T. Yang, R. G. Parr, *Phys. Rev. B*, 1988, **37**, 785-789.
25. A. D. Becke, *J. Chem. Phys*., 1993, **98**, 5648-5653.
26. Gaussian 09, Revision B.01, M. J. Frisch, G. W. Trucks, H. B. Schlegel, G. E. Scuseria, M. A. Robb, J. R. Cheeseman, G. Scalmani, V. Barone, B. Mennucci, G. A. Petersson, H. Nakatsuji, M. Caricato, X. Li, H. P. Hratchian, A. F. Izmaylov, J. Bloino, G. Zheng, J. L. Sonnenberg, M. Hada, M. Ehara, K. Toyota, R. Fukuda, J. Hasegawa, M. Ishida, T. Nakajima, Y. Honda, O. Kitao, H. Nakai, T. Vreven, J. A. Montgomery, Jr., J. E. Peralta, F. Ogliaro, M. Bearpark, J. J. Heyd, E. Brothers, K. N. Kudin, V. N. Staroverov, R. Kobayashi, J. Normand, K. Raghavachari, A. Rendell, J. C. Burant, S. S. Iyengar, J. Tomasi, M. Cossi, N. Rega, J. M. Millam, M. Klene, J. E. Knox, J. B. Cross, V. Bakken, C. Adamo, J. Jaramillo, R. Gomperts, R. E. Stratmann, O. Yazyev, A. J. Austin, R. Cammi, C. Pomelli, J. W. Ochterski, R. L. Martin, K. Morokuma, V. G. Zakrzewski, G. A. Voth, P. Salvador, J. J. Dannenberg, S. Dapprich, A. D. Daniels, Ö. Farkas, J. B. Foresman, J. V. Ortiz, J. Cioslowski, D. J. Fox, Gaussian, Inc., Wallingford CT, 2009.
27. E. Ruiz, J. Cano, S. Alvarez, P. Alemany, *J. Comput. Chem*., 1999, **20**, 1391-1400.
28. E. Ruiz, S. Alvarez, A. Rodríguez-Fortea, P. Alemany, Y. Pouillon, C. Massobrio, *Magnetism: Molecules to Materials* (Eds.: J. S. Miller, M. Drillon), Wiley-VCH, Weinheim, Germany, 2001, **2**, 5572.
29. E. Ruiz, A. R. -Fortea, J. Cano, S. Alvarez, P. Alemany, *J. Comput. Chem*., 2003, **24**, 982-989.
30. E. Ruiz, S. Alvarez, J. Cano, V. Polo, *J. Chem. Phys*., 2005, **123**, 164110-164117.
31. P. J. Baesjou, W. L. Driessen, J. Reedjic, A. L. Spek, *Inorg. Chim. Acta*, 2000, **306**, 237-240.
32. C. Adhikari, S. Koner, *Coord. Chem. Rev*., 2010, **254**, 2933-2958.
33. J. H. Aiu, Z. R. Liao, X. J. Meng, L. Zhu, Z. M. Wang, K. B. Yu, *Polyhedron*, 2005, **24**, 1617-1623.
34. L. Y. Wang, B. Zaho, C. X. Zhang, D. Z. Liao, Z. H. Jiang, S. P. Yan, *Inorg. Chem*., 2003, **43**, 5804-5806.

35. E. Q. Gao, S. Q. Bai, Z. M. Wang, C. H. Yan, *J. Am. Chem. Soc.*, 2003, **125**, 4984-4985.
36. F. Murata, M. Arakawa, A. Nakao, K. Satoh, Y. Fukuda, *Polyhedron*, 2007, **26**, 1570-1578.
37. O. Kahn, M. F. Charlot, *Novu. J. Chim.*, 1980, **4**, 567-576.
38. O. Castillo, A. Luque, P. Román, F. Lloret, M. Julve, *Inorg. Chem.*, 2001, **40**, 5526-5535.
39. H. Oshio, U. Nagashima, *Inorg. Chem.*, 1992, **31**, 3295-3301.
40. O. Castillo, A. Luque, F. Lloret, P. Román, *Inorg. Chim. Acta*, 2001, **324**, 141-149.
41. M. L. Calatayud, I. Castro, J. Sletten, F. Lloret, M. Julve, *Inorg. Chim. Acta*, 2000, **300–302**, 846-854.
42. O. Castillo, A. Luque, F. Lloret, P. Roman, *Inorg. Chem. Commun.*, 2001, **4**, 350-353.
43. B. Bag, N. Mondal, S. Mitra, V. Gramlich, J. Ribas, M. S. El. Fallah, *Polyhedron*, 2001, **20**, 2113-2116.
44. M. Du, Y. M. Guo, X. H. Bu, *Inorg. Chim. Acta*, 2002, **335**, 136-140.
45. S. Youngme, G. A. V. Albada, N. Chaichit, P. Gunnasoot, P. Kongsaeree, I. Mutikainen, O. Roubeau, J. Reedijk, U. Turpeinen, *Inorg. Chim. Acta*, 2003, **353**, 119-128.
46. A. Bauzá, T. J. Mooibroek, A. Frontera, *Chem. Commun*., 2015, **51**, 1491-1493.
47. S. Saha, A. Sasmal, G. Pilet, A. Bauzá, A. Frontera, S. Mitra, *Cryst. Eng. Comm.*, 2014, **16**, 654-666.
48. A. Choudhary, D. Gandla, G. R. Krow, R. T. Raines, *J. Am. Chem. Soc.*, 2009, **131**, 7244-7246.
49. F. Weinhold, R. A. Klein, *Angew. Chem. Int. Ed*., 2014, **53**, 11214-11217.
50. R. F. W. Bader, *Chem. Rev.*, 1991, **91**, 893-928.
51. M. Nishio, *Cryst. Eng. Comm.*, 2004, **6**, 130-158.
52. B. K. Mishra, *J. Phys. Chem. A*, 2005, **109**, 6-8.

CHAPTER 4

Formation of supramolecular associations involving C–H···Cl and π···π interactions in M^{II} - 2,2':6',2"-terpyridine complexes (M: Ni, Cu): Synthetic and theoretical perspective

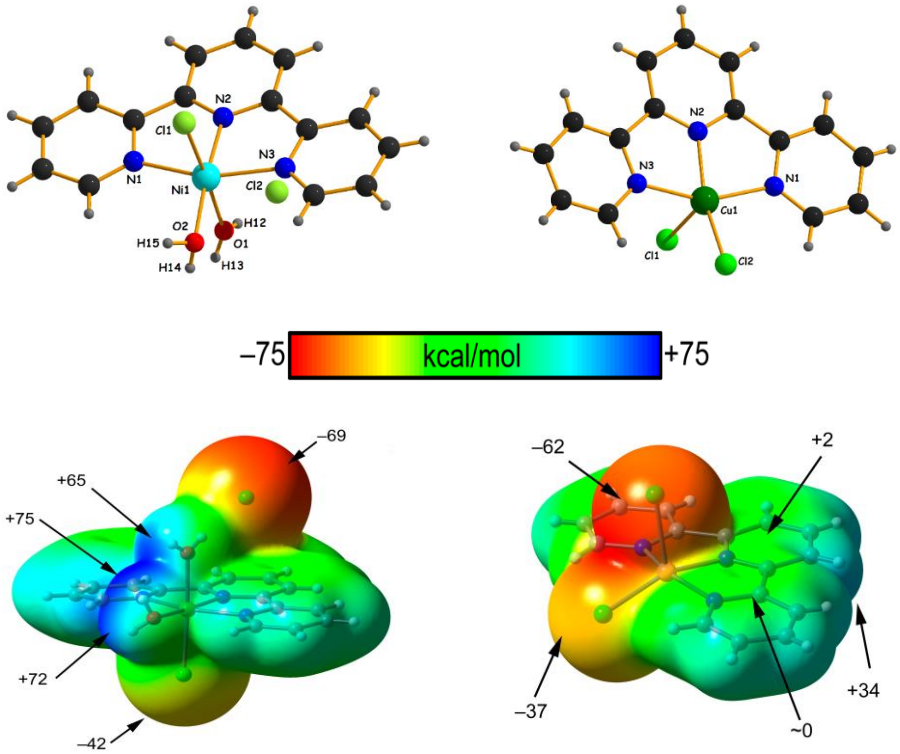

Published in New Journal of Chemistry, 2020, 44, 7310-7318

Formation of supramolecular associations involving C–H···Cl and π···π interactions in M^{II} - 2,2':6',2"-terpyridine complexes (M: Ni, Cu): Synthetic and theoretical perspective

4.1. INTRODUCTION

Noncovalent interactions namely intra and intermolecular hydrogen bonding, hydrophobic interaction, dispersion interaction, halogen bonding, cation···π, C–H···π, π···π, N–H···π, S–H···π, lone pair···π, salt bridge···π arrest significant interests beside traditional covalent interactions to elucidate the outstanding importance of such weak chemical forces in controlling both structure and function of macromolecules in current years [1-3]. Although these interactions were recognized approximately three decades ago, their significant roles in controlling structural integrity have been established in recent years [2, 3]. Quantification of these weak non-covalent interactions that direct the molecular aggregation into supramolecular assembly is of necessary importance [4, 5]. Hydrogen bonding has been extremely well studied and recognized as the most important of all noncovalent interactions [6, 7]. In classical notation of the hydrogen bond as D–H···A, reflects the strongly polar hydrogen bond donor groups D–H (D = O, N, or halogen) on one side and hydrogen bond acceptor atoms A (A = O, N, halogen, etc.) on the other. In contrary, a weak non-traditional hydrogen bond of type C–H···X (X: halogen atoms) arrests interest in the broad field of host–guest chemistry and anion recognition. In addition to commonly occurring C–H···N/ O hydrogen bonding the existence of C–H···Cl hydrogen bonding is much less frequent but well appreciated in recent years [8-10]. If the heterocyclic ring is associated with a donor moiety that reduces the electron density in the ring that in turn induces the ring C–H groups to produce C–H···Cl hydrogen bonding interaction [11]. For having a good C–H···Cl interaction, it has been reported that the C–H···Cl distance should be less than the sum of the van der Waals radii (2.95Å) of the hydrogen atom and the neutral chlorine atom [12]. Here in this present work the aforesaid distances range from 2.64 to 2.82 Å.

The π···π non covalent interaction is rather frequent for transition metal complexes that may play a significant role in formation of a supramolecular architecture. For such interaction a preferable geometrical conformation is required through which the π lobes of aromatic 'N' containing ligands should place either face to face or to some extent parallel having distance up to 3.8 Å [13]. Here the said distance ranges from 3.49 to 3.74 Å.

2,2′:6′,2″-terpyridine or their structural analogs are one of the prototypes oligopyridine metal-binding motifs that play a pivotal role in metallo-supramolecular chemistry and have grown much interest in contemporary research as functional templates in the fields of coordination chemistry as well as materials science [14-16]. The chelating ability of 2,2′:6′,2″-terpyridine enhances the stability of the metal complex, and planarity of the ligand leads to strong intercalative interaction of the complex in biological systems [17]. This ligand used as renowned building blocks in supramolecular chemistry because of its π stacking ability [18-20], H-bond acceptor sites and possibility of formation of either anion···π, metal cation···π depending on the acidity/ basicity of the π-cloud, which depends on the coordination (type of metal and its oxidation state). Hence many metal complexes have been synthesized chemically using 2,2′:6′,2″- terpyridine which prefers to adopt a planar geometry to get maximum conjugation, thus containing three nitrogen atoms in *cis*, *cis* fashion. Therefore, it acts as N–heterocycle that has very high binding potentiality towards the transition metal ions due to dπ–pπ* back bonding of the metal to pyridine rings and chelate effect [21].

The crystal as a whole is an organization of different kind of supramolecular interactions. The introduction of the supramolecular synthons concept was an extremely important step for easy understanding of the organization of molecular crystals. The concept of supramolecular synthons is nothing but a retrosynthetic approach to supramolecular chemistry where one can fragment the crystal structures into supramolecular synthons, and based on their relative abundance in the crystallographic database, new synthetic strategies can be planned. Therefore, when one starts with a crystal structure and deconstructs it to the smallest non reducible unit, i.e., synthon, both geometrical and chemical factors get deconstructed, and it is here where synthons score over individual molecules (or functional groups) in terms of consistency and robustness [22]. This created an opportunity for the preparation of molecular crystals with targeted patterns of binding between molecules similar to the synthesis of organic molecules using molecular building blocks or synthons [23].

Two terpyridine derived transition metal complexes have been synthesized [complex **1** bears Ni(II) as metal center and **2** has Cu(II)] in aqueous methanol solvent. Strategically 1:1 molar ratio is maintained to synthesize mixed ligand complexes (to avoid *bis*-terpyridine complexes) having at least one chlorine coordinated to metal centers. In both complexes title ligand acts as a neutral tridentate NNN donor in *cis*, *cis*- fashion to execute more effective binding through chelate rings around the metal centers. Unlike other metal cations, Cu(II) is

not regarded to take part in a cation···π interaction because this metal tends to oxidize the π electron system [24]. To the best of my knowledge this is the first example of a Cu(II) complex derived from 2,2′:6′,2″-terpyridine that exhibits Cu(II)···π interaction. For **1**, an intermolecular π···π stacking interaction results a 1D arrangement which is further extended through two different types of O–H···Cl hydrogen bonding to ensure a 2D arrangement. Another 2D chain was constituted by only intermolecular H-bonding of both C–H···Cl and O–H···Cl types. Complex **2** shows a dimeric distribution utilizing a metal cation···π interaction which in turn connected through two types of π···π interaction results to execute a 2D assembly. A variety of 2D layer is generated comprising only different kinds of π···π interactions. Finally, complex **2** utilizes two different C–H···Cl intermolecular H-bonding in two different planes that are able to constitute another 2D arrangement.

Finally, it combines theory (DFT calculations) and experiment to analyze the noncovalent interactions and their interplay governing the solid-state architecture of complexes **1** and **2**. In particular, the influence of intermolecular C–H···Cl and π···π interaction along with other non-covalent interactions like O–H···Cl, anion···π, cation···π is investigated using $[LM(Cl)_x]$ (x= 1 or 2, M = Ni, Cu) unit as the key building block.

4.2. EXPERIMENTAL SECTION

4.2.1. Materials and Physical Measurements

All chemicals were of reagent grade, purchased from commercial sources and used without further purification. 2,2′:6′,2″-terpyridine (**L**) and methanol were purchased from Aldrich Chemical Company, USA and used without further purification. All reactions were carried out in aerobic condition and in methanol-water medium (Scheme 4.1). During the whole experiment freshly boiled, doubly distilled water was used. Perkin-Elmer RXI FT-IR spectrophotometer was used to record the IR spectra in the range of 4000−400 cm^{-1} and Elemental analyses (carbon, hydrogen and nitrogen) of the metal complexes were determined with a Perkin–Elmer CHN analyzer 2400. UV-Vis-NIR spectra for both **1** and **2** were collected on UV-Visible/ NIR spectrophotometer Hitachi UH 4150. The PXRD data of the powdered sample were collected on a Rigaku-TTRAX-III diffractometer using Cu Kα radiation (λ = 1.5406 Å). Thermogravimetric analysis (TGA) data were collected with an SDT 2960 thermoanalyzer under nitrogen (50°C to 850°C) at a heating rate of 10°C per minute for both

the complexes. The room temperature magnetic moments of the complexes were taken from magnetic susceptibility balance MK1 Sherwood.

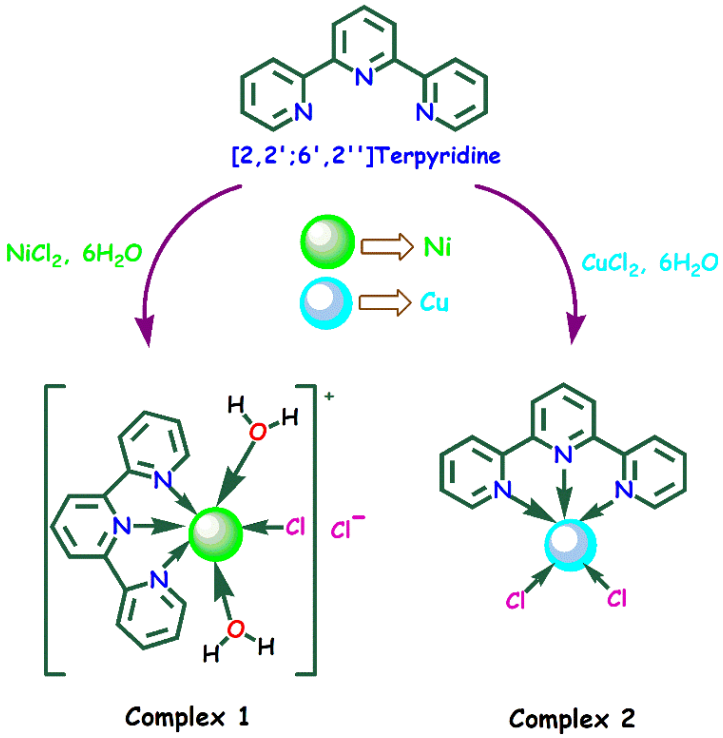

Scheme 4.1: Schematic representations of the synthesis of complex **1** and **2**

4.2.2. Synthesis

4.2.2.1. *Synthesis of [Ni(L)Cl(H$_2$O)$_2$]Cl (Complex 1)*

A methanolic solution (10 mL) of the ligand '**L**' (0.233g, 1mmol) was added drop wise to a solution of $NiCl_2$, $6H_2O$ (0.237g, 1mmol) in the same solvent (10 mL) with constant stirring which continued for 3 hours. Then the solution was filtered and the filtrate was left for slow evaporation. After one-week, deep green X-ray quality crystals of **1** were isolated. (Yield: 67%). Anal. Calc. for $C_{15}H_{15}NiN_3O_2Cl_2$: C, 45.12; H, 3.76; N, 10.52. Found: C, 44.98; H, 3.69; N, 10.17%. Main FT- IR absorptions, (KBr, cm^{-1}): 3207 (s), 3057 (s), 3018 (s), 1599 (vs), 1576 (s), 1477 (s), 1451 (s), 1323 (w), 1253 (m) (Fig. 4.1). $\lambda_{max/\ nm}$ = 281, 447 and 581 (Fig. 4.2). Room temperature magnetic moment (μ_{eff}) = 2.99 B.M.

4.2.2.2. *Synthesis of [Cu(L)Cl_2] (Complex 2)*

A methanolic solution (20 mL) of the ligand '**L**' (0.233g, 1mmol) was added drop wise to a solution of $CuCl_2$, $6H_2O$ (0.242g, 1mmol) in the same solvent (10 mL) with constant stirring for 2 hours. Then the green colored solution was filtered and the filtrate was kept undisturbed for slow evaporation. After one-week, green X-ray quality crystals of **2** were obtained. (Yield: 63.5%). Anal. Calc. for $C_{15}H_{11}CuN_3Cl_2$: C, 48.97; H, 2.99; N, 11.42. Found: C, 48.67; H, 2.91; N, 11.33%. Main FT- IR absorptions, (KBr, cm^{-1}): 3087 (s), 3013 (s), 2965 (s), 1598 (s), 1575 (m), 1473 (s), 1448 (s), 1327 (m), 1252 (m) (Fig. 4.3). $\lambda_{max/\ nm}$ = 377 and 469 (Fig. 4.4). Room temperature magnetic moment (μ_{eff}) = 1.83 B.M.

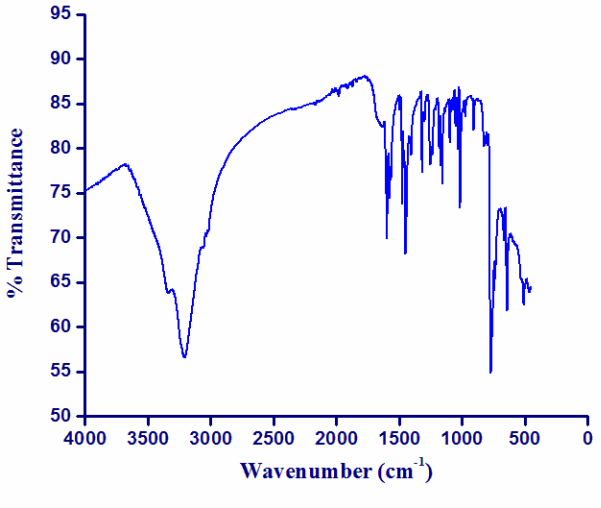

Fig. 4.1: IR spectra for Complex **1**

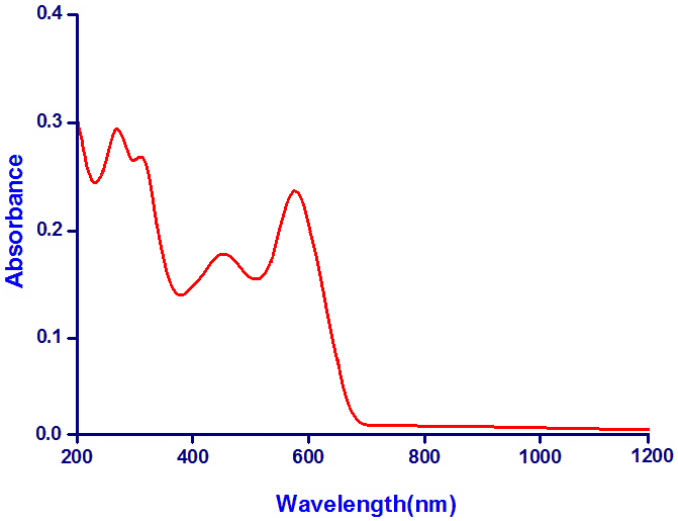

Fig. 4.2: UV-Vis-NIR spectra for Complex **1**

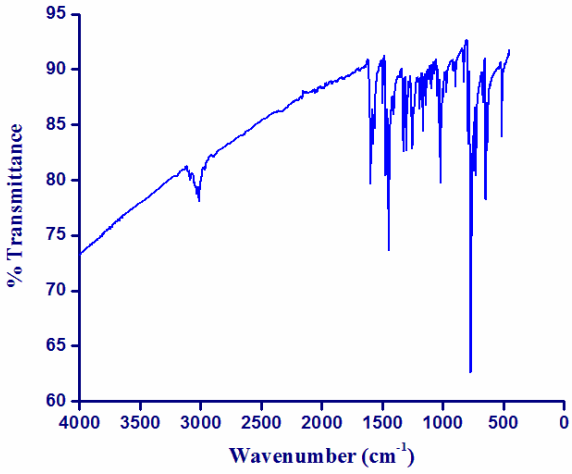

Fig. 4.3: IR spectra for Complex **2**

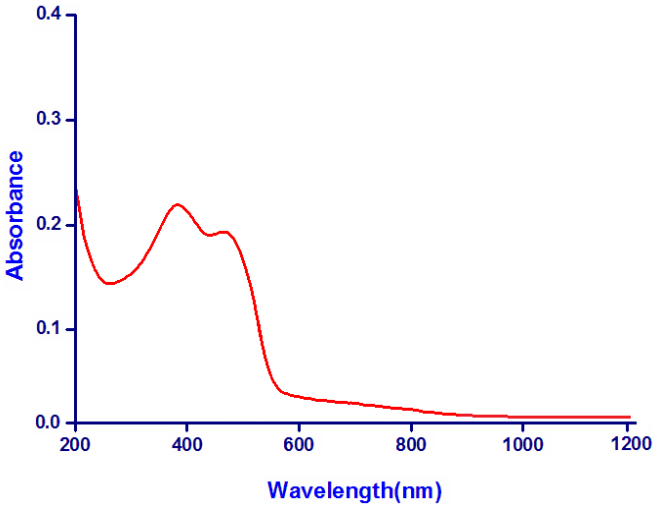

Fig. 4.4: UV-Vis-NIR spectra for Complex **2**

4.2.3. X-ray Crystallographic Analysis

Data collections were made using Bruker SMART APEX II CCD area detector equipped with graphite monochromated Mo Kα radiation (λ = 0.71073 Å) source in φ and ω scan mode at 293(2) K for **1** and 273(2) K for **2**. Cell parameters refinement and data reduction were carried out using the Bruker SMART APEX II. Cell parameters refinement and data reduction were carried out using Bruker SMART and Bruker SAINT softwares [25] for all the complexes.

Table 4.1: Selected crystallographic features of structures **1** and **2**

Compound	**1** **(CCDC: 1922811)**	**2** **(CCDC: 1922812)**
Empirical formula	$C_{15}H_{15}Cl_2N_3NiO_2$	$C_{15}H_{11}Cl_2CuN_3$
Formula weight	398.89	367.72
Temperature (K)	293 K	273 K
Wavelength (Å)	0.71073	0.71073
Crystal system	Monoclinic	Monoclinic
Space group	P $2_1/n$	P $2_1/c$
Unit cell dimensions		
a (Å)	12.485(6)	10.671(10)
b (Å)	9.687(4)	8.258(7)
c (Å)	14.318(6)	16.090(16)
α (°)	90	90
β (°)	105.290(15)	94.686(3)
γ (°)	90	90
Volume ($Å^3$)	1670.4(13)	1413.2(2)
Crystal size (mm^3)	0.07x0.13x0.21	0.08x0.12x0.17
z	4	4
$Density_{cal}$ (Mgm^{-3})	1.586	1.728
Absorption coefficient (mm^{-1})	1.492	1.917
F(000)	816.0	740.0
θ Range (˚) for data collection	2.87 – 25.88	1.915 – 27.218
Index ranges	$-16 \le h \le 16$ $-12 \le k \le 12$ $-18 \le l \le 18$	$-13 \le h \le 13$ $-10 \le k \le 10$ $-20 \le l \le 20$
Goodness-of-fit on F^2	0.893	0.938
Independent reflections [R_{int}]	3686 (0.035)	3130
Absorption correction	Multi-scan	Multi-scan
Refinement method	Full-matrix least squares on F^2	Full-matrix least squares on F^2
Data/restraints/parameters	3686/ 0/ 224	3130/ 0/ 234
Reflections collected	24244	20311
Final R indices [I > 2σ (I)]	R=0.0273 wR_2=0.1204	R=0.0240 wR_2=0.1103
Largest difference peak & hole($eÅ^{-3}$)	-1.27, 0.83	-0.92, 0.83

The structure of both the complexes were solved by conventional direct methods and refined by full-matrix least square methods using F^2 data. SHELXS-97 and SHELXL-97 programs [26] were used for structure of all the complexes solution and refinement respectively. CCDC 1922811 (**1**) and 1922812 (**2**) include additional crystallographic information. Selected crystal data for **1** and **2** is given in Table 4.1 and selected metrical parameters of the complexes were given in Table 4.2.

Table 4.2: Selected bond distances (Å) and angles (°) in **1** and **2**

Selected Bonds	Value (Å)	Selected Angles	(°)
Complex 1			
Ni1–N1	2.105(2)	N1–Ni1–N2	78.65(9)
Ni1–N2	1.985(19)	N2–Ni1–N3	78.69(9)
Ni1–N3	2.087(2)	N2–Ni1–O2	174.33(8)
Ni1–O1	2.097(2)	N2–Ni1–O1	91.07(8)
Ni1–O2	2.055(18)	N3–Ni1–O2	98.01(8)
Ni1–Cl1	2.386(13)	N3–Ni1–N1	157.34(9)
		Cl1–Ni1–O1	174.75(6)
		Cl1–Ni1–O2	90.51(5)
		N1–Ni1–O2	104.59(8)
		N3–Ni1–O1	89.04(9)
		Cl1–Ni1–N1	89.67(6)
		Cl1–Ni1–N2	94.18(6)
		Cl1–Ni1–N3	91.90(6)
		O2–Ni1–O1	84.25(8)
Complex 2			
Cu1–N1	2.055(18)	N1–Cu1–N2	78.96(7)
Cu1–N2	1.961(16)	N2–Cu1–N3	78.82(7)
Cu1–N3	2.057(17)	Cl1–Cu1–N1	99.51(5)
Cu1–Cl1	2.469(6)	Cl1–Cu1–N2	98.36(5)
Cu1–Cl2	2.249(6)	Cl1–Cu1–N3	92.57(5)
		Cl1–Cu1–Cl2	104.39(2)
		Cl2–Cu1–N1	97.24(5)
		Cl2–Cu1–N2	157.25(5)
		Cl2–Cu1–N3	99.74(5)
		N1–Cu1–N3	156.00(7)

4.3. THEORETICAL METHODS

To compute the interaction energies in the solid state the crystallographic coordinates at the PB1PBE-D3/def2-TZVP level of theory have been used where only the position of the H-atoms has been optimized. For the calculations, the GAUSSIAN-16 program has been used

[27]. The D3 Grimme's dispersion correction has also been used as implemented in GAUSSIAN-16 program since it is adequate for the evaluation of non-covalent interactions where dispersion effects are relevant like those reported herein [28]. The basis set superposition error for the calculation of interaction energies has been corrected using the counterpoise method [29]. The NCI index and NCI plot isosurfaces have been used to characterize the non-covalent interactions [30]. They correspond to both favorable and unfavorable interactions, as differentiated by the sign of the second density Hessian eigenvalue and defined by the isosurface color. The color scheme is a red-yellow-green-blue scale with red for ρ^{+}_{cut} (repulsive) and blue for ρ^{-}_{cut} (attractive), whereas yellow and green isosurfaces correspond to weak repulsive and weak attractive interactions, respectively [31].

4.4. RESULTS AND DISCUSSION

Single-crystal X-ray structural analysis confirms that the asymmetric unit of the title complexes consist of one heterocyclic ligand (**L**) [2,2′: 6′,2″-terpyridine] moiety with nickel (II), chloride ion and solvent water molecules (in **1**) and copper (II) and chloride ions (in **2**). In both complexes, the ligand (**L**) acts as a neutral tridentate NNN donor moiety in cis, cis- fashion and form two five membered chelate rings around the central metal ions. The molecular representation with atom numbering scheme (only coordinated atom numbering was done for maintaining the clarity of the picture) of the complexes are shown in Fig. 4.5 and 4.6**.**

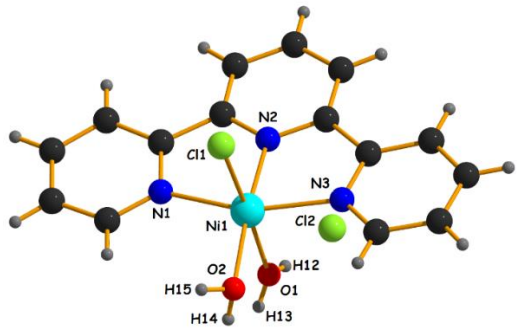

Fig. 4.5: Asymmetric unit of Complex **1**

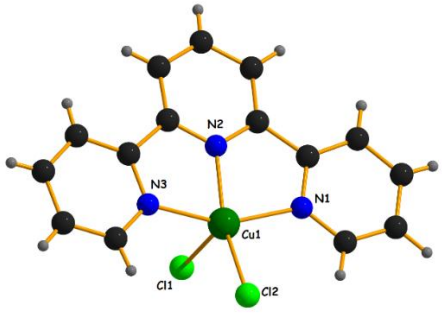

Fig. 4.6: Asymmetric unit of Complex **2**

PXRD has been carried out at room temperature with the powdered sample of both the complexes (**1** and **2**). The bulk purity of both the complexes has been confirmed by PXRD pattern. The major peaks of the PXRD pattern of the synthesized complexes match well with the simulated pattern generated from the single crystal data (Fig. 4.7), representing phase purity of the bulk. The minor shifts and the differences in the intensities might be attributed to the changes either in crystal lattice orientation with respect to an inertial frame of reference or sample thickness. It might also be due to the baseline drift of the PXRD diffractometer and the temperature difference in measuring for single crystal diffraction and powered X-ray diffraction [32, 33].

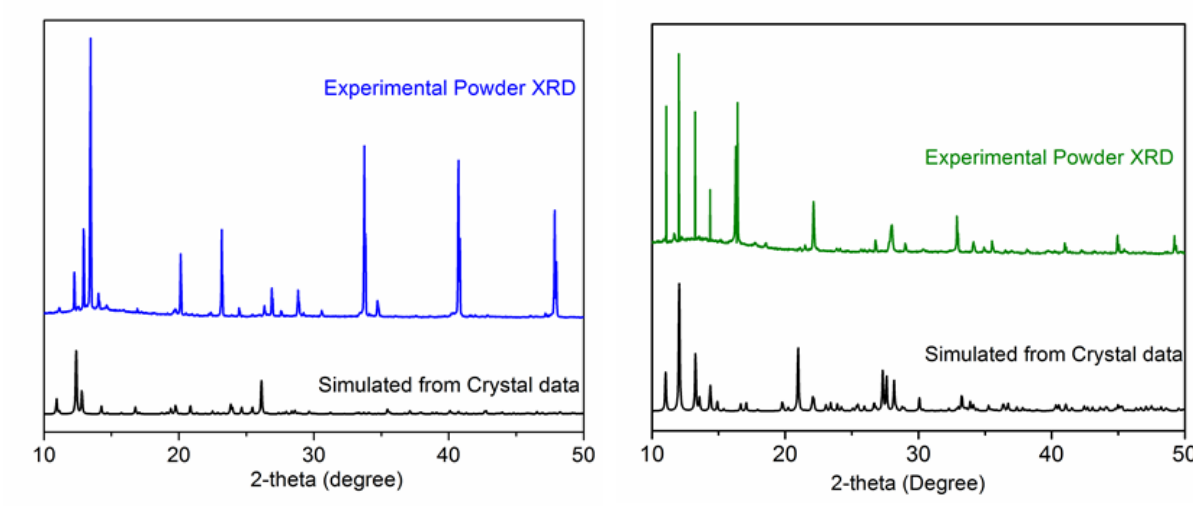

Complex 1 **Complex 2**

Fig. 4.7: PXRD patterns of experimental powder XRD (blue) for complex **1** and green for complex **2** and simulated pattern from single crystal data (black)

4.4.1. Structural description of Complex 1

The perspective view of molecular structure of complex **1** with atom numbering scheme is shown in Fig. 4.5 whereas selected bond lengths (Å) and bond angles (°) are listed in Table 4.2. Complex **1** crystallizes in a space group $P2_1/n$ and unit cell is comprised of four molecules. Complex **1** is distorted octahedral where the title ligand (**L**) spans in meridional position [N1–Ni1–N2 = 78.65(9)°, N2–Ni1–N3 = 78.69(9)° and N3–Ni1–N1 = 157.34(9)°] as a neutral tridentate NNN donor via three pyridyl nitrogen atoms (N1, N2 and N3). The residual positions of the octahedral geometry are satisfied by two oxygen atoms from two different water molecules (O1 and O2) and one chloride atom (Cl1). The monopositive charge of **1** is taken care by another chloride ion (Cl2) present at the outside of the metal coordination sphere.

In **1** among three *trans* angles two [N2–Ni1–O2 = 174.33(8)^o and Cl1–Ni1–O1 = 174.75(6)^o] are close to ideal 180^o while the rest one [N3–Ni1–N1 = 157.34(9)^o] was departed more may be due to small bite angles [N1–Ni1–N2 = 78.65(9)^o and N2–Ni1–N3 = 78.69(9)^o] of the tridentate ligand that possibly induces a distortion in this *trans* angle and in overall octahedral geometry (Table 4.2). The average Ni–N and Ni–O bond distances are 2.059 Å [Ni1–N1 = 2.105(2) Å, Ni1–N2 = 1.9854(19) Å and Ni1–N3 = 2.087(2) Å] and 2.076Å [Ni1–O1 = 2.097(2) Å and Ni1–O2 = 2.0557(18) Å] respectively, which are in accord with previously reported six coordinated Ni(II) complexes [34]. Ni1 atom sits almost in the same mean plane (deviated by only 0.04 Å) constituted by O2N1N2N3. The monomeric unit of complex **1** propagates to ensure a 1D polymeric association through a π···π interaction (Table 4.3) between Cg(3) of one unit with Cg(5) of other unit (Fig. 4.8).

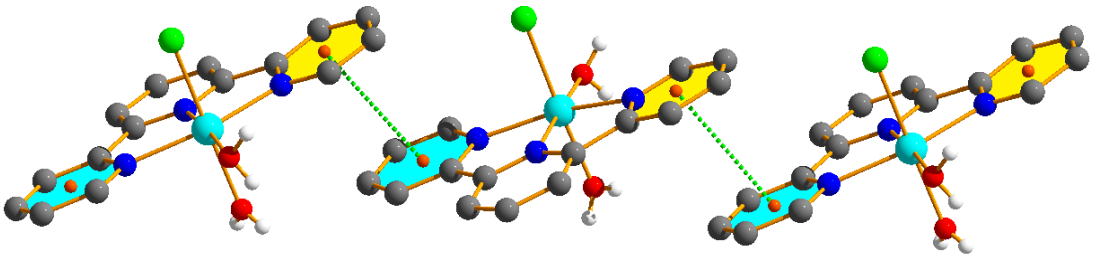

Fig. 4.8: 1D chain of **1** incorporating π···π interaction [π···π interaction is shown by green dotted lines, Cg(3): yellow coloured filled rings and Cg(5): aqua coloured filled rings]. Aromatic hydrogen atoms have been omitted for clarity.

Table 4.3: Geometric features (distances in Å and angles in degrees) of π···π interactions obtained for **1**

Cg(ring I) - Cg(ring J)	Cg···Cg (Å)	Cg(I) ···perp (Å)	Cg(J) ···perp (Å)	α (°)	β (°)	γ (°)	Symmetry
Cg(3)···Cg(5)	3.593(2)	3.453	3.493	2.84	13.53	16.04	-1/2+x, 1/2-y, -1/2+z
Cg(5)···Cg(3)	3.593(2)	3.493	3.453	2.84	16.04	13.53	1/2+x, 1/2-y,1/2+z

α = Dihedral angle between ring I and ring J (°); β = Cg(I) →Cg(J) or Cg(I) → Me vector and normal to plane I (°); γ = Cg(I) → Cg(J) vector and normal to plane J (°); Cg···Cg = distance between ring centroids (Å); Cg(I)···Perp = perpendicular distance of Cg(I) on ring J (Å); Cg(J)···Perp = perpendicular distance of Cg(J) on ring I (Å).

Cg(3) = Centre of gravity of ring [N1/C1/C2/C3/C4/C5] and Cg(5) = Centre of gravity of ring [N3/C11/C12/C13/C14/C15] for complex **1**.

This 1D arrangement is further extended to 2D layers using two different types of intermolecular hydrogen bonding (Table 4.4).

Table 4.4: Details of Hydrogen bond distances (Å) and angles (°) for **1**

D – H ···A	D (D – H)	D (HA)	D(D···A)	<DHA
O1–H12···Cl2	0.78(4)	2.28(4)	3.052(3)	173(3)
O1–H13···Cl2	0.72(3)	2.44(4)	3.115(3)	156(4)
O2–H15···Cl1	0.83(4)	2.26(4)	3.073(2)	167(3)
C4–H4···Cl1	0.93	2.82	3.693(3)	156

The first type (Type 1) of intermolecular hydrogen bonding was shaped by the hydrogen atom H15 (attached with O2 of coordinated water molecule) of one unit and the coordinated chlorine atom (Cl1) that leads to the formation of $R_2^2(8)$ ring motif. Second type (Type 2) of intermolecular hydrogen bonding is formed by non-coordinated chloride ion (Cl2) and two hydrogen atoms (H12 and H13) from two different oxygen atom (O1) of coordinated water molecules belonging to two different complex units (Fig. 4.9). Thus π···π interaction along with these two types of H-bonding enhance the dimensionality from 1D to 2D.

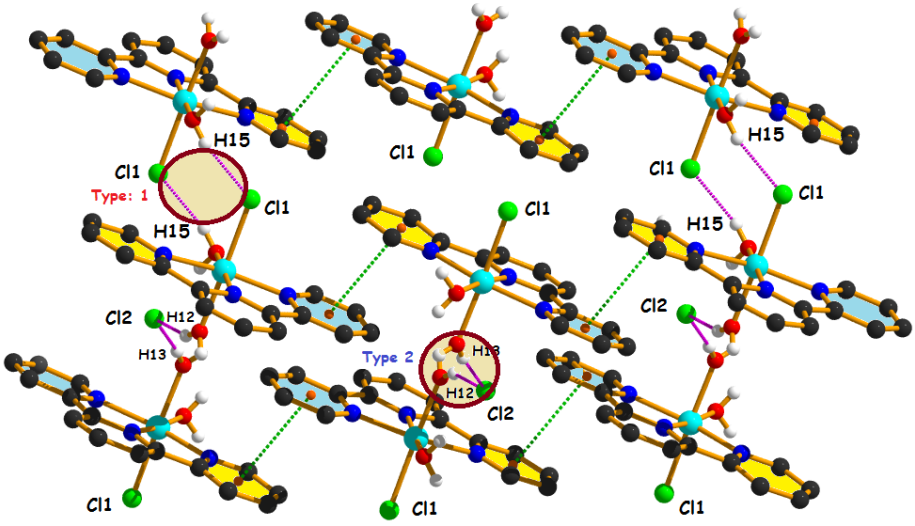

Fig. 4.9: 2D chain of **1** incorporating H-bonding and π···π interaction [π···π interaction is shown by green dotted lines and O – H···Cl hydrogen bonding is shown by pink dotted lines, Cg(3): yellow coloured filled rings and Cg(5): aqua coloured filled rings. Aromatic hydrogen atoms have been omitted for clarity].

A different 2D layer is formed in complex **1** using three different types of hydrogen bonding (Table 4.4). Type 1 and Type 2 have been already described above. The third type (Type 3) of intermolecular hydrogen bonding is formed between the hydrogen atom H4 attached to pyridine ring carbon C4 of one unit and coordinated chlorine atom, Cl1 from another complex unit) in association with other two types of intermolecular hydrogen bonding. It constitutes a new 2D architecture (Fig. 4.10). This 2D layer includes four different types of synthons namely $R_2^2(8)$, $R_2^2(16)$, $R_3^6(20)$ and $R_6^4(22)$.

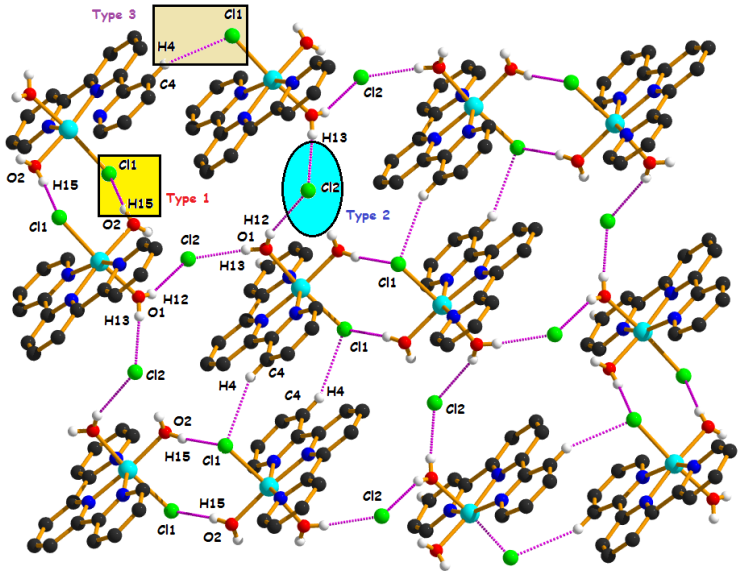

Fig. 4.10: 2D layer of **1** incorporating H-bonding interactions [O–H···Cl and C–H···Cl hydrogen bonding is shown by pink dotted lines. Aromatic hydrogen atoms have been omitted for clarity].

4.4.2. Structural Description of Complex 2

The molecular structure of Cu(II) complexes with atom numbering scheme is shown in Fig. 4.6 while its selected bond lengths (Å) and bond angles (°) are listed in Table 4.2. Complex **2** crystallizes in a monoclinic system under space group $P2_1/c$ and unit cell was contained of four molecules. Complex **2** is a mononuclear species comprising neutral $[Cu(L)Cl_2]$ where **L**: [2,2′: 6′,2″-terpyridine] molecule. Central Cu(II) ion is placed itself in a square pyramidal [the τ value [35] is 0.077, ideally 1 for trigonal bipyramidal geometry and 0 for square pyramidal geometry] pocket where the equatorial plane was constituted by the pyridyl nitrogen atoms (N1, N2 and N3) of terpyridine ligand and one chloride ion (Cl2) while the axial position was

occupied by another chloride ion (Cl1). Cu(II) ion is shifted by a distance of 0.327Å and 0.20Å towards apical Cl1 atom from the equatorial plane (N1N2N3Cl2) and pyridine plane (N1N2N3) respectively. Here ligand (**L**) is able to bind the metal ion through two five-membered chelate rings. The average Cu–N bond distance is 2.0246 Å [Cu1–N1 = 2.0552(18) Å, Cu1–N2 = 1.9614(16) Å and Cu1–N3 = 2.0572(17) Å]. The Cu(II)–nitrogen bond between Cu(II) and the central pyridine atom (N2) is somewhat shorter [Cu1–N2 = 1.9614(16) Å] than those concerning the terminal 'N' atoms (N1 and N3) (Table 4.2), which is usual and results from chelating ligand constrains [36-38]. The axial chloride (Cl1) is comparatively at a larger distance [Cu1–Cl1 = 2.4699(6) Å] than the equatorial one [Cu1–Cl2 = 2.2496(6) Å] likely due to the less 's' character of the orbital involved in the coordination bond, which makes axially coordinated chloride ion more electronegative (stronger hydrogen bond acceptor). The average axial-equatorial and equatorial-equatorial bond angles are 98.70^{o} and 88.69^{o} respectively. Equatorial trans angles Cl2–Cu1–N2 [157.25(5)^{o}] and N1–Cu1–N3 [156.00(7)^{o}] are departed from ideal trans angle 180^{o} due to steric and electronic effects. The electrical charge of the central Cu ion is compensated by two coordinated chloride ions (Cl1 and Cl2).

The existence of C–H···Cl hydrogen bonds along with charge-assisted terminal M–Cl bonds in particular, have been well appreciated in recent times besides commonly occurring C–H···N/ O/ S hydrogen-bonding interactions. Through a closer look it was evident that two different planes are propagating through intermolecular C–H···Cl hydrogen bonding [C2–H2···Cl1] (Table 4.5) incorporating the axially coordinated chloride ion (Cl1) to produce a 1D infinite chain (Fig. 4.11).

Table 4.5: Details of Hydrogen bond distances (Å) and angles (^{o}) for **2**

D – H ···A	**D (D – H) (Å)**	**D (HA) (Å)**	**D(D···A) (Å)**	**<DHA (^{o})**
C2–H2···Cl1	0.97(3)	2.76(3)	3.446(2)	128(2)
C4–H4···Cl1	0.88(3)	2.64(3)	3.479(2)	159(2)

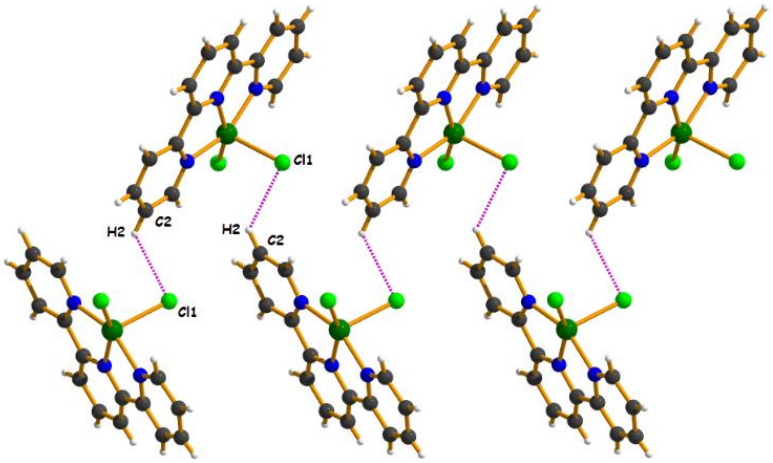

Fig. 4.11: Perspective view of the formation of a single 1D architecture of Complex **2** by H-bonding [C–H···Cl hydrogen bonding is shown by pink dotted lines].

In association with this intermolecular hydrogen bonding interaction another intermolecular hydrogen bonding interaction [C4–H4···Cl1] extends the dimensionality to 2D. Hence it is the perfect self-assembly of a [$CuLCl_2$] coordination motif held together by C–H···Cl hydrogen bonding interaction. Possibly the non-equivalency of the terminal chloride generated from square pyramidal geometry adopted by the central Cu(II) ion along with secondary C–H···Cl interaction provides the required turn almost orthogonally. In this 2D arrangement two different planes are propagating through intermolecular hydrogen bonding incorporating one coordinated chloride ion (Cl1). In individual planes ('A' and 'B') two complex units are oriented in such a manner so that hydrogen H4 (attached with pyridine C4) of one unit faces Cl1 atom of other unit. Now these two planes are connected by another intermolecular H-bonding forming between the aromatic fragment C2–H2 of 'plane A' and Cl1 atom of 'plane B' and vice versa. These two planes ('A' and 'B') are almost orthogonal (86^o) repeating alternately and repeating themselves alternately to enhance the dimensionality from 1D to 2D (Fig. 4.12).

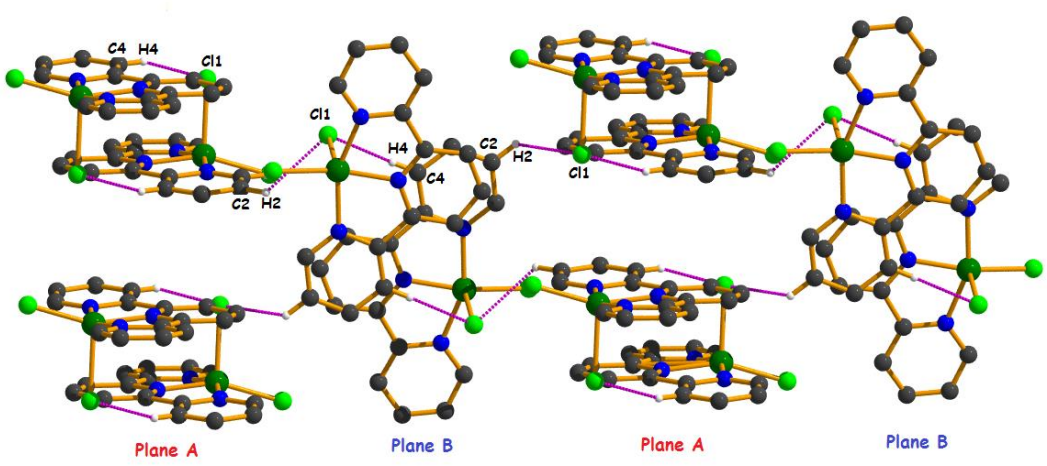

Fig. 4.12: 2D polymeric chain of Complex **2** by two different kinds of C–H···Cl hydrogen bonding [C–H···Cl hydrogen bonding is shown by pink dotted lines. Hydrogen atoms not involving in hydrogen bonding have been omitted for clarity].

In complex **2** a dimeric distribution is shown in Fig. 4.13 that is formed by a cation···π interaction which is quite unusual because Cu(II) likely to oxidize the π electron system. Here two units are arranged almost in opposite orientation one above another to accomplish a cation···π interaction (Table 4.6) between Cu(1) and Cg(5). The Cu···Cu separation in this dimeric integrity is 5.535Å.

Table 4.6: Geometric features (distances in Å and angles in degrees) of metal cation···π interaction obtained for complex **2**

Cation ···Cg	Cg(I)···Cation (Å)	Cation(J)···Perp (Å)	β (°)	Symmetry
Cu1···Cg (5)	3.848	3.465	25.8	1-x, 1-y, 1-z

Cg(5) = Centre of gravity of ring [N3/C11/C12/C13/C14/C15]

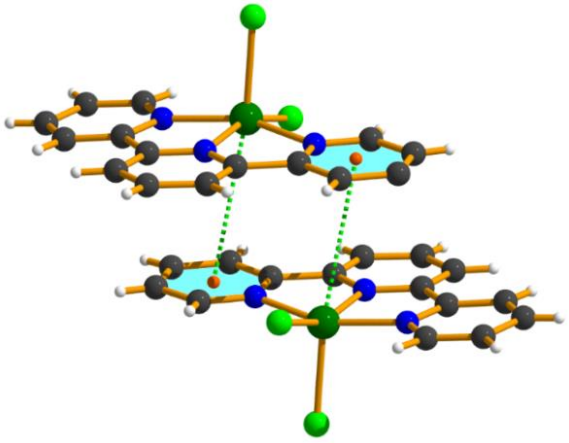

Fig. 4.13: Cation···π interaction in complex **2 [**Cu(II)···π interaction is shown by green dotted lines, Cg(5): aqua coloured filled rings].

The interplanar distances of successive terpyridine moieties suggest the possibilities of π···π interaction. Interestingly the dimeric units [through cation···π interaction as depicted in Fig. 4.13] of **2** forms a 1D chain implementing a π···π interaction between Cg(3) and Cg(4). Such kind of 1D chains are further stabilized though another π···π interaction (Table 4.7) between Cg(5) centroids of different layers almost parallel to increase the dimensionality (Fig. 4.14).

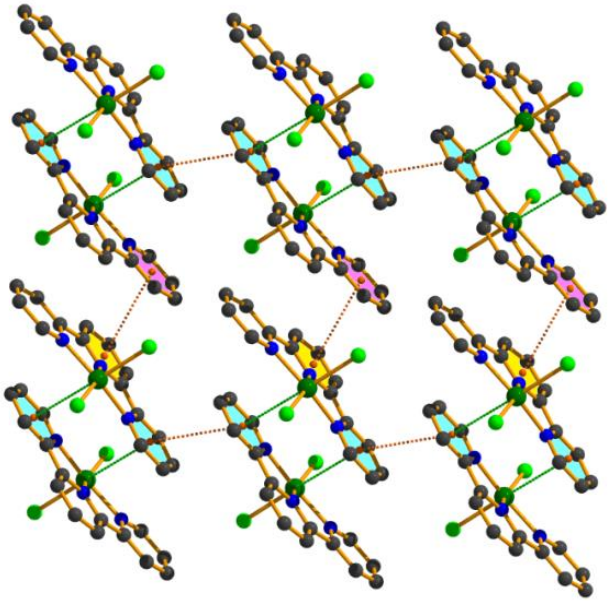

Fig. 4.14: 2D chain of **2** incorporating cation···π and π···π interaction [Cu(II)···π interaction is shown by green dotted lines and π···π interaction is shown by orange dotted lines, Cg(3): pink coloured filled rings, Cg(4): yellow coloured filled rings and Cg(5): aqua coloured filled rings].

Table 4.7: Geometric features (distances in Å and angles in degrees) of π···π interactions obtained for **2**

Cg(ring I) - Cg(ring J)	Cg···Cg (Å)	Cg(I) ···perp (Å)	Cg(J) ···perp (Å)	α (°)	β (°)	γ (°)	Symmetry
Complex 2							
Cg(1)···Cg(5)	3.4970(12)	3.277	3.342	5.59	17.11	20.43	1-x, 1-y, 1-z
Cg(5)···Cg(1)	3.4969(12)	3.342	3.277	5.59	20.43	17.11	1-x, 1-y, 1-z
Cg(2)···Cg(2)	3.5839(11)	3.348	3.348	0.02	20.90	20.90	1-x, 1-y, 1-z
Cg(2)···Cg(5)	3.5184(12)	3.346	3.354	2.51	17.56	18.02	1-x, 1-y, 1-z
Cg(5)···Cg(2)	3.5183(12)	3.354	3.346	2.51	18.02	17.56	1-x, 1-y, 1-z
Cg(3)···Cg(4)	3.7469(12)	3.341	3.473	4.93	22.05	26.9	-x, 1-y, 1-z
Cg(4)···Cg(3)	3.7468(12)	3.473	3.341	4.93	26.9	22.05	-x, 1-y, 1-z
Cg(4)···Cg(5)	3.6812(13)	3.299	3.281	2.31	26.95	26.34	1-x, 1-y, 1-z
Cg(5)···Cg(4)	3.6811(13)	3.281	3.299	2.31	26.34	26.95	1-x, 1-y, 1-z
Cg(5)···Cg(5)	3.6706(13)	3.288	3.288	0.02	26.40	26.40	1-x, -y, 1-z

α = Dihedral angle between ring I and ring J (°); β = Cg(I) →Cg(J) or Cg(I) → Me vector and normal to plane I (°); γ = Cg(I) → Cg(J) vector and normal to plane J (°); Cg–Cg = distance between ring centroids (Å); Cg(I)···Perp = perpendicular distance of Cg(I) on ring J (Å); Cg(J)···Perp = perpendicular distance of Cg(J) on ring I (Å).

Cg(1): Centre of gravity of ring [Cu1/N1/C5/C6/N2], Cg(2): Centre of gravity of ring [Cu1/N2/C10/C11/N3], Cg(3): Centre of gravity of ring [N1/C1/C2/C3/C4/C5], Cg(4): Centre of gravity of ring [N2/C6/C7/C8/C9/C10] and Cg(5): Centre of gravity of ring [N3/C11/C12/C13/C14/C15] for Complex **2**

Another interesting interpretation has been drawn from the structural integrity through different kinds of π···π interactions that play a crucial role in forming a different 1D polymeric chain. Here Cg(5) of one complex unit interacts simultaneously with Cg(1), Cg(2) and Cg(4) to form a dimeric unit. This dimeric unit is further stabilized by another π···π interaction, i.e., Cg(2)–Cg(2) (Table 4.7). Again the dimeric units are interconnected by Cg(3)···Cg(4) interaction which leads to the formation of a 1D chain (Table 4.7). All these cumulatively associated with another π···π interaction between two Cg(5) centroids of different 1D chain extrapolates to generate a 2D arrangement (Fig. 4.15).

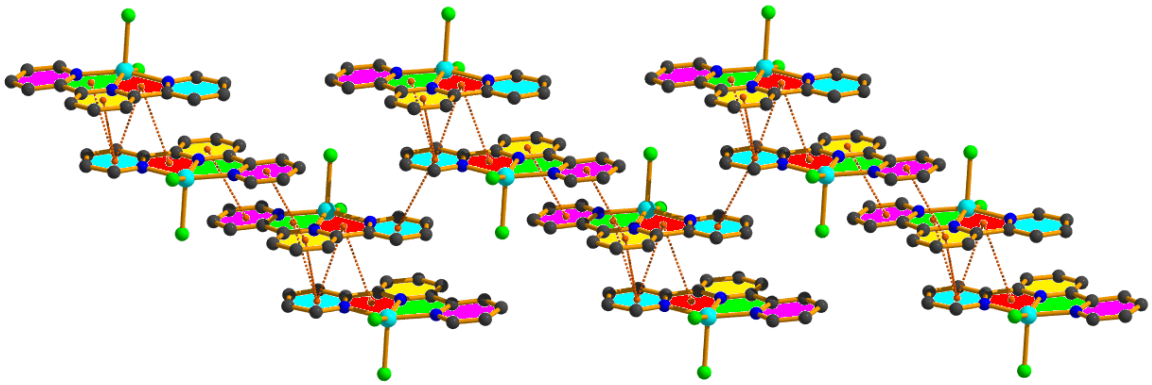

Fig. 4.15: 2D chain of **2** incorporating π···π interaction [π···π interaction is shown by orange dotted lines, Cg(1): green coloured filled rings, Cg(2): red coloured filled rings Cg(3): pink coloured filled rings, Cg(4): yellow coloured filled rings and Cg(5): aqua coloured filled rings].

4.4.3. Thermal analysis

Thermal analysis was carried out to obtain an insight into the thermal stability of the complexes. The TG curves for both the complexes are shown in Fig. 4.16.

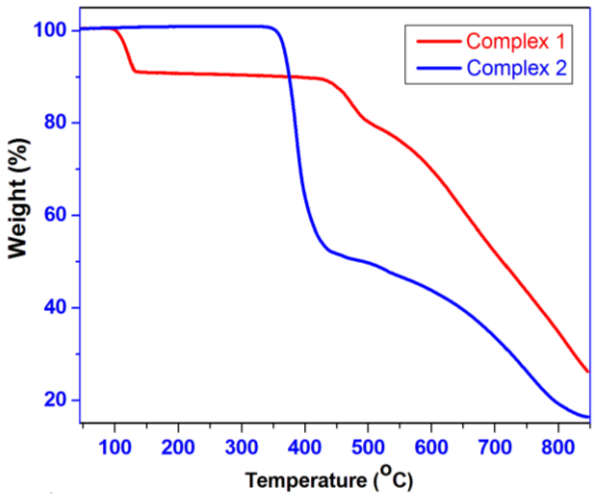

Fig. 4.16: TGA of Complex **1** and **2** measured under N_2 atmosphere

For complex **1**, it clearly shows that the complex is thermally stable up to 100°C. In the temperature range 100°C to 135°C, the complex **1** loses two coordinated water molecules (calculated mass loss 9%, found 8.7%). After that the complex **1** shows thermal stability up to 430°C even after removal of the two water molecules. The complex **1** then exhibits multistep decomposition after 430°C that did not exactly match with the calculated mass loss [21]. The TG curve for complex **2** displays that the complex is thermally stable up to 350°C and then

decomposes with no evident intermediate steps found in the TG analysis. The thermal decomposition pattern of complex **2** is complicated and no definite conclusion can be drawn as weight loss at different stages cannot be matched with the predicted decomposition and consequent loss in weight indicating multistep decomposition [39].

4.4.4. Theoretical study

First of all, the molecular electrostatic potential (MEP) surfaces of complexes **1** and **2** have been computed in order to know the most electrophilic and nucleophilic parts of the complexes. The MEP surfaces for both compounds are illustrated in Fig. 4.17 and, for complex **1** [Fig. 4.17 (a)], the most positive region (+75 kcal/mol) is located at the H-atoms of the coordinated water molecules. The acidity and thus the ability of these H-atoms to participate in H-bonding interactions is enhanced due to the coordination of the O-atom to the Ni(II) metal center. The most negative region corresponds to the chloride counterion (–69 kcal/mol) and the coordinated chlorido ligand also exhibits a large and negative MEP value (–42 kcal/mol). In complex **2** [Fig. 4.17 (b)], the most positive region is located at the aromatic H-atoms (+34 kcal/mol) and the most negative value at the axial chlorido ligand (–62 kcal/mol) that is considerably more negative than the other chlorido ligand (–37 kcal/mol). The MEP values over the aromatic rings are very small or negligible.

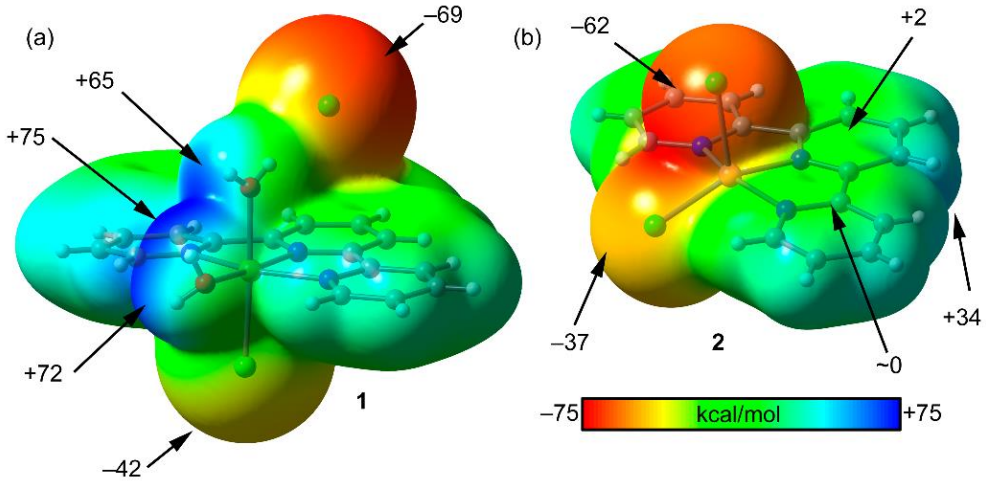

Fig. 4.17: MEP surfaces of complex **1** (a) and **2** (b) using the 0.001 a.u. isosurface at the PBE1PBE-D3/def2-TZVP level of theory. The values at selected points of the surface are indicated in kcal/mol.

The theoretical models used to evaluate the different assemblies observed in the solid state of complex **1** are given in Fig. 4.18. To evaluate the H-bonds (red dashed lines) the monomeric {[Ni(L)Cl(H_2O)$_2$]Cl} unit has been utilized. The dimerization energy [Fig. 4.18 (a)] is very large (ΔE_1 = –35.9 kcal/mol) in agreement with the strong MEP value at the H-atoms [Fig. 4.17 (a)] involved in the H-bonds. This confirms the robustness of these H-bonds in the formation of the 2D layer shown in Fig. 4.10. The interaction modes of the chloride counterion with the cationic part of complex **1** [Ni(L)Cl(H_2O)$_2$]$^+$ have also been evaluated. That is, on one hand the Cl^- anion interacts with [Ni(L)Cl(H_2O)$_2$]$^+$ by a combination of H-bond and anion···π interaction [Fig. 4.18 (b)] and, on the other hand, by means of a bifurcated Cl···H_2O–Ni(II) H-bonds [Fig. 4.18 (c)]. Both binding modes are energetically very favorable due to strong electrostatic attraction between the counterions. As expected, the bifurcated H-bond is more favored (around 9 kcal/mol) than the combination of H-bond and anion···π interactions.

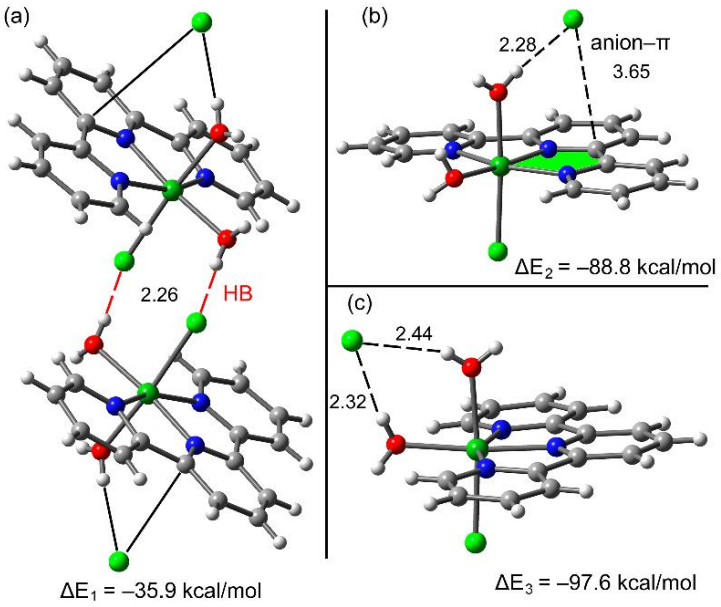

Fig. 4.18: Theoretical models used to evaluate the noncovalent interactions in the dimer of **1** (a) and the two different binding modes of the chloride (b, c). Distances in Å.

In complex **2** both π···π stacking modes that are important in the X-ray packing have been analyzed as illustrated above in Fig. 4.15. Fig. 4.19 (a) shows the π···π dimer where the chelate rings (CR) participate in the binding in addition to the pyridine rings. The dimerization energy is large (ΔE_4 = –27.4 kcal/mol) due to the participation of the CR as previously demonstrated [40-47] and also due to the antiparallel arrangement of the monomers that enhances the

dipole···dipole interaction. In the other π···π stacking binding mode, in addition to the π···stacking interaction, two symmetrically equivalent hydrogen bonds are also established. The formation of these H-bonds strongly agrees with the MEP surface of this complex [Fig. 4.17 (b)] since the most negative and most positive parts of the molecule correspond to the axial chlorido ligand and the aromatic H-atoms, respectively. Consequently, the binding energy computed for this dimer [Fig. 4.19 (b)] is larger (ΔE_5 = –33.4 kcal/mol) than the other one [Fig. 4.19 (a)] where only π···stacking interactions are present.

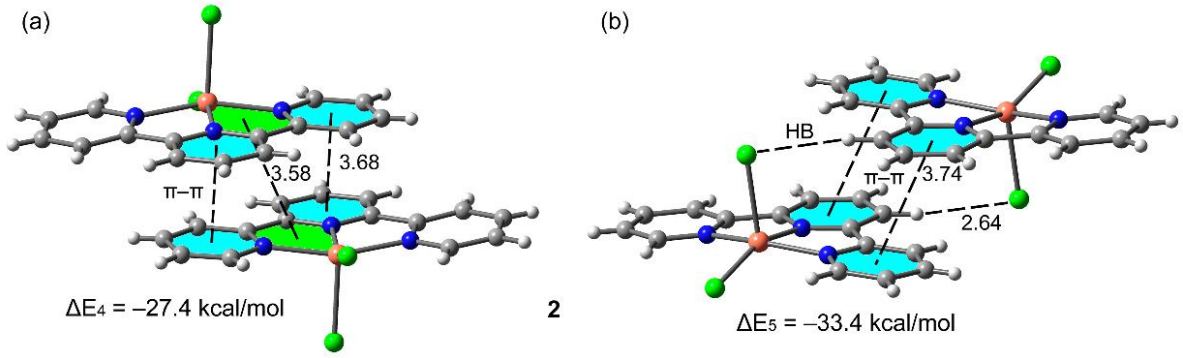

Fig. 4.19: Theoretical models used to evaluate the noncovalent interactions in both π···π binding modes of **2** (a, b). Distances are in Å.

Finally, the noncovalent interaction plot (NCI plot) index [31] has been used to further characterize the noncovalent interactions in the assemblies of the complexes **1** and **2**. This index facilitates a direct assessment and shows the extent to which non-covalent interactions stabilize a complex. Fig. 4.20 shows the NCI plot representation obtained for the self-assembled dimer commented above in Fig. 4.18 (a). The NCI index confirms the existence of anion···π and H-bonding interactions between the chloride counterion and the Ni(II) complex, which are characterized by green and blue isosurfaces, respectively. The NCI plot also evidences the strong nature of the O–H···Cl interactions between the $[Ni(L)Cl(H_2O)_2]^+$ moieties (blue and small isosurfaces) and reveals the existence of secondary C–H···Cl weak H-bonding interactions involving the aromatic ring, that also contribute to the dimerization.

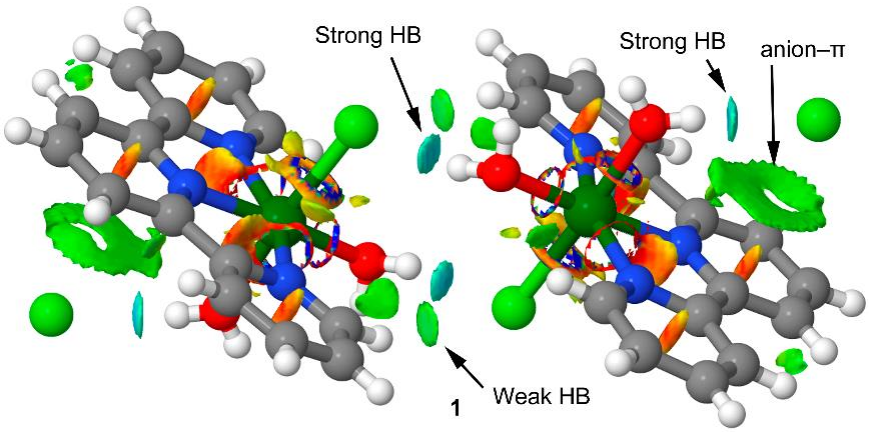

Fig. 4.20: NCI plot of the self-assembled dimer of **1**. The gradient cut-off is $s = 0.35$ au, and the color scale is $-0.04 < \rho < 0.04$ au.

Fig. 4.21 shows the NCI plot for the two π···stacking modes analyzed above for complex **2**. For the dimer shown in Fig. 4.21 (a) the π···stacking interaction is characterized by a green and very large isosurface that embraces the whole π-systems and even the Cu(II) metal center and explains the strong interaction energy. For the other dimer [Fig. 4.21 (b)], the overlap of the π-systems is smaller compared to the one shown in Fig. 4.21 (a), because of the antiparallel displacement of the complexes. The NCI plot confirms the existence of the C–H···Cl H-bonds that are characterized by bluish and small isosurfaces located between the Cl and H-atoms.

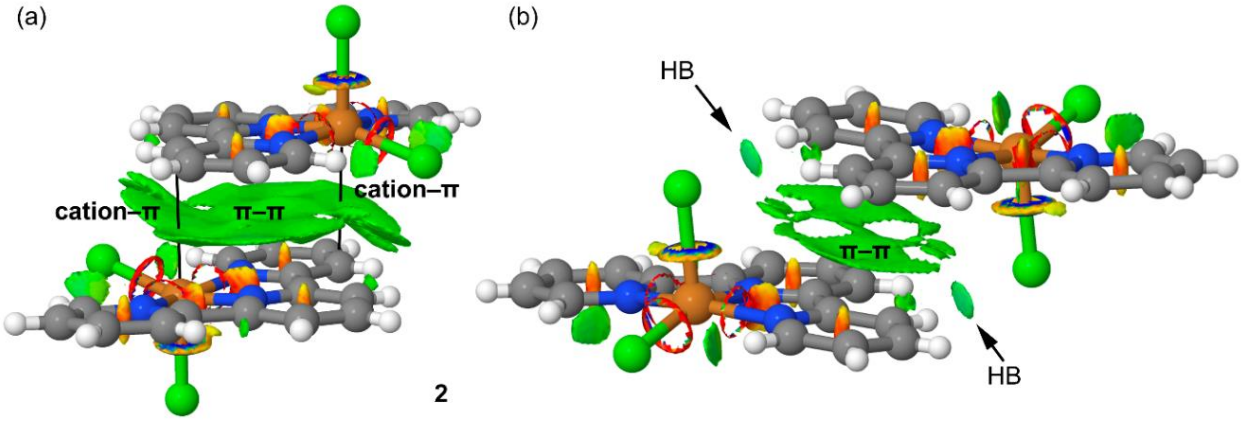

Fig. 4. 21: (a, b) NCI plots of two self-assembled π···π dimers of **2**. The gradient cut-off is $s = 0.35$ au, and the color scale is $-0.04 < \rho < 0.04$ au.

4.5. CONCLUSION

2,2′:6′,2″-terpyridine based complexes of Ni(II) (**1**) and Cu(II) (**2**) have been synthesized using their chloro salts purposefully so that at least one chloride ion should be attached with the metal centers. The aim of this work was to explore the role of π-rich aromatic rings and ancillary chloride ions in producing supramolecular interactions. The structural insights reveal that intermolecular hydrogen bonding (C–H···Cl, O–H···Cl), π···π and metal cation···π supramolecular interactions play a pivotal role in stabilizing the structures of the complexes in solid state. To the best of my knowledge this is the first report of Cu(II)···π interaction with terpyridine moiety. Keeping these interesting supramolecular interactions in hand, new supramolecular synthons have been constructed in solid state by exploiting their robustness in the supramolecular architecture. The supramolecular synthons in this structural family are generated through polarization induced interactions. The DFT study has been used to evaluate the noncovalent interactions energetically and confirm their crucial role determining the supramolecular architecture of both complexes. Finally, the interactions have been characterized using the NCI plot index and rationalized using the MEP surfaces. Theoretically strong O–H···Cl and weak C–H···Cl in complex **1** and π···π, metal cation···π and C–H···Cl interaction in complex **2** can be verified. In complex **2** the MEP surface evidences that the axial chlorido ligand is better H-bond acceptor (C–H···Cl interaction) than the equatorial one, in agreement with the supramolecular assemblies observed in the solid state.

REFERENCES

1. M. O. Sinnokrot, E. F. Valeev, C. D. Sherrill, *J. Am. Chem. Soc.*, 2002, **124**, 10887-10893.
2. F. Biedermann, H. J. Schneider, *Chem. Rev*., 2016, **116**, 5216-5300.
3. S. Scheiner, (Ed) *Noncovalent forces*, Springer, Dordrecht, 2015.
4. A. S. Mahadevi, G. N. Sastry, *Chem. Rev.*, 2016, **116**, 2775-2825.
5. A. Bauzá, T. J. Mooibroek, A. Frontera, *Chem. Commun*., 2014, **50**, 12626-12629.
6. H. Schneider, *Angew. Chem., Int. Ed*., 2009, **48**, 3924-3977.
7. A. M. Maharramov, K. T. Mahmudov, M. N. Kopylovich, A. J. L. Pombeiro, (Edn) *Non-covalent interaction in the synthesis and design of new compounds*, John Wiley & Sons. Inc., Hoboken, NJ, 2016.
8. L. M. Eytel, H. A. Fargher, M. M. Haley, D. W. Johnson, *Chem. Comm*., 2019, **55**, 5195-5206.
9. Y. Liu, W. Zhao, C. H. Chen, A. H. Flood, *Science*, 2019, **365**, 159-161.
10. G. R. Desiraju, T. Steiner, *The weak hydrogen bond in structural chemistry and biology*, Oxford University Press Inc, New York, 1999.
11. V. Balamurugen, M. S. Hundal, R. Mukherjee, *Chem. Eur. J*., 2004, **10**, 1683-1690.
12. G. Aullon, D. Bellamy, A. G. Orpen, L. Brammer, E. A Bruton, *Chem. Comm*., 1998, **6**, 653-654.
13. C. Janiak, *J. Chem. Soc. Dalton. Trans*., 2000, **21**, 3885-3896.
14. E. C. Constable, *Chem. Soc. Rev*., 2007, **36**, 246-253.
15. M. W. Cooke, G. S. Hanan, *Chem. Soc. Rev*., 2007, **36**, 1466-1476.
16. A. Wild, A. Winter, F. Schluetter, S.U. Schubert, *Chem. Soc. Rev*., 2011, **40**, 1459-1511.
17. V. S. Stafford, K. Suntharalingam, A. Shivalingam, A. J. P. White, D. J. Mann, R. Vilar, *Dalton Trans*., 2015, **44**, 3686-3700.
18. *Themed Issue on 'Stacking Interactions', Phys. Chem. Chem. Phys*., 2008, **10**, 2561-2868.
19. J. Sponer, K. E. Riley, P. Hobza, *Phys. Chem. Chem. Phys*., 2008, **10**, 2595-2610.
20. L. M. Salonen, M. Ellermann, F. Diederich, *Angew. Chem., Int. Ed.*, 2011, **50**, 4808-4842.
21. G. Barone, G. Gennaro, A. M. Giuliani, M. Giustini, *RSc. Adv*., 2016, **6**, 4936-4945.
22. A. Mukherjee, *Cryst. Growth Des.*, 2015, **15**, 3076-3085.

23. O. V. Shishkin, R. I. Zubatyuk, S. V. Shishkina, V. V. Dyakonenko, V. V. Medviediev, *Phys. Chem. Chem. Phys.*, 2014, **16**, 6773-6786.
24. H. Yorita, K. Otomo, H. Hiramatsu, A. Toyama, T. Miura, H. Takeuchi, *J. Am. Chem. Soc*., 2008, **46**, 15266-15267.
25. Bruker, *SMART* v5.631, Bruker AXS Inc., Madison, WI, USA, 2001.
26. G. M. Sheldrick, *SHELXS-97* and *SHELXL-97*, University of Göttingen, Germany, 1997.
27. M. J. Frisch, G. W. Trucks, H. B. Schlegel, G. E. Scuseria, M. A. Robb, J. R. Cheeseman, G. Scalmani, V. Barone, B. Mennucci, G. A. Petersson, H. Nakatsuj, M. Caricato, X. Li, H. P. Hratchian, A. F. Iamaylov, J. Bloino, G. Zheng, J. L. Sonnenberg, M. Hada, M. Ehara, K. Toyota, R. Fukuda, J. Hasegawa, M. Ishida, T. Nakajima, Y. Honda, O. Kitao, H. Nakai, T. Vreven, J. A. Montgomery jr, J. E. Peralta, F. Ogliaro, M. Bearpark, J. J. Heyd, E. Brothers, K. N. Kudin, V. N. Staroverov, R. Kobayashi, J. Normand, K. Raghavachari, A. Rendell, J. C. Burant, S. S. Lyengar, J. Tomasi, M. Cossi, N. Rega, J. M. Millam, M. Klene, J. E. Knox, J. B. Cross, V. Bakken, C. Adamo, J. Jaramillo, R. Gomperts, R. E. Stratmann, O. Yazyev, A. J. Austin, R. Cammi, C. Pomelli, J. W. Ochterski, R. L. Martin, K. Morokuma, V. G. Zakrzewski, G. A. Voth, P. Salvador, J. J. Dannenberg, S. Dapprich, A. D. Daniels, O. Farkas, J. B. Foresman, J. V. Ortiz, J. Cioslowski, D. J. Fox, Gaussian 09, Revision A.1, Gaussian Inc., Wallingford CT, 2016.
28. S. Grimme, J. Antony, S. Ehrlich, H. Krieg, *J. Chem. Phys.*, 2010, **132**, 154104.
29. S. F. Boys, F. Bernardi, *Mol. Phys*., 1970, **19**, 553-566.
30. J. Contreras-García, E. R. Johnson, S. Keinan, R. Chaudret, J.-P. Piquemal, D. N. Beratan, W. Yang, *J. Chem. Theory Comput*., 2011, **7**, 625-632.
31. E. R. Johnson, S. Keinan, P. Mori-Sánchez, J. Contreras-García, A. J. Cohen, W. Yang, *J. Am. Chem. Soc*., 2010, **132**, 6498-6506.
32. C. F. Holder, R. E. Schaak, *ACS Nano*., 2019, **13**, 7359-7365.
33. H. Zaho, B. G. Zhang, X. X. Zhang, S. Wang, B. L. Wu, *Synthesis and Reactivity in Inorganic, Metal-Organic, and Nano-Metal Chemistry*, 2015, **45**, 572-580.
34. E. C. Constable, D. Phillips, P. R. Raithby, *Inorg. Chem. Commun.*, 2002, **5**, 519-521.
35. A. W. Addison, T. N. Rao, J. Reedijk, J. Rijn, G. C. Verschoor, *J. Chem. Soc. Dalton Trans*.,1984, **7**, 1349-1356.
36. G. Zhang, E. Liu, C. Yang, L. Li, J. A. Golen, A. L. Rheingold, *Eur. J. Inorg. Chem*., 2015, **6**, 939-947.

37. Z. Ma, L. Wei, E. C. B. A. Alegria, L. M. D. R. S. Martins, M. F. C. Guedes da Silva, A. J. L. Pombeiro, *Dalton Trans*., 2014, **43**, 4048-4058.
38. R. J. Allenbaugh, A. L. Rheingold, L. H. Doerrer, *Dalton Trans.*, 2009, **7**, 1155-1163.
39. Z. Ma, B. Zhang, M. F. C. Guedes da Silva, J. Silva, A. S. Mendo, P. V. Baptista, A. R. Fernandes, A. J. L. Pombeiro, *Dalton Trans*., 2016, **45**, 5339-5365.
40. S. Mirdya, S. Roy, S. Chatterjee, A. Bauza, A. Frontera, S. Chattopadhyay, *Cryst Growth Des*., 2019, **19**, 5869-5881.
41. M. K. Bhattacharyya, U. Saha, D. Dutta, A. Das, A. K. Verma, A. Frontera, *RSc Adv*., 2019, **9**, 16339-16356.
42. S. Khan, P. Giri, A. Bauza, K. Harms, A. Frontera, S. Chattopadhyay, *Polyhedron*, 2019, **157**, 487-494.
43. M. K. Bhattacharyya, D. Dutta, S. M. Nashre-ul-Islam, A Frontera, P. Sharma, A. K. Verma, A. Das, *Inorg. Chim. Acta*, 2020, **501**, 119233.
44. H. Nath, P. Sharma, A. Frontera, A. K. Verma, A. Das, M. Barceló-Oliver, M. K. Bhattacharyya, *Polyhedron*, 2020, **176**, 114266.
45. I. Alkorta, F. Blanco, P. M. Deya, J. Elguero, C. Estarellas, A. Frontera, *Theor. Chem. Acc.*, 2010, **126**, 1-14.
46. M. Mitra, P. Manna, A. Bauzá, P. Ballester, S. K. Seth, S. R. Choudhury, A. Frontera, S. Mukhopadhyay, *J. Phys. Chem. B*, 2014, **118**, 14713-14726.
47. A. Bauzá, T. J. Mooibroek, A. Frontera, *Chem. Eur. J*., 2014, **20**, 10245-10248.

CHAPTER 5

On the importance of orchestrated interplay between anion···π, π···π and hydrogen bonding interactions in simultaneous binding of Nickel (II) cation and chloride anion by 2,4,6 tris-(2-pyridyl)-1,3,5 triazine: Synthetic, supramolecular and theoretical aspects

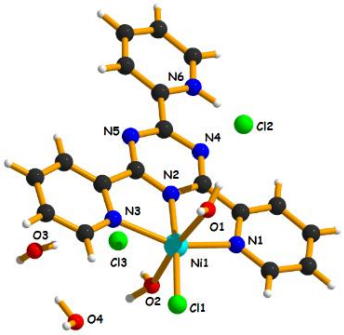

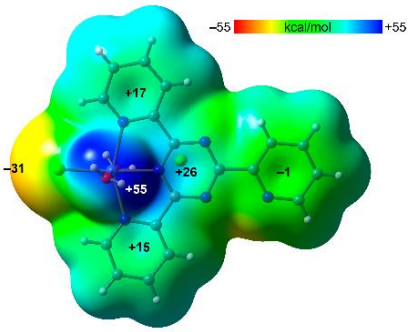

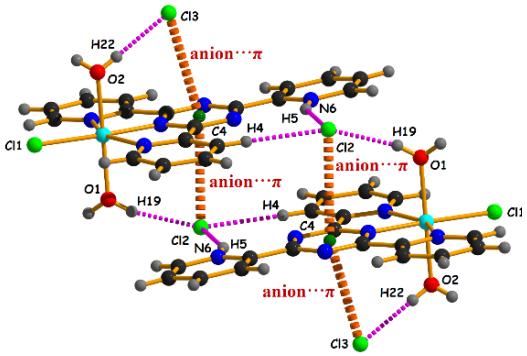

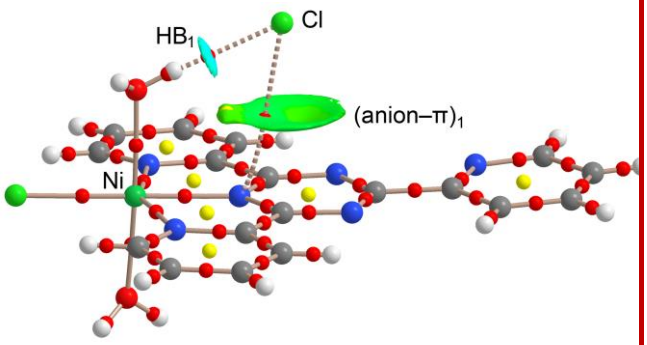

Published in New Journal of Chemistry, 2021, 11689, 7310-11696

On the importance of orchestrated interplay between anion···π, π···π and hydrogen bonding interactions in simultaneous binding of Nickel (II) cation and chloride anion by 2,4,6 tris-(2-pyridyl)-1,3,5 triazine: Synthetic, supramolecular and theoretical aspects

5.1. INTRODUCTION

Recent years have witnessed an extensive growth in designing metallo-organic frameworks propelled by numerous supramolecular synthons using different types of non-covalent interactions that play a significant role in structural integrity in the solid state [1, 2]. Based on relative abundance of the supramolecular synthons in the database new synthetic strategies can be planned [3]. This created an opportunity for the synthesis of molecular crystals with targeted pattern of binding in the solid state [4]. Although the structure-directing role of weak noncovalent interactions (NCIs) was reported about three decades ago, a deeper understanding of NCIs is needed to control and modulate the solid-state architecture of molecular crystals [5, 6]. 2,4,6-tris(2-pyridyl)-1,3,5-triazine (**tptz**) or their structural analogs are well established metal binding ligands that can arrest a colossal interest in the field of contemporary metallo-supramolecular chemistry [7-10]. As a flexidentate coordinating ligand **tptz** shows various coordination modes with the transition metal centers [Scheme 5.1(a-f)].

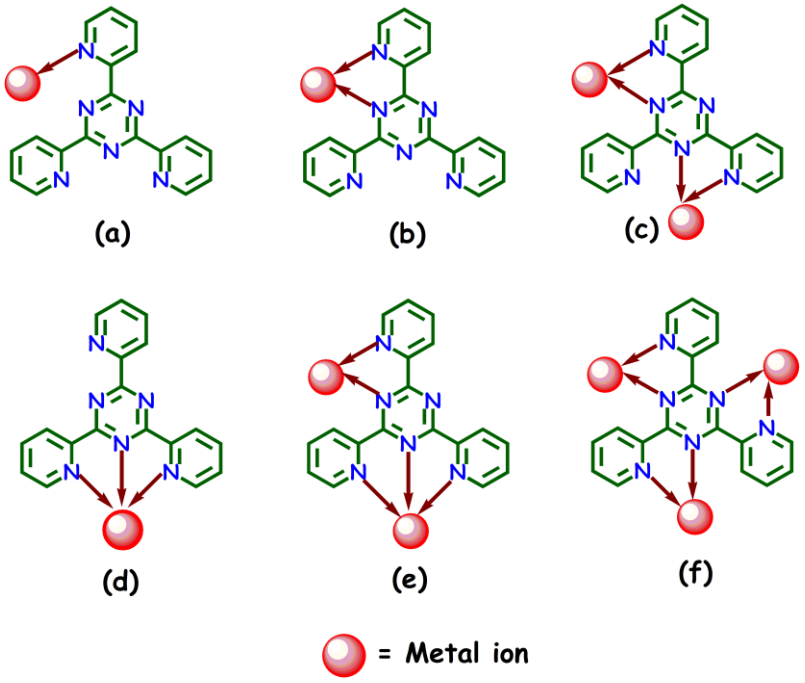

Scheme 5.1: Schematic representation of the possible coordination modes of the ligand '**tptz**'

From the structural database it was evident that the predominant coordination mode of '**tptz**' is tridentate terpyridine like [Scheme 5.1 (d)]. Moreover, it is also able to coordinate two metal centers in one terpyridine and one bipyridine like coordination modes [Scheme 5.1 (e)] or bind three metal centers simultaneously *via* all bipyridine-like coordination [Scheme 5.1 (f)], although the later binding mode is quite rare. Several mononuclear complexes of transition metal ions with '**tptz**' ligand have been reported including Cr^{+2} [9], Mn^{+2} [9, 11], Fe^{+3} [12], Co^{+2} [13], Ni^{+2} [10, 14], Cu^{+2} [15], Ag^{+} [16] etc. The '**tptz**' has also been used to separate trivalent lanthanides and actinides [17, 18] from nitric acid media (> 0.1M) in which '**tptz**' is protonated as '**Htptz**$^{+}$'. For coordination chemists, '**tptz**' is a ligand of immense interest because of its multiple coordination sites, large π conjugation for stabilization and variable hapticities to be used for designing building blocks, that recognizes each other through direction specific interactions to form extended supramolecular architectures [9, 13].

The underappreciation of anion···π interactions relied on the intuitive assumption of repulsive force between anion and the electron rich π system of an arene [19]. But in recent years the anion···π interaction, i.e., the non-covalent force between electron deficient aromatic system and anions has been recognized as a potential non-covalent bonding interaction [20, 21]. From crystallographic database it was evident that the interplay between anion···π and π···π or anion···π and hydrogen bonding interactions play a significant role in a synergistic manner to stabilize the crystal structure in solid state. But the challenging task to ensure both anion···π and π···π interactions simultaneously because for the former electron deficient π system and for the later electron rich π systems are required. When the heterocycle ring is coordinated to the metal center, the ring became electron deficient, but not to such extent so that it can be utilized to ensure a strong anion···π interaction but this interaction became a significant one if the aromatic ring moiety is protonated [22].

Keeping all these factors in mind, here one peripheral pyridine ring of '**tptz**' has been protonated strategically (to restrict coordination of the second metal center as shown in scheme 5.1e) to ensure not only NNN tridentate terpyridine like major coordination site active, leaving moderate and minor coordination sites inactive in the coordination game towards the metal center [Scheme 5.2 (a) and 5.2 (b)] but also make the triazine ring sufficiently electron deficient to encourage it to participate in strong anion···π interaction.

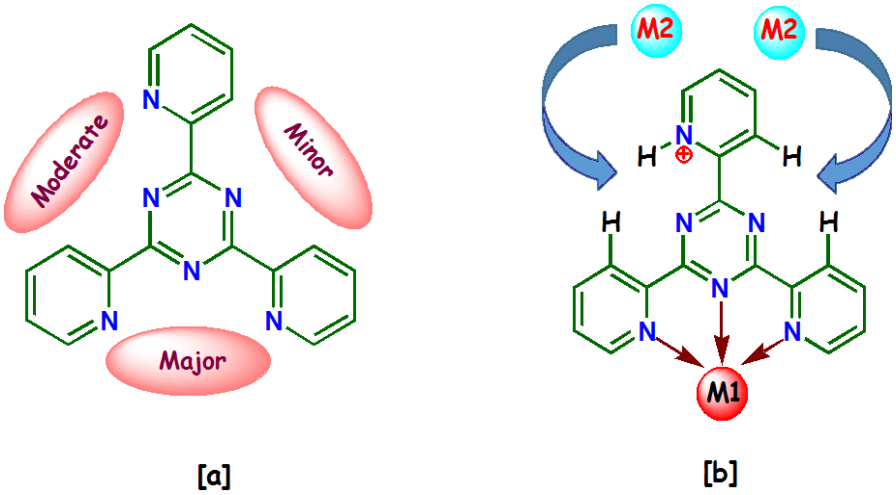

Scheme 5.2: [a] Availability and the nature of coordination pockets in **tptz** and **[b]** Schematic representation of steric constrain of the protonated ligand (**Htptz**$^{+}$) executed by the hydrogen atoms on the approach of second metal ion (M2) when it is already coordinated to the first metal ion (M1)

A Ni(II) complex of the protonated ligand (**Htptz**$^{+}$) has been successfully synthesized and characterized by single crystal X-ray analysis. As anticipated the electron deficient triazine ring (one nitrogen of triazine ring is coordinated to the metal Ni(II) and one peripheral substituted pyridine ring is protonated) participates in anion···π interaction and the substituted non-protonated pyridine rings are engaged in π···π and π^{+}···π (using one protonated pyridine ring) along with several hydrogen bonding interactions (classical O–H···O, O–H···Cl, N–H···Cl and non-classical C–H···Cl type) to construct different networks of varying dimensionalities. Finally, the present work uses DFT calculations and several computational tools (QTAIM and NCI Plot) to rationalize the noncovalent interactions and their decisive role in forming the solid-state architecture of complex **1**.

5.2. EXPERIMENTAL SECTION

5.2.1. Materials and Physical Measurements

All chemicals were of reagent grade, purchased from commercial sources and used without further purification. 2,4,6-tris(2-pyridyl)-1,3,5-triazine (**tptz**) and ethanol were purchased from Aldrich Chemical Company, USA and used without further purification. All reactions were carried out in aerobic condition and in ethanol-water medium (Scheme 5.3).

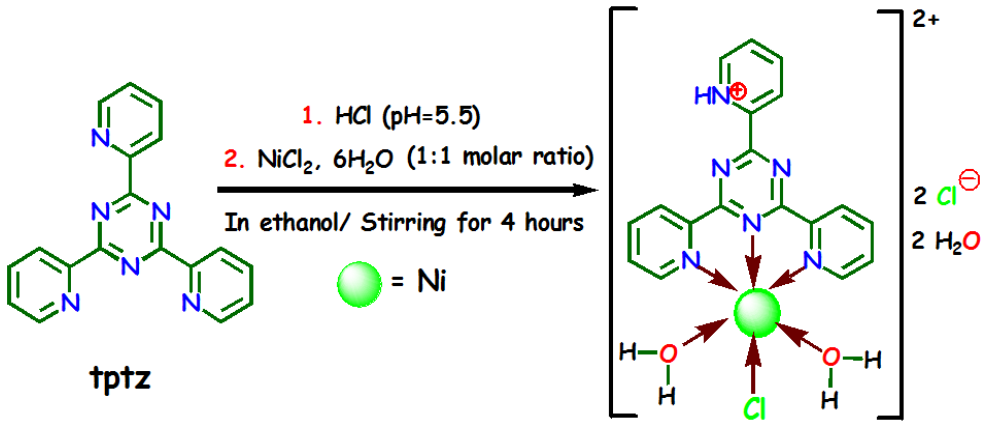

Scheme 5.3: Schematic representation of the synthesis of complex **1**

During the whole experiment freshly boiled, doubly distilled water was used. Perkin-Elmer RXI FT-IR spectrophotometer was used to record the IR spectra in the range of 4000−400 cm^{-1} and an Elemental analysis (carbon, hydrogen and nitrogen) of the metal complex was determined with a Perkin–Elmer CHN analyzer 2400. UV-Visible spectra were collected on UV-Visible spectrophotometer Hitachi UH 4150. Thermogravimetric analysis (TGA) data was collected with an SDT 2960 thermoanalyzer under nitrogen (50°C to 850°C) at a heating rate of 10°C per minute for **1**. The room temperature magnetic moment of the complex was taken from magnetic susceptibility balance MK1 Sherwood.

5.2.2. Synthesis

5.2.2.1. *Synthesis of protonated ligand ($Htptz^+$)*

Protonated '**tppz**' [2,4,6-tris(2-pyridyl)-1,3,5-triazine] was synthesized by following the reported procedure [17].

5.2.2.2. *Synthesis of $[Ni(Htptz^+)Cl(H_2O)_2]$ 2Cl. $2H_2O$ (Complex 1)*

The protonated ligand, **$Htptz^+$** (0.376g, 1.2 mmol) was dissolved in ethanol (15 mL) and drop wise an aqueous ethanolic solution of $NiCl_2$, $6H_2O$ (0.284g, 1.2 mmol) was added with constant stirring that continued for 4 hours. Then the solution was filtered and the filtrate was left for slow evaporation. After one-week, brownish green X-ray quality crystals of **1** were isolated. (Yield: 73%). Anal. Calc. for $C_{18}H_{21}NiN_6O_4Cl_3$: C, 39.21; H, 3.81; N, 15.26. Found: C, 38.98; H, 3.83; N, 15.28%. Main FT-IR absorptions, (KBr, cm^{-1}): 3407 (m), 3260

(m), 3047 (s), 3027 (s), 1730 (s), 1577 (s), 1561 (s), 1547 (s), 1473 (s), 1439 (s), 1377 (s) (Fig. 5.1). $\lambda_{max/\ nm}$ = 233, 311 and 379 (Fig. 5.2). Room temperature magnetic moment (μ_{eff}) = 2.79 B.M.

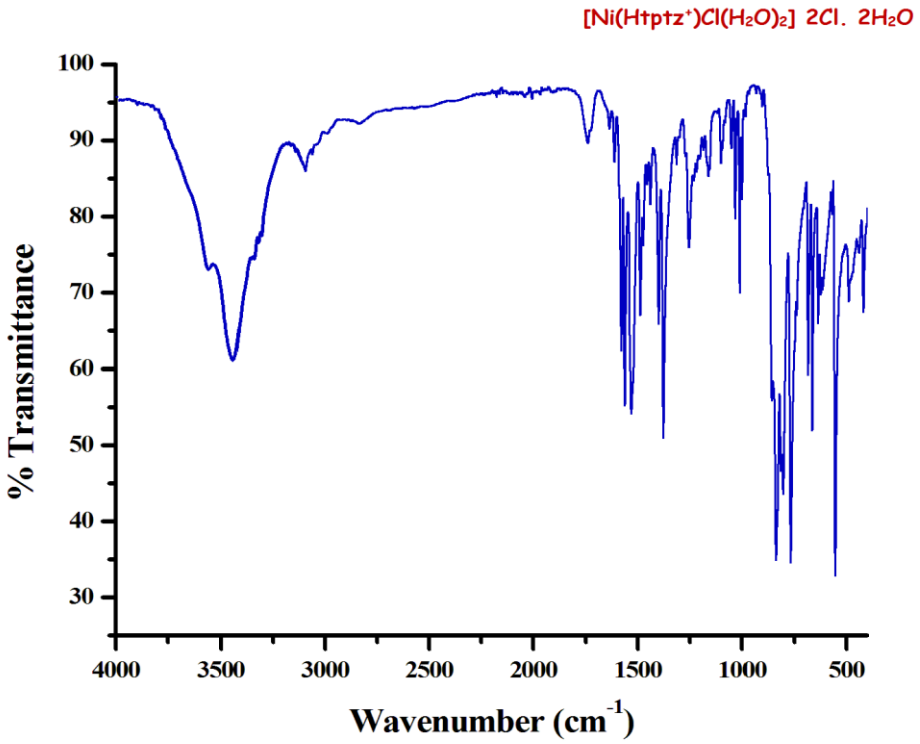

Fig. 5.1: IR spectrum for Complex **1**

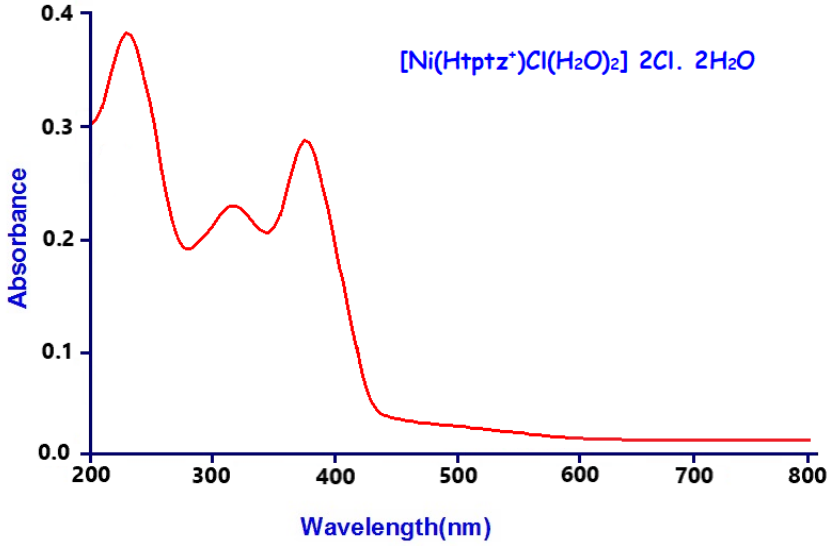

Fig. 5.2: UV-Visible spectrum for Complex **1**

5.2.3. X-ray Crystallographic Analysis

Data collection was made using Bruker SMART APEX II CCD area detector equipped with graphite monochromated Mo Kα radiation (λ = 0.71073 Å) source in φ and ω scan mode at 150(2) K for **1**. Cell parameters refinement and data reduction were carried out using the Bruker SMART APEX II. Cell parameters refinement and data reduction were carried out using Bruker SMART and Bruker SAINT software [23] for the complex. The structure of the complex was solved by conventional direct methods and refined by full-matrix least square methods using F^2 data. SHELXS-97 and SHELXL-97 programs [24] were used for the solution and refinement of the structure of the complex respectively. **CCDC 2024203** (**1**) include additional crystallographic information. Selected crystallographic features for **1** are given in Table 5.1 and selected metrical parameters of the complex are shown in Table 5.2.

5.3. THEORETICAL METHODS

The calculation of the interaction energies was carried out using the Gaussian-16 [25] and the PBE0-D3/def2-TZVP level of theory and using the crystallographic coordinates. The Grimme's D3 dispersion correction has been used in the calculations since it is important to evaluate anion···π interactions properly [26]. This procedure and level of theory has been successfully used to evaluate similar interactions [27-30]. The interaction energies were computed by calculating the difference between the energies of the isolated monomers and their assembly and they have been BSSE corrected [31]. The QTAIM [32] and NCI Plot calculations [33] have been performed at the same level of theory and using the AIMAll program.

5.4. RESULTS AND DISCUSSION

Single-crystal X-ray structural analysis confirms that the asymmetric unit of the title complex (**1**) consists of one protonated heterocyclic ligand (**Htptz**$^+$) [**tptz** = 2,4,6-tris(2-pyridyl)-1,3,5-triazine] moiety with Ni(II), chloride ion and solvent water molecules. In this complex, the protonated ligand acts as a monopositive tridentate NNN donor moiety in cis,

cis- fashion and form two five membered chelate rings around the central metal ion. Two non-coordinated chloride ions and two water molecules are there to complete the asymmetric unit of **1**. The molecular representation with atom numbering scheme (only selected atom numbering was done for maintaining the clarity of the picture) of the complex is shown in Fig. 5.3**.**

Table 5.1: Selected crystallographic features of complex **1**

Compound	**1** (CCDC: 2024203)
Empirical formula	$C_{18}H_{21}Cl_3N_6NiO_4$
Formula weight	550.47
Temperature (K)	150 (2) K
Wavelength (Å)	0.71073
Crystal system	Monoclinic
Space group	P 2_1/n
Unit cell dimensions	
a (Å)	12.5147(10)
b (Å)	14.4871(13)
c (Å)	13.4749(11)
α (˚)	90
β (˚)	107.825(2)
γ (˚)	90
Volume ($Å^3$)	2325.7(3)
Crystal size (mm^3)	0.10x0.11x0.13
z	4
$Density_{cal}$ (Mgm^{-3})	1.572
Absorption coefficient (mm^{-1})	1.216
F (000)	1128
θ Range (˚) for data collection	2.1 – 27.1
Index ranges	$-16 \leq h \leq 16$ $-18 \leq k \leq 18$ $-17 \leq l \leq 17$
Goodness-of-fit on F^2	1.049
Independent reflections [R_{int}]	5038 (0.0407)
Absorption correction	Multi-scan
Refinement method	Full-matrix least squares on F^2
Data/ restraints/ parameters	5038/ 0/ 325
Reflections collected	34100
Final R indices [$I > 2\sigma(I)$]	R=0.0246, wR_2=0.0591
Largest difference peak & hole($eÅ^{-3}$)	-0.317, 0.292

Table 5.2: Coordination bond distances (Å) and angles (°) for **1**

Selected Bonds	Value (Å)	Selected Angles	(°)
Ni1–N1	2.1486(12)	N1–Ni1–N2	76.62(4)
Ni1–N2	2.0010(11)	N2–Ni1–N3	75.96(5)
Ni1–N3	2.1721(12)	N1–Ni1–O1	85.35(5)
Ni1–O1	2.0726(13)	N1–Ni1–O2	88.69(5)
Ni1–O2	2.0822(12)	N1–Ni1–Cl1	106.6(3)
Ni1–Cl1	2.3072(4)	N2–Ni1–O1	91.88(5)
		N2–Ni1–Cl1	176.55(4)
		N2–Ni1–O2	91.15(5)
		N3–Ni1–O1	94.38(6)
		N3–Ni1–O2	93.00(5)
		N3–Ni1–Cl1	100.83(3)
		N1–Ni1–N3	152.56(5)
		O1–Ni1–O2	172.51(5)
		O1–Ni1–Cl1	89.64(4)
		Cl1–Ni1–O2	87.72(4)

5.4.1. Structural description of Complex 1

The perspective view of the molecular structure of complex **1** with selected atom numbering scheme is shown in Fig. 5.3 whereas selected bond lengths (Å) and bond angles (°) are listed in Table 5.2. Complex **1** crystallizes in the space group P 2_1/n and its unit cell is comprised of four molecules. Complex **1** is a distorted octahedron where the title ligand 'tptz' in its protonated form (**Htptz**$^+$) spans in the meridional position [N1–Ni1–N2 = 76.62(4)°, N2–Ni1–N3 = 75.96(5)° and N1–Ni1–N3 = 152.56(5)°] as a monopositive [due to protonation of third pendant pyridine ring nitrogen (N6)] NNN donor via two pyridyl nitrogen atom (N1 and N3) and one triazine ring nitrogen (N2). In association with the ligand (**Htptz**$^+$) two oxygen atoms (O1 and O2) from two different water molecules and one chlorine atom (Cl1) complete the octahedral geometry (Table 5.2).

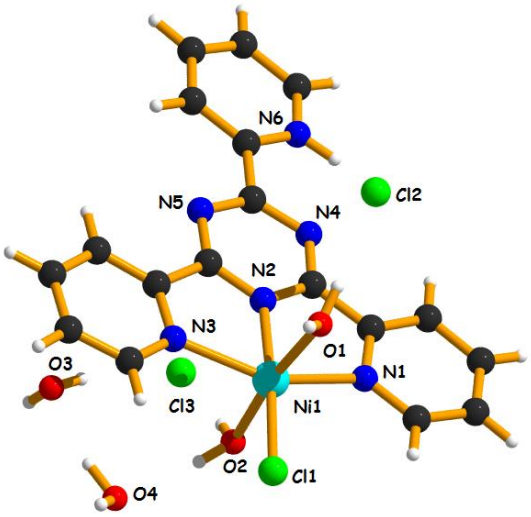

Fig. 5.3: Asymmetric unit of Complex **1**

The dipositive charge of the heteroleptic complex is taken care by two non-coordinated chloride ions (Cl2 and Cl3) present at the outside of the metal coordination sphere. Beside coordinating water molecules two non-coordinated water molecules are also present in **1**. Among the three trans angles two [O1–Ni1–O2 = 172.51(5)^o and N2–Ni1–Cl1 = 176.55(4)^o] are close to ideal trans angle 180^o, while the third one [N1–Ni1–N3 = 152.56(5)^o] is deviated more probably due to small bite angles (form two five membered chelate rings towards the central metal ion) of the title ligand [N1–Ni1–N2 = 76.62(4)^o, N2–Ni1–N3 = 75.96(5)^o] that may induce a distortion in the trans angle in the entire octahedral geometry (Table 5.2). The average Ni–N and Ni–O bond lengths are 2.107Å [Ni1–N1 = 2.1486(12) Å, Ni1–N2 = 2.0010(11) Å and Ni1–N3 = 2.1721(12) Å] and 2.077 Å [Ni1–O1 = 2.0726(13) Å and Ni1–O2 = 2.0822(12) Å], those are consistent with reported six coordinated Ni(II) complexes available at Cambridge Crystallographic database [7, 10, 14, 34, 35].

Ni–$N_{triazine}$ (Ni1–N2) bond length is to some extent shorter than those of Ni–$N_{pyridyl}$ (Ni1–N1 and Ni1–N3) that may be due to the stronger π-accepting properties of the triazine ring or due to the constricted coordination geometry imposed by the triazine ligand [10]. The dihedral angle between the ring C1C2C3C4C5N1, C14C15C16C17C18N3 and C8C9C10C11C12N6 with the triazine ring N2C6N4C7N5C13 are 2.88^o, 1.28^o and 4.22^o respectively. This shows that the coordinated pyridyl rings are almost coplanar and the uncoordinated, protonated pyridyl ring is slightly nonplanar with respect to the triazine ring. The pendant protonated pyridine ring makes an angle 6.34^o with the equatorial plane

(N1N2N3Cl1) displaying the maximum degree of twisting. The central Ni atom is placed almost in the equatorial plane constituted by N1N2N3Cl1.

In the present structure both coordinated and non-coordinated chloride ions participate in several hydrogen bonding interactions. According to Jeffrey's categorization based on donor-acceptor distances of hydrogen bond, they are found to be moderate and weakly electrostatic [36]. Though C–H···Cl hydrogen bonding is comparatively less frequent but well appreciated in recent years [7, 37-40]. When the heterocyclic ring bears a donor atom that is capable to reduce the electron density in the ring sufficiently that produce non-classical C–H···Cl hydrogen bonding interactions. For better C–H···Cl interaction the H···Cl distance should be less than the sum of their van der Waals radii (2.95Å) [41]. In this work that such distance ranges from 2.60 to 2.82 Å (Table 5.3).

Table 5.3: Details of Hydrogen bond distances (Å) and angles (°) for **1**

D – H ···A	D (D – H) (Å)	D (HA) (Å)	D(D···A) (Å)	<DHA (°)
N6–H5···Cl2	0.90(2)	2.32(2)	3.1405(15)	152.1(19)
O1–H19···Cl2	0.84(2)	2.26(2)	3.0833(14)	166(2)
O1–H20···Cl1	0.84(2)	2.26(2)	3.0980(14)	173.2(19)
O2–H21···O4	0.82(2)	1.88(2)	2.694(2)	171(2)
O2–H22···Cl3	0.80(2)	2.28(2)	3.0721(14)	175(2)
O3–H23···Cl3	0.75(2)	2.49(2)	3.232(2)	169(2)
O3–H24···Cl2	0.75(3)	2.39(3)	3.133(2)	171(3)
O4–H25···O3	0.89(3)	1.99(3)	2.837(3)	159(3)
O4–H26···Cl3	0.73(3)	2.39(3)	3.1020(17)	165(2)
C2–H2···Cl2	0.9500	2.8200	3.6237(19)	143
C3–H3···Cl1	0.9500	2.6000	3.4598(18)	150
C4–H4···Cl2	0.9500	2.6600	3.6126(17)	177

Both the coordinated and one non-coordinated chloride ions (Cl1 and Cl2 respectively) engaged in these C–H···Cl type non-classical hydrogen bonding interactions [C3–H3···Cl1, C2–H2···Cl2 and C4–H4···Cl2] leading to the generation of $R_3^2(11)$ synthons. An additional electrostatic attraction enables N6–H5 in hydrogen bonding interaction only to the chloride ion (non-coordinated Cl2) and not to either coordinated or non-coordinated water molecules. The N–H···Cl distance is short (2.32 Å) because the hydrogen bonding occurs through non-coordinated ionic chloride (Table 5.3) that is expected to be stronger compared to the chloride attached to the metal ion. The N–H···Cl interaction along with C4–H4···Cl2 constitutes a $R_2^1(10)$ synthons. These $R_3^2(11)$ and $R_2^1(10)$ synthons propagate to generate a 1D tape (Fig. 5.4).

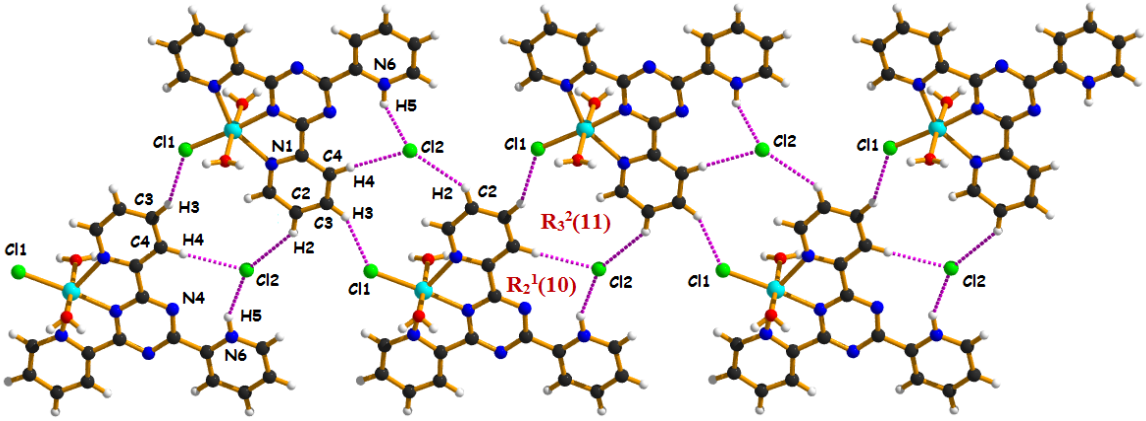

Fig. 5.4: 1D tape formed by various hydrogen bonding interactions incorporating both coordinated (Cl1) and non-coordinated ionic chloride (Cl2) ions viewing along 'c' axis.

This 1D arrangement is further stabilized by intermolecular π···π and π^{+}···π interactions between the six membered coordinated pyridine ring [Cg(3) centroid] of one layer with the six membered coordinated pyridine ring [Cg(5) centroid] and another six membered non-coordinated, protonated pyridine ring [Cg(6) centroid] from two different (almost parallel) layers with the shortest centroid-centroid distances 3.6757(9) Å and 3.8936 (10) Å respectively (Table 5.4).

Table 5.4: Geometric features (distances in Å and angles in degrees) of π···π interactions obtained for **1**

Cg(ring I) - Cg(ring J)	Cg···Cg (Å)	Cg(I) ···perp (Å)	Cg(J) ···perp (Å)	α (°)	β (°)	γ (°)	Symmetry
Cg(3)···Cg(5)	3.6757(9)	3.3674(6)	3.4849(6)	5.11(8)	18.5	23.6	½+x, 3/2-y, ½+z
Cg(3)···Cg(6)	3.8936(10)	3.5380(6)	3.3513(7)	6.84(8)	30.6	24.7	1-x, 1-y, 1-z
Cg(5)···Cg(3)	3.6757(9)	3.4850(6)	3.3673(6)	5.11(8)	23.6	18.5	-½+x, 3/2-y, -½+z
Cg(6)···Cg(3)	3.8939(10)	3.3515(7)	3.5381(6)	6.84(8)	24.7	30.6	1-x, 1-y, 1-z

α = Dihedral angle between ring I and ring J (°); β = Cg(I) →Cg(J) or Cg(I) → Me vector and normal to plane I (°); γ = Cg(I) → Cg(J) vector and normal to plane J (°); Cg···Cg = distance between ring centroids (Å); Cg(I)···Perp: perpendicular distance of Cg(I) on ring J (Å); Cg(J)···Perp: perpendicular distance of Cg(J) on ring I (Å).

Cg(3): Centre of gravity of ring [N1/C1/C2/C3/C4/C5], Cg(5): Centre of gravity of ring [N3/C14/C15/C16/C17/C18] and Cg(6): Centre of gravity of ring [N6/C8/C9/C10/C11/C12]

These π···π and π^+···π stacking interactions increase the dimensionality of the tape from 1D (Fig. 5.4) to 2D (Fig. 5.5).

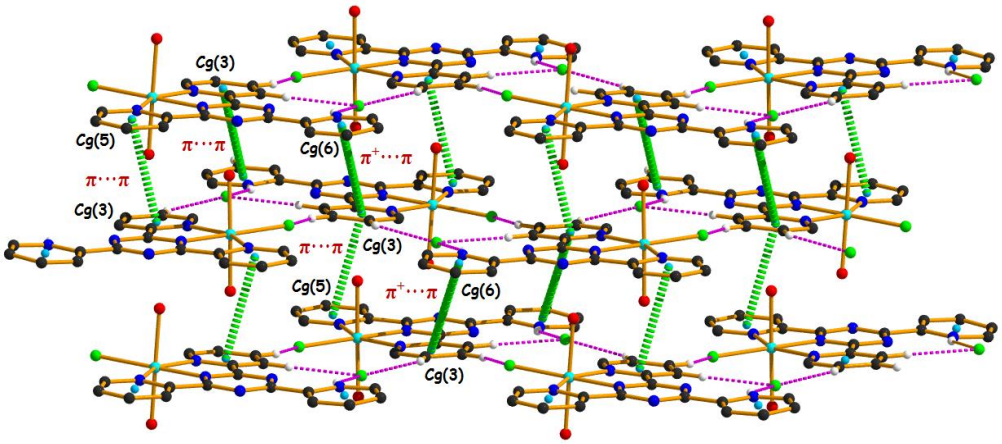

Fig. 5.5: 2D layer formed by hydrogen bonding, π···π and π^+···π stacking interactions (H-atoms not involved in hydrogen bonding have been omitted for clarity).

Here the triazine ring is trisubstituted by three pyridyl groups among which one pyridine ring is protonated. One triazine nitrogen (N2) and two pyridyl nitrogen atoms (N1 and N3) are directly coordinated to the Ni(II) center. From database it was evident that simple metal coordination will not provide sufficient polarization to produce strong anion···π interaction. But ab initio calculation has provided evidence that these weak interactions can afford a significant degree of stability if the aromatic moiety is protonated [22, 42].

In structure **1**, two non-coordinated chloride ions (Cl2 and Cl3) are located above and below the electron deficient triazene ring to form an effective anion···π interactions in association with a hydrogen bonding interaction with the hydrogen atoms of axially coordinated water molecules [O1–H19···Cl2 and O2–H22···Cl3] available in proximity (Fig. 5.6). In **1**, there is a dimeric distribution as shown in Fig. 5.7 that is formed by anion···π and hydrogen bonding involving coordinated water along with two different hydrogen bonding interactions involving N–H···Cl (N6–H5···Cl2) and C–H···Cl (C4–H4···Cl2). Hence the combined effect mutually strengthens each other.

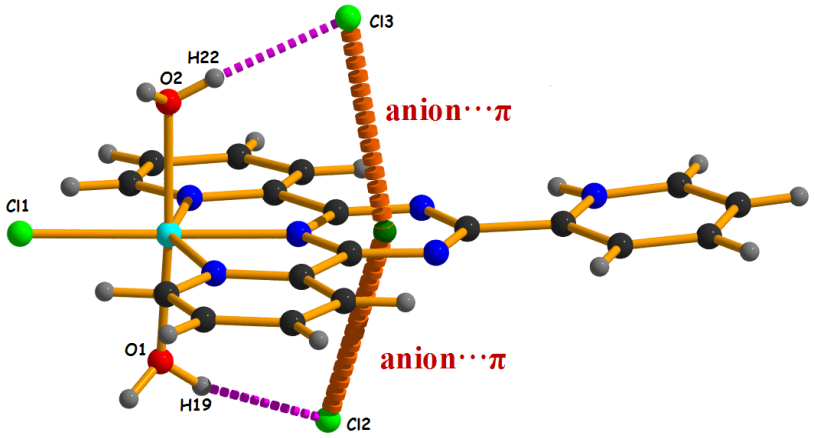

Fig. 5.6: Anion···π interactions along with hydrogen bonding interactions in complex **1**

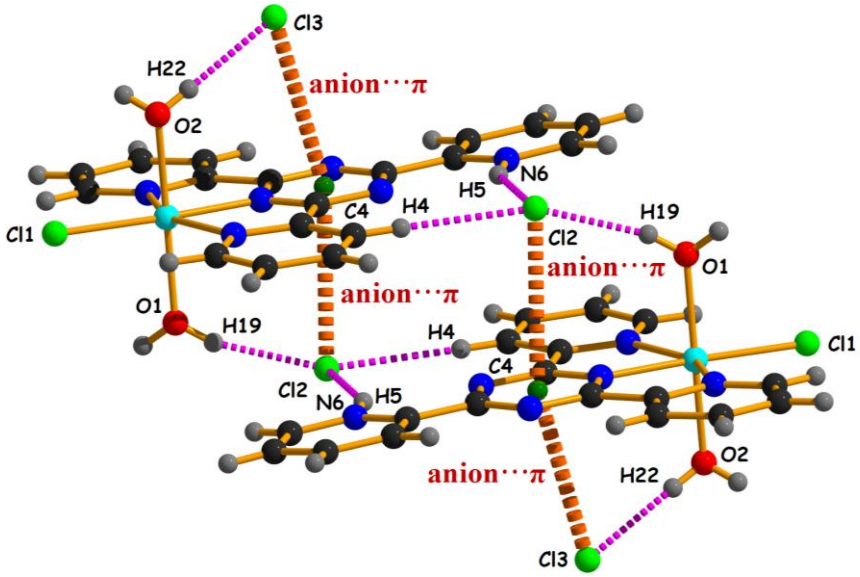

Fig. 5.7: Dimeric distribution of **1** using anion···π and different hydrogen bonding interactions

Non-coordinated water molecules are also susceptible to form several hydrogen bonding interactions with coordinated as well as non-coordinated chloride ions [O1–H20···Cl1, O3–H23···Cl3, O4–H26···Cl3 and O3–H24···Cl2]. In solid state complex **1** form an infinite chain through O2–H21···O4, O2–H22···Cl3, O4–H25···O3 and O3–H23···Cl3 classical hydrogen bonding interactions are responsible to generate a $R_4^3(8)$ synthon that are interconnected those are interconnected through O4–H26···Cl3 to form a 1D chain. These 1D chains are interconnected through symmetric $R_2^2(8)$ synthon and produce a 2D layer structure through intermolecular hydrogen bonding interactions between

O1–H20···Cl1. In association with anion···π interactions, the non-coordinating Cl2 atom further strengthen the stability of the 2D layer as it introduces strong O3–H24···Cl2 and O1–H19···Cl2 interactions (Fig. 5.8).

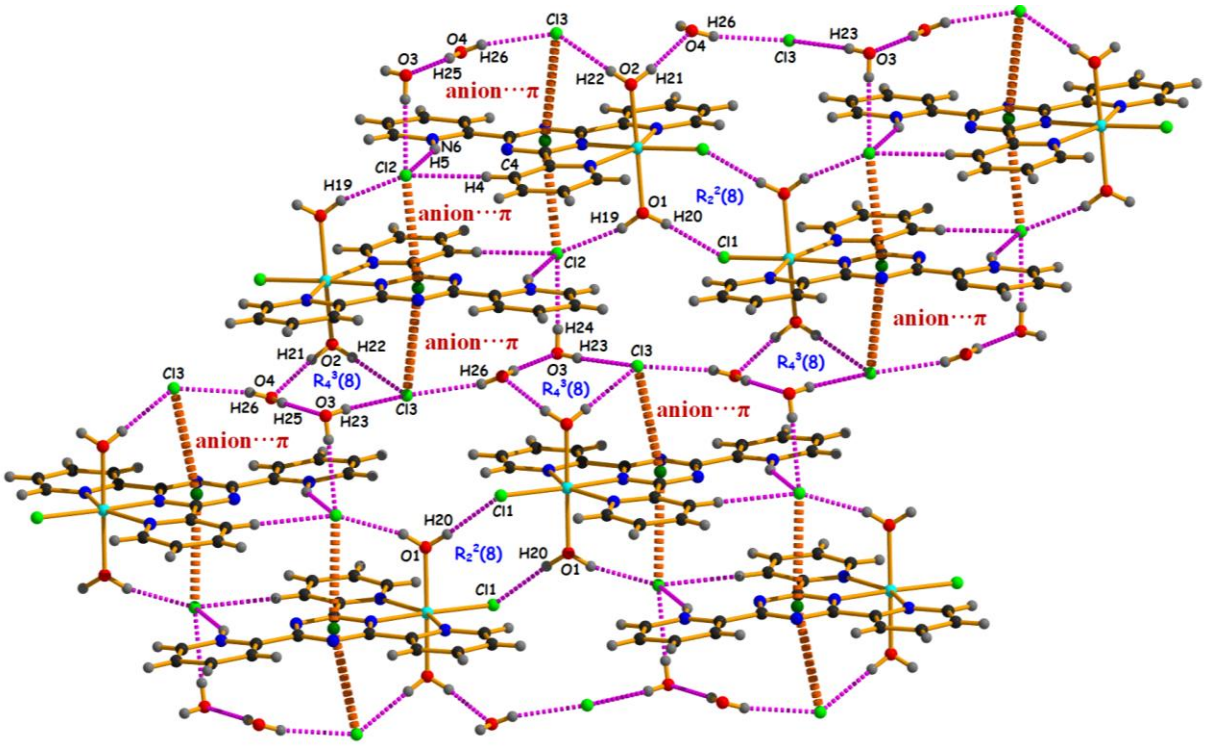

Fig. 5.8: 2D network generated by the anion···π, several hydrogen bonding interactions and $R_4^3(8)$ and $R_2^2(8)$ synthons.

5.4.2. Thermal analysis

Thermal analysis was carried out to obtain an idea about the thermal stability of the complex. The TG curves for complex **1** is shown in Fig. 5.9. For **1** it clearly shows that the complex is thermally stable up to 110°C. In the temperature range 110°C to 125°C complex **1** loses two non-coordinated water molecules (calculated mass loss 6.54%, found 6.4%). A second weight loss is observed in the temperature range 170°C to 187°C due to decomposition of two coordinated water molecules (calculated mass loss 7%, found 6.8%). Then the complex is stable thermally up to 378°C and finally **1** exhibits a consequent weight loss indicating multistep decomposition above 400°C.

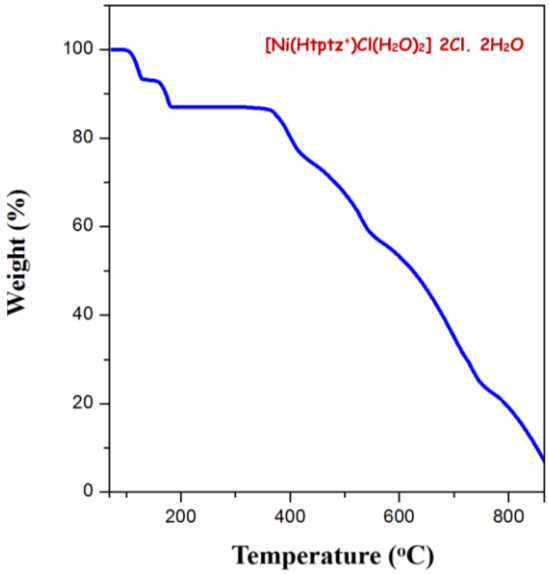

Fig. 5.9: TGA of Complex **1** measured under N_2 atmosphere

5.4.3. Theoretical study

The theoretical study is focused on the analysis and rationalization of both types of anion···π interactions that are observed in the solid state of the Ni-complex **1**. The dication $[Ni(\mathbf{Htptz})(H_2O)_2Cl]^{2+}$ interact with the chloride counterions by means of collaborative H-bonds and anion···π interactions, as represented in [Fig. 5.10 (a)]. The O–H···Cl distances are similar (2.26 and 2.27 Å) and also the anion···π distances (measured from the anion to the triazine ring centroid).

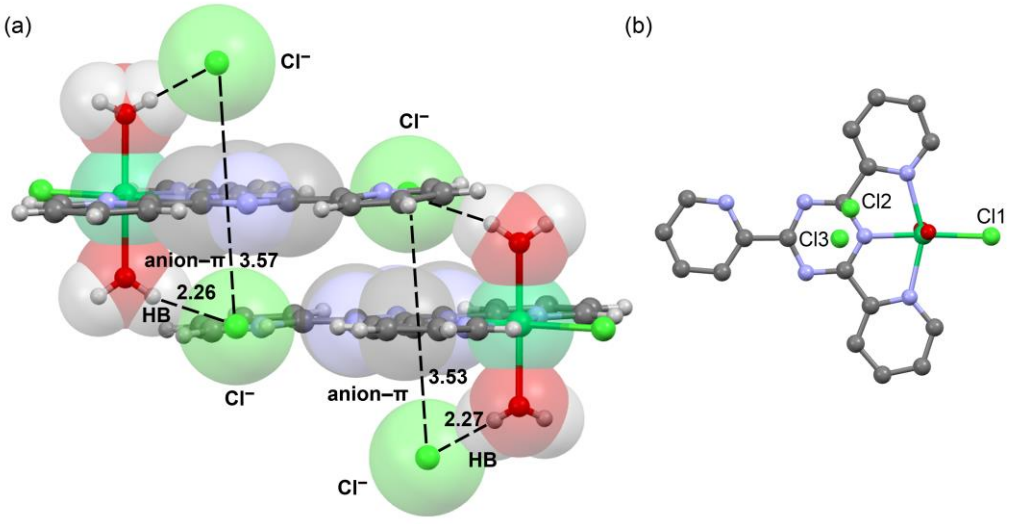

Fig. 5.10: (a) Partial view of the X-ray structure of **1** with indication of the anion···π and O–H···Cl interactions. (b) on top view of the complex

The zenithal view of the complex [Fig. 5.10 (b)] illustrates the difference of both anion···π interactions, in one case (Cl3), the anion is located approximately over the center of the ring, slightly displaced toward the coordinated N-atom. In the other case (Cl2), the anion is located approximately over one C-atom of the triazine ring. At first the molecular electrostatic potential (MEP) surface of hypothetical [Ni(tptz)(H_2O)$_2$Cl](Cl) has been computed where the **tptz** has been considered as de-protonated ligand in order to visualize the most electrophilic parts of the molecule in a neutral system. The surface is represented in Fig. 5.11 and it can be observed that the MEP maximum is located at the H-atoms of the coordinated water molecules, due to the enhanced acidity of these protons as a consequence of coordination of the O-atom to Ni(II) metal center. The MEP is also positive over the center of the three aromatic rings coordinated to the Ni(II) ion. The MEP values over the pyridine ring (15-17 kcal/mol) are smaller than those over the triazine ring (+26 kcal/mol), thus revealing that the coordinated triazine ring is significantly more acidic than the pyridine ring (Fig. 5.11). This explains the location of the non-coordinated chloride ions that are located above and below the triazine ring (Fig. 5.10). The MEP minimum is located at the non-coordinated Cl^- atom (–55 kcal/mol) and that at the coordinated Cl-atom is –31 kcal/mol.

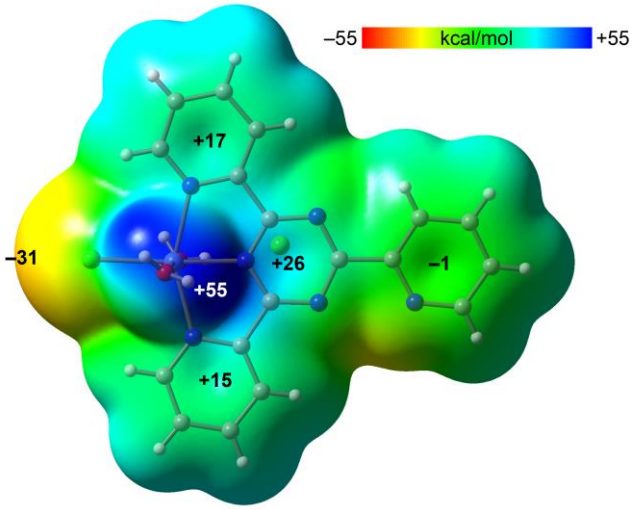

Fig. 5.11: MEP surface (isosurface 0.001 a.u.) of [Ni(**tptz**)(H_2O)$_2$Cl](Cl) at the PBE0-D3/def2-TZVP level of theory. The values at selected points of the surface are given in kcal/mol.

The interaction energies associated to the H-bonds and anion···π interactions described above have analyzed and studied the effect of the positive charge on one of the pyridine rings of the **tptz** ligand. Two different types of anion···π interactions are observed in

the solid state of **1**, as represented in Fig. 5.12, which have been denoted as (anion···π)$_1$ and (anion–π)$_2$. In the former the Cl anion is located approximately over the center of the ring and in the latter, it is displaced toward one C-atom of the ring [Fig. 5.10 (b)]. Fig. 5.12 (a) shows the binding energy of the interaction of the two possible cationic {[Ni(**Htptz**$^+$)(H$_2$O)$_2$Cl](Cl)}$^+$ moieties and chloride.

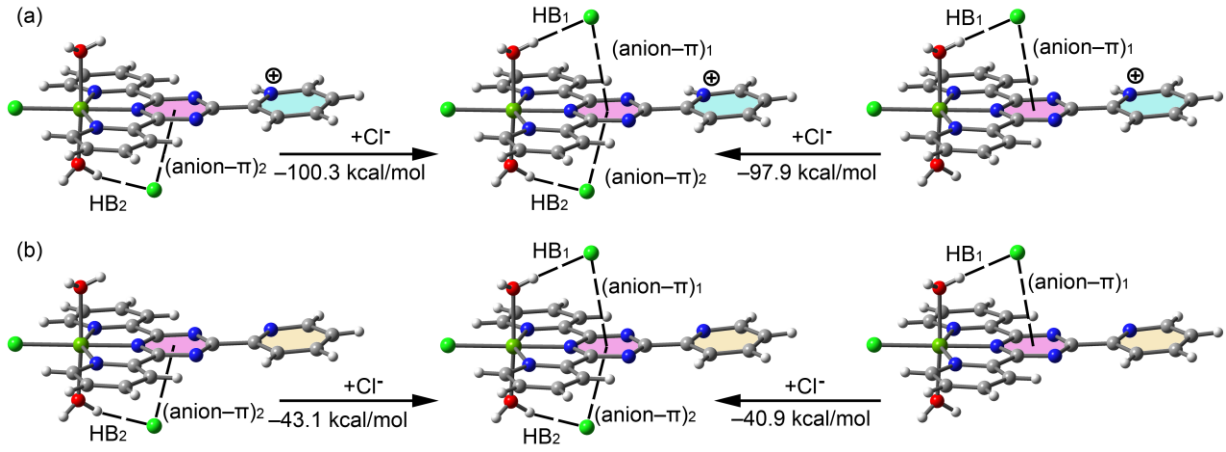

Fig. 5.12: Models used to evaluate the interaction energies for both combination of anion···π and HB interactions by using charged (a) and neutral models (b) in complex **1**.

It can be observed that both binding energies are very large (–100.3 kcal/mol and –97.9 kcal/mol) due to the strong electrostatic attraction between the counter ions. In an effort to estimate the energetic features of the anion···π and hydrogen bonds in the absence of strong electrostatic effects, the neutral {[Ni(**tptz**)(H$_2$O)$_2$Cl](Cl)} moieties have been used as shown in Fig. 5.12 (b) where the pyridine ring of **tptz** ligand is not protonated. Consequently, the binding energies are significantly reduced to –43.1 and –40.9 kcal/mol for (anion···π)$_1$ and (anion···π)$_2$, respectively, that correspond to the contribution of both the H-bonds and anion···π interactions. These large interaction energies agree well with the strong electrophilicity of the complex, as shown by the MEP surface. The combination of interactions labelled as (anion···π)$_1$ and HB$_1$, where the chloride anion is located over the center of the triazine, is stronger than the combination (anion···π)$_2$ and HB$_2$, where the chloride anion is located over one carbon atom of the triazine ring. In order to analyze the relative importance of H-bond and anion···π interactions in complex **1**, additional models have used where one of the water molecules has been eliminated [Fig. 5.13 (a) and 5.13 (b)], therefore only the anion···π interaction is evaluated. The results included in Fig. 5.13 reveal

that the (anion···π)$_1$ is around 4 kcal/mol stronger than (anion···π)$_2$. Moreover, the contributions of the HBs can be deduced by comparing the energies gathered in Fig. 5.12 (b) with those of Fig. 5.13. which are –13.8 and –15.5 kcal/mol for HB$_1$ and HB$_2$, respectively. This energetic analysis suggests that the anion···π interactions are stronger than the HBs.

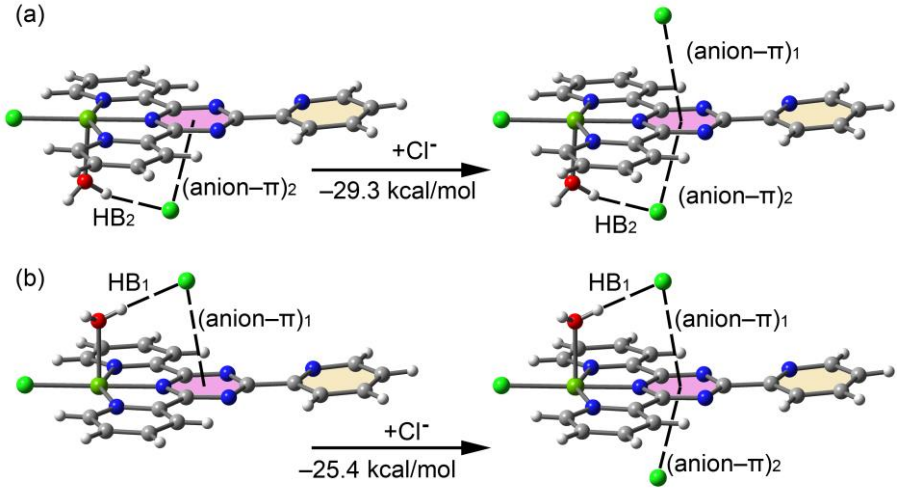

Fig. 5.13: Models used to evaluate the anion···π interaction in complex **1**.

Finally, a combined QTAIM/ NCI plot analysis in both combination of interactions has performed. Each HB is characterized by a bond critical point (CP, red sphere) and bond path interconnecting the H and Cl atoms [Fig. 5.14 (a) and 5.14 (b)]. Moreover, a small blue (strong interaction) NCI plot isosurface is also located between the Cl and H-atoms that coincides with the position of the bond CP. The (anion···π)$_1$ binding mode is characterized by a bond CP connecting the Cl to the Ni(II) coordinated N-atom of triazine ring. Moreover, a large green NCI plot isosurface (attractive interaction) embracing the whole π-system is also observed that further corroborates the existence of the anion···π interaction. The (anion···π)$_2$ binding mode is characterized by a bond CP and bond path connecting the Cl to closest C-atom of triazine ring. The green NCI plot isosurface that characterizes the anion···π interaction is smaller compared to that of (anion···π)$_1$ binding mode and also displaced toward the C-atom, in good agreement with the smaller binding energy obtained for this interaction.

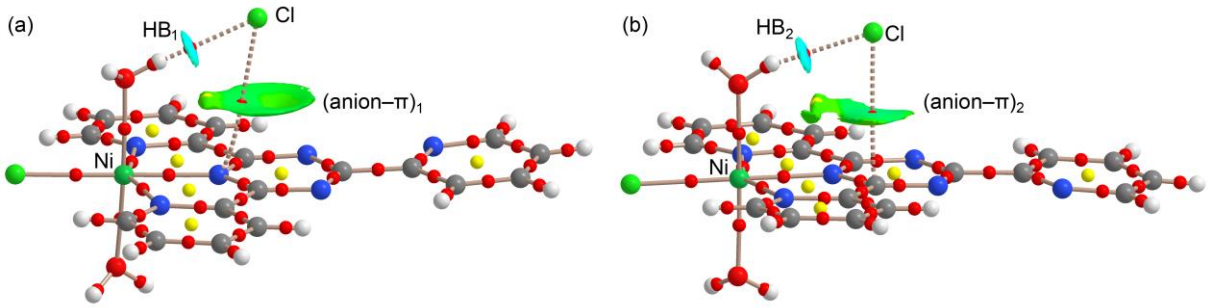

Fig. 5.14: Distribution of bond and ring CP (red and yellow spheres, respectively) and bond paths for both for (anion···π)$_1$ (a) and (anion···π)$_2$ (b) binding modes at the PBE0-D3/def2-TZVP level of theory. The overlapped NCI plot has been constructed using the 0.5 a.u. |RGD| isosurface and the sign(λ_2)ρ has been mapped using the ρ = 0.04 a.u. cut-off. For clarity, only the intermolecular isosurfaces have been plotted.

5.5. A BRIEF COMPARATIVE ACCOUNT ON ANION···π INTERACTIONS OF SOME RELATED 2,4,6 tris-(2-pyridyl)-1,3,5 triazine BASED Ni(II) COMPLEXES:

Anion···π interactions, i.e., the attraction between anions and electron deficient π system, are gaining a significant recognition and their pivotal role in many chemical and biological processes is being appreciated increasingly. Such interactions largely depend not only on the nature and shape of the anions but also the position of the π lobes offered by heterocyclic aromatic moieties. The design and quantification of highly selective anion···π interactions arrests recent interests in the nascent field of supramolecular chemistry [43-45].

In 2002, almost simultaneous pioneering theoretical studies by Alkorta et. al, [46] Deya et. al, [47] and Mascal et. al, [48] confirmed the presence of favorable non-covalent interactions between electron deficient aromatic rings and anion. Its binding energy are almost comparable to hydrogen bonds (20-50 kJmol^{-1}). The term anion···π was first coined by Deya et. al to descried such interactions [47]. Mascal et. al, [48] first pointed out about the effect of substitution by electron withdrawing groups in the aromatic ring. They provide a theoretical justification that the central triazine ring of trifluoro 1,3,5-triazine has a greater positive potential than 1,3,5-triazine due to the presence of electron withdrawing fluoride groups and hence are more susceptible to ensure anion···π interactions.

The first X-ray crystal structures with recognized and unambiguous anion···π interactions were independently reported by Meyer et. al, [49] and Reedijik et. al, [50] in 2004 using electron deficient ligand hexakis-(pyridine-2-yl)-[1,3,5]-triazine-2,4,6-triamine. In their report the anion···π distance is 3.11Å and the angle of contact is 88^o both of which

are close to theoretically as predicted by Deya [47] and Mascal [48]. Both crystallographic database and theoretical elucidation proved that the strength of this anion···π interaction is dependent on anion···π non-covalent interaction distance and as well as on the angle (θ) that is defined as the angle of the $[X]^-$···aryl centroid axis and the line connecting the ring centroid with a ring atom.

Meyer's work [49] inspired chemists to use a substituted triazine ring for inducing an anion···π interaction employing several anions like fluoride, chloride, bromide, nitrate, perchlorate etc.

Giese et. al, [51, 52] performed a series of studies in order to investigate the role of anions in anion···π interactions and are able to prove the centroid to anion distances increases in the order chloride < bromide < iodide.

To explore the role of anion···π interactions in the stabilization of Ni(II) complexes derived from 2,4,6 tris-(2-pyridyl)-1,3,5 triazine ligand in the solid state some of the related complexes reported earlier have been chosen for a brief comparison. It was found that in these earlier communications [53-55] the presence and as well as role of anion···π interactions had not been explored, though the existence of π···π or hydrogen bonding interactions had been reported. In consequence to this present work (the presence of anion···π along with other supramolecular interactions have been elucidated and quantified energetically with detailed DFT calculations) a comparative account has made focusing on only anion···π interactions (Table 5.5).

The potential versatility of 2,4,6 tris-(2-pyridyl)-1,3,5 triazine (**tptz**) system and its Ni(II) coordination chemistry was explored by Barclay et. al in 1967. In 1977 this group communicated [53] a Ni(II) complex (Complex **7** as mentioned in the Table 5.5) of **tptz** in its protonated form (**Htptz**$^+$). The charge of the cationic part was taken care by three bromide counter ions. The prospect of anion···π interactions have investigated in this complex (from crystallographic database) and have found that the bromide ion forms an anion···π interaction with central triazine ring. Due to more polarizability (charge delocalization) of the bromide ion here the anion···π distance is larger as compared to chlorides. In 2005, Zibaseresht et. al, [54] reported several Ni(II) complexes (complex **3**, **4**, **5**, **8**, **9** and **10** as mentioned in the Table 5.5) derived from **tptz** (either non-protonated or protonated) with different metal to ligand ratio. Complex **3**, **5** and **9** exhibit 1:1 metal to ligand ratio with chloride (for complex **3**

and **5**) and nitrate (complex **9**) counterions. In **3** the triazine ring became electron deficient not only due to substitution of three pyridine rings but also one nitrogen atom of triazine ring was coordinated to Ni(II) made it suitable for strong anion···π interaction with (Cg···Cl=3.307Å) non-coordinated chloride ion. In complex **5** though both coordinated and non-coordinated chloride ions were present but only non-coordinated chloride ions play a significant role in anion···π interactions with central triazine ring. These two anion···π interactions were found to bear different strength as two anion···π distances and the angle differs widely. Complex **4** is actually a mixture of two different crystallographic units of Ni(II). In this complex the non-coordinated chloride ion was engaged in anion···π interaction with the triazine ring having comparatively large Cg···Cl distance (3.8789Å) and the angle (θ) also deviated quite largely. There is no halide ions in complex **8**, **9** and **10**. Complex **8** is a bis chelated Ni(II)-tptz crystal where two perchlorate ions were responsible to balance the charge of the cationic moiety. In **8** there is two triazine rings coordinated to the metal like terpyridine motif. The oxygen atoms of perchlorate (non-compressible anion) were actively engaged in anion···π interaction with central triazine ring strongly (Cg···O distances range from 3.0 to 3.1Å and the angle θ also deviate slightly). Complex **9** is a mononuclear 1:1 complex with nitrate counter anions. Three coordinated water molecules along with **tptz** complete the octahedral geometry of **9**. Complex **10** is 2:1 (metal to ligand ratio) species formed by using nickel (II) nitrate as a metal precursor. The complex was synthesized in an aqueous ethanol solvent and both water and ethanol were present in the cationic unit of **10**. Complexes **9** and **10** exhibit active participation of terminal pyridine ring besides the triazine ring in anion···π interaction. From crystallographic database it was found that such participation of terminal pyridine ring in anion···π interaction is comparatively scarce with halides. In both **9** and **10** the oxygen atoms associated with non-coordinated ionic nitrate ions participate in anion···π interactions. Here the anion···π interaction distance ranges from 2.94Å (strong interaction) to 3.48Å (moderate interaction). From the comparative study it was evident that Cg···Cl distances incorporating triazine π is comparatively higher than that of Cg···O (oxygen may derived from nitrate or perchlorate anions). Nitrate and perchlorate ions are considered as a non-compressible hard anion (less polarizable) and hence expected to participate in strong to moderate anion···π interactions compared to more polarizable bromide (~3.7Å) or iodide (~3.9Å). Though in this article no anion···π interactions were elucidated but this consists of a pool of Ni(II) complexes not only with diverse metal to ligand molar ratio but also variation of counterions. From structural database available we

have analyzed qualitatively the possibility of existence of anion···π interactions in those complexes.

Table 5.5: Comparison of anion···π interactions in Ni(II) – 2,4,6 tris-(2-pyridyl)-1,3,5 triazine complexes

Complexes	X(I)···Cg(J)	X···Cg (Å)	X···Cg···$Z_{(Min)}$ (°)	X···Cg···$Z_{(Max)}$ (°)	Ref
$[Ni(tptz)(H_2O)Cl_2]H_2O$ **(2)**	Cl(2)···Cg(4)	3.3937	76.72	102.18	**14**
	Cg(4): [N2/C6/N3/C8/N6/C7]				
$[Ni(tptz)(H_2O)_3]Cl_2.2H_2O$ **(3)**	Cl(1)···Cg(3)	3.307	82.37	97.05	**54**
	Cg(3): [N1/C1/N2/C2/N3/C3]				
$[Ni(tptz)Cl(H_2O)_2]Cl.[Ni(tptz)(H_2O)Cl_2].4H_2O$ **(4)**	Cl(1)···Cg(3)	3.8789	67.34	113.26	**54**
	Cg(3): [N1'/C1'/N2'/C2'/N3'/C3']				
$[Ni(Htptz^+)(H_2O)_2Cl]Cl_2.H_2O$ **(5)**	Cl(4)···Cg(3)	3.951	63.04	118.74	**54**
	Cl(3)···Cg(3)	3.513	67.96	111.45	
	Cg(3): [N1/C1/N2/C2/N3/C3]				
$[Ni(tptz)(H_2O)_3Cl_2]$ $[Ni(tptz)(H_2O)Cl]Cl.5H_2O$ **(6)**	Cl(3)···Cg(11)	3.204	84.40	96.91	**CSD ref. code EREWEF**
	Cl(4)···Cg(5)	3.506	76.72	104.02	
	Cg(5): [N23/C211/N24/C213/N25/C212] **Cg(11): [N13/C111//N15/C113/N14/C112]**				
$[Ni(Htptz^+)(H_2O)_3]Br_3.H_2O$ **(7)**	Br(1)···Cg(3)	3.729	64.69	116.68	**53**
	Cg(3): [N1/C1/N2/C2/N3/C3]				
$[Ni(tptz)_2](ClO_4)_2$ **(8)**	O(11)···Cg(6)	3.109	74.01	104.97	**54**
	O(21)···Cg(5)	3.016	79.49	99.71	
	Cg(5): [N1/C1/N2/C2/N3/C3] **Cg(6): [N1'/C1'/N2'/C2'/N3'/C3']**				
$[Ni(tptz)(H_2O)_3](NO_3)_2$ **(9)**	O(1")···Cg(3)	3.485	63.00	117.07	**54**
	O(2")···Cg(4)	3.248	79.94	99.87	
	O(3")···Cg(3)	3.470	67.47	113.58	
	Cg(3): [N1/C1/N2/C2/N3/C3] **Cg(4): [N4/C4/C5/C6/C7/C8]**				
$[Ni_2(tptz)(EtOH)_2(NO_3)_3(H_2O)]NO_3$ **(10)**	O(73)···Cg(5)	2.944	74.84	105.58	**54**
	O(93)···Cg(7)	3.114	71.00	109.81	
	Cg(5): [N1/C1/N2/C2/N3/C3] **Cg(7): [N5/C9/C10/C11/C12/C13]**				
$[Ni(Htptz^+)(H_2O)_2Cl]Cl_2.H_2O$ **(1)**	Cl(2)···Cg(4)	3.549	67.69	111.64	**This work**
	Cl(3)···Cg(4)	3.527	80.69	99.05	
	Cg(4): [N2/C6/N4/C7/N5/C13]				

Complex **6** (DOI.10.5517/ccdc.csd.cclm7vl9, CSD ref. code EREWEF) as mentioned in Table 5.5, consists of two non-equivalent crystallographic units. Here the central triazine ring of two different crystallographic units interact with chloride ions as complex **4** analyzed earlier but in **6** the anion···π interaction is comparatively stronger probably due to different crystal packing force.

In 2017 Yagci et. al, [14] contributed a heteroleptic Ni(II) complex (**2**) (as mentioned in Table 5.5) where the octahedral geometry around central Ni(II) was constituted by one **tptz** ligand, one water and two chloride ions. Here the equatorially coordinated chloride (that is placed at trans to triazine coordinating nitrogen atom) ion is engaged in anion···π interaction. Possibly, other reported supramolecular interactions (π···π and hydrogen bonding interactions) were responsible to generate suitable electronic distribution for such anion···π interaction and may play a contributory role in this regard.

Though these crystallographic data confirmed the presence of anion···π interactions but this is not sufficient to ensure the strength of such interaction without performing detailed DFT calculations. To elucidate the strength and as well as the role of anion···π interaction in consequence to the stabilization of said synthesized complex (**1**) the DFT studies have been performed. Here the existence of two Cl···π (triazine ring) interactions (moderately strong) in **1** along with π···π and hydrogen bonding interactions have reported. From the theoretical insights it can be concluded that two non-coordinated chloride ions participate in anion···π interactions that cooperatively strengthened by more directional supramolecular interactions like π···π and hydrogen bonding interactions. Finally, NCI plot unambiguously shows the existence of such interactions.

5.6. CONCLUSION

A new metal-organic complex has successfully synthesized and crystallographically characterized that possesses several functional groups responsible to construct supramolecular architectures employing the coordination of a protonated heterocyclic ligand. Crystal structure of **1** is distorted octahedron using the protonated '**tptz**' ligand meridionally as a tridentate terpyridine like coordinating agent. The protonated pyridine ring acts as a potential π^+ ring that ensure a $\pi^+\cdots\pi$ interactions in conjugation with $\pi\cdots\pi$ interactions between π-enriched non-protonated pyridine moieties. Both coordinated and non-coordinated water molecules and chloride ions are actively engaged in forming various classical and non-classical hydrogen bonding interactions. Finally, an orchestrated interplay between anion$\cdots\pi$ and hydrogen bonding interactions have demonstrated. This can lead to a strong cooperative effect. Hence, the protonated ligand plays a dual role to interact with the metal and as well as counter anions. A DFT study has been used to evaluate the cooperative influence of both types of anion$\cdots\pi$ and hydrogen bonding interaction quantitively and demonstrating that the former is stronger. Finally, both interactions have been characterized using a combination of QTAIM and NCI plot tools, confirming the attractive nature of both interactions.

REFERENCES

1. N. H. Evan, P. D. Beer, *Angew. Chem., Int. Ed*., 2014, **53**, 11716-11756.
2. J. L. Atwood, G. W. Gokel, L. J. Barbour, *Comprehensive supramolecular chemistry II*, Elsevier, 2017.
3. A. Mukherjee, *Cryst. Growth Des.*, 2015, **15**, 3076-3085.
4. O. V. Shishkin, R. I. Zubatyuk, S. V. Shishkina, V. V. Dyakonenko, V. V. Medviediev, *Phys. Chem. Chem. Phys*., 2014, **16**, 6773-6786.
5. I. Alkorta, J. Elguero, A. Frontera, *Crystals*, 2020, **10**, 180.
6. S. Scheiner, *Non covalent forces*, ed., Springer, Dordrecht, 2015.
7. P. Pal, K. Das, A. Hossain, A. Frontera, S. Mukhopadhyay, *New J. Chem.*, 2020, **44**, 7310-7318.
8. A. M. Maharramov, K. T. Mahmudov, M. N. Kopylovich and A. J. L. Pombeiro, (Edn) *Non-covalent interaction in the synthesis and design of new compounds*, John Wiley & Sons. Inc., Hoboken, NJ, 2016.
9. M. G. Alexandru, D. Visinescu, B. B. Cula, F. Lloret, M. Julve, *Eur. J. Inorg. Chem.*, 2018, **3-4**, 349-359.
10. H. Hadadzadeh, M. Maghami, J. Simpson, A. D. Khalaji, K. Abdi, *J. Chem. Crystallogr*., 2012, **42**, 656-667.
11. K. N. Lazarou, I. Stamatopoulos, V. Psycharis, C. Duboc, C. P. Raptopou, Y. Sanaki, *Polyhedron*, 2018, **155**, 291-301.
12. A. Majumder, G. Pilet, M. S. El. Fallah, J. Ribas, S. Mitra, *Inorg. Chim. Acta*. 2007, **360**, 2307-2312.
13. A. Das, C. Marschner, J. Cano, J. Baumgartner, J. Ribas, M. S. El. Fallah, S. Mitra, *Polyhedron*, 2009, **28**, 2436-2442.
14. N. K. Yagci, K. Guven, G. D. Yildiz, *Z. Kristallogr.*, *NCS*, 2017, **232(3)**, 485-487.
15. K. Abdi, H. Hadadzadeh, M. Salimi, J. Simpson, A. D. Khalaji, *Polyhedron*, 2012, **44**, 101-112.
16. L. Zhang, X-Q. Lu, Q. Zhang, C. L. Chen, B. S. Kang, *Trans. Met. Chem.*, 2005, **30**, 76-81.
17. P. Byers, G. Y. S. Chan, M. G. B. Drew, M. J. Hudson, C. Madic, *Polyhedron*, 1996, **15**, 2845-2849.
18. R. Weitzke, M. Mazzanti, J. M. Latour, J. Picaut, *Inorg. Chem*., 1999, **38**, 3581-3585.
19. M. Giese, M. Albrecht, K. Rissanen, *Chem. Comm.*, 2016, **52**, 1778-1795.

20. A. Frontera, *Coord. Chem. Rev*., 2013, **257**, 1716-1727.
21. A. Frontera, P. Gamez, M. Mascal, T. J. Mooibroek, J. Reedijk, *Angew. Chem. Int. Ed*., 2011, **50**, 9564-9583.
22. C. Biswas, M. G. B. Drew, D. Escudero, A. Frontera, A. Ghosh, *Eur. J. Inorg. Chem*., 2009, 2238-2246.
23. *Bruker*, *SMART* v5.631, Bruker AXS Inc., Madison, WI, USA, 2001.
24. G. M. Sheldrick, *SHELXS-97* and *SHELXL-97*, University of Göttingen, Germany, 1997.
25. M. J. Frisch, G. W. Trucks, H. B. Schlegel, G. E. Scuseria, M. A. Robb, J. R. Cheeseman, G. Scalmani, V. Barone, B. Mennucci, G. A. Petersson, H. Nakatsuji, M. Caricato, X. Li, H. P. Hratchian, A. F. Izmaylov, J. Bloino, G. Zheng, J. L. Sonnenberg, M. Hada, M. Ehara, K. Toyota, R. Fukuda, J. Hasegawa, M. Ishida, T. Nakajima, Y. Honda, O. Kitao, H. Nakai, T. Vreven, J. A. Montgomery Jr., J. E. Peralta, F. Ogliaro, M. Bearpark, J. J. Heyd, E. Brothers, K. N. Kudin, V. N. Staroverov, R. Kobayashi, J. Normand, K. Raghavachari, A. Rendell, J. C. Burant, S. S. Iyengar, J. Tomasi, M. Cossi, N. Rega, J. M. Millam, M. Klene, J. E. Knox, J. B. Cross, V. Bakken, C. Adamo, J. Jaramillo, R. Gomperts, R. E. Stratmann, O. Yazyev, A. J. Austin, R. Cammi, C. Pomelli, J. W. Ochterski, R. L. Martin, K. Morokuma, V. G. Zakrzewski, G. A. Voth, P. Salvador, J. J. Dannenberg, S. Dapprich, A. D. Daniels, O. Farkas, J. B. Foresman, J. V. Ortiz, J. Cioslowski, D. J. Fox, Gaussian 16, Gaussian Inc., Wallingford CT, 2016.
26. S. Grimme, J. Antony, S. Ehrlich, H. Krieg, *J. Chem. Phys*., 2010, **132**, 154104.
27. L. E. Zelenkov, D. M. Ivanov, E. K. Sadykov, N. A. Bokach, B. Galmes, A. Frontera, V. Yu. Kukushkin, *Crys. Growth Des*., 2020, **20**, 6956-6965.
28. L. Bofill, R. Prohens, R. Barbas, A. Frontera, *Cryst. Growth Des*., 2020, **20**, 6691-6698.
29. C. Alvarez-Lorenzo, A. Castiñeiras, A. Frontera, I. Garcia-Santos, J. Gonzalez-Perez, J. Niclos-Gutierrez, I. Rodriguez-Gonzalez, E. Vilchez, J. K. Zareba, *Cryst. Eng. Comm.*, 2020, **22**, 6674-6689.
30. J. C. Belmont-Sánchez, M. E. García-Rubiño, A. Frontera, J. M. González-Pérez, A. Castiñeiras, J. Niclós-Gutiérrez, *Crystals*, 2021, **11**, 48.
31. S. F. Boys, F. Bernardi, *Mol. Phys*. 1970, **19**, 553-566.
32. R. F. W. Bader, *Chem Rev*., 1991, **91**, 893-928.

33. J. Contreras-Garcia, E. R. Johnson, S. Keinan, R. Chaudret, J. P. Piquemal, D. N. Beratan, W. Yang, *J. Chem. Theory Comput*., 2011, **7,** 625-632.
34. E. Freire, S. Baggio, C. J. Munoz, R. Baggio, *Acta Crystallogr.*, 2002, **C 58**, m 221-m 224.
35. M. E. Diazde Vivar, S. Baggio, R. Baggio, *Acta Crystallogr.*, 2006, **E 62**, m986-m 988.
36. George A. Jeffrey, *An introduction to Hydrogen bonding*, Oxford University Press, New York, 1997.
37. L. M. Eytel, H. A. Fargher, M. M. Haley, D. W. Johnson, *Chem. Comm*., 2019, **55**, 5195-5206.
38. Y. Liu, W. Zhao, C. H. Chen, A. H. Flood, *Science*, 2019, **365**, 159-161.
39. M. Maghami, F. Farzaneh, J. Simpson, M. Ghiasi, M. Azarkish, *J. Mol. Struct*., 2015, **1093**, 24-32.
40. G. R. Desiraju, T. Steiner, *The weak hydrogen bond in structural chemistry and biology*, Oxford University Press Inc, New York, 1999.
41. G. Aullon, D. Bellamy, A. G. Orpen, L. Brammer, E. A Bruton, *Chem. Comm*., 1998, **6**, 653-654.
42. S. Scheiner, T. Kar, J. Pattanayak, *J. Am. Chem. Soc*., 2002, **124**, 13257-13264.
43. Y. Li, Z. Yang, M. Zhou, Y. Li, J. He, X. Wang, Z. Lin, *RSC Adv*., 2017, **7**, 41527-41539.
44. I. A. Rather, S. A. Wagay, R. Ali, *Coord. Chem. Rev.*, 2020, **415**, 213327.
45. B. L. Schottel, H. T. Chifotides, K. R. Dunber, *Chem. Soc. Rev.*, 2008, **37**, 68-83.
46. I. Alkorta, I. Rozas, J. Elguero, *J. Am. Chem. Soc*., 2002, **124**, 8593-8598.
47. D. Quinonero, C. Garau, C. Rotger, A. Frontera, P. Ballester, A. Costa, P. M. Deya, *Angew. Chem. Int. Ed*., 2002, **41**, 3389-3392.
48. M. Mascal, A. Armstrong, M. D. Bartberger, *J. Am. Chem. Soc*., 2002, **124**, 6274-6276.
49. S. Demeshko, S. Dechert, F. Meyer, *J. Am. Chem. Soc*., 2004, **126**, 4508-4509.
50. P. de Hoog, P. Gamez, I. Mutikainen, U. Turpeinen, J. Reedijik, Angew. *Chem. Int. Ed.*, 2004, **43**, 5815-5817.
51. M. Giese, M. Albrecht, G. Ivanova, A. Valkonen, K. Rissanen, *Supramol. Chem*., 2012, **24**, 48-55.
52. M. Giese, M. Albrecht, A. Valkonen, K. Rissanen, *Eur. J. Org. Chem*., 2013, **16**, 3247-3253.

53. G. A. Barclay, R. S. Vagg, E. C. Watton, *Acta. Crystallogr., Sect. A: Cryst. Phys., Theor. Gen. Crystallogr*, 1977, **B33**, 3487-3491.

54. R. Zibaseresht, R. M. Hartshorn, *Aust. J. Chem.*, 2005, **58**, 345-353.

55. C. Garau, D. Quinonero, A. Frontera, P. Ballester, A. Costa, P. M. Deya, *Org. Letter.*, 2003, **5**, 2227-2229.

APPENDIX

LIST OF PUBLICATIONS

RSC Advances

PAPER View Article Online View Journal | View Issue

CrossMark click for updates

Cite this: *RSC Adv.*, 2015, 5, 45082

Synthesis, crystal structures, magnetic properties and DFT calculations of nitrate and oxalate complexes with 3,5 dimethyl-1-(2′-pyridyl)-pyrazole-Cu(II)†

Pampi Pal,[a] Saugata Konar,*[b] Mohamed Salah El Fallah,[c] Kinsuk Das,*[d] Antonio Bauzá,[e] Antonio Frontera*[e] and Subrata Mukhopadhyay[b]

THE JOURNAL OF PHYSICAL CHEMISTRY B Article pubs.acs.org/JPCB

On the Importance of Noncovalent Carbon-Bonding Interactions in the Stabilization of a 1D Co(II) Polymeric Chain as a Precursor of a Novel 2D Coordination Polymer

Pampi Pal,[†] Saugata Konar,*[,†] Prem Lama,[‡] Kinsuk Das,*[,§] Antonio Bauzá,[∥] Antonio Frontera,*[,∥] and Subrata Mukhopadhyay[†]

NJC

ROYAL SOCIETY OF CHEMISTRY

PAPER View Article Online View Journal | View Issue

Check for updates

Cite this: *New J. Chem.*, 2020, 44, 7310

Supramolecular and theoretical perspectives of 2,2′:6′,2″-terpyridine based Ni(II) and Cu(II) complexes: on the importance of C–H···Cl and π···π interactions†

Pampi Pal,[a] Kinsuk Das,[b] Anowar Hossain,[a] Antonio Frontera *[c] and Subrata Mukhopadhyay*[a]

NJC

ROYAL SOCIETY OF CHEMISTRY

PAPER View Article Online View Journal | View Issue

Check for updates

Cite this: *New J. Chem.*, 2021, 45, 11689

Synthesis and crystal structure of the simultaneous binding of Ni(II) cation and chloride by the protonated 2,4,6 tris-(2-pyridyl)-1,3,5 triazine ligand: theoretical investigations of anion···π, π···π and hydrogen bonding interactions†

Pampi Pal,[a] Kinsuk Das,*[b] Anowar Hossain,[a] Rosa M. Gomila,[c] Antonio Frontera *[d] and Subrata Mukhopadhyay*[a]

1. **Synthesis, crystal structures, magnetic properties and DFT calculations of nitrate and oxalate complexes with 3,5 dimethyl-1-(2′-pyridyl)-pyrazole-Cu(II).**

   P. Pal, S. Konar, M. S. El Fallah, K. Das, A. Bauzá, A. Frontera, S. Mukhopadhyay.

   RSC Advances 5 (2015) 45082-45091.

2. **On the Importance of Noncovalent Carbon-Bonding Interactions in the Stabilization of a 1D Co(II) Polymeric Chain as a Precursor of a Novel 2D Coordination Polymer.**

   P. Pal, S. Konar, P. Lama, K. Das, A. Bauzá, A. Frontera, S. Mukhopadhyay.

   The Journal of Physical Chemistry B 120 (2016) 6803-6811.

3. **Supramolecular and theoretical perspective of 2,2′:6′,2″-terpyridine based Ni(II) and Cu(II) complexes: On the importance of C–H···Cl and π···π interactions.**

   P. Pal, K. Das, A. Hossain, A. Frontera, S. Mukhopadhyay

   New J. Chem. 44 (2020) 7310-7318.

4. **Synthetic, supramolecular and theoretical aspects of the simultaneous binding of Ni(II) cation and chloride anion by 2,4,6 tris-(2-pyridyl)-1,3,5 triazine: On the importance of anion···π, π···π and hydrogen bonding interactions.**

   P. Pal, K. Das, A. Hossain, R. M. Gomila, A. Frontera, S. Mukhopadhyay.

   New J. Chem. 45 (2021) 11689–11696.

RSC Advances

PAPER

View Article Online
View Journal | View Issue

Cite this: *RSC Adv.*, 2015, **5**, 45082

Synthesis, crystal structures, magnetic properties and DFT calculations of nitrate and oxalate complexes with 3,5 dimethyl-1-(2′-pyridyl)-pyrazole-Cu(II)†

Pampi Pal,[a] Saugata Konar,*[b] Mohamed Salah El Fallah,[c] Kinsuk Das,*[d] Antonio Bauzá,[e] Antonio Frontera*[e] and Subrata Mukhopadhyay[b]

Received 10th March 2015
Accepted 12th May 2015

DOI: 10.1039/c5ra04241k

www.rsc.org/advances

The synthesis, crystal structures and magnetic property of an uncommon oxalate-containing copper(II) chain of formula $[Cu(L)(Ox)_2(H_2O)]_n$ (**2**), where L = 3,5 dimethyl-1-(2′-pyridyl)-pyrazole and a mononuclear Cu(II) complex $[Cu(L)(NO_3)_2]$ (**1**) derived from the same ligand, which can be used as the precursor of compound **2** are reported. The structure of **2** consists of tridentate oxalate-bridged ($\mu_{1,2,3}$) copper(II) chains, ligand (L) and crystallization water molecules. Variable-temperature magnetic susceptibility measurements of **2** show the occurrence of a weak ferromagnetic interaction through the oxalate bridge [$J = +1.95 \pm 0.08$ cm^{-1}]. The small J value can be interpreted as a consequence of the almost zero overlap between the Cu(II) ions through the bridging ligand due to the different character (axial and equatorial), giving quasi-orthogonal magnetic orbitals. DFT calculations have been used to rationalize several aspects including the magnetic coupling mechanism and the interesting noncovalent interactions observed in the solid state architecture of compounds **1** and **2**.

Introduction

Inorganic chemists have shown interest in synthesizing coordination complexes of heterocyclic base ligands because of their broad applicability in catalysis, in designing molecular ferromagnets, in biological modeling as liquid crystals and as heterogeneous catalysts.[1,2] It is well known that the careful selection of organic ligands is one of the key factors for the synthesis of coordination compounds with novel structures.

The oxalate ion has been demonstrated to be an excellent connector for the construction of organic–inorganic hybrid polymeric compounds. The oxalate group (dianion of the ethanedioic acid, H_2Ox) is a classical ligand in coordination chemistry and in magneto-structural studies due to the great number of coordination modes that it exhibits in its metal complexes[3–6] together with its remarkable ability to mediate strong magnetic interactions between the paramagnetic metal ions when acting as a bis-bidentate bridge, the metal–metal separation being larger than 5.4 Å.[6] In the available oxalate copper(II) complexes, the $\mu_{1,2,3,4}$-bis-chelating mode is more frequently exhibited, while the number of structurally characterized complexes in which the oxalate group acts as tridentate ligand is scarce[7] that exhibit weak antiferromagnetic interactions between copper(II) ions.[8–13] The ferromagnetic complexes with tridentate coordination mode are very rarely reported. Here, we report a weak ferromagnetic tridentate oxalato bridged 1D Cu(II) polymeric complex along with a monomeric Cu(II) complexes derived from strongly coordinating bidentate pyridyl-pyrazole (L) ligand. Magnetic susceptibility measurements reveal a weak ferromagnetic interaction between the adjacent Cu(II) ions separated by 5.399 Å. There are several oxalato bridged Cu(II) complexes among which some are antiferromagnetic in nature and some other shows ferromagnetic behaviour (*vide infra*). Keeping all these results in mind we extend our work beyond the monomeric Cu(II) complex (complex **1**) derived from pyridyl-pyrazole (L) ligand and finally have synthesized a weak ferromagnetic tridentate oxalato bridged 1D Cu(II) polymeric complex (complex **2**) from the same ligand in two different ways (Scheme 1). The first one was synthesized by 1 : 1 condensation between $K_2[Cu(Ox)_2]$ and the ligand 'L' in methanol solvent and the second one was synthesized from the condensation of the complex **1** with oxalic acid in aqueous media. Even though a great variety of oxalato-bridged polynuclear complexes have been

[a]*Assistant Teacher in Chemistry, Ghoshpara Nischinda Balika Vidyapith, Bally, Howrah 711227, India*

[b]*Department of Chemistry, Jadavpur University, Jadavpur, Kolkata 700032, India. E-mail: saugata.konar@gmail.com*

[c]*Departament de Química Inorganica, Universitat de Barcelona, Marti I Franques, 1-11, 08028 Barcelona, Catalunya, Spain*

[d]*Department of Chemistry, Chandernagore College, Hooghly, 712136 West Bengal, India. E-mail: kdaschem@yahoo.in*

[e]*Departament de Química, Universitat de les Illes Balears, Crta. de Valldemossa km 7.5, 07122 Palma, Baleares, Spain. E-mail: toni.frontera@uib.es*

† Electronic supplementary information (ESI) available. CCDC 945288 and 945289. For ESI and crystallographic data in CIF or other electronic format see DOI: 10.1039/c5ra04241k

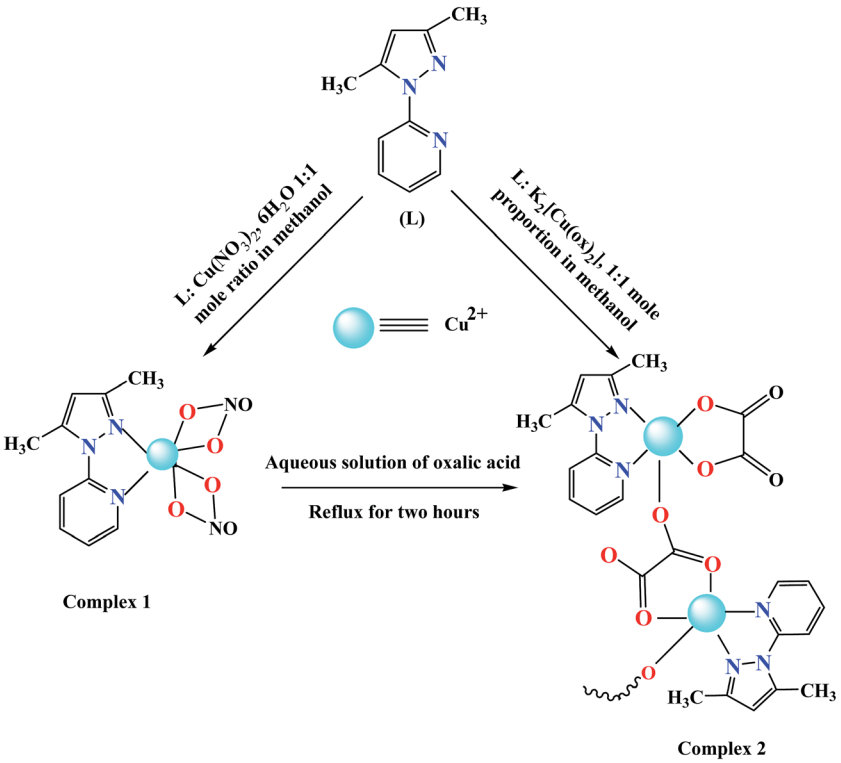

Scheme 1

structurally and magnetically characterized (from discrete dimers to three-dimensional systems), to the best of our knowledge only a few weak ferromagnetically one-dimensional $\mu_{1,2,3}$ tridentate oxalato-bridged copper(II) compounds are known.[14] Moreover, compound **2** is the first example of a the tridentate oxalate-bridged ($\mu_{1,2,3}$) copper(II) based on pyridyl pyrazole ligand. Finally, we also report herein density functional theory (DFT) calculations where we analyze two interesting aspects of the complexes. First, we study the interesting π-hole noncovalent interactions involving the coordinated nitro ligands in compound **1**. As a matter of fact, the importance of this particular interaction in supramolecular chemistry has been recently investigated[15] combining a comprehensive analysis of the CSD and theoretical calculations. Second, the magnetic properties of compound **2** have been rationalized using the broken-symmetry approach and analyzing the spin density of a Cu_2 dimeric model of the polymeric chain.

Experimental section

Materials

All chemicals were of reagent grade, purchased from commercial sources and used without further purification. 2-Chloro pyridine, acetyl acetone and hydrazine hydrate (Aldrich) were used without further purification.

Physical measurements

Elemental analyses (C, H and N) of the ligand and the metal complexes were determined with a Perkin–Elmer CHN analyzer 2400. Magnetic susceptibilities were measured on a Quantum Design MPMSXL5 (SQUID) magnetometer. Diamagnetic corrections were estimated from Pascal's constants for all constituent atoms. The electronic spectra of the complexes in methanol solution were recorded on a Hitachi model U-3501 spectrophotometer. FT–IR spectra were recorded on a Perkin Elmer; model RX–1 (KBr disk, 4000–400 cm^{-1}) spectrometer.

Synthesis of 3,5 dimethyl-1-(2′-pyridyl) pyrazole (L)

The ligand L (3-5 dimethyl-1-(2′-pyridyl) pyrazole) was synthesized following the reported method.[16]

Synthesis of compound $[Cu(L)(NO_3)_2]$ (1). A methanolic solution (10 mL) of the ligand L (0.173 g, 1 mmol) was added drop wise to a solution of $Cu(NO_3)_2 \cdot 6H_2O$ (0.295 g, 1 mmol) in the same solvent (10 mL) with constant stirring which continued for 2 h. The separated resulting green compound was filtered and dried over silica gel in desiccators. Then the solution was left for slow evaporation. After one week deep green X-ray quality crystals of **1** were isolated (yield: 62%). Anal. calc. for $C_{10}H_{11}CuN_5O_6$: C, 33.26; H, 3.05; N, 19.40. Found: C, 33.21; H, 3.01; N, 19.42. μ_{eff} (at 298 K) = 1.72 B.M. $\lambda_{max/nm}$ = 287 and 327 (Fig. S1†). Main FT-IR absorptions, (KBr pellets): ν = 1429 (s), 1315 (s), 1051 (m) (Fig. S2†).

Synthesis of compound $[Cu(L)(Ox)_2(H_2O)]_n$ (2). The methanolic solution of $K_2[Cu(Ox)_2] \cdot 2H_2O$ (0.354 g, 1 mmol) was added to an aqueous methanolic solution of the ligand L (0.173 g, 1 mmol). The mixture was stirred for 2 h, filtered and kept for slow evaporation. After one week blue X-ray quality crystals of **2** were obtained (yield: 69.5%). Anal. calc. for

$C_{24}H_{24}Cu_2N_6O_9$: C, 43.14; H, 3.59; N, 12.58. Found: C, 43.11; H, 3.57; N, 12.60. $\lambda_{max/nm}$ = 291 and 318 (Fig. S3†). FT-IR absorptions, (KBr pellets): ν = 1640 (s), 1484 (m), 1341 (s), 1059 (m), 795 (s) (Fig. S4†).

X-ray crystallographic data collection and refinement

Selected crystal data for **1** and **2** are given in Table S1† and selected metrical parameters of the complexes are given in Table S2.† For both complexes **1** and **2** data collections were made using Bruker SMART APEX II CCD area detector equipped with graphite monochromated Cu and Mo Kα radiation (λ = 0.71073 Å) source in φ and ω scan mode at 90(2) and 150(2) K respectively. Cell parameters refinement and data reduction were carried out using the Bruker SMART and Bruker SAINT softwares[17] for all the complexes. The structure of all the complexes were solved by conventional direct methods and refined by full-matrix least square methods using F^2 data. SHELXS-97 and SHELXL-97 programs[18] were used for structure of all the complexes solution and refinement respectively. For both complexes non hydrogen atoms were refined anisotropically till the convergence is attained.

Theoretical methods

The energies of all complexes included in this study were computed at the BP86-D3/def2-TZVP level of theory. We have used the crystallographic coordinates for the theoretical analysis of the non-covalent interactions observed in the solid state. This level of theory has been shown useful and reliable to study noncovalent interactions like those analyzed herein.[19a,b] The calculations have been performed by using the program TURBOMOLE version 6.5.[20] For the calculations we have used the BP86 functional with the latest available correction for dispersion (D3).[21] The Bader's "Atoms in molecules" theory has been used to study the interactions discussed herein by means of the AIM all calculation package.[22]

The magnetic coupling constants are described using the Heisenberg model. The hybrid B3LYP functional[23a–c] has been used in all calculations as implemented in Gaussian-09,[24] using the 6-31+G* basis set for all atoms. The approach used to determine the exchange coupling constants for dinuclear and trinuclear complexes has been described before in the literature.[25a–d]

Results and discussion

Crystal structure description of complex 1

The perspective view of molecular structure of complex **1** with atom numbering scheme is shown in Fig. 1. Complex **1** crystallizes in space group P-1 in which the unit cell is comprised of two molecules.

Complex **1** is distorted octahedral where the ligand L, spans the adjacent positions [N1–Cu1–N3 = 81.54(6)°] as a neutral bidentate NN donor *via* one pyridyl nitrogen (N3) and one pyrazolyl nitrogen (N1). The other four positions of the octahedral geometry are occupied by two oxygen atoms from two different bidentate nitrate anions (O1, O2 and O4, O5). The

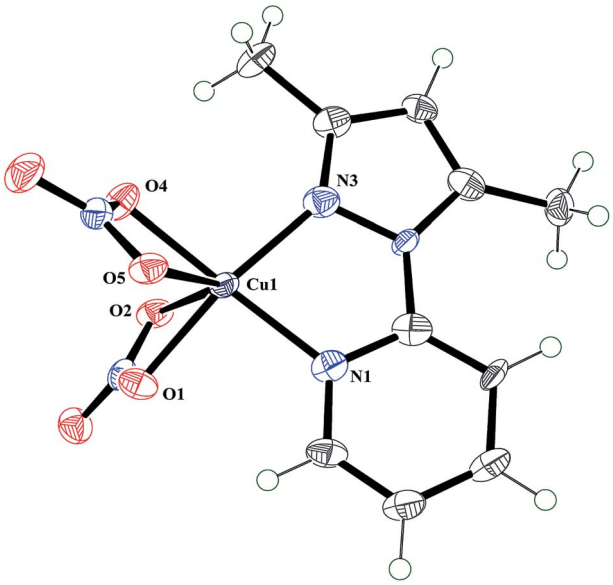

Fig. 1 Molecular structure of complex **1** with ellipsoids drawn at 50% probability. Color code: Cu(II), sky; O, red; N, blue; C, grey; H, light green.

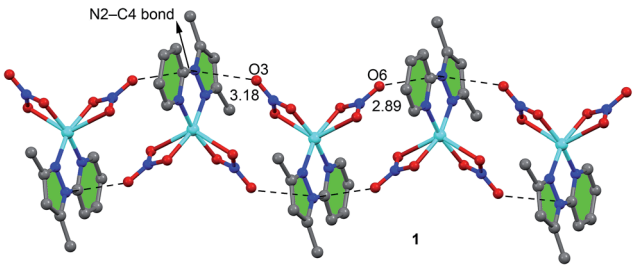

Fig. 2 Anion–π interaction along *a* axis in **1** to form an infinite 1D chain. Distances to the N–C ring centroid are given in Å. Hydrogen atoms are omitted for clarity. Color code: Cu(II), sky; O, red; N, blue; C, grey.

Cu–N bond distances [Cu1–N1 = 1.947(18) Å, Cu1–N3 = 1.977(17) Å] and the copper–oxygen bond lengths [Cu1–O1 = 2.419(16) Å, Cu1–O2 = 1.972(16) Å, Cu1–O4 = 2.481(16) Å and Cu1–O5 = 1.991(16) Å] are in accord with those values reported previously for similar type of six coordinated octahedral Cu(II) complexes.[26–28] Cu(II) atom sits in the same mean plane constituted by N1N3O5O2 atoms. The three *trans* angles are N1–Cu1–O5 (160.05°), N3–Cu1–O2 (163.47°) and O4–Cu1–O1 (128.69°) departed from the ideal trans angle of 180° due to some steric obligations. This is most likely due to the small bite angles [O1–Cu1–O2 = 58.05(5)° and O4–Cu1–O5 =

Table 1 Geometric features (distances in Å and angles in degrees) of the anion–π interactions observed in complex **1** (Cg = centre of gravity C4–N2 bond)

Interaction	O···N	O···C	∠N–O···Cg	∠O···Cg–N
N(4)-O(3)···π	3.128(5)	3.387(6)	132.8	79.1
N(5)-O(6)···π	2.964(5)	2.974(7)	134.4	89.6

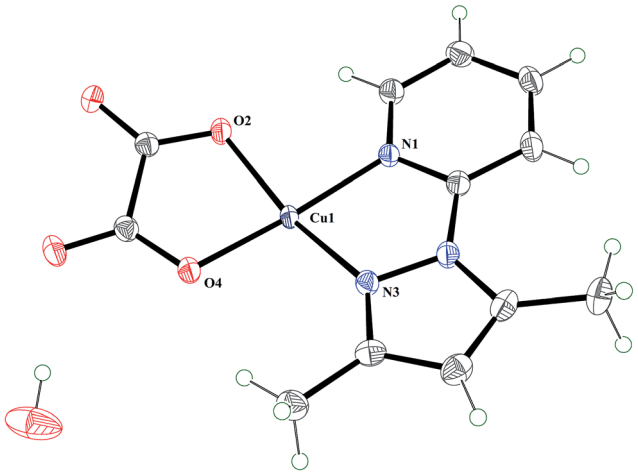

Fig. 3 Molecular structure of complex **2** with ellipsoids drawn at 50% probability. Color code: Cu(II), sky; O, red; N, blue; C, grey; H, light green.

56.74(5)°] of the bidentate nitrate ligand, which may induce a distortion in the geometry of the complex.[29] In this coordination game the pyridyl part is slightly twisted by 9.25° with respect to the pyrazole part. There are two types of anion–π interactions involving the non coordinating atoms O(6) and O(3) of the nitrate anions that are orientated towards the π-face (Fig. 2) of the ligand, pointing to the middle of the N2–C4 bond (the anion–π distances are summarized in Table 1). It is remarkably the short distance observed for the N(5)–O(6)···π contact (<3.0 Å) that is indicative of a strong interaction. As demonstrated below in the theoretical study by molecular electrostatic potential (MEP) calculations this part of the π-system is the most adequate for interacting with electron rich moieties.

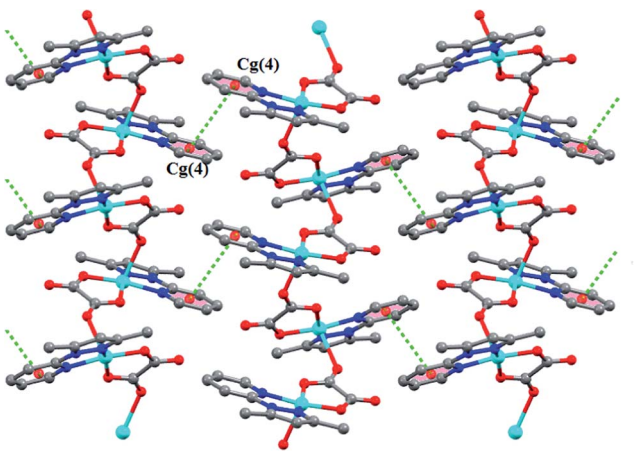

Fig. 4 π–π interaction along *c* axis in **2** to form 2D sheet. Hydrogen atoms are omitted for clarity. Color code: Cu(II), sky; O, red; N, blue; C, grey.

Structural description of complex 2

The perspective view of complex **2** with atom numbering schemes is shown in Fig. 3. The complex crystallizes in space group *C*2/*c*. The crystal structure of title compound reveals the presence of water molecule of crystallization with the neutral [Cu(Ox)(L)] moiety. The unit cell of **2** comprises of four molecules. The complex units are stacked in parallel and linked one to other through long Cu–O distances forming a one dimensional chain along the crystallographic '*a*' axis (Fig. S5†). As indicated in the structural part of **2** two oxygen atoms of one bridging oxalate anions (O2 and O4), one oxygen of other bridging oxalate anion (O1) and two *cis*-coordinated nitrogen atoms [one from pyrazole (N3) and other from pyridine (N1)] of the ligand constitute a slightly distorted tetragonal square pyramid surrounding the Cu(II) ion. Two copper atoms are crystallographically indistinguisible. The equatorial Cu–O_{basal} [Cu1–O2 (1.951 Å) and Cu1–O4 (1.924 Å)] and Cu–N [Cu1–N1 (1.988 Å) and Cu1–N3 (1.988 Å)] bond distances are comparatively shorter than Cu–O_{axial} bond distance (Cu1–O1 = 2.284 Å). The lengthening of the axial bond distance can be explained by the fact that informing the axial bond less s-character has been utilized. In this situation the unpaired electron resides in a $d_{x^2-y^2}$ type orbital pointing to the four atoms with short metal–ligand distances (in the basal plane). The overlapping density between σ type orbitals should be rather small, while the 2p orbitals of the bridging axial oxygen (O1) atom, which is involved in the axial interaction, is approximately orthogonal to the $d_{x^2-y^2}$ orbital of the Cu(II) ion. Cu atom is displaced by 0.226 Å from the N_2O_2 least square plane (N1O2O4N3) towards the axial O1 atom. The angles around the copper atom in it are close to ideal angle 90°. The metal–metal separation (Cu–Cu) within the chain of stacked molecules is 5.393 Å. These values are more or less similar to the intramolecular Cu–Cu distance (5.399 Å) in the asymmetrical binuclear cation $[(dien)Cu(\mu\text{-}ox)Cu(H_2O)_2\text{-}(tmen)]_2$ (dien = diethylenetriamine and tmen = *NNN′N′*-tetramethylenediamine),[30] but are somewhat longer than the value of 5.29 Å, reported for the sheet like polymer $[Cu_2(ox)_2(pyz)_3]_n$ (pyz = pyrazine).[31] Pyrazole part is slightly twisted by an angle 2.31° with respect to the pyridyl ring. The oxalate and pyridyl

Table 2 Geometric features (distances in Å and angles in degrees) of the π–π interactions obtained for **2**[a]

Cg(ring I)–Cg(ring J)	Cg–Cg	Cg(I)···Perp	Cg(J)···Perp	*A*	*B*	*Γ*	Symmetry
Cg(4)–Cg(4)	3.731(3)	3.372	3.372	0.02	25.34	25.34	1 − X, −Y, 1 − Z

[a] α = dihedral angle between ring I and ring J (°); β = Cg(I) → Cg(J) or Cg(I) → Me vector and normal to plane I (°); γ = Cg(I) → Cg(J) vector and normal to plane J (°); Cg–Cg = distance between ring centroids (Å); CgI···Perp = perpendicular distance of Cg(I) on ring J (Å); CgJ···Perp = perpendicular distance of Cg(J) on ring I (Å); Cg(4) = centre of gravity of ring [N1–C1–C2–C3–C4–C5] for complex **2**.

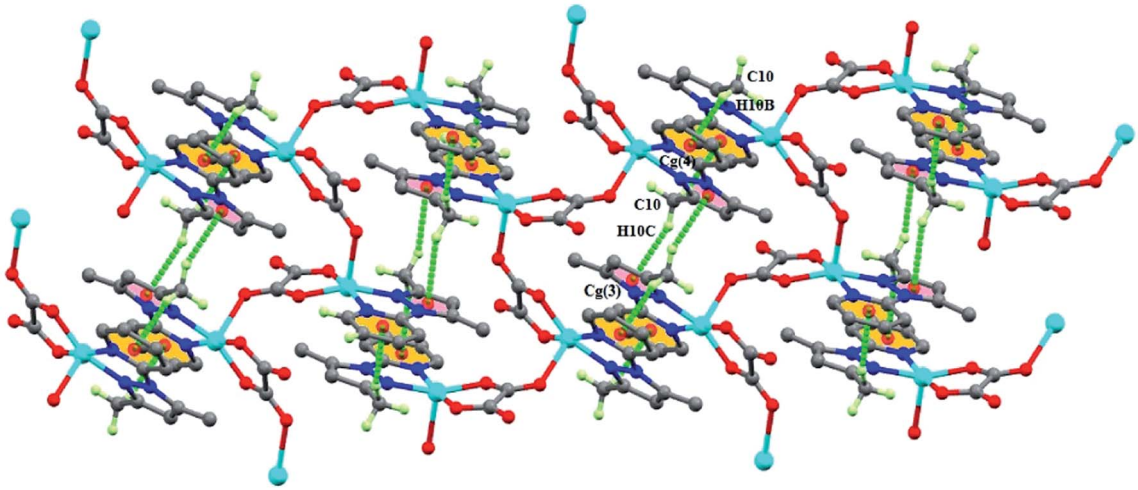

Fig. 5 C–H/π along *a* axis to form 2D sheet in **2**. Non related hydrogen atoms are omitted for clarity. Color code: Cu(II), sky; O, red; N, blue; C, grey; H, light green.

part is twisted by an angle 17.03° whereas the same with pyrazole part is 17.8°.

A two-dimensional supramolecular sheet (Fig. 4) is formed in complex **2** by multiple face-to-face π–π stacking interactions between the 1D infinite chains that involve the pyridine rings [Cg(4)], N1–C1–C2–C3–C4–C5] of one chain with the symmetry related (1 − X, −Y, 1 − Z) pyridine rings [Cg(4)] of the neighboring chain (Table 2). Each molecule of [Cu(L)(Ox)] is assembled by C–H/π interactions along *c*-axis (Fig. 5) involving the one C(methyl)–H group, C(10)–H(10B) donor group of pyrazole ring and another pyridine ring Cg(4) [the ring centroid defined by N1–C1–C2–C3–C4–C5 atoms] of symmetry 3/2 − X, 1/2 − Y, 1 − Z and another type involving C(10)–H(10C) donor group of pyrazole ring and aromatic pyrazole ring Cg(3) (the ring centroid defined by N2–N3–C6–C7–C8 atoms) of symmetry 3/2 − X, −1/2 − Y, 1 − Z (Fig. 5) (Table 3).

For complex **2**, Cg(4) = centre of gravity of ring [N1–C1–C2–C3–C4–C5], Cg(3) = centre of gravity of ring [N2–N3–C6–C7–C8].

Magnetic properties

The magnetic property of complex **2** is shown in Fig. 6 as $\chi_M T$ *vs.* T and $M/N\mu_B$ *vs.* H (inset) respectively. The values of $\chi_M T$ at 300 K are 0.5 $cm^3\ mol^{-1}$ K which is as expected for magnetically quasi-isolated spin doublets ($g > 2.00$). Starting from the room temperature $\chi_M T$ values remain practically constant up to 50 K and below 50 K it increase quickly to 1.1 $cm^3\ mol^{-1}$ K at 2 K. This global feature is characteristic of very weak ferromagnetic interactions. The $M/N\mu_B$ value at 5 T is close to 1.1 and the curve practically follows the Brillouin law, assuming $g > 2.0$, logical for any Cu(II) ion. Complex **2** is, actually, a one-dimensional system in which the copper atoms are linked by oxalato bridging ligands in axial-equatorial form. This feature gives a uniform $S = 1/2$ system (with J = coupling parameter for the Cu-bridge-Cu pathway). The fit of the magnetic data has been carried out using the formula given by Kahn for this kind of uniform ferromagnetic $S = 1/2$ chains.[32] According to Kahn's model,[6,32] the coupling constant 'J' can be decomposed into two terms, one positive (ferromagnetic, J_F) and the other negative (antiferromagnetic, J_{AF}), the expression being $J = J_F + J_{AF}$. In such a model, the value of the negative term is proportional to the square of the overlap integral (S^2) between the two metal centered magnetic orbitals. In the case of complex **2**, the poor overlap between the two parallel magnetic orbitals through the two OCO oxalate set of atoms would lead to a weak ferro- or antiferromagnetic coupling. The best-fit parameters obtained with this model are $J = +1.95 \pm 0.08\ cm^{-1}$, $g = 2.21 \pm 0.01$ and $R = 1.1 \times 10^{-4}$. This result is a signature of the very weak ferromagnetic coupling mediated through the bridging ligands. The small J value can be interpreted as a consequence of the almost nil overlap between the Cu(II) ions through the ligand due to the different character (axial and equatorial), giving quasi-orthogonal magnetic orbitals. The symmetry of the Cu(II) ion is distorted square-pyramidal (τ parameter = 0.18; 0 for square pyramidal and **1** for trigonal bipyramidal). The major tendency to adopt the square pyramidal geometry avoids the necessary molecular overlap because the electronic density in a square pyramidal is in the $d_{x^2-y^2}$ orbital. No important density is in the d_{z^2} orbital (which corresponds to axial direction). The

Table 3 Geometric features (distances in Å and angles in degrees) of the C–H/π interactions obtained for **2**

C–H···Cg(ring)	H···Cg (Å)	C–H···Cg (°)	C···Cg (Å)	Symmetry
C10–H10B···Cg(4)	2.82	165	3.752(4)	3/2 − X, 1/2 − Y, 1 − Z
C10–H10C···Cg(3)	2.60	138	3.368(3)	3/2 − X, −1/2 − Y, 1 − Z

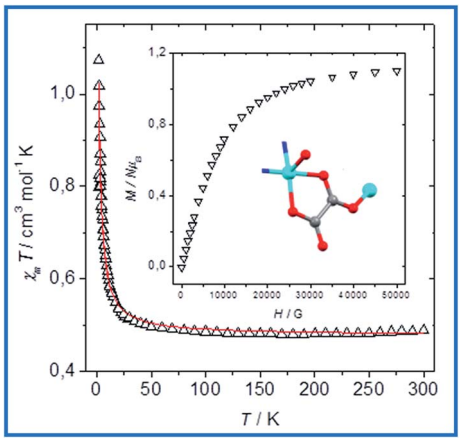

Fig. 6 $\chi_M T$ *vs.* T and $M/N\mu_B$ *vs.* H (inset) for complex **2**.

calculated J value must be taken with care, because being so small, any interchain coupling will be of the similar order of magnitude (but antiferromagnetic).

Magneto-structural comparison

The versatility in coordination modes of oxalate ion in metal complexes (Fig. S6†) constitutes the basis for the development of synthesis and magneto-structural investigation of oxalate bridged complexes [here Cu(II) complex] where the magnetic metal centers are as far away as 5 Å. The magnetic coupling in oxalato complexes ranging from weak ferromagnetic (**6–9**)[32,33,35,36] to weak antiferromagnetic (**3–5**)[33,34] through the moderate (**10,11**)[37,38] to strong (**12,13**)[39,40] antiferromagnetic are shown in Table S3† (our synthesized oxalato bridged copper complex is listed as number **2**). Detailed analysis of oxalate bridged Cu(II) complexes establish that their magnetic exchange interactions are strongly dependent on the geometry around the Cu(II) ion, sensitive to the orientation of the magnetic orbital of each Cu(II) ion relative to the oxalate plane and the bridging mode of the oxalate group. It has been found in oxalate-bridged copper(II) complexes that strong antiferromagnetic coupling (J ranging from -260 to -400 cm^{-1}) results when the short Cu(II)–ligand bonds are coplanar with the bridging ligand (topology A in Fig. S7†) and the singly occupied molecular orbitals (SOMO's) are built up from metal 'd' orbitals ($d_{x^2-y^2}$ type orbitals in square pyramidal or elongated octahedral geometry) well oriented to interact with the bridging ligand. When one of the Cu(II)–oxalate bridge distance is long (oxalate bridge is asymmetrically coordinated) the two metal-centred magnetic orbitals are parallel to each other and perpendicular to the bridging oxalate (topology B in Fig. S7†) and the interaction is poor which results a weak magnetic coupling (J ranging from +3 to -45 cm^{-1}). An intermediate case is that for which one of the magnetic orbitals is coplanar with the oxalate bridge whereas the other one is perpendicular to it (topology C in Fig. S7†),[37] as in complex **2**.

Theoretical study

We have divided the theoretical study into two parts. Firstly, we have analyzed the noncovalent interactions energetically focusing our attention to the C–H/π, anion–π and π–π interactions observed in the solid state of compounds **1** and **2**. In addition, we have also examined the antiparallel intermolecular $NO_3\cdots NO_3$ interaction observed in compound **1**. Similar interactions have been recently attracted attention due to their increasing interest in supramolecular chemistry and crystal engineering.[41] Secondly, we have used DFT calculations combined with the broken symmetry approach to gain insight into the qualitative theoretical interpretation on the overall magnetic behavior of the complex.

Noncovalent interactions

We have focused the theoretical study of compound **1** to the supramolecular 1D chain found in its solid state structure that is characterized by the presence of self-complementary anion–π interactions (Fig. 2). First of all, we have computed and analyzed the MEP surface of complex **1** (X-ray asymmetric unit), that is shown in Fig. 7A. It can be observed that the most positive electrostatic potential isovalue is located close to the aromatic hydrogen atoms of the ligand, which are more acidic than in the free ligand due to the coordination to the Cu^{II} ion. The blue (positive electrostatic potential) contours also include the π-system and, remarkably, the contour corresponding to the isovalue = +30 kcal mol^{-1} reaches the region of the N2–C4 bond. The electrostatic potential over the center of the pyridine ring is smaller (+26 kcal mol^{-1}). This result is helpful to explain the location of the uncoordinated oxygen atom (O6, see Fig. 7B) of the nitrate in the X-ray geometry that is pointing to the middle of the C–N bond. We have computed the interaction energy of the self-assembled dimer (see Fig. 7B), which is large and negative ($\Delta E_1 = -22.4$ kcal mol^{-1}). A detailed analysis of this dimeric unit reveals that the coordinated nitrate ligands are also interacting to each other (see Fig. 7C). That is, the O4 oxygen atom of one complex is located at 3.065(5) Å from the N5 nitrogen atom of the other complex and *vice versa* (the O4⋯N5 distance is slightly shorter than the sum of van der Waals radii that is 3.07 Å). This interaction is similar to antiparallel CO⋯CO interactions described in the literature;[42] however, it should emphasized that in complex **1** the antiparallel NO⋯NO interaction involves two anionic ligands (even though part of the charge is transfer to the metal center). Therefore this interaction can be considered as a *pseudo* antielectrostatic interaction that has been recently described for hydrogen bonds.[43] In order to investigate if this NO⋯NO interaction is energetically favored we have used a theoretical model (see Fig. 7D) where the aromatic ligands have been eliminated and only the NO⋯NO interaction is evaluated. As a result the computed interaction energy is $\Delta E_2 = -9.1$ kcal mol^{-1} that indicates a favorable contribution of this interaction. It should be mentioned that this is only a rough estimation of the NO⋯NO interaction energy because the coordination environment of the Cu ion has changed in this reduced model with respect to complex **1**. However, it likely demonstrates (at least qualitatively) that this *pseudo* antielectrostatic interaction is energetically favorable. Moreover, in an effort to evaluate the anion–π interaction, we have used an additional theoretical

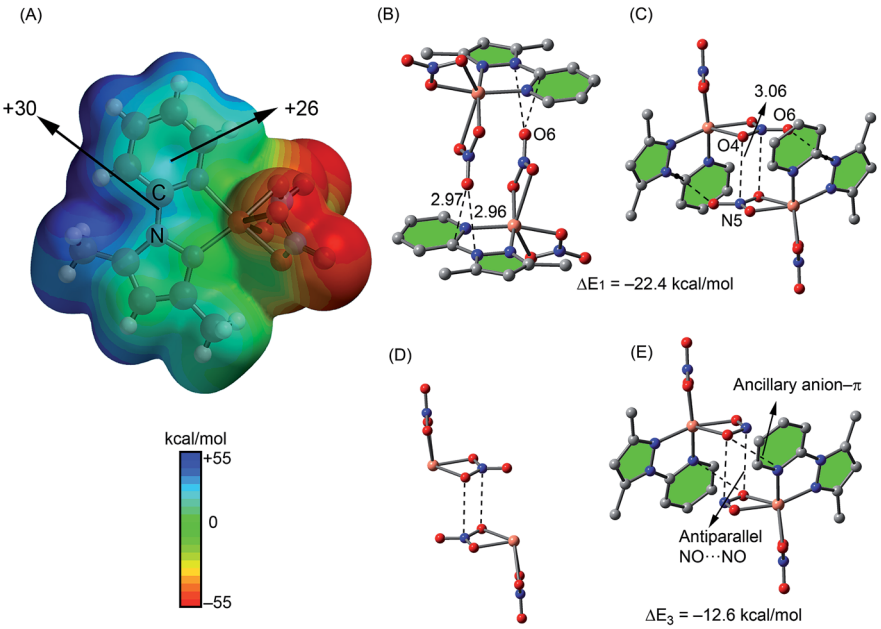

Fig. 7 (A) MEP surface computed for **1**. (B and C) Two views of the self-assembled dimer observed in the solid state of **1**. (D) Theoretical model without the organic ligands. (E) Theoretical model where the nitrate ligands have been replaced by nitrite ligands.

model where the nitrate counterions have been replaced by nitrite ligands (see Fig. 7E). This model does not have the contribution of the O6···π interaction that can be then estimated by comparing ΔE_1 and ΔE_3. As a result the contribution of the anion–π interaction (O6···π) to the formation of the dimer is $\Delta E_1 - \Delta E_3 = -9.8$ kcal mol^{-1}. We have also used the Bader's[44] "atoms-in-molecules" to further characterize and these interactions and the results are discussed in the ESI.†

In the polymeric complex **2** we have evaluated energetically the noncovalent interactions that are relevant to rationalize the crystal packing described in Fig. 4 and 5. We have used a repeating structural unit of the polymeric chain of compound **2** for the calculations. The theoretical models to analyze the CH/π and π–π interactions are shown in Fig. 8. The interaction energy of the C–H/π self-assembled complex (Fig. 8A) is larger in absolute value ($\Delta E_4 = -15.0$ kcal mol^{-1}) than expected for this type of interaction.[45] This is likely due to additional electrostatic forces between the anionic oxalate ligands and the hydrogen atoms of the methyl groups that are separated by ~3.8 Å (see Fig. 8A). We have also computed a theoretical model where only the organic ligands are considered (see Fig. 8B). As a result the interaction energy is reduced to $\Delta E_5 = -6.8$ kcal mol^{-1} indicating that each C–H/π interaction contributes in 3.4 kcal mol^{-1}. The π–π interaction mode observed for the coordinated pyridine rings in antiparallel. Previous studies[46] have demonstrated that this arrangement is energetically favored over the parallel binding model. The interaction energy of the π–π model dimer is $\Delta E_6 = -6.7$ kcal mol^{-1} that is similar to previously reported in coordinated pyridine and pyrimidine rings (see Fig. 8C).[46] We have also examined the distribution of critical points of both dimeric complexes and a good agreement with the energetic analysis is found (see Fig. S9 in ESI† for the results).

Finally, we have analyzed the magnetic coupling interaction theoretically in a dinuclear model of compound **2** by computing the spin density distribution. According to the molecular orbital theory, spin delocalization is the result of electron transfer from the magnetic centers to the ligand atoms. A spin-exchange model was generated for theoretical studies using the crystal structure geometry. The theoretical

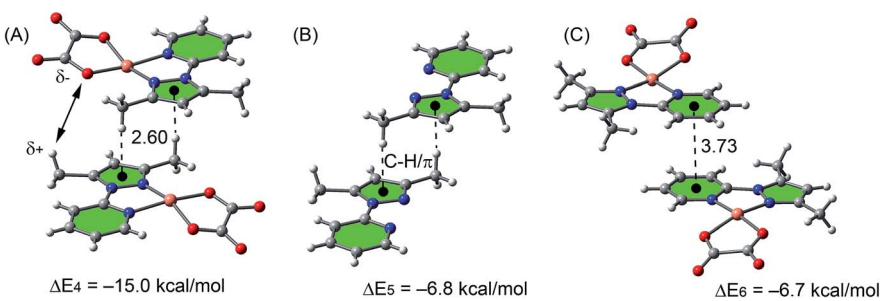

Fig. 8 Theoretical models used to evaluate the noncovalent interactions observed in the solid state of **2** (A–C).

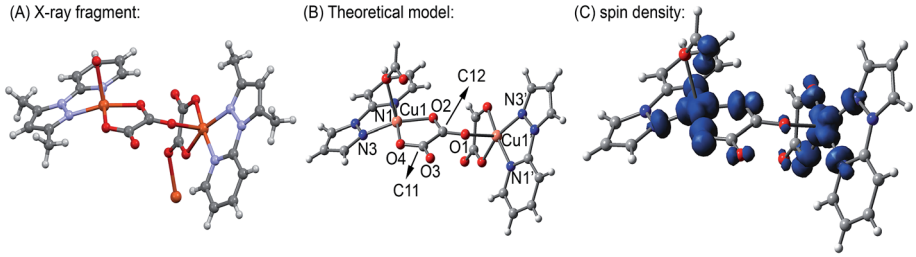

Fig. 9 X-ray, theoretical model and spin density plot (isovalue = 0.004 e Å^{-3}) of the dinuclear fragment of complex **2**.

model has been simplified, *i.e.* hydrogen atoms instead of methyl groups have been used in order to keep the size of the system computationally approachable (Fig. 9A and B). The calculation of the individual pair-wise exchange constant has been carried out by means of spin-unrestricted DFT calculations using the B3LYP method and employing the 6-31+G* basis set. The theoretical J value calculation has been performed computing the difference between the energy values of the highest spin state and the broken-symmetry state. Using this methodology and the simplified dinuclear model the theoretical J is 2.4 cm^{-1} that is in good agreement with the experimental value (1.95 cm^{-1}) and confirms the weak ferromagnetic coupling between both metal centers. The Mulliken spin population analysis (Table 4) indicates that a significant spin (*ca.* 0.73 e) is delocalized through the ligands, and the rest (1.27 e) is carried by the copper atoms. The spin density plot is shown in Fig. 9C for the high spin state of **2**. The spin density distribution shows a delocalization mechanism in which the Cu atoms carry 64% of net spin and the remaining part is delocalized through coordinating atoms.

In a square-pyramidal Cu^{II} complex, the $d_{x^2-y^2}$ orbital contains the unpaired electron; consequently these orbitals along with the local orbitals of the bridging ligands are involved in the super-exchange pathway, which is confirmed by the spin density plot shown in Fig. 9C. The spin density at the O1 is very small (0.01 e) therefore a very weak ferromagnetic coupling is mediated through the bridging ligand communicating the quasi-orthogonal magnetic orbitals. Interestingly, the spin density computed at the carbon atoms of the bridging oxalate group C11 and C12 are negative (−0.003 and −0.010 e, respectively), indicating a spin polarization mechanism that facilitates the ferromagnetic interaction.

Table 4 Mulliken spin densities (e) computed for the high spin configuration of the Cu_2 dimer model of compound **2**. See Fig. 9 for numbering scheme

Atom label	Spin density	Atom label	Spin density
Cu1	0.62	N1	0.07
Cu1′	0.65	N1′	0.10
O1	0.01	N3	0.05
O2	0.10	N3′	0.06
O3	0.03	C11	−0.00
O4	0.15	C12	−0.01

Conclusion

A new one-dimensional oxalate-containing copper(II) complex, namely $[Cu(L)(Ox)_2(H_2O)]_n$ (**2**) has been synthesized by condensing the metal salt with the ligand in methanol solvent and then again by condensing the precursor complex $[Cu(L)(NO_3)_2]$ (**1**) with oxalic acid in aqueous media. The geometry around each Cu(II) in **2** is axially elongated square pyramidal with the intrachain copper–copper separation being 5.399 Å. The magnetic studies reveal a weak ferromagnetic interaction through the oxalate bridge, its nature and magnitude being in a good agreement with available magneto-structural data for oxalate-bridged copper(II) complexes where the same out-of-plane exchange pathway is involved. The DFT calculations combined with the broken symmetry approach provide a good estimate of the weak ferromagnetic coupling that is mediated through the tridentate $\mu_{1,2,3}$ oxalate bridging ligand as corroborated by the spin density plot. Moreover, the interesting non-covalent interactions observed in the solid state have been studied by means of DFT calculations assigning discrete energetic values to them. The most important finding is the *pseudo* antielectrostatic interaction between the nitrato ligands that has been characterized both energetically and using the "atoms-in-molecules" methodology.

Acknowledgements

S. K. acknowledges the financial support provided by University Grants Commission, India (Award letter no. F.4-2/2006(BSR)/13-1089/2013(BSR), dated September, 2013) through the Dr D. S. Kothari Post Doctoral Fellowship (DSKPDF). M. S. E. F. acknowledges the financial support from the Spanish Government (Grant CTU2012-30662). Financial support from UGC-UPE (II) program of Jadavpur University is thankfully acknowledged. AF and AB thank the MINECO of Spain for financial support (CONSOLIDER-Ingenio 2010 project CSD2010-0065, FEDER funds) and CTI (UIB) for computational facilities.

References

1 K. Biradha, M. Sarkar and L. Rajput, *Chem. Commun.*, 2006, 4169–4179.
2 N. Hoshino, *Coord. Chem. Rev.*, 1998, **174**, 77–108.
3 M. H. Molina, P. A. Lorenzo-Luis and C. Ruiz-Pérez, *CrystEngComm*, 2001, **16**, 1–4.

4 S. Youngme, G. A. van Albada, N. Chaichit, P. Gunnasoot, I. Multikainen, O. Roubeau, J. Reedijk and U. Turpeinen, *Inorg. Chim. Acta*, 2003, **353**, 119–128.
5 G. Marinescu, M. Andruh, F. Lloret and M. Julve, *Coord. Chem. Rev.*, 2011, **255**, 161–185.
6 O. Kahn, *Molecular Magnetism*, Wiley-VCH, New York, 1993, and references therein.
7 H. Núñez, J.-J. Timor, J. Server-Carrió, L. Soto and E. Escrivà, *Inorg. Chim. Acta*, 2001, **318**, 8–14.
8 A. S. Olszewska, B. Matura, J. Mrozinski, B. Kaliuska, R. Kruszynski and M. Penkala, *New J. Chem.*, 2014, **38**, 1611–1626.
9 D. Y. Jeter and W. E. Hatfield, *Inorg. Chim. Acta*, 1972, **6**, 523–525.
10 A. Bentana, O. Schott, J. F. Soria, S. E. Stiriba, J. Pasan, C. R. Perez and M. Julve, *Inorg. Chim. Acta*, 2012, **389**, 52–59.
11 U. Geiser, B. L. Ramakrishna, R. D. Wilett, F. B. Hulsbergen and J. Reedijk, *Inorg. Chem.*, 1987, **26**, 3750–3756.
12 A. Gleizes, F. Maury and J. Galy, *Inorg. Chem.*, 1980, **19**, 2074–2078.
13 (*a*) K. Kadir, T. M. Ahmed, D. Noreus and L. Eriksson, *Acta Crystallogr., Sect. E: Struct. Rep. Online*, 2006, **62**, 1139–1141; (*b*) M.-L. Zhu, *Acta Crystallogr., Sect. E: Struct. Rep. Online*, 2006, **62**, 1985–1987.
14 O. Castillo, A. Luque, F. Lloret, M. Julve and P. Román, *Inorg. Chim. Acta*, 2001, **315**, 9–17.
15 (*a*) A. Bauzá, T. J. Mooibroek and A. Frontera, *Chem. Commun.*, 2015, **51**, 1491–1493; (*b*) S. Roy, A. Bauza, A. Frontera, R. Banik, A. Purkayastha, M. G. B. Drew, B. M. Reddy, B. Sridhar, S. Kr. Dasa and S. Das, *CrystEngComm*, 2015, **17**, DOI: 10.1039/c5ce00453e.
16 N. Saha and S. K. Kar, *J. Inorg. Nucl. Chem.*, 1977, **39**, 1236–1238.
17 *Bruker, SMART v5.631*, Bruker AXS Inc., Madison, WI, USA, 2001.
18 G. M. Sheldrick, *SHELXS-97 and SHELXL-97*, University of Göttingen, Germany, 1997.
19 (*a*) L. K. Das, R. M. Kadam, A. Bauzá, A. Frontera and A. Ghosh, *Inorg. Chem.*, 2012, **51**, 12407–12418; (*b*) M. Mitra, P. Manna, A. Bauzá, P. Ballester, S. Kumar Seth, S. R. Choudhury, A. Frontera and S. Mukhopadhyay, *J. Phys. Chem. B*, 2014, **118**, 14713–14726; (*c*) S. Saha, A. Sasmal, C. R. Choudhury, G. Pilet, A. Bauzá, A. Frontera, S. Chakraborty and S. Mitra, *Inorg. Chim. Acta*, 2015, **425**, 211–220; (*d*) A. Bauzá and A. Frontera, *Angew. Chem., Int. Ed.*, 2015, **54**, DOI: 10.1002/anie.201502571.
20 R. Ahlrichs, M. Bär, M. Hacer, H. Horn and C. Kömel, *Chem. Phys. Lett.*, 1989, **162**, 165–169.
21 S. Grimme, J. Antony, S. Ehrlich and H. Krieg, *J. Chem. Phys.*, 2010, **132**, 154104–154119.
22 *AIMAll (Version 13.05.06), Todd A. Keith, TK Gristmill Software*, Overland Park KS, USA, 2013.
23 (*a*) A. D. Becke, *Phys. Rev. A*, 1988, **38**, 3098–3100; (*b*) C. T. Lee, W. T. Yang and R. G. Parr, *Phys. Rev. B: Condens. Matter Mater. Phys.*, 1988, **37**, 785–789; (*c*) A. D. Becke, *J. Chem. Phys.*, 1993, **98**, 5648–5653.
24 M. J. Frisch, G. W. Trucks, H. B. Schlegel, G. E. Scuseria, M. A. Robb, J. R. Cheeseman, G. Scalmani, V. Barone, B. Mennucci, G. A. Petersson, H. Nakatsuji, M. Caricato, X. Li, H. P. Hratchian, A. F. Izmaylov, J. Bloino, G. Zheng, J. L. Sonnenberg, M. Hada, M. Ehara, K. Toyota, R. Fukuda, J. Hasegawa, M. Ishida, T. Nakajima, Y. Honda, O. Kitao, H. Nakai, T. Vreven, J. A. Montgomery Jr, J. E. Peralta, F. Ogliaro, M. Bearpark, J. J. Heyd, E. Brothers, K. N. Kudin, V. N. Staroverov, R. Kobayashi, J. Normand, K. Raghavachari, A. Rendell, J. C. Burant, S. S. Iyengar, J. Tomasi, M. Cossi, N. Rega, J. M. Millam, M. Klene, J. E. Knox, J. B. Cross, V. Bakken, C. Adamo, J. Jaramillo, R. Gomperts, R. E. Stratmann, O. Yazyev, A. J. Austin, R. Cammi, C. Pomelli, J. W. Ochterski, R. L. Martin, K. Morokuma, V. G. Zakrzewski, G. A. Voth, P. Salvador, J. J. Dannenberg, S. Dapprich, A. D. Daniels, Ö. Farkas, J. B. Foresman, J. V. Ortiz, J. Cioslowski and D. J. Fox, *Gaussian 09, RevisionB.01*, Gaussian, Inc., Wallingford CT, 2009.
25 (*a*) E. Ruiz, J. Cano, S. Alvarez and P. Alemany, *J. Comput. Chem.*, 1999, **20**, 1391–1400; (*b*) E. Ruiz, S. Alvarez, A. Rodríguez-Fortea, P. Alemany, Y. Pouillon and C. Massobrio, in *Magnetism: Molecules to Materials*, ed. J. S. Miller and M. Drillon, Wiley-VCH, Weinheim, Germany, 2001, vol. 2, p. 5572; (*c*) E. Ruiz, A. R. Fortea, J. Cano, S. Alvarez and P. Alemany, *J. Comput. Chem.*, 2003, **24**, 982–989; (*d*) E. Ruiz, S. Alvarez, J. Cano and V. Polo, *J. Chem. Phys.*, 2005, **123**, 164110–164117.
26 P. J. Baesjou, W. L. Driessen, J. Reedjic and A. L. Spek, *Inorg. Chim. Acta*, 2000, **306**, 237–240.
27 C. Adhikari and S. Koner, *Coord. Chem. Rev.*, 2010, **254**, 2933–2958.
28 J. H. Aiu, Z. R. Liao, X. J. Meng, L. Zhu, Z. M. Wang and K. B. Yu, *Polyhedron*, 2005, **24**, 1617–1623.
29 L. Y. Wang, B. Zaho, C. X. Zhang, D. Z. Liao, Z. H. Jiang and S. P. Yan, *Inorg. Chem.*, 2003, **43**, 5804–5806.
30 E. Q. Gao, S. Q. Bai, Z. M. Wang and C. H. Yan, *J. Am. Chem. Soc.*, 2003, **125**, 4984–4985.
31 F. Murata, M. Arakawa, A. Nakao, K. Satoh and Y. Fukuda, *Polyhedron*, 2007, **26**, 1570–1578.
32 O. Kahn and M. F. Charlot, *Nouv. J. Chim.*, 1980, **4**, 567–576.
33 O. Castillo, A. Luque, P. Román, F. Lloret and M. Julve, *Inorg. Chem.*, 2001, **40**, 5526–5535.
34 H. Oshio and U. Nagashima, *Inorg. Chem.*, 1992, **31**, 3295–3301.
35 O. Castillo, A. Luque, F. Lloret and P. Román, *Inorg. Chim. Acta*, 2001, **324**, 141–149.
36 M. L. Calatayud, I. Castro, J. Sletten, F. Lloret and M. Julve, *Inorg. Chim. Acta*, 2000, **300–302**, 846–854.
37 O. Castillo, A. Luque, F. Lloret and P. Roman, *Inorg. Chem. Commun.*, 2001, **4**, 350–353.
38 B. Bag, N. Mondal, S. Mitra, V. Gramlich, J. Ribas and M. S. El. Fallah, *Polyhedron*, 2001, **20**, 2113–2116.
39 M. Du, Y. M. Guo and X. H. Bu, *Inorg. Chim. Acta*, 2002, **335**, 136–140.

40 S. Youngme, G. A. V. Albada, N. Chaichit, P. Gunnasoot, P. Kongsaeree, I. Mutikainen, O. Roubeau, J. Reedijk and U. Turpeinen, *Inorg. Chim. Acta*, 2003, **353**, 119–128.
41 (*a*) A. Bauzá, T. J. Mooibroek and A. Frontera, *Chem. Commun.*, 2015, **51**, 1491–1493; (*b*) S. Saha, A. Sasmal, G. Pilet, A. Bauzá, A. Frontera and S. Mitra, *CrystEngComm*, 2014, **16**, 654–666.
42 A. Choudhary, D. Gandla, G. R. Krow and R. T. Raines, *J. Am. Chem. Soc.*, 2009, **131**, 7244–7246.
43 F. Weinhold and R. A. Klein, *Angew. Chem., Int. Ed.*, 2014, **53**, 11214–11217.
44 R. F. W. Bader, *Chem. Rev.*, 1991, **91**, 893–928.
45 M. Nishio, *CrystEngComm*, 2004, **6**, 130–158.
46 B. K. Mishra, *J. Phys. Chem. A*, 2005, **109**, 6–8.

THE JOURNAL OF PHYSICAL CHEMISTRY B

Article

pubs.acs.org/JPCB

On the Importance of Noncovalent Carbon-Bonding Interactions in the Stabilization of a 1D Co(II) Polymeric Chain as a Precursor of a Novel 2D Coordination Polymer

Pampi Pal,[†] Saugata Konar,[*,†] Prem Lama,[‡] Kinsuk Das,[*,§] Antonio Bauzá,[∥] Antonio Frontera,[*,∥] and Subrata Mukhopadhyay[†]

[†]Department of Chemistry, Jadavpur University, Jadavpur, Kolkata 700032, India

[‡]Department of Chemistry and Polymer Science, University of Stellenbosch, Stellenbosch 7600, South Africa

[§]Department of Chemistry, Chandernagore College, Hooghly 712136, West Bengal, India

[∥]Departament de Química, Universitat de les Illes Balears, Crta. de Valldemossa km 7.5, Palma 07122, Baleares, Spain

Supporting Information

ABSTRACT: A new cobalt(II) coordination polymer **2** with $\mu_{1,5}$ dicyanamide (dca) and a bidentate ligand 3,5-dimethyl-1-(2′-pyridyl)pyrazole (*pypz*) is prepared in a stepwise manner using the newly synthesized one-dimensional linear Co(II) coordination polymer **1** as a precursor. The structural and thermal characterizations elucidate that the more stable complex **2** shows a two-dimensional layer structural feature. Here, Co(II) atoms with $\mu_{1,5}$ dicyanamido bridges are linked by the ligand *pypz* forming a macrocyclic chain that runs along the crystallographic '*c*' axis having 'sql' (Shubnikov notation) net topology with a 4-connected uninodal node having point symbol $\{4^4.6^2\}$. The remarkable noncovalent carbon-bonding contacts detected in the X-ray structure of compound **1** are analyzed and characterized by density functional theory calculations and the analysis of electron charge density (atoms in molecules).

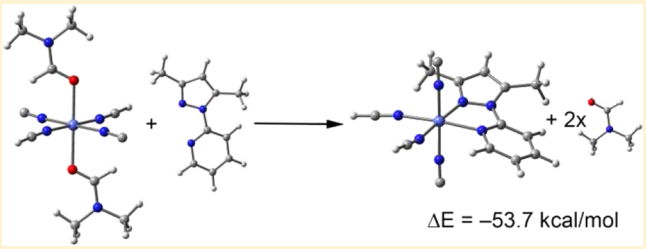

INTRODUCTION

Recent years have witnessed an extensive advancement in organic and inorganic materials chemistry propelled by the noncovalent interactions that play an instrumental role in the syntheses of crystalline substances. Metal−ligand compounds are designated as coordination polymers, especially called metal−organic coordination networks, and they extend "infinitely" into different dimensionalities via metal−ligand bonding.[1−3] The basic objective of crystal engineering in coordination polymers is to achieve the desired structural topology that obviously needs judicious choice of ligand and metal precursors.[4−8] Generally, the combination of transition metals and adequate "spacers" generating the structure and topology of a coordination polymer needs the proper selection of metal centers, ligands, experimental conditions, nature of spacers, and so forth.[9,10] Either the main ligand or ancillary ligands must have bridging sites, at least in one extended dimension to facilitate the metal atoms to be bridged only by this ligand. The coordination polymers derived from the bridging ligand dicyanamide (dca) with a captivating architectural framework have drawn much attention in coordination chemistry in the recent past due to their several functionalities[11−21] (Scheme 1). The coordination properties of the central metal ions (flexibility and signature) enable the creation of different architectures.[22−25] These architectures include one-dimensional (1D) linear chains,[26] nanotube-like structures,[27] two-dimensional (2D) (4,4) nets,[28] and triangular[29] and herringbone-like lattices.[30] Hence, the overall framework of the coordination polymers formed in the self-assembly process mostly depends upon the specialty of the bridging linker, and one such bridging ligand is dca.

In this work, a $\mu_{1,5}$ dicyanamido-bridged 1D linear Co(II) polymer (**1**) with two axially coordinated *N,N*′-dimethylformamide (DMF) molecules is synthesized. Moreover, polymer **1** is used to prepare a new Co(II) coordination polymer (**2**) of $\mu_{1,5}$ dca with a strongly coordinated bidentate 3,5-dimethyl-1-(2′-pyridyl)pyrazole (*pypz*) as an ancillary ligand (Scheme S1). During the entire process, complex **1** (1D coordination polymer) was metamorphosed to complex **2** with increased dimensionality (2D) and forming a macrocyclic chain that runs along the '*c*' axis with a 4-connected uninodal system representing a 'sql' (Shubnikov notation) net topology with point symbol $\{4^4.6^2\}$. Thermal analysis reveals that complex **2** is more stable thermally than complex **1**. Moreover, the relevant role of noncovalent carbon-bonding interactions in compound **1** has also been analyzed in solid state. In particular, the $-CH_3$

Received: April 21, 2016
Revised: June 10, 2016
Published: June 13, 2016

DOI: 10.1021/acs.jpcb.6b04046
J. Phys. Chem. B 2016, 120, 6803−6811

Scheme 1. Known Coordination Modes of dca[a]

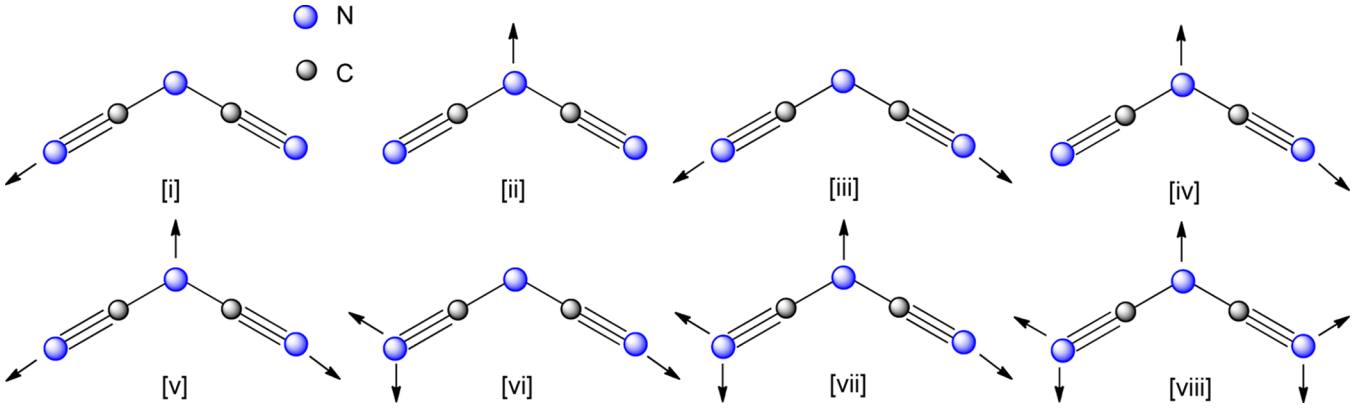

[a] i: μ_1, ii: μ_3, iii: $\mu_{1,5}$, iv: $\mu_{1,3}$, v: $\mu_{1,3,5}$, vi: $\mu_{1,1,5}$, vii: $\mu_{1,1,3,5}$, viii: $\mu_{1,1,3,5,5}$.

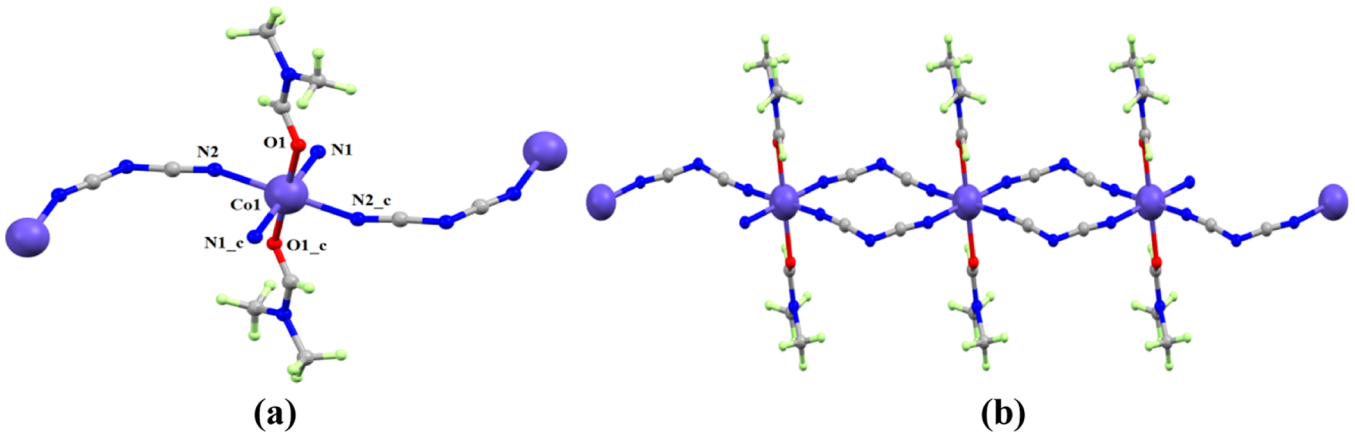

Figure 1. (a) Asymmetric unit of complex **1**. (b) 1D chain running along the *a* axis in **1**. Color code: Co(II), Majorelle Blue; O, red; N, Duke blue; C, grey; H, light green.

group of the coordinated DMF interacts with the central N atom of the end-to-end (EE) doubly bridging dca. Theoretical calculations have shown that sp^3-hybridized carbon and silicon atoms are able to form noncovalent complexes with electron-rich entities.[31−53] Furthermore, important proof of carbon···oxygen/carbon noncovalent interactions in complexes of carbon monoxide with haloalkanes has been recently described[54] and referred to as carbon and dicarbon bonds. In addition, carbon-bonding interactions with hydride donors have been reported by Li et al.[55] Finally, carbon-bonding interactions involving π-holes instead of σ-holes have been recently described in XCN derivatives (X = halogen atom).[56]

Experimental works confirming these theoretical predictions are scarcely found in the literature.[57] Recently, evidence of carbon-bonding interactions in sarcosine salts has been provided by means of solid nuclear magnetic resonance spectroscopy.[58] In this article, we demonstrate the existence of noncovalent carbon-bonding interactions in complex **1** using charge-density analysis and other computational tools. To our knowledge, this is the first experimental evidence of non-covalent carbon bonding using nitrogen as an electron donor (RCH_3···N motif).

EXPERIMENTAL SECTION

All of the chemicals were procured from commercial sources (Aldrich or Merck), with high purity.

Elemental analyses of carbon, hydrogen, and nitrogen were performed with a PerkinElmer CHN analyzer 2400. Infrared (IR) spectra were recorded on a PerkinElmer IR spectrophotometer (model 883). Thermogravimetric analysis (TGA) data were collected with an SDT 2960 thermoanalyzer under nitrogen (50−800 °C) at a heating rate of 10 °C/min.

The ligand *pypz* was synthesized using a reported procedure.[59]

Preparation of Complex $[Co(dca)_2(DMF)_2]_n$ (1). An aqueous solution (10 mL) of sodium dca (0.534 g, 6 mmol) was added dropwise with constant stirring to a methanolic solution (10 mL) of $CoCl_2{\cdot}6H_2O$ (0.238 g, 1 mmol). The resulted reddish compound was dissolved in DMF and excess (1:20) methanol. Then, the solution was left for slow evaporation. After 1 week, blue-colored X-ray quality crystals of **1** were isolated (yield: 0.231 g, 46%). Anal. Calcd for $C_{10}H_{14}CoN_8O_2$: C, 35.61; H, 4.15; N, 33.23. Found: C, 35.58; H, 4.13; N, 33.21.

Preparation of Complex $[Co(dca)_2(pypz)]_n$ (2). The solid crystals of complex **1** (0.337 g, 1 mmol) were mixed with the methanolic solution of the ligand *pypz* (0.173 g, 1 mmol). The heterogeneous mixture was kept undisturbed for 10 h, filtered, and the filtrate was reserved for slow evaporation. After 1 week, dark blue crystals of **2** were obtained. (yield: 0.421 g, 39.5%). Anal. Calcd for $C_{14}H_{11}CoN_9$: C, 46.15; H, 3.02; N, 34.61. Found: C, 46.11; H, 3.00; N, 34.58. IR (KBr; ν/cm): 2310 (s), 2244 (m), 2159 (s).

DOI: 10.1021/acs.jpcb.6b04046
J. Phys. Chem. B 2016, 120, 6803−6811

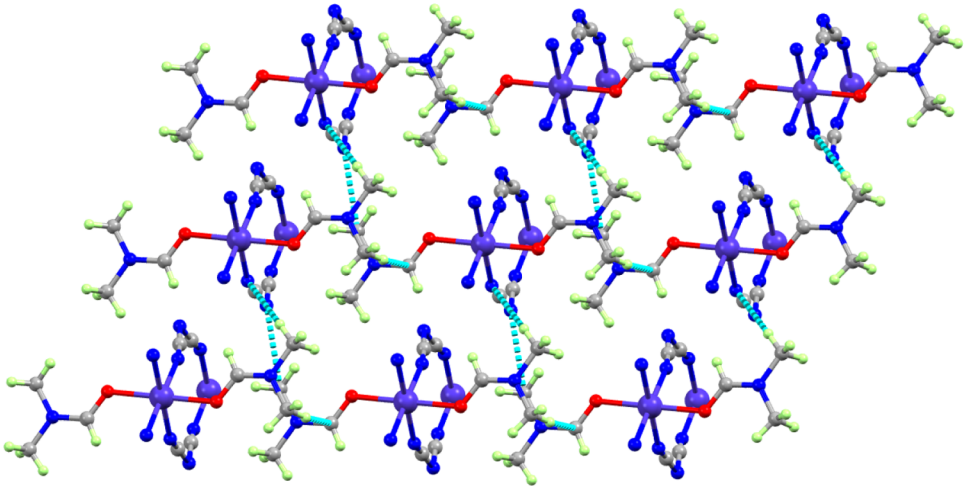

Figure 2. $CH_3\cdots N$ noncovalent interactions in complex **1**.

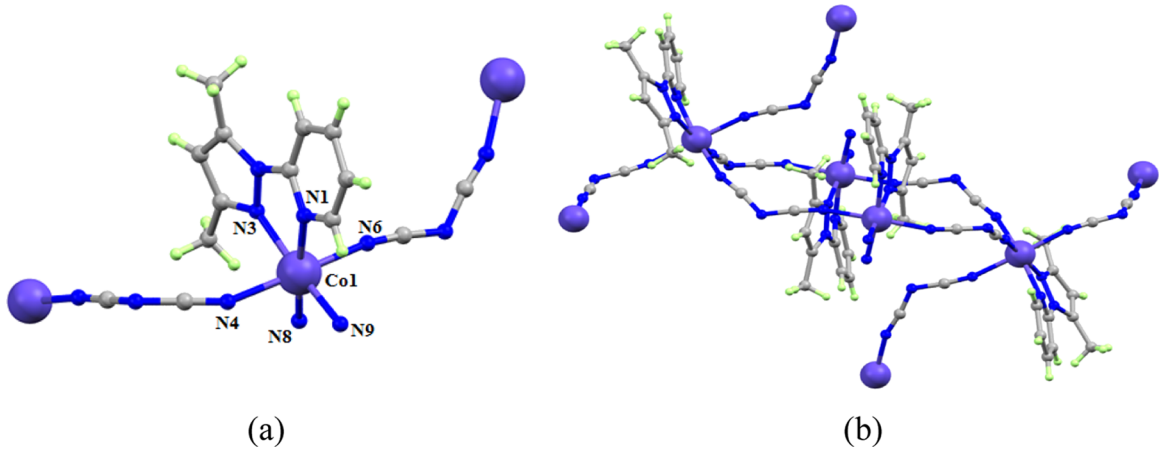

Figure 3. (a) Coordination mode of the metal complex in **2**. (b) Chair arrangement of complex **2**. Color code: Co(II), Majorelle Blue; O, red; N, Duke blue; C, grey; and H, light green.

Crystallographic Data Collection and Refinement for 1 and 2. The crystallographic data and geometric data (bond lengths and angles) are tabulated in Tables S1 and S2 of Supporting Information, respectively. For both **1** and **2**, data sets were collected using Bruker SMART APEX II CCD area detector at 293(2) and 296(2) K, respectively. The Bruker SMART and Bruker SAINT software packages[60] were used for cell parameters' refinement and data reduction. The structures were solved by conventional direct techniques and refined using F^2 data. The programs SHELXS-97 and SHELXL-97[61] were utilized for refinement and structure solution. For **1** and **2**, anisotropic refinement for non-H-atoms was used. CCDC 877582 (**1**) and 877583 (**2**) include additional crystallographic information.

Theory. The energies were calculated at the density functional theory-D3/def2TZVP level of theory using the functional BP86 and the program TURBOMOLE version 7.0.[62] The interaction energies are corrected for the basis set superposition error (BSSE).[63] The latest accessible dispersion correction (D3) was used in the calculations.[64] Atoms-in-molecules (AIM)[65] analysis was carried out using the AIMall program.[66]

RESULTS AND DISCUSSION

The asymmetric unit with atom numbering scheme and the polymeric 1D chain of complex **1** are given in Figure 1a,b. Complex **1** is made of well-defined chain of cobalt atoms bridged by double EE ($\mu_{1,5}$) dca ligands. Complex **1** crystallizes in space group $P\bar{1}$, and the asymmetric entity consists of only one dca molecule with one DMF molecule and a half-occupancy Co(II) ion. The geometry around the Co(II) center is a distorted octahedron, where the four N atoms of the nitrile groups in dca form the basal plane (the average deviation is 0.03 Å) with the subtended angles at the Co(II) center ranging from 88.08(12) to 91.92(12)°, whereas two oxygen atoms of DMF engaged themselves in the axial coordination position with exactly linear O1−Co−O1^i ($i = -x, -y, -z$) disposition (180°). The dca ligand chain propagates in such a manner that each DMF molecule of the adjacent chain lies between two DMF molecules (Figure 2). The Co(II) ion is placed exactly in the equatorial plane N2−N1−N2−N1.

In complex **1**, dca anions bind through nitrile nitrogen atoms and expand the metals over 7.379(3) Å, which is analogous to the length of the crystallographic '*b*' axis. The bond angles associated with the bridging dca ligands are 159.7(3) and 151.7(3)° for Co1−N2−C5 and Co1−N1−C4, respectively. A rough C_{2v} symmetry is noticed for the dca ligands with the C5−

DOI: 10.1021/acs.jpcb.6b04046
J. Phys. Chem. B 2016, 120, 6803−6811

N2 and C4−N1 bond distances of 1.153(4) and 1.147(4) Å, respectively, as is typical for the $[N(CN)_2]^-$ anion.[17,33−37] The small degree of π-conjugation results in longer C5−N3 [1.289(4) Å] and N3−C4 [1.302(4) Å]. The DMF molecules in compliance with symmetry requirements are trans to each other. Weak $CH_3\cdots N$ noncovalent interactions (Table S3) prevail along the neighboring chains. The 1D chain in **1** formed by the interaction of coordinated DMF molecules and dca ligands runs parallel along the crystallographic '*b*' axis (Figure 2). The $CH_3\cdots N$ interaction can be viewed as a trifurcated H-bonding interaction (with poor directionality because the C−H···N angle ranges from 76 to 100°) or as a noncovalent carbon-bonding (C···N interaction). As a matter of fact, all three H···N distances are higher than the sum of their van der Waals radii ($\sum R_{vdW}$), and, conversely, the C···N distance is shorter than the $\sum R_{vdW}$ of C and N. The nature of this interaction is further analyzed below in the theoretical study. Moreover, further description of the Co environment in **1** and a comparison with related structures retrieved from the Cambridge structural database (CSD) have been included in the Supporting Information.

The crystal structure of complex **2** is represented in Figure 3a; it crystallizes in the space group $P2_1/c$. Each six-coordinated Co(II) ion is surrounded by four six-coordinated N atoms (two nitrile nitrogen atoms from 'dca' and two nitrogen atoms of *pypz*) at equatorial sites, and the two axial nitrile nitrogen atoms N6 and N4 subtend an angle of 174.08(12)° at the Co(II) center. The dca ligands adopt the $\mu_{1,5}$ EE bridging mode, and they join any one metal ion to other four nearer Co(II) centers developing parallelogram grid sheets (the opposite sides and angles of the geometrical plane created by Co^{II}_4 units are exactly equal) almost parallel to the crystallographic "*bc*" plane.

Keeping the Co^{II}_4 unit in a mean plane, two $\mu_{1,5}$ dca linkers are above the plane (distances of the amide nitrogen of the bridging dca from the mean Co^{II}_4 plane are 1.202 and 1.704 Å, respectively) and other two $\mu_{1,5}$ dca linkers are below the same plane by the same measurement, finally, constituting a 24-membered chair arrangement (Figure 3b). In chairlike conformation, each Co(II) center of the Co^{II}_4 unit corresponds to the hexacoordinated $[Co^{II}(pypz)(dca)_4]$ unit. Each Co(II) center on an arm of chair is coordinated through a strongly bidentated NN donor ligand, and four 'dca' anions work as linkers between these Co(II) centers. The intralayer Co···Co separation through the dca bridge is 8.899 Å, whereas the Co···Co distances through the diagonals are different (7.851 and 13.802 Å, respectively), indicating that the neutral center in the Co^{II}_4 units adopts a parallelogram arrangement rather than a rhombus or square disposition. The TOPOS 4.0 software[67,68] was used for topological analysis of the network. The Co(II) centers create a 4-connected uninodal net (Figure 4) described by point symbol $\{4^4, 6^2\}$, which corresponds to the 'sql' topological type.

The network forming macrocyclic chains in **2** that stack in 2D layers along the '*b*' axis is shown in Figure 5, exhibiting a uninodal 4-connected net. The hydrogen-bonding interactions that contribute to the further stabilization of the neutral layers are given in Table S3.

Thermal analysis was carried out to obtain an insight into the thermal stability of the complexes. The TGA curve obtained for **1** (Figure S1) clearly displays two stages of decomposition. The first weight loss (43.9%) in the range of 180−240 °C corresponds to the loss of DMF molecule (calcd, 43.29).

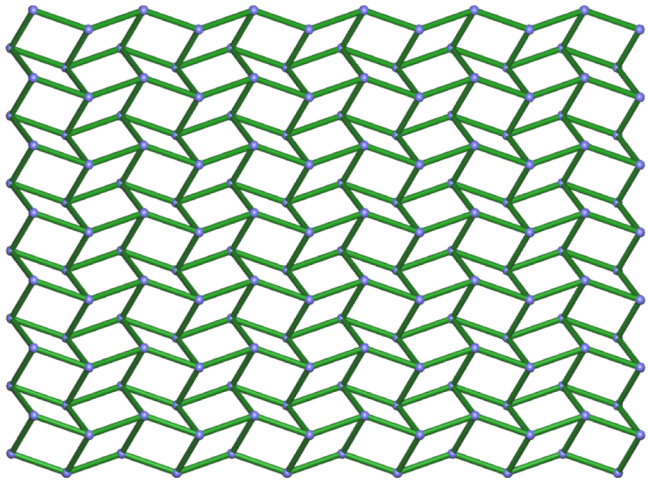

Figure 4. Topological view of **2** having a 4-connected 'sql' net with point symbol $\{4^4.6^2\}$.

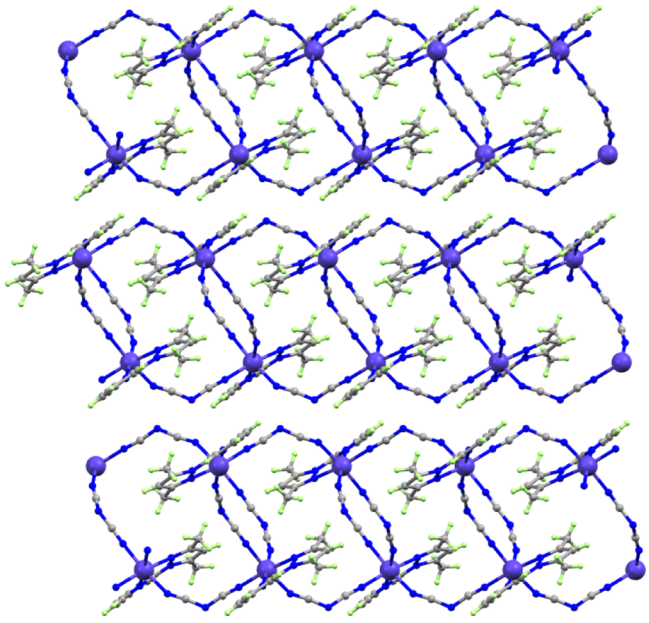

Figure 5. Stacking of macrocyclic chains along the '*b*' axis in **2**.

Then, the compound shows thermal stability up to 300 °C. The second step (found, 40.1%; calcd, 39.14%) in the region 300−460 °C indicates loss of two dca molecules. The TGA curve for **2** (Figure S2) shows that the compound is thermally stable up to 400 °C and decomposition occurs in the temperature range 400−530 °C. The weight loss of 51.76% of the total weight taken can be assigned to the decomposition of the ligand *pypz* (calcd, 47.49), and the collapse of the whole framework occurs in the temperature range 530−680 °C. The residual species was supposed to be CoO (found, 18.17%; calcd, 22.21% for **1** and found, 16.86%; calcd, 20.56% for **2**). Overall, thermal analysis reveals that complex **2** is more thermally stable than complex **1**.

As mentioned above, the theoretical study is devoted to the study of the $CH_3\cdots N$ carbon-bonding interaction observed in **1** that interconnects the 1D polymeric chains (see Figure 2). First, we have computed the molecular electrostatic potential (MEP) surface in DMF to investigate the existence of a σ-hole in the carbon atom. Moreover, we have also computed the MEP surface in DMF coordinated to $CoCl_2$ to explore the

DOI: 10.1021/acs.jpcb.6b04046
J. Phys. Chem. B 2016, 120, 6803−6811

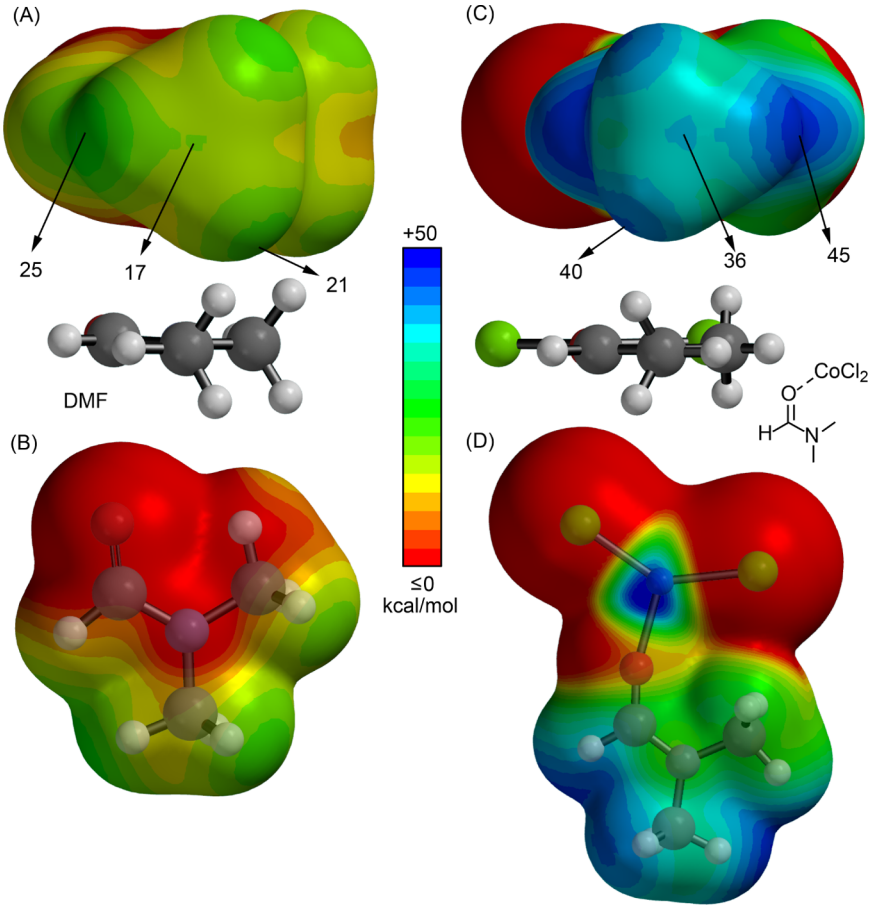

Figure 6. MEP surfaces of DMF (A), on-top view of DMF (B), DMF O-coordinated to $CoCl_2$ (C) and on-top view of coordinated DMF (D).. The electrostatic potential values at some points of the surface are shown.

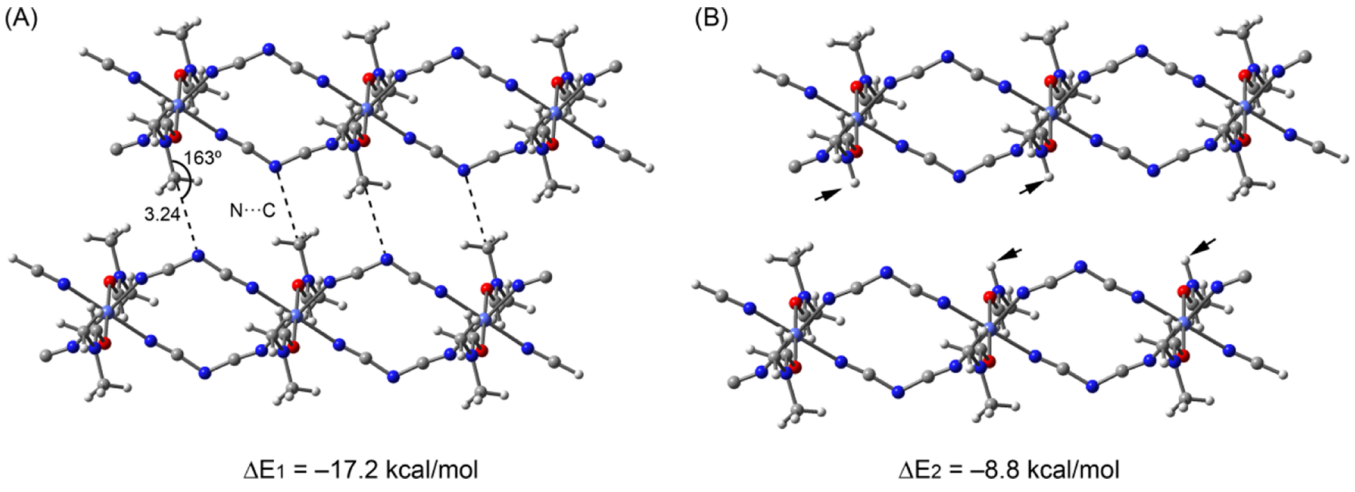

Figure 7. Theoretical models used to evaluate the carbon-bonding (A) and long-range dispersion (B) interactions in **1**.

effect of the coordination of the CO group to a metal on the MEP values. The MEP surfaces are plotted in Figure 6 in two different orientations. MEP analysis indicates that DMF has several green isocontours in the methyl group and a positive electrostatic potential value at the carbon atom (+17 kcal/mol; see Figure 6A,B). For the coordinated DMF (see Figure 6C,D), the shape of the MEP is very similar; however, the MEP values are significantly more positive. In fact, the MEP at the C atom increases from 17 to 36 kcal/mol. In general, the MEP values measured at the hydrogen atoms of the methyl group are more positive than those measured at the σ-hole of the carbon atom. Consequently, both coordinated and uncoordinated DMF molecules are better suited to form hydrogen-bonding rather than carbon-bonding interactions in terms of electrostatic effects.

We have used a theoretical model of compound **1** using the crystallographic coordinates (see Figure 7) to evaluate energetically the carbon (or trifurcated H-bonding) interactions. To use a neutral fragment of the X-ray structure (see Figure 7A), we have used a model of polymeric chains, where

DOI: 10.1021/acs.jpcb.6b04046
J. Phys. Chem. B 2016, 120, 6803–6811

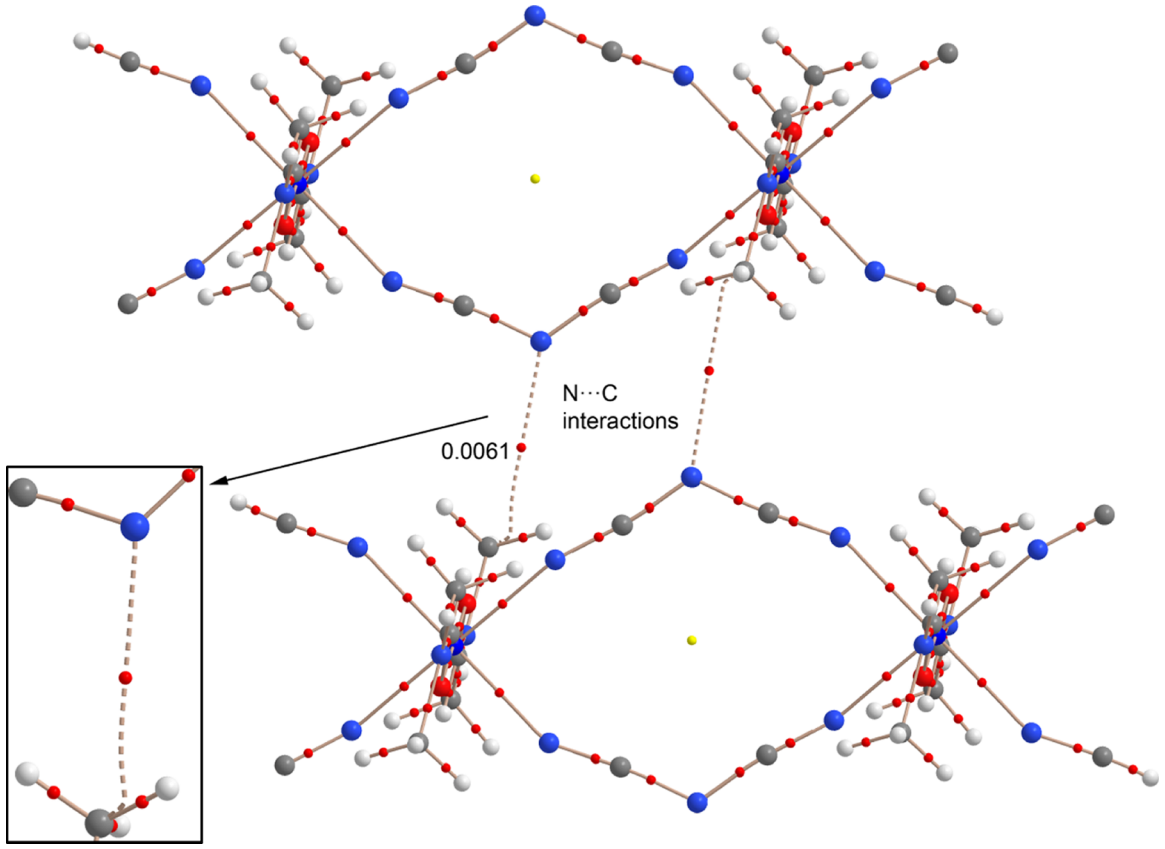

Figure 8. Bond and ring CPs (red and yellow spheres, respectively) and bond paths for the model of compound **1** at the BP86-D3/def2-TZVP level of theory. The ρ(r) value at the bond CP that characterized the noncovalent carbon-bonding interaction is given in atomic units.

some dca ligands have been substituted by either CN^- or hyperpolarization-activated cyclic nucleotide-modulated (HCN) ligands at the ends of the chain. In the theoretical model, we have used two discrete polymeric chains including three Co ions in each chain. Using this model, the octahedral coordination environment of the central Co of each chain is not changed with respect to the real one present in the crystal structure. In this dimer, four concurrent N···C interactions are established, and the computed interaction energy is significant (ΔE_1 = −17.2 kcal/mol). As other long-range dispersion interactions may also be present between the chains, we have computed another model, in which the CH_3 groups are substituted by H-atoms (see arrows in Figure 7B). Using this frozen model, we can roughly estimate the contribution of long-range dispersion interactions as they operate in the model in Figure 7A. The resulting interaction energy decreases to ΔE_2 = −8.8 kcal/mol; therefore, the carbon-bonding interaction can be estimated by calculating the difference, that is, $\Delta E_1 - \Delta E_2$ = −8.4 kcal/mol.

The characterization of the noncovalent interaction in complex **1** has been performed by means of charge-density analysis and distribution of critical points (CPs). The existence of a bond path linking two atoms and the concomitant bond CP provide strong evidence of interaction. The allocation of CPs and bond paths computed for a reduced model of compound **1** is shown in Figure 8. The carbon-bonding N···C interaction is characterized by the existence of a bond CP that links the N atom with the carbon atom, consequently validating the C-bonding nature of this contact. The value of ρ(r) at the bond CP is comparable to that previously reported for O···C interactions.[40,47] It should be emphasized that the analysis of **1** exhibited a bond path starting from the N atom and ending at the $-CH_3$ carbon atom and, more importantly, that there exist no other bond paths connecting the N atom to the H atoms of the methyl group. Therefore, the motif observed in the solid state certainly represents a C···N noncovalent carbon-bonded motif. The value at the Laplacian of ρ supports the closed-shell nature of the interaction. Finally, it can be inferred that the coordination of DMF to Co(II) communicates a charge-depletion effect to the carbon atom, thus supporting the carbon-bonding interaction.

Moreover, with the purpose of examining the N···C interaction from an orbital perspective, we have carried out natural bond orbital (NBO) analysis for the model in Figure 8.[69] Interestingly, second-order perturbation analysis shows electron donation from the lone pair of the central N atom of the dca ligand to the C−N antibonding orbital (BD*) of the coordinated DMF with an associated stabilization energy of $E^{(2)}$ = 0.40 kcal/mol for each LP(N) → BD*(CN) interaction. Interestingly, no other donor−acceptor orbital interaction from the ligand to DMF is found in this complex. Therefore, the presence of noncovalent C-bonding instead of hydrogen-bonding interactions is confirmed.

Finally, we have also analyzed theoretically the easy transformation of 1D Co(II) polymeric chain **1** to polymer **2** in methanol. That is, when *pypz* is added to the methanolic solution of polymer **1**, the DMF molecules that are axially coordinated in polymer (**1**) are substituted by the bidentate *pypz* ligand. This substitution likely gives the extra stabilization to **2** through the chelate effect. To give theoretical support to

DOI: 10.1021/acs.jpcb.6b04046
J. Phys. Chem. B 2016, 120, 6803−6811

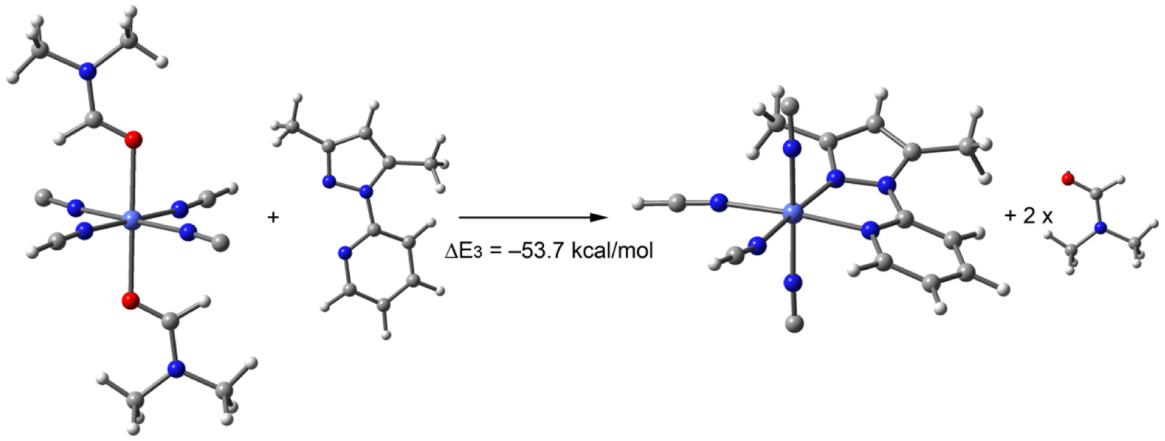

Figure 9. Optimized geometries of the monomeric models and reaction energy to evaluate the chelate effect of the ligand *pypz*.

this explanation, we have computed the reaction energy associated with the substitution of two DMF molecules in the axial position by bidentate *pypz*. As the system is polymeric, we have used a monomeric model, which is shown in Figure 9 along with the reaction energy. In the minimalistic model, each dca ligand has been substituted by either CN^- or HCN ligand to use a neutral Co(II) octahedral complex. It can be observed that the substitution of both axial-coordinated DMF molecules by *pypz* is energetically favored in 53.7 kcal/mol, thus confirming the strong chelate effect of the bidentate ligand. Moreover, it supports the formation of polymer **2** from compound **1** upon addition of the ligand in MeOH.

CONCLUSIONS

We were able to synthesize a novel 2D Co(II) coordination polymer **2** in a stepwise manner from a 1D Co(II) polymer **1** by incorporating the ligand *pypz*, and they were characterized both structurally and thermally. From a structural point of view, 2D Co(II) polymer **2** is based on a 24-membered chairlike arrangement, which in turn creates a 4-connected uninodal net with sql topology having the point symbol $\{4^4.6^2\}$. Polymer **2** is thermally more stable than polymer **1**, so it may be used as a precursor to design and construct thermally more stable polymeric materials by incorporating ancillary ligands. Remarkably, compound **1** exhibits noncovalent carbon-bonding interactions that involve the N atom of the interconnecting dca ligand and the methyl group of DMF. MEP calculations demonstrate the enhanced ability of coordinated DMF to be involved in noncovalent carbon-bonding interactions compared to that of noncoordinated DMF. AIM analysis of CPs and bond path confirms the existence of C···N, not the H-bonding interaction. This investigation may be claimed as a testimony to the importance of nascent interactions in the solid state.

ASSOCIATED CONTENT

Supporting Information

The Supporting Information is available free of charge on the ACS Publications website at DOI: 10.1021/acs.jpcb.6b04046.

Scheme S1 exhibiting schematic representation, Table S1 exhibiting crystallographic data of **1** and **2**, Table S2 exhibiting geometrical features of **1** and **2**, Table S3 exhibiting hydrogen-bond distances and angles, Table S4 exhibiting intermetallic distances of 1D $[Co(dca)_2L_2]_n$ polymeric chains, Figures S1 and S2 exhibiting thermogravimetric curves of **1** and **2**, and Figure S3 exhibiting different conformations of the dca anion (PDF)

PLATON report (PDF, CIF)

PLATON report (PDF, CIF)

AUTHOR INFORMATION

Corresponding Authors

*E-mail: saugata.konar@gmail.com. Phone: +91 (033) 2414-6666 (S.K.).

*E-mail: kdaschem@yahoo.in. Phone: +91 (033) 2685-5002 (K.D.).

*E-mail: toni.frontera@uib.es. Phone: +34 971 173498 (A.F.).

Notes

The authors declare no competing financial interest.

ACKNOWLEDGMENTS

S.K. thanks the University Grants Commission, India (Award letter No. F.4-2/2006(BSR)/13-1089/2013(BSR)) for the Dr. D.S. Kothari Post Doctoral Fellowship. Financial support from the Innovative Research Program of University Grants Commission (New Delhi) is thankfully acknowledged. We thank the MINECO of Spain (projects CSD2010-0065 and CTQ2014-57393-C2-1-P FEDER funds) for financial support. The CTI(UIB) is gratefully acknowledged for free allocation of computer time.

REFERENCES

(1) Blatov, V. A.; Proserpio, D. M. In *Modern Methods of Crystal Structure Prediction*; Oganov, A. R., Ed.; Wiley-VCH: Weinheim, 2011; Chapter 1.

(2) Bradshaw, D.; Garai, A.; Huo, J. Metal−Organic Framework Growth at Functional Interfaces: Thin Films and Composites for Diverse Applications. *Chem. Soc. Rev.* **2012**, *41*, 2344−2381.

(3) Zhu, Q.-L.; Xu, Q. Metal−Organic Framework Composites. *Chem. Soc. Rev.* **2014**, *43*, 5468−5512.

(4) Hoskins, B. F.; Robson, R. Design and Construction of a New Class of Scaffolding-Like Materials Comprising Infinite Polymeric Frameworks of 3D-Linked Molecular Rods. A Reappraisal of the Zinc Cyanide and Cadmium Cyanide Structures and the Synthesis and Structure of the Diamond-Related Frameworks $[N(CH_3)_4][Cu^IZn^{II}(CN)_4]$ and $Cu^I[4,4',4'',4'''$-tetracyanotetraphenylmethane$]BF_4.xC_6H_5NO_2$. *J. Am. Chem. Soc.* **1990**, *112*, 1546−1554.

(5) Singh, M.; Ramanan, A. Crystal Engineering of Polyoxomolybdates Based Metal−Organic Solids: The Case of Chromium Molybdate Cluster Based Metal Complexes and Coordination Polymers. *Cryst. Growth Des.* **2011**, *11*, 3381−3394.

DOI: 10.1021/acs.jpcb.6b04046
J. Phys. Chem. B 2016, 120, 6803−6811

(6) Batten, S. R.; Robson, R. Interpenetrating Nets: Ordered, Periodic Entanglement. *Angew. Chem., Int. Ed.* **1998**, *37*, 1460−1494.
(7) Adarsh, N. N.; Dastidar, P. A New Series of Zn^{II} Coordination Polymer Based Metallogels Derived from Bis-pyridyl-bis-amide Ligands: A Crystal Engineering Approach. *Cryst. Growth Des.* **2011**, *11*, 328−336.
(8) Blake, A. J.; Champness, N. R.; Hubberstey, P.; Li, W. S.; Withersby, M. A.; Schroder, M. Inorganic Crystal Engineering Using Self-Assembly of Tailored Building-Blocks. *Coord. Chem. Rev.* **1999**, *183*, 117−138.
(9) Maji, T. K.; Uemura, K.; Chang, H. C.; Matsuda, R.; Kitagawa, S. Expanding and Shrinking Porous Modulation Based on Pillared-Layer Coordination Polymers Showing Selective Guest Adsorption. *Angew. Chem., Int. Ed.* **2004**, *43*, 3269−3272.
(10) Shiga, T.; Okawa, H.; Kitagawa, S.; Ohba, M. Stepwise Synthesis and Magnetic Control of Trimetallic Magnets $[Co_2Ln(L)_2(H_2O)_4]$-$[Cr(CN)_6]\cdot nH_2O$ (Ln = La, Gd; H_2L = 2,6-Di(acetoacetyl)pyridine) with 3-D Pillared-Layer Structure. *J. Am. Chem. Soc.* **2006**, *128*, 16426−16427.
(11) Potocnak, I.; Jurco, M. D.; Miklos, D.; Kabesova, M.; Jager, L. Bis(dicyanamide)bis(1,10-phenanthroline)Copper(II). *Acta Crystallogr., Sect. C* **1995**, *51*, 600−602.
(12) Das, L. K.; Ghosh, A. Structural Diversity in the Complexes Based on a Hetero-trimetallic Cu_2Cd Node and Dicyanamide Spacer: A Hexanuclear Cluster, a 1D Stair Polymer and a 1D Zigzag Chain as Supramolecular Isomers and a 3D Network. *CrystEngComm* **2013**, *15*, 9444−9456.
(13) Sun, B. W.; Gao, S.; Ma, B. Q.; Niu, D. Z.; Wang, Z. M. Syntheses, Structures and Magnetic Properties of Three-Dimensional Co-ordination Polymers Constructed by Dimer Subunits. *J. Chem. Soc., Dalton Trans.* **2000**, 4187−4191.
(14) Xu, J.-Y; Xie, C.-Z; Xue, F.; Hao, L.-F; Ma, Z.-Y; Liao, D.-Z; Yan, S.-P Directed Assembly and Characterization of 1D Polymers Based on $[M^{II}(BMA)]^{2+}$ node (M = Cu, Mn, Ni and Zn; BMA = N,N-bis (benzimidazol-2-yl-methyl)amine) with Linear Bridging Dicyanamide and Terephthalate Ligands. *Dalton Trans.* **2010**, *39*, 7159−7166.
(15) Wang, Z. M.; Sun, B. W.; Luo, J.; Gao, S.; Liao, C. S.; Yan, C. H.; Li, Y. Bimetallic Sandwiches Assembled with Chelated Cu/Zn Cations and Manganese Dicyanamide Polymeric Ladders. *Polyhedron* **2003**, *22*, 433−439.
(16) van der Werff, P. M.; Batten, S. R.; Jensen, P.; Moubaraki, B.; Murray, K. S. Cation Templation of Anionic Metal Dicyanamide Networks. *Inorg. Chem.* **2001**, *40*, 1718−1722.
(17) Batten, S. R.; Jensen, P.; Moubaraki, B.; Murray, K. S.; Rubson, R. Structure and Molecular Magnetism of the Rutile-Related Compounds M $(dca)_2$, M = Co^{II}, Ni^{II}, Cu^{II}, dca = dicyanamide, N $(CN)_2^-$. *Chem. Commun.* **1998**, 439−440.
(18) Manson, J. L.; Kmety, C. R.; Palacio, F.; Epstein, A. J.; Miller, J. S. Low-Field Remanent Magnetization in the Weak Ferromagnet $Mn[N(CN)_2]_2$. Evidence for Spin-Flop Behavior. *Chem. Mater.* **2001**, *13*, 1068−1073.
(19) Miller, J. S.; Manson, J. L. Designer Magnets Containing Cyanides and Nitriles. *Acc. Chem. Res.* **2001**, *34*, 563−570.
(20) Chow, Y. M.; Britton, D. The Crystal Structures of Dimethylthallium Acetate, Tropolonate, Acetylacetonate and Dibenzoylmethide. *Acta Crystallogr., Sect. B* **1975**, *31*, 1929−1934.
(21) Shi, Y. J.; Chen, X. T.; Li, Y. Z.; Xue, Z. L.; You, X. Z. $Pb(dca)_2$ (dca = dicyanamide): A Novel 3D Compound with Unusual Coordination Modes of Dicyanamide. *New J. Chem.* **2002**, *26*, 1711−1713.
(22) Janiak, C. Engineering Coordination Polymers Towards Applications. *Dalton Trans.* **2003**, 2781−2804.
(23) Wei, Y.; Yu, Y.; Sa, R.; Li, Q.; Wu, K. Two Cobalt(II) Coordination Polymers $[Co_2(H_2O)_4(Hbidc)_2]_n$ and $[Co(Hbidc)]_n$ (Hbidc = 1H-benzimidazole-5,6-dicarboxylate): Syntheses, Crystal Structures and Magnetic Properties. *CrystEngComm* **2009**, *11*, 1054−1060.
(24) Sun, H. L.; Wang, Z. M.; Gao, S. Synthesis, Crystal Structures and Magnetism of Cobalt Coordination Polymers Based on Dicyanamide and Pyrazine-dioxide Derivatives. *Inorg. Chem.* **2005**, *44*, 2169−2176.
(25) Massoud, S. S.; Louka, F. R.; Mautner, F. A. Polynuclear and Polymeric Squarato-Bridged Coordination Compounds. *CrystEngComm* **2015**, *17*, 7604−7617.
(26) Dasna, I.; Golhen, S.; Ouahab, L.; Pena, O.; Guillevic, J.; Fettouhi, M. 1-D Mixed Stack of Coordinated and Uncoordinated Radicals in $Mn^{II}(NITpPy)_4[N(CN)_2]_2$ (NITpPy = nitronyl nitroxide radical). *J. Chem. Soc., Dalton Trans.* **2000**, 129−132.
(27) Jensen, P.; Batten, S. R.; Moubaraki, B.; Murray, K. S. Infinite Molecular Tubes: Structure and Magnetism of $M(dca)_2(apym)$ [M = Co, Ni, apym = 2-aminopyrimidine, dca = dicyanamide, $N(CN)_2^-$]. *Chem. Commun.* **2000**, 793−794.
(28) Manson, J. L.; Schlueter, J. A.; Geiser, U.; Stone, M. B.; Reich, D. H. Crystal Structures and Magnetic Properties of $Mn[N(CN)_2]_2L$ {L = 2,5-dimethylpyrazine and aminopyrazine}. *Polyhedron* **2001**, *20*, 1423−1429.
(29) Sun, H. L.; Gao, S.; Ma, B. Q.; Su, G. Long-Range Ferromagnetic Ordering in Two-Dimensional Coordination Polymers $Co[N(CN)_2]_2(L)$ [L = Pyrazine Dioxide (pzdo) and 2-Methyl Pyrazine Dioxide (mpdo)] with Dual μ- and μ_3-$[N(CN)_2]$ Bridges. *Inorg. Chem.* **2003**, *42*, 5399−5404.
(30) Luo, J. L.; Hong, M. C.; Weng, J. B.; Zhao, Y. J.; Cao, R. The Complexes with End-To-End Dicyanamide Bridges: Syntheses, Characterization and Crystal Structures of $[Cu(\mu_{1,5}\text{-dca})_2(phen)]_n$ and $[Cd(\mu_{1,5}\text{-dca})_2(py)_2]_n$ (phen = phenanthroline; py = pyridine; dca = dicyanamide, $N(CN)_2^-$). *Inorg. Chim. Acta* **2002**, *329*, 59−65.
(31) Bauzá, A.; Mooibroek, T. J.; Frontera, A. Tetrel Bonding Interactions. *Chem. Rec.* **2016**, *16*, 473−487.
(32) Bauzá, A.; Mooibroek, T. J.; Frontera, A. Tetrel-Bonding Interaction: Rediscovered Supramolecular Force? *Angew. Chem., Int. Ed.* **2013**, *52*, 12317−12321.
(33) Politzer, P.; Murray, J. S.; Clark, T. Halogen Bonding and Other σ-Hole Interactions: A Perspective. *Phys. Chem. Chem. Phys.* **2013**, *15*, 11178−11189.
(34) Murray, J. S.; Riley, K. E.; Politzer, P.; Clark, T. Directional Weak Intermolecular Interactions: σ-Hole Bonding. *Aust. J. Chem.* **2010**, *63*, 1598−1607.
(35) Clark, T. σ-Holes. *Wiley Interdiscip. Rev.: Comput. Mol. Sci.* **2013**, *3*, 13−20.
(36) Politzer, P.; Murray, J. S.; Clark, T. Halogen Bonding: An Electrostatically-Driven Highly Directional Noncovalent Interaction. *Phys. Chem. Chem. Phys.* **2010**, *12*, 7748−7757.
(37) Bundhun, A.; Ramasami, P.; Murray, J. S.; Politzer, P. Trends in σ-Hole Strengths and Interactions of F_3MX Molecules (M= C, Si, Ge and X= F, Cl, Br, I). *J. Mol. Model.* **2013**, *19*, 2739−2746.
(38) Grabowski, S. J. Tetrel Bond−σ-Hole Bond as a Preliminary Stage of the S_N2 Reaction. *Phys. Chem. Chem. Phys.* **2014**, *16*, 1824−1834.
(39) Bauzá, A.; Mooibroek, T. J.; Frontera, A. Small Cycloalkane $(CN)_2C\text{-}C(CN)_2$ Structures are Highly Directional Non-Covalent Carbon-Bond Donors. *Chem. Eur. J.* **2014**, *20*, 10245−10248.
(40) Bauzá, A.; Mooibroek, T. J.; Frontera, A. 1,1,2,2-Tetracyanocyclopropane (TCCP) as Supramolecular Synthon. *Phys. Chem. Chem. Phys.* **2016**, *18*, 1693−1698.
(41) Adán, E. C. E.; Bauzá, A.; Frontera, A.; Ballester, P. Nature of Noncovalent Carbon-Bonding Interactions Derived from Experimental Charge-Density Analysis. *ChemPhysChem* **2015**, *16*, 2530−2533.
(42) Mani, D.; Arunan, E. The X−C···Y (X = O/F, Y = O/S/F/Cl/Br/N/P) 'Carbon Bond' and Hydrophobic Interactions. *Phys. Chem. Chem. Phys.* **2013**, *15*, 14377−14383.
(43) McDowell, S. A. C. Sigma-hole Cooperativity in Anionic $[FX\cdots CH_3\cdots YF]-$ (X, Y = Cl, Br) Complexes. *Chem. Phys. Lett.* **2014**, *598*, 1−4.
(44) Tang, Q.; Li, Q. Interplay between Tetrel Bonding and Hydrogen Bonding Interactions in Complexes Involving F_2XO (X = C and Si) and HCNO. *Comput. Theor. Chem.* **2014**, *1050*, 51−57.
(45) Guo, X.; Liu, Y.-W.; Li, Q.-Z.; Li, W.-Z.; Cheng, J. B. Competition and Cooperativity between Tetrel Bond and Chalcogen

DOI: 10.1021/acs.jpcb.6b04046
J. Phys. Chem. B 2016, 120, 6803−6811

Bond in Complexes Involving F_2CX (X = Se and Te). *Chem. Phys. Lett.* **2015**, *620*, 7−12.
(46) Esrafili, M. D.; Mohammadirad, N.; Solimannejad, M. Tetrel Bond Cooperativity in Open-Chain $(CH_3CN)_n$ and $(CH_3NC)_n$ clusters (n = 2−7): An Ab Initio Study. *Chem. Phys. Lett.* **2015**, *628*, 16−20.
(47) Esrafili, M. D.; Mohammadian-Sabet, F. Cooperativity of Tetrel Bonds Tuned by Substituent Effects. *Mol. Phys.* **2016**, *114*, 1528−1538.
(48) Scheiner, S. Comparison of CH···O, SH···O, Chalcogen, and Tetrel Bonds Formed by Neutral and Cationic Sulfur-Containing Compounds. *J. Phys. Chem. A* **2015**, *119*, 9189−9199.
(49) Marín-Luna, M.; Alkorta, I.; Elguero, J. Cooperativity in Tetrel Bonds. *J. Phys. Chem. A* **2016**, *120*, 648−656.
(50) Metrangolo, P.; Neukirch, H.; Pilati, T.; Resnati, G. Halogen Bonding Based Recognition Processes: A World Parallel to Hydrogen Bonding. *Acc. Chem. Res.* **2005**, *38*, 386−395.
(51) Politzer, P.; Murray, J. S. Halogen Bonding: An Interim Discussion. *ChemPhysChem* **2013**, *14*, 278−294.
(52) Bauzá, A.; Mooibroek, T. J.; Frontera, A. The Bright Future of Unconventional σ/π-Hole Interactions. *ChemPhysChem* **2015**, *16*, 2496−2517.
(53) Politzer, P.; Murray, J. S.; Clark, T. Halogen Bonding: An Electrostatically-Driven Highly Directional Noncovalent Interaction. *Phys. Chem. Chem. Phys.* **2010**, *12*, 7748−7757.
(54) Varadwaj, P. R.; Varadwaj, A.; Jin, B.-Y. Significant Evidence of C···O and C···C Long-Range Contacts in Several Heterodimeric Complexes of CO with CH_3−X, Should One Refer to them as Carbon and Dicarbon bonds. *Phys. Chem. Chem. Phys.* **2014**, *16*, 17238−17252.
(55) Li, Q.-Z.; Zhuo, H.-Y.; Li, H.-B.; Liu, Z.-B.; Li, W.-Z.; Cheng, J.-B. Tetrel−Hydride Interaction between XH_3F (X = C, Si, Ge, Sn) and HM (M = Li, Na, BeH, MgH). *J. Phys. Chem. A* **2015**, *119*, 2217−2224.
(56) Nziko, V. de. P. N.; Scheiner, S. Comparison of π-Hole Tetrel Bonding with σ-Hole Halogen Bonds in Complexes of XCN (X = F, Cl, Br, I) and NH_3. *Phys. Chem. Chem. Phys.* **2016**, *18*, 3581−3590.
(57) Thomas, S. P.; Pavan, M. S.; Row, T. N. G. Experimental Evidence for 'Carbon Bonding' in the Solid State from Charge Density Analysis. *Chem. Commun.* **2014**, *50*, 49−51.
(58) Southern, S. A.; Bryce, D. L. NMR Investigations of Noncovalent Carbon Tetrel Bonds. Computational Assessment and Initial Experimental Observation. *J. Phys. Chem. A* **2015**, *119*, 11891−11899.
(59) Saha, N.; Kar, S. K. Chelating Behaviour of a New Pyridyl Pyrazole: Tris-Complexes of Cu(II)-, Ni(II)- and Co(II)-perchlorates and Fluoborates with 3,5-dimethyl-1-(2′-pyridyl) pyrazole. *J. Inorg. Nucl. Chem.* **1977**, *39*, 1236−1238.
(60) *Bruker, SMART*, v5.631; Bruker AXS Inc.: Madison, WI, 2001.
(61) Sheldrick, G. M. *SHELXS-97 and SHELXL-97*; University of Göttingen: Germany, 1997.
(62) Ahlrichs, R.; Bär, M.; Hacer, M.; Horn, H.; Kömel, C. Electronic Structure Calculations on Workstation Computers: The Program System Turbomole. *Chem. Phys. Lett.* **1989**, *162*, 165−169.
(63) Boys, S. B.; Bernardi, F. The Calculation of Small Molecular Interactions by the Differences of Separate Total Energies. Some Procedures with Reduced Errors. *Mol. Phys.* **1970**, *19*, 553−566.
(64) Grimme, S.; Antony, J.; Ehrlich, S.; Krieg, H. A Consistent and Accurate ab initio Parametrization of Density Functional Dispersion Correction (DFT-D) for The 94 Elements H-Pu. *J. Chem. Phys.* **2010**, *132*, 154104−154119.
(65) Bader, R. F. W. *Atoms in Molecules - A Quantum Theory*; Oxford University Press: Oxford, U.K., 1990.
(66) Todd, A.; Keith, T. K. *AIMA11*, version 13.05.06; Gristmill Software: Overland Park, KS, 2013.
(67) Blatov, V. A. Nanocluster Analysis of Intermetallic Structures with the Program Package TOPOS. *Struct. Chem.* **2012**, *23*, 955−963.
(68) Li, M.; Li, D.; O'Keeffe, M.; Yaghi, O. M. Topological Analysis of Metal−Organic Frameworks with Polytopic Linkers and/or Multiple Building Units and the Minimal Transitivity Principle. *Chem. Rev.* **2014**, *114*, 1343−1370.
(69) Weinhold, F. Natural Bond Orbital Analysis: A Critical Overview of Relationships to Alternative Bonding Perspectives. *J. Comput. Chem.* **2012**, *33*, 2363−2379.

DOI: 10.1021/acs.jpcb.6b04046
J. Phys. Chem. B 2016, 120, 6803−6811

NJC

ROYAL SOCIETY OF CHEMISTRY

PAPER

View Article Online
View Journal | View Issue

Cite this: *New J. Chem.*, 2020, 44, 7310

Supramolecular and theoretical perspectives of 2,2′:6′,2″-terpyridine based Ni(II) and Cu(II) complexes: on the importance of C–H···Cl and π···π interactions†

Pampi Pal,[a] Kinsuk Das,[b] Anowar Hossain,[a] Antonio Frontera *[c] and Subrata Mukhopadhyay*[a]

Received 7th January 2020,
Accepted 30th March 2020

DOI: 10.1039/d0nj00094a

rsc.li/njc

Two new complexes [Ni(L)Cl(H$_2$O)$_2$]Cl (complex **1**) and [Cu(L)Cl$_2$] (complex **2**) [L = 2,2′:6′,2″ terpyridine] have been synthesized and characterized by single crystal X-ray analysis. The noncovalent interactions and supramolecular assemblies observed in the crystal packing of both complexes have been described focusing on non-traditional C–H···Cl and 'traditional' O–H···Cl hydrogen bonding interactions along with π···π interactions. A DFT study has been carried out to analyze the π···π, hydrogen bonding interactions with their rationalization and characterization using molecular electrostatic potential (MEP) surfaces and NCI plot computational tools.

Introduction

Besides traditional covalent interactions, noncovalent interactions, namely, intra and intermolecular hydrogen bonding, hydrophobic interactions, dispersion interactions, halogen bonding, cation···π, C–H···π, π···π, N–H···π, S–H···π, lone pair···π, salt bridge···π, have attracted interest to elucidate the outstanding importance of these weak forces in controlling the structure and function of macromolecules in recent years.[1–3] Although these interactions were noticed about three decades ago, their pivotal role in deciding structural integrity has been established in current years.[2,3] Quantification of these weak interactions that direct molecular aggregation into supramolecular assembly is of importance.[4,5] Hydrogen bonding has been extremely well studied and recognized as the most important of all noncovalent interactions.[6,7] The classical definition of the hydrogen bond also reflects what many are taught in introductory chemistry courses: X–H···A reflects the strongly polar hydrogen bond donor groups X–H (X = O, N, or halogen) on one side and hydrogen bond acceptor atoms A (A = O, N, halogen, *etc.*) on the other. In contrast, a weak non-traditional hydrogen bond of type C–H···X attracts interest in the broad field of host–guest chemistry and anion recognition. In addition to commonly occurring C–H···N/O hydrogen bonding the existence of C–H···Cl hydrogen bonding has been much less frequent but well appreciated in recent years.[8–10] If the heterocyclic ring is associated with a donor center that reduces the electron density in the ring that in turn induces the ring C–H groups to produce C–H···Cl hydrogen bonding interactions.[11] For having a good C–H···Cl interaction, the C–H···Cl distance should be less than the sum of the van der Waals radii (2.95 Å) of the hydrogen atom and the neutral chlorine atom.[12] We find in our work that such distances range from 2.64 to 2.82 Å.

The π···π non covalent interaction is rather common for transition metal complexes that may play a decisive role in the formation of a supramolecular architecture. For this interaction a suitable geometrical conformation is necessary through which the π lobes of aromatic 'N' containing ligands should place either face to face or to some extent parallel with a distance of up to 3.8 Å.[13] Here in this paper the said distance ranges from 3.49 to 3.74 Å.

2,2′:6′,2″-Terpyridine or their structural analogs are one of the prototype oligopyridine metal-binding motifs that play a pivotal role in metallo-supramolecular chemistry and have attracted much interest in contemporary research as functional templates in the fields of coordination chemistry as well as materials science.[14–16] The chelating ability of 2,2′:6′,2″-terpyridine enhances the stability of the metal complex, and planarity of the ligand leads to strong intercalative interactions of the complex in biological systems.[17] This ligand is used as a renowned building block in supramolecular chemistry because

[a] *Department of Chemistry, Jadavpur University, Kolkata 700032, India. E-mail: toni.frontera@uib.es, ju_subrata@yahoo.in*
[b] *Department of Chemistry, Chandernagore College, Hooghly, West Bengal 712136, India*
[c] *Departament de Química, Universitat de les IllesBalears, Crta. deValldemossa km 7.5, Palma 07122, Baleares, Spain*

† Electronic supplementary information (ESI) available. CCDC 1922811 and 1922812. For ESI and crystallographic data in CIF or other electronic format see DOI: 10.1039/d0nj00094a

of its π stacking ability,[18–20] H-bond acceptor sites and possibility of formation of either anion···π or metal cation···π depending on the acidity/basicity of the π-cloud, which depends on the coordination (type of metal and its oxidation state). Hence many metal complexes have been synthesized using 2,2′:6′,2″-terpyridine that prefers to adopt a planar geometry to achieve maximum conjugation, thus containing three nitrogen atoms in *cis*, *cis* fashion. Therefore, it acts as an N-heterocycle that has very high binding potentiality towards transition metal ions due to dπ–pπ* back bonding of the metal to pyridine rings and the chelate effect.[21]

The crystal as a whole is an organization of different kinds of supramolecular interactions. The concept of introduction of supramolecular synthons was an extremely important step for the understanding of the organization of molecular crystals. The concept of supramolecular synthons is nothing but a retrosynthetic approach to supramolecular chemistry where one can fragment the crystal structures into supramolecular synthons, and based on their relative abundance in the database, new synthetic strategies can be formulated. Therefore, when one starts with a crystal structure and deconstructs it into the smallest nonreducible unit, *i.e.*, synthon, both geometrical and chemical factors get deconstructed, and it is here where synthons score over individual molecules (or functional groups) in terms of consistency and robustness.[22] This created an opportunity for the preparation of molecular crystals with targeted patterns of binding between molecules similar to the synthesis of organic molecules using molecular building blocks or synthons.[23]

Considering our interest in the field of novel noncovalent interactions we have planned to synthesize two terpyridine derived transition metal complexes [complex **1** bears Ni(II) as the metal center and **2** has Cu(II)] in aqueous methanol solvent. Strategically 1 : 1 molar ratio is maintained to synthesize mixed ligand complexes (to avoid bis-terpyridine complexes) having at least one chlorine coordinated to metal centers. In both complexes the title ligand acts as a neutral tridentate NNN donor in *cis*, *cis* fashion to execute more effective binding through chelate rings around the metal centers. Unlike other metal cations, Cu(II) is not regarded to take part in a cation···π interaction because this metal tends to oxidize the π electron system.[24] To the best of our knowledge this is the first reported Cu(II) complex with 2,2′:6′,2″-terpyridine (**L**) that exhibits Cu(II)···π interactions. For **1**, an intermolecular π···π stacking interaction results in a 1D arrangement which is further extended through two different types of O–H···Cl hydrogen bonding to ensure a 2D arrangement. Another 2D chain was observed by only intermolecular H-bonding of both C–H···Cl and O–H···Cl types. Complex **2** exhibits a dimeric distribution utilizing a metal cation···π interaction that in turn connected through two types of π···π interaction results in the execution of a 2D assembly. A new type of 2D layer is generated comprising only different kinds of π···π interactions. Finally, complex **2** utilizes two different C–H···Cl intermolecular H-bonding in two different planes that are able to constitute another 2D arrangement.

The present work combines theory (DFT calculations) and experiment to analyze the noncovalent interactions and their interplay governing the solid state architecture of complexes **1** and **2**. In particular, the influence of intermolecular C–H···Cl and π···π interactions along with other non-covalent interactions like O–H···Cl, anion···π, and cation···π is investigated using a $[LM(Cl)_x]$ (x = 1 or 2, M = Ni, Cu) unit as the key building block.

Experimental section

Materials and measurements

All chemicals were of reagent grade, purchased from commercial sources and used without further purification. 2,2′:6′,2″-terpyridine (**L**) and methanol were purchased from Aldrich Chemical Company, USA, and used without further purification. All reactions were carried out under aerobic conditions and in methanol–water medium (Scheme S1, ESI†). During the whole experiment freshly boiled, doubly distilled water was used. A PerkinElmer RXI FT-IR spectrophotometer was used to record the IR spectra in the range of 4000–400 cm^{-1} and elemental analyses (carbon, hydrogen and nitrogen) of the metal complexes were performed with a PerkinElmer CHN analyzer 2400. UV-Vis-NIR spectra for both **1** and **2** were collected on a Hitachi UH 4150 UV-Visible/NIR spectrophotometer. The PXRD data of the powdered sample were collected on a Rigaku-TTRAX-III diffractometer using Cu Kα radiation (λ = 1.5406 Å). Thermogravimetric analysis (TGA) data were collected with an SDT 2960 thermoanalyzer under nitrogen (50° to 850 °C) at a heating rate of 10 °C per minute for both the complexes. The room temperature magnetic moments of the complexes were obtained from a magnetic susceptibility balance MK1 Sherwood.

Synthesis

Synthesis of $[Ni(L)Cl(H_2O)_2]Cl$ (complex 1)

A methanolic solution (10 mL) of the ligand (0.233 g, 1 mmol) was added dropwise to a solution of $NiCl_2{\cdot}6H_2O$ (0.237 g, 1 mmol) in the same solvent (10 mL) with constant stirring which continued for 3 hours. Then the solution was filtered and the filtrate was left for slow evaporation. After one week, deep green X-ray quality crystals of **1** were isolated (yield: 67%). Anal. calc. for $C_{15}H_{15}NiN_3O_2Cl_2$: C, 45.12; H, 3.76; N, 10.52. Found: C, 44.98; H, 3.69; N, 10.17%. Main FT- IR absorptions, (KBr, cm^{-1}): 3207 (s), 3057 (s), 3018 (s), 1599 (vs), 1576 (s), 1477 (s), 1451 (s), 1323 (w), 1253 (m) (Fig. S3, ESI†). $\lambda_{max/nm}$ = 281, 447 and 581 (Fig. S4, ESI†). Room temperature magnetic moment (μ_{eff}) = 2.99 B.M.

Synthesis of $[Cu(L)Cl_2]$ (complex 2)

A methanolic solution (20 mL) of the ligand (0.233 g, 1 mmol) was added dropwise to a solution of $CuCl_2{\cdot}6H_2O$ (0.242 g, 1 mmol) in the same solvent (10 mL) with constant stirring for 2 hours. Then the green coloured solution was filtered and the filtrate was kept undisturbed for slow evaporation. After one

week, green X-ray quality crystals of **2** were obtained (yield: 63.5%). Anal. calc. for $C_{15}H_{11}CuN_3Cl_2$: C, 48.97; H, 2.99; N, 11.42. Found: C, 48.67; H, 2.91; N, 11.33%. Main FT-IR absorptions, (KBr, cm^{-1}): 3087 (s), 3013 (s), 2965 (s), 1598 (s), 1575 (m), 1473 (s), 1448 (s), 1327 (m), 1252 (m) (Fig. S3, ESI†). $\lambda_{max/nm}$ = 377 and 469 (Fig. S4, ESI†). Room temperature magnetic moment (μ_{eff}) = 1.83 B.M.

X-ray crystallographic analysis

Data collections were made using a Bruker SMART APEX II CCD area detector equipped with a graphite monochromated Mo Kα radiation (λ = 0.71073 Å) source in φ and ω scan mode at 293(2) K for **1** and 273(2) K for **2**. Cell parameter refinement and data reduction were carried out using a Bruker SMART APEX II instrument and Bruker SMART and Bruker SAINT software[25] for all the complexes. The structure of all the complexes was solved by conventional direct methods and refined by full-matrix least-squares methods using F^2 data. SHELXS-97 and SHELXL-97 programs[26] were used for the solution and refinement of the structure of all the complexes, respectively. CCDC 1922811 (**1**) and 1922812 (**2**) include additional crystallographic information. Selected crystal data for **1** and **2** are given in Table S1 (ESI†) and selected metrical parameters of the complexes are given in Table S2, ESI.†

Theoretical methods

To compute the interaction energies in the solid state we have used the crystallographic coordinates at the PB1PBE-D3/def2-TZVP level of theory where only the position of the H-atoms has been optimized. For calculations, the GAUSSIAN-16 program has been used.[27] The D3 Grimme's dispersion correction has also been used as implemented in the GAUSSIAN-16 program since it is adequate for the evaluation of non-covalent interactions where dispersion effects are relevant like those reported herein.[28] The basis set superposition error for the calculation of interaction energies has been corrected using the counterpoise method.[29] The NCI index and NCI plot isosurfaces have been used to characterize the non-covalent interactions.[30] They correspond to both favorable and unfavorable interactions, as differentiated by the sign of the second density Hessian eigenvalue and defined by the isosurface color. The color scheme is a red-yellow-green-blue scale with red for ρ_{cut}^{+} (repulsive) and blue for ρ_{cut}^{-} (attractive), whereas yellow and green isosurfaces correspond to weak repulsive and weak attractive interactions, respectively.[31]

Results and discussion

Single-crystal X-ray structural analysis confirms that the asymmetric unit of the title complexes consist of one heterocyclic ligand (**L**) [2,2′: 6′,2″-terpyridine] moiety with nickel(II), chloride ions and solvent water molecules (in **1**) and copper(II) and chloride ions (in **2**). In both complexes, the ligand (**L**) acts as a neutral tridentate NNN donor moiety in *cis*, *cis* fashion and forms two five membered chelate rings around the central metal ions. The molecular representation with the atom numbering scheme (only coordinated atom numbering was done for maintaining the clarity of the picture) of the complexes are shown in Fig. S1 and S2 (ESI†).

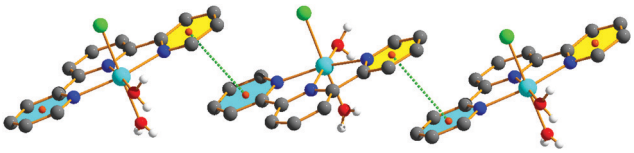

Fig. 1 1D chain of **1** incorporating π···π interactions [π···π interaction is shown by green dotted lines, Cg(2): pink coloured filled rings, Cg(3): yellow coloured filled rings and Cg(5): aqua coloured filled rings]. Aromatic hydrogen atoms have been omitted for clarity.

PXRD has been carried out at room temperature with the powdered sample of both the complexes (**1** and **2**). The bulk purity of both the complexes has been confirmed by the PXRD pattern. The major peaks of the PXRD pattern of the synthesized complexes match well with the simulated pattern generated from the single crystal data, representing phase purity of the bulk (Fig. S5, ESI†). The minor shifts and the differences in the intensities might be attributed to the changes either in crystal lattice orientation with respect to an inertial frame of reference or sample thickness. It might also be due to the baseline drift of the PXRD diffractometer and the temperature difference in measuring single crystal diffraction and powder X-ray diffraction.[32,33]

Structural description of complex 1

The perspective view of the molecular structure of complex **1** with the atom numbering scheme is shown in Fig. S1 (ESI†) whereas selected bond lengths (Å) and bond angles (°) are listed in Table S2 (ESI†). Complex **1** crystallizes in the space group $P2_1/n$ and its unit cell is composed of four molecules. Complex **1** is a distorted octahedron where the title ligand (**L**) spans in the meridional position [N1–Ni1–N2 = 78.65(9)°, N2–Ni1–N3 = 78.69(9)° and N3–Ni1–N1 = 157.34(9)°] as a neutral tridentate NNN donor *via* three pyridyl nitrogen atoms (N1, N2 and N3). The residual positions of the octahedral geometry are satisfied by two oxygen atoms from two different water molecules (O1 and O2) and one chloride atom (Cl1). The monopositive charge of **1** is taken care by another chloride ion (Cl2) present at the outside of the metal coordination sphere. In **1** among the three *trans* angles two [N2–Ni1–O2 = 174.33(8)° and Cl1–Ni1–O1 = 174.75(6)°] are close to ideal 180° while the third one [N3–Ni1–N1 = 157.34(9)°] deviated more maybe due to small bite angles [N1–Ni1–N2 = 78.65(9)° and N2–Ni1–N3 = 78.69(9)°] of the tridentate ligand that possibly induces a distortion in this *trans* angle and in the overall octahedral geometry (Table S2, ESI†). The average Ni–N and Ni–O bond distances are 2.059 Å [Ni1–N1 = 2.105(2) Å, Ni1–N2 = 1.9854(19) Å and Ni1–N3 = 2.087(2) Å] and 2.076 Å [Ni1–O1 = 2.097(2) Å and Ni1–O2 = 2.0557(18) Å] respectively, which are in accord with previously reported six coordinated Ni(II) complexes.[34] The Ni1 atom sits almost in the same mean plane (deviated by only 0.04 Å) formed by O2N1N2N3.

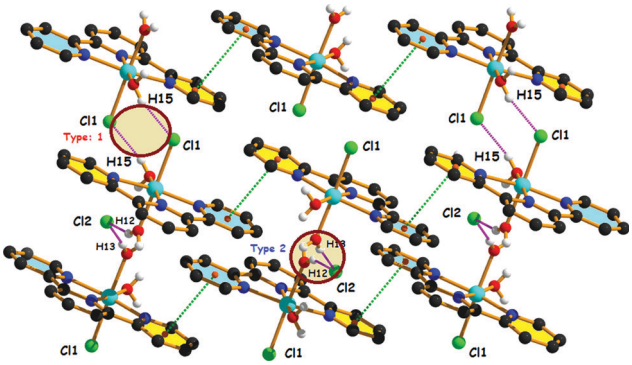

Fig. 2 2D chain of **1** incorporating H-bonding and π···π interactions [π···π interaction is shown by green dotted lines and O–H···Cl hydrogen bonding is shown by pink dotted lines, Cg(3): yellow coloured filled rings and Cg(5): aqua coloured filled rings]. Aromatic hydrogen atoms have been omitted for clarity.

The monomeric unit of complex **1** propagates to ensure a 1D polymeric association through a π···π interaction (Table S3, ESI†) between Cg(3) of one unit with Cg(5) of the other unit (Fig. 1).

This 1D arrangement is further extended to 2D layers using two different types of intermolecular hydrogen bonding (Table S4, ESI†). The first type (Type 1) of intermolecular hydrogen bonding was shaped by the hydrogen atom H15 (attached with O2 of coordinated water molecule) of one unit and the coordinated chlorine atom (Cl1) that leads to the formation of an $R_2^2(8)$ ring motif. The second type (Type 2) of intermolecular hydrogen bonding is formed by a non-coordinated chloride ion (Cl2) and two hydrogen atoms (H12 and H13) attached with two different oxygen atoms (O1) of coordinated water molecules belonging to two different complex units (Fig. 2). Thus π···π interactions along with these two types of H-bonding enhance the dimensionality from 1D to 2D.

A different 2D layer is formed in complex **1** using three different types of hydrogen bonding (Table S4, ESI†). Type 1 and Type 2 have already been described above. The third type (Type 3) of intermolecular hydrogen bonding is formed between the hydrogen atom H4 attached to the pyridine ring carbon C4 of one unit and coordinated chlorine atom (Cl1 from another complex unit) in association with the other two types of intermolecular hydrogen bonding. It constitutes a new 2D architecture (Fig. 3). This 2D layer includes four different types of synthons, namely, $R_2^2(8)$, $R_2^2(16)$, $R_3^6(20)$ and $R_6^4(22)$.

Structural description of complex 2

The molecular structure of Cu(II) complex **2** with the atom numbering scheme is shown in Fig. S2 (ESI†) while its selected bond lengths (Å) and bond angles (°) are listed in Table S2 (ESI†). Complex **2** crystallizes in a monoclinic system with the space group $P2_1/c$ and its unit cell contains four molecules. Complex **2** is a mononuclear species comprising neutral $[Cu(L)Cl_2]$ where **L** is a 2,2′:6′,2″-terpyridine molecule. The central Cu(II) ion is placed in a square pyramidal [the τ value[35] is 0.077, ideally 1 for trigonal bipyramidal geometry and 0 for square pyramidal geometry] pocket where the equatorial plane

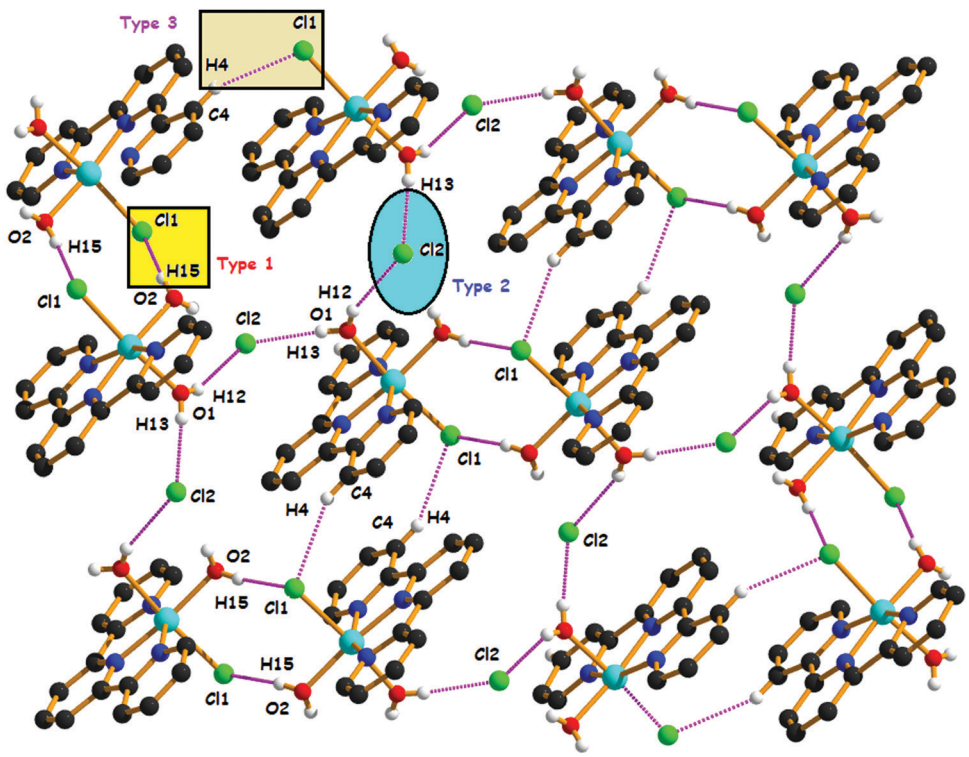

Fig. 3 2D layer of **1** incorporating H-bonding interactions [O–H···Cl and C–H···Cl hydrogen bonding is shown by pink dotted lines]. Aromatic hydrogen atoms have been omitted for clarity.

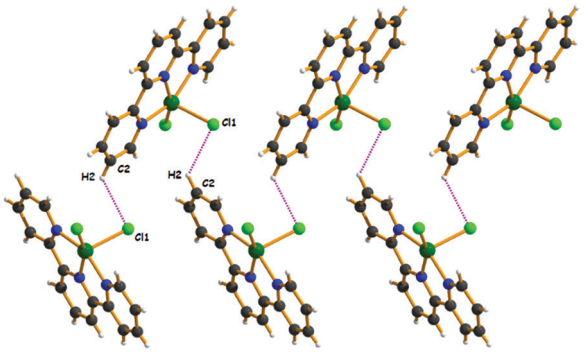

Fig. 4 Perspective view of the formation of a single 1D architecture of complex **2** by H-bonding [C–H···Cl hydrogen bonding is shown by pink dotted lines].

is formed by the pyridyl nitrogen atoms (N1, N2 and N3) of the terpyridine ligand and one chloride ion (Cl2) while the axial position is occupied by another chloride ion (Cl1). The Cu(II) ion is shifted by a distance of 0.327 Å and 0.20 Å towards the apical Cl1 atom from the equatorial plane (N1N2N3Cl2) and pyridine plane (N1N2N3) respectively. Here the ligand (**L**) is able to bind the metal ion through two five-membered chelate rings. The average Cu–N bond distance is 2.0246 Å [Cu1–N1 = 2.0552(18) Å, Cu1–N2 = 1.9614(16) Å and Cu1–N3 = 2.0572(17) Å]. The Cu(II)–nitrogen bond between Cu(II) and the central pyridine atom (N2) is somewhat shorter [Cu1–N2 = 1.9614(16) Å] than those concerning the terminal 'N' atoms (N1 and N3) (Table S2, ESI†), which is usual and results from chelating ligand constraints.[36–38] The axial chloride (Cl1) is comparatively at a larger distance [Cu1–Cl1 = 2.4699(6) Å] than the equatorial one [Cu1–Cl2 = 2.2496(6) Å] likely due to the less 's' character of the orbital involved in the coordination bond, which makes the axially coordinated chloride ion more electronegative (stronger hydrogen bond acceptor). The average axial–equatorial and equatorial–equatorial bond angles are 98.70° and 88.69° respectively. Equatorial trans angles Cl2–Cu1–N2 [157.25(5)°] and N1–Cu1–N3 [156.00(7)°] deviated from the ideal trans angle 180° due to steric and electronic effects. The electrical charge of the central Cu ion is compensated for by two coordinated chloride ions (Cl1 and Cl2).

The existence of C–H···Cl hydrogen bonds along with charge-assisted terminal M–Cl bonds, in particular, has been well appreciated in recent times besides the commonly occurring C–H···N/O/S hydrogen-bonding interactions. Through a closer look it was evident that two different planes propagate through intermolecular C–H···Cl hydrogen bonding [C2–H2···Cl1] (Table S4, ESI†) incorporating the axially coordinated chloride ion (Cl1) to produce a 1D infinite chain (Fig. 4).

In association with this intermolecular hydrogen bonding interaction another intermolecular hydrogen bonding interaction [C4–H4···Cl1] extends the dimensionality to 2D. Hence it is the perfect self-assembly of a [$CuLCl_2$] coordination motif held together by C–H···Cl hydrogen bonding interactions. Possibly the nonequivalency of the terminal chloride generated from the square pyramidal geometry adopted by the central Cu(II) ion along with the secondary C–H···Cl interaction provides the required turn almost orthogonally. In this 2D arrangement two different planes propagate through intermolecular hydrogen bonding incorporating one coordinated chloride ion (Cl1). In individual planes ('A' and 'B') two complex units are oriented in such a manner that hydrogen H4 (attached with pyridine C4) of one unit faces the Cl1 atom of the other unit. Now these two planes are connected by another intermolecular H-bonding formed between the aromatic fragment C2–H2 of 'plane A' and the Cl1 atom of 'plane B' and *vice versa*. These two planes ('A' and 'B') are almost orthogonal (86°) and repeating themselves alternately to enhance the dimensionality from 1D to 2D (Fig. 5).

In **2** there is a dimeric distribution as shown in Fig. 8 that is formed by a cation···π interaction (Fig. 6), which is quite unusual because Cu(II) is likely to oxidize the π electron system. Here two units are arranged almost in opposite orientations one above the other to accomplish a cation···π interaction (Table S5, ESI†) between Cu(1) and Cg(5). The Cu···Cu separation in this dimeric integrity is 5.535 Å.

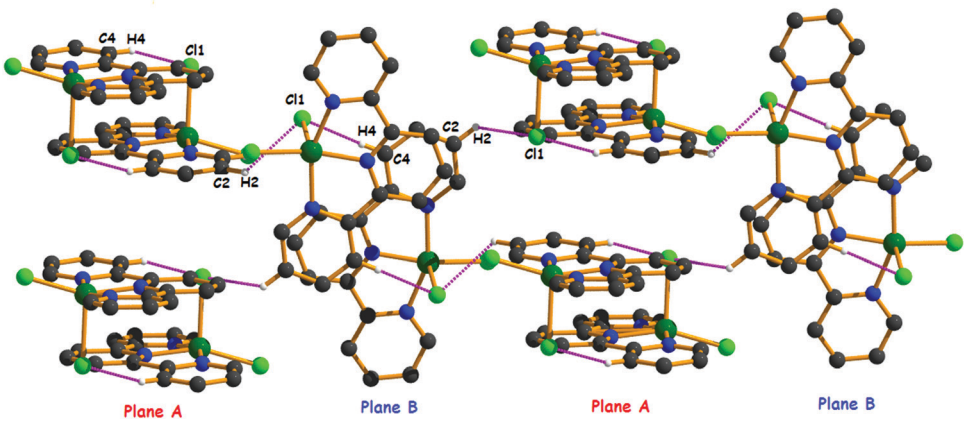

Fig. 5 2D polymeric chain of complex **2** by two different kinds of C–H···Cl hydrogen bonding [C–H···Cl hydrogen bonding is shown by pink dotted lines]. Hydrogen atoms not involved in hydrogen bonding have been omitted for clarity.

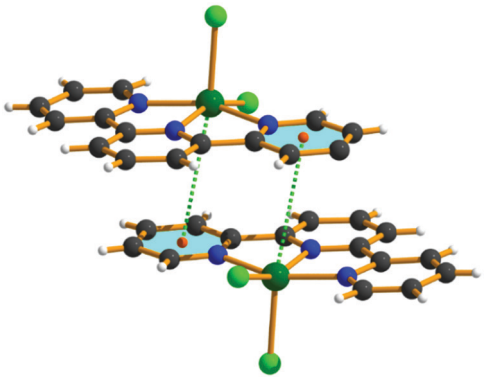

Fig. 6 Cation···π interactions in complex **2** [Cu(II)···π interaction is shown by green dotted lines, Cg(5): aqua coloured filled rings].

The interplanar distances of successive terpyridine moieties suggest the possibilities of π···π interactions. Interestingly the dimeric units [through cation···π interaction as depicted in Fig. 6] of **2** forms a 1D chain implementing a π···π interaction between Cg(3) and Cg(4). Such 1D chains are further stabilized through another π···π interaction (Table S3, ESI†) between Cg(5) centroids of different layers that are almost parallel to increase the dimensionality (Fig. 7).

Another interesting interpretation has been drawn from the structural integrity through different kinds of π···π interactions that play a crucial role in the formation of a different 1D polymeric chain. Here Cg(5) of one complex unit interacts simultaneously with Cg(1), Cg(2) and Cg(4) to form a dimeric unit. This dimeric unit is further stabilized by another π···π interaction, *i.e.*, Cg(2)–Cg(2) (Table S3, ESI†). Again the dimeric units are interconnected by a Cg(3)–Cg(4) interaction which leads to the formation of a 1D chain (Table S3, ESI†). All these interactions are cumulatively associated with another π···π interaction between two Cg(5) centroids of different extrapolated 1D chains to generate a 2D arrangement (Fig. 8).

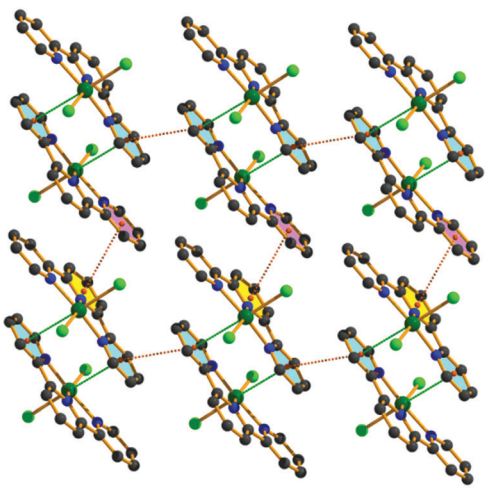

Fig. 7 2D chain of **2** incorporating cation···π and π···π interactions [Cu(II)···π interaction is shown by green dotted lines and π···π interaction is shown by orange dotted lines, Cg(3): pink coloured filled rings, Cg(4): yellow coloured filled rings and Cg(5): aqua coloured filled rings].

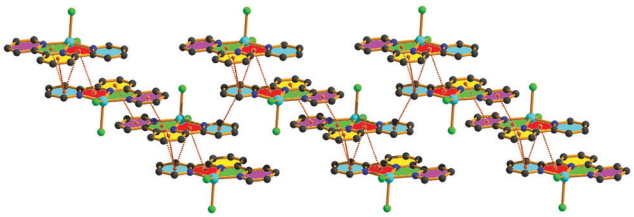

Fig. 8 2D chain of **2** incorporating π···π interactions [π···π interaction is shown by orange dotted lines, Cg(1): green coloured filled rings, Cg(2): red coloured filled rings Cg(3): pink coloured filled rings, Cg(4): yellow coloured filled rings and Cg(5): aqua coloured filled rings].

Thermal analysis

Thermal analysis was carried out to obtain an insight into the thermal stability of the complexes. The TG curves for both the complexes are shown in Fig. S6 (ESI†). For **1**, it clearly shows that the complex is thermally stable up to 100 °C. In the temperature range from 100 to 135 °C, complex **1** loses two coordinated water molecules (calculated mass loss 9%, found 8.7%). After that complex **1** shows thermal stability up to 430 °C even after the removal of the two water molecules. Complex **1** then exhibits multistep decomposition after 430 °C that did not exactly match with the calculated mass loss.[21] The TG curve for complex **2** indicates that the complex is thermally stable up to 350 °C and then decomposes with no evident intermediate steps found in the TG analysis. The thermal decomposition pattern of complex **2** is complicated and no definite conclusion can be drawn as weight loss at different stages cannot be matched with the predicted decomposition and consequent loss in weight indicating multistep decomposition.[39]

Theoretical study

First of all, we have computed the molecular electrostatic potential (MEP) surfaces of complexes **1** and **2** in order to find the most electrophilic and nucleophilic parts of the complexes. The MEP surfaces for both complexes are illustrated in Fig. 9 and, for complex **1**, the most positive region (+75 kcal mol^{-1}) is located at the H-atoms of the coordinated water molecules. The acidity and thus the ability of these H-atoms to participate in H-bonding interactions are enhanced due to the coordination of the O-atom to the Ni(II) metal center. The most negative

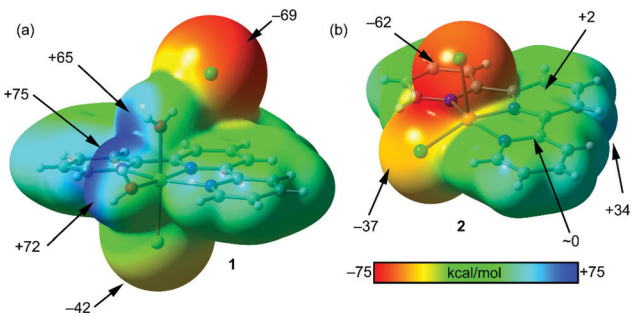

Fig. 9 MEP surfaces of complexes **1** (a) and **2** (b) using the 0.001 a.u. isosurface at the PBE1PBE-D3/def2-TZVP level of theory. The values at selected points of the surface are indicated in kcal mol^{-1}.

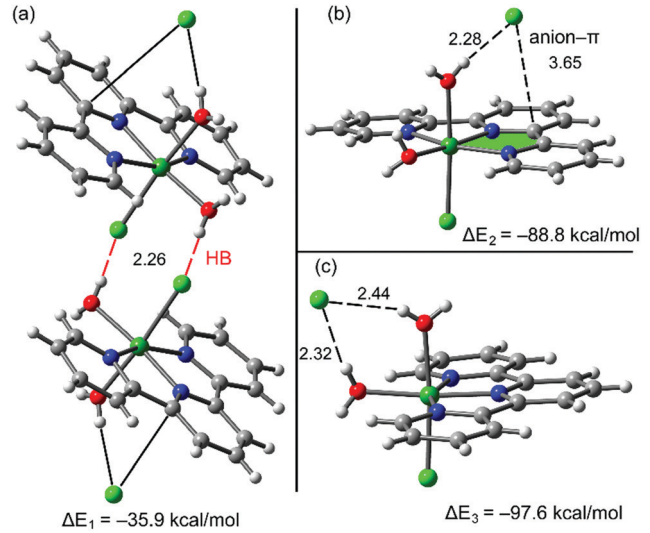

Fig. 10 Theoretical models used to evaluate the noncovalent interactions in the dimer of **1** (a) and the two different binding modes of the chloride (b and c). Distances are in Å.

region corresponds to the chloride counterion (−69 kcal mol^{-1}) and the coordinated chlorido ligand also exhibits a large and negative MEP value (−42 kcal mol^{-1}). In complex **2**, the most positive region is located at the aromatic H-atoms (+34 kcal mol^{-1}) and the most negative value is at the axial chlorido ligand (−62 kcal mol^{-1}) that is considerably more negative than the other chlorido ligand (−37 kcal mol^{-1}). The MEP values over the aromatic rings are very small or negligible.

The theoretical models used to evaluate the different assemblies observed in the solid state of complex **1** are given in Fig. 10. To evaluate the H-bonds (red dashed lines) we have used as monomer the whole {[Ni(L)Cl(H$_2$O)$_2$]Cl} unit. The dimerization energy (see Fig. 10a) is very large (ΔE_1 = −35.9 kcal mol^{-1}) in agreement with the strong MEP value at the H-atoms (see Fig. 9) involved in the H-bonds. This confirms the robustness of these H-bonds in the formation of the 2D layer shown in Fig. 3. We have also evaluated the interaction modes of the chloride counterion with the cationic part of complex **1** [Ni(L)Cl(H$_2$O)$_2$]$^+$. That is, on one hand, the Cl$^-$ anion interacts with [Ni(L)Cl(H$_2$O)$_2$]$^+$ by a combination of H-bond and anion–π interactions (see Fig. 10b) and, on the other hand, by means of bifurcated Cl···H$_2$O–Ni(II) H-bonds (see Fig. 10c). Both binding modes are energetically very favorable due to strong electrostatic attraction between the counterions. As expected the bifurcated H-bond is more favored (around 9 kcal mol^{-1}) than the combination of H-bond and anion–π interactions.

In complex **2** we have analyzed both π–π stacking modes that are important in the X-ray packing as illustrated above in Fig. 8. Fig. 11a shows the π–π dimer where the chelate rings (CR) participate in the binding in addition to the pyridine rings. The dimerization energy is large (ΔE_4 = −27.4 kcal mol^{-1}) due to the participation of the CR as previously demonstrated[40–43] and also due to the antiparallel arrangement of the monomers that enhances the dipole···dipole interaction. In the other π–π stacking binding mode, in addition to the π-stacking interaction, two symmetrically equivalent hydrogen bonds are also established (see Fig. 11b). The formation of these H-bonds strongly agrees with the MEP surface of this complex (see Fig. 9b), since the most negative and most positive parts of the molecule correspond to the axial chlorido ligand and the aromatic H-atoms, respectively. Consequently, the binding energy computed for this dimer (b) is larger (ΔE_5 = −33.4 kcal mol^{-1}) than the other one (a) where only π-stacking interactions are present.

Finally, the noncovalent interaction plot (NCI plot) index[31] has been used to further characterize the noncovalent interactions in the assemblies of complexes **1** and **2**. This index facilitates a direct assessment and shows the extent to which non-covalent interactions stabilize a complex. Fig. 12 shows the NCI plot representation obtained for the self-assembled dimer commented above in Fig. 10a. The NCI index confirms the

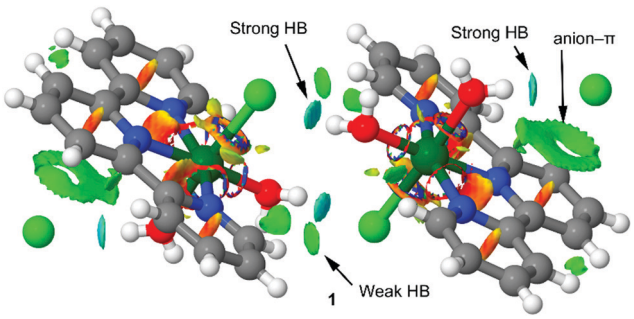

Fig. 12 NCI plot of the self-assembled dimer of **1**. The gradient cut-off is s = 0.35 a.u., and the color scale is $-0.04 < \rho < 0.04$ a.u.

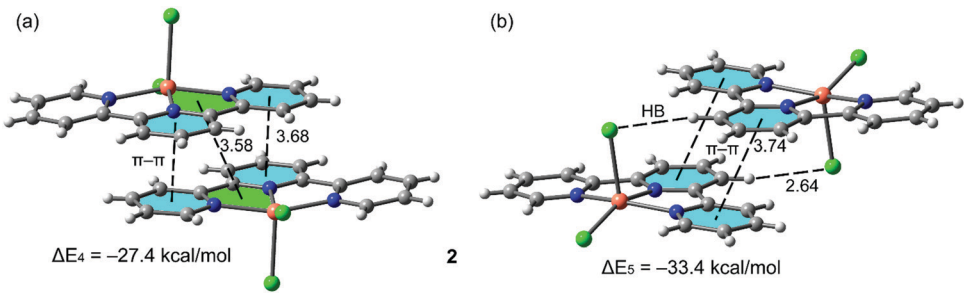

Fig. 11 Theoretical models used to evaluate the noncovalent interactions in both π···π binding modes of **2** (a and b). Distances are in Å.

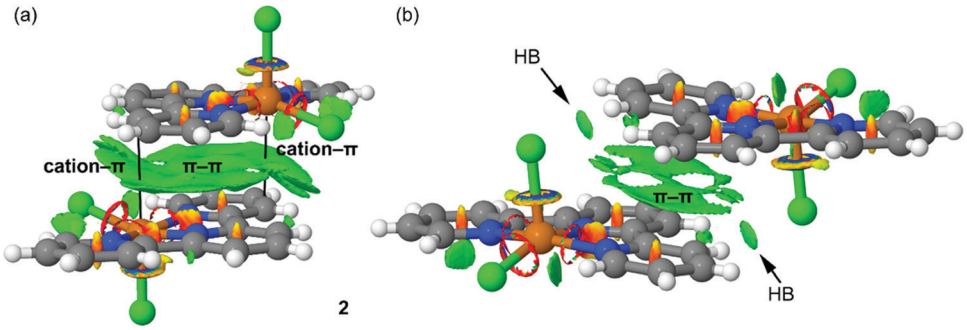

Fig. 13 (a and b) NCI plots of two self-assembled π–π dimers of **2**. The gradient cut-off is s = 0.35 a.u., and the color scale is $-0.04 < \rho < 0.04$ a.u.

existence of anion–π and H-bonding interactions between the chloride counterion and the Ni(II) complex, which are characterized by green and blue isosurfaces, respectively. The NCI plot also evidences the strong nature of the O–H···Cl interactions between the $[Ni(L)Cl(H_2O)_2]^+$ moieties (blue and small isosurfaces) and reveals the existence of secondary C–H···Cl weak H-bonding interactions, involving the aromatic ring, that also contribute to the dimerization.

Fig. 13 shows the NCI plot for the two π-stacking modes analyzed above for complex **2**. For the dimer shown in Fig. 13a the π-stacking interaction is characterized by a green and very large isosurface that embraces the whole π-systems and even the Cu(II) metal center and explains the strong interaction energy. For the other dimer (Fig. 13b), the overlap of the π-systems is smaller compared to the one shown in Fig. 13a, because of the antiparallel displacement of the complexes. The NCI plot confirms the existence of the C–H···Cl H-bonds that are characterized by bluish and small isosurfaces located between the Cl and H-atoms.

Conclusions

We have synthesized 2,2′:6′,2″-terpyridine based complexes of Ni(II) (**1**) and Cu(II) (**2**) using their chloro salts purposefully so that at least one chloride ion should be attached with the metal centers. The aim of this work was to explore the role of π-rich aromatic rings and ancillary chloride ions in producing supramolecular interactions. The structural insights reveal that intermolecular hydrogen bonding (C–H···Cl, O–H···Cl), π···π and metal cation···π supramolecular interactions play a pivotal role in stabilizing the structures of the complexes in the solid state. To the best of our knowledge this is the first report of Cu(II)···π interactions with a terpyridine moiety. Due to their robustness, these supramolecular interactions can be used as synthons for the construction of new supramolecular architectures in the solid state. A DFT study has been used to evaluate the noncovalent interactions energetically and confirm their crucial role determining the supramolecular architecture of both complexes. Finally, the interactions have been characterized using the NCI plot index and rationalized using the MEP surfaces. Theoretically strong O–H···Cl and weak C–H···Cl in complex **1** and π···π, metal cation···π and C–H···Cl interactions in complex **2** can be verified. In complex **2** the MEP surface evidences that the axial chlorido ligand is a better H-bond acceptor (C–H···Cl interaction) than the equatorial one, in agreement with the supramolecular assemblies observed in the solid state.

Conflicts of interest

There are no conflicts to declare.

Acknowledgements

A. H. gratefully acknowledges the University Grants Commission (New Delhi) for a senior research fellowship. A. F. thanks MICIU/AEI from Spain (project number CTQ2017-85821-R, FEDER funds) for financial support.

References

1 M. O. Sinnokrot, E. F. Valeev and C. D. Sherrill, *J. Am. Chem. Soc.*, 2002, **124**, 10887–10893.
2 (*a*) I. Alkorta, J. Elguero and A. Frontera, *Crystals*, 2020, **10**, 180; (*b*) F. Biedermann and H. J. Schneider, *Chem. Rev.*, 2016, **116**, 5216–5300.
3 *Noncovalent forces*, ed. S. Scheiner, Springer, Dordrecht, 2015.
4 A. S. Mahadevi and G. N. Sastry, *Chem. Rev.*, 2016, **116**, 2775–2825.
5 (*a*) I. Alkorta, F. Blanco, P. M. Deya, J. Elguero, C. Estarellas and A. Frontera, *Theor. Chem. Acc.*, 2010, **126**, 1–14; (*b*) A. Bauzá, T. J. Mooibroek and A. Frontera, *Chem. Commun.*, 2014, **50**, 12626–12629; (*c*) M. Mitra, P. Manna, A. Bauza, P. Ballester, S. K. Seth, S. R. Choudhury, A. Frontera and S. Mukhopadhyay, *J. Phys. Chem. B*, 2014, **118**, 14713–14726; (*d*) A. Bauzá, T. J. Mooibroek and A. Frontera, *Chem. – Eur. J.*, 2014, **20**, 10245–10248.
6 H. Schneider, *Angew. Chem., Int. Ed.*, 2009, **48**, 3924–3977.
7 *Non-covalent interaction in the synthesis and design of new compounds*, ed. A. M. Maharramov, K. T. Mahmudov, M. N. Kopylovich and A. J. L. Pombeiro, John Wiley & Sons, Inc., Hoboken, NJ, 2016.
8 L. M. Eytel, H. A. Fargher, M. M. Haley and D. W. Johnson, *Chem. Commun.*, 2019, **55**, 5195–5206.

9 Y. Liu, W. Zhao, C. H. Chen and A. H. Flood, *Science*, 2019, **365**, 159–161.
10 G. R. Desiraju and T. Steiner, *The weak hydrogen bond in structural chemistry and biology*, Oxford University Press Inc., New York, 1999.
11 V. Balamurugen, M. S. Hundal and R. Mukherjee, *Chem. – Eur. J.*, 2004, **10**, 1683–1690.
12 G. Aullon, D. Bellamy, A. G. Orpen, L. Brammer and E. A. Bruton, *Chem. Commun.*, 1998, 653–654.
13 C. Janiak, *J. Chem. Soc., Dalton Trans.*, 2000, **21**, 3885–3896.
14 E. C. Constable, *Chem. Soc. Rev.*, 2007, **36**, 246–253.
15 M. W. Cooke and G. S. Hanan, *Chem. Soc. Rev.*, 2007, **36**, 1466–1476.
16 A. Wild, A. Winter, F. Schluetter and S. U. Schubert, *Chem. Soc. Rev.*, 2011, **40**, 1459–1511.
17 V. S. Stafford, K. Suntharalingam, A. Shivalingam, A. J. P. White, D. J. Mann and R. Vilar, *Dalton Trans.*, 2015, **44**, 3686–3700.
18 P. Hobza, Themed Issue on 'Stacking Interactions', *Phys. Chem. Chem. Phys.*, 2008, **10**, 2561–2868.
19 J. Sponer, K. E. Riley and P. Hobza, *Phys. Chem. Chem. Phys.*, 2008, **10**, 2595–2610.
20 L. M. Salonen, M. Ellermann and F. Diederich, *Angew. Chem., Int. Ed.*, 2011, **50**, 4808–4842.
21 G. Barone, G. Gennaro, A. M. Giuliani and M. Giustini, *RSC Adv.*, 2016, **6**, 4936–4945.
22 A. Mukherjee, *Cryst. Growth Des.*, 2015, **15**, 3076–3085.
23 O. V. Shishkin, R. I. Zubatyuk, S. V. Shishkina, V. V. Dyakonenko and V. V. Medviediev, *Phys. Chem. Chem. Phys.*, 2014, **16**, 6773–6786.
24 H. Yorita, K. Otomo, H. Hiramatsu, A. Toyama, T. Miura and H. Takeuchi, *J. Am. Chem. Soc.*, 2008, **46**, 15266–15267.
25 *Bruker, SMART v5.631*, Bruker AXS Inc., Madison, WI, USA, 2001.
26 G. M. Sheldrick, *SHELXS-97 and SHELXL-97*, University of Göttingen, Germany, 1997.
27 M. J. Frisch, G. W. Trucks, H. B. Schlegel, G. E. Scuseria, M. A. Robb, J. R. Cheeseman, G. Scalmani, V. Barone, B. Mennucci, G. A. Petersson, H. Nakatsuj, M. Caricato, X. Li, H. P. Hratchian, A. F. Iamaylov, J. Bloino, G. Zheng, J. L. Sonnenberg, M. Hada, M. Ehara, K. Toyota, R. Fukuda, J. Hasegawa, M. Ishida, T. Nakajima, Y. Honda, O. Kitao, H. Nakai, T. Vreven, J. A. Montgomery Jr, J. E. Peralta, F. Ogliaro, M. Bearpark, J. J. Heyd, E. Brothers, K. N. Kudin, V. N. Staroverov, R. Kobayashi, J. Normand, K. Raghavachari, A. Rendell, J. C. Burant, S. S. Lyengar, J. Tomasi, M. Cossi, N. Rega, J. M. Millam, M. Klene, J. E. Knox, J. B. Cross, V. Bakken, C. Adamo, J. Jaramillo, R. Gomperts, R. E. Stratmann, O. Yazyev, A. J. Austin, R. Cammi, C. Pomelli, J. W. Ochterski, R. L. Martin, K. Morokuma, V. G. Zakrzewski, G. A. Voth, P. Salvador, J. J. Dannenberg, S. Dapprich, A. D. Daniels, O. Farkas, J. B. Foresman, J. V. Ortiz, J. Cioslowski and D. J. Fox, *Gaussian 09, Revision A.1*, Gaussian Inc., Wallingford CT, 2016.
28 S. Grimme, J. Antony, S. Ehrlich and H. Krieg, *J. Chem. Phys.*, 2010, **132**, 154104.
29 S. F. Boys and F. Bernardi, *Mol. Phys.*, 1970, **19**, 553–566.
30 J. Contreras-García, E. R. Johnson, S. Keinan, R. Chaudret, J.-P. Piquemal, D. N. Beratan and W. Yang, *J. Chem. Theory Comput.*, 2011, **7**, 625–632.
31 E. R. Johnson, S. Keinan, P. Mori-Sánchez, J. Contreras-García, A. J. Cohen and W. Yang, *J. Am. Chem. Soc.*, 2010, **132**, 6498–6506.
32 C. F. Holder and R. E. Schaak, *ACS Nano*, 2019, **13**, 7359–7365.
33 H. Zaho, B. G. Zhang, X. X. Zhang, S. Wang and B. L. Wu, *Synth. React. Inorg., Met.-Org., Nano-Met. Chem.*, 2015, **45**, 572–580.
34 E. C. Constable, D. Phillips and P. R. Raithby, *Inorg. Chem. Commun.*, 2002, **5**, 519–521.
35 A. W. Addison, T. N. Rao, J. Reedijk, J. Rijn and G. C. Verschoor, *J. Chem. Soc., Dalton Trans.*, 1984, **7**, 1349–1356.
36 G. Zhang, E. Liu, C. Yang, L. Li, J. A. Golen and A. L. Rheingold, *Eur. J. Inorg. Chem.*, 2015, 939–947.
37 Z. Ma, L. Wei, E. C. B. A. Alegria, L. M. D. R. S. Martins, M. F. C. Guedes da Silva and A. J. L. Pombeiro, *Dalton Trans.*, 2014, **43**, 4048–4058.
38 R. J. Allenbaugh, A. L. Rheingold and L. H. Doerrer, *Dalton Trans.*, 2009, 1155–1163.
39 Z. Ma, B. Zhang, M. F. C. Guedes da Silva, J. Silva, A. S. Mendo, P. V. Baptista, A. R. Fernandes and A. J. L. Pombeiro, *Dalton Trans.*, 2016, **45**, 5339–5365.
40 S. Mirdya, S. Roy, S. Chatterjee, A. Bauza, A. Frontera and S. Chattopadhyay, *Cryst. Growth Des.*, 2019, **19**, 5869–5881.
41 M. K. Bhattacharyya, U. Saha, D. Dutta, A. Das, A. K. Verma and A. Frontera, *RSC Adv.*, 2019, **9**, 16339–16356.
42 S. Khan, P. Giri, A. Bauza, K. Harms, A. Frontera and S. Chattopadhyay, *Polyhedron*, 2019, **157**, 487–494.
43 (*a*) M. K. Bhattacharyya, D. Dutta, S. M. Nashre-ul-Islam, A. Frontera, P. Sharma, A. K. Verma and A. Das, *Inorg. Chim. Acta*, 2020, **501**, 119233; (*b*) H. Nath, P. Sharma, A. Frontera, A. K. Verma, A. Das, M. Barceló-Oliver and M. K. Bhattacharyya, *Polyhedron*, 2020, **176**, 114266.

NJC

ROYAL SOCIETY OF CHEMISTRY

PAPER

View Article Online
View Journal | View Issue

Cite this: *New J. Chem.*, 2021, 45, 11689

Synthesis and crystal structure of the simultaneous binding of Ni(II) cation and chloride by the protonated 2,4,6 tris-(2-pyridyl)-1,3,5 triazine ligand: theoretical investigations of anion···π, π···π and hydrogen bonding interactions†

Pampi Pal,[a] Kinsuk Das,*[b] Anowar Hossain,[a] Rosa M. Gomila,[c] Antonio Frontera*[d] and Subrata Mukhopadhyay*[a]

Received 17th April 2021,
Accepted 27th May 2021

DOI: 10.1039/d1nj01880a

rsc.li/njc

A new octahedral Ni(II) complex **1** of protonated ligand **Htptz**$^+$ (**tptz**: 2,4,6-tris(2-pyridyl)-1,3,5-triazine) has been synthesized and characterized by single crystal X-ray analysis. It is noteworthy that the protonated ligand concomitantly chelates the Ni(II) and interacts with two non-coordinated chloride ions *via* anion···π and hydrogen bonding interactions. Moreover, N$^+$–H hydrogen bonding occurs with the non-coordinated anion rather than with the coordinated or lattice water molecules. In this work, we demonstrate the role of the protonated ligand and chloride ions in stabilizing the structural integrity through several supramolecular interactions. Besides π···π interactions, theoretical investigations provide significant insight about the interplay between anion···π and hydrogen bonding interactions that in turn conclusively confirm the decisive role of protonation as well as coordination to the metal center [here Ni(II)]. The different contributions to the complexation energies have been evaluated by using several theoretical models.

Introduction

Recent years have witnessed an extensive advancement in designing metallo–organic frameworks propelled by numerous supramolecular synthons using several non-covalent interactions that play a crucial role in structural integrity in the solid state.[1,2] Based on relative abundance of the supramolecular synthons in the database, new synthetic strategies can be planned.[3] This created an opportunity for the preparation of molecular crystals with targeted patterns of binding in the solid state.[4] Although the structure-directing role of weak noncovalent interactions (NCIs) was noticed about three decades ago, a deeper understanding of NCIs is needed to control and modulate the solid-state architecture of molecular crystals.[5,6] 2,4,6-Tris(2-pyridyl)-1,3,5-triazine (**tptz**) or its structural analogs are well known metal binding sites that have aroused a colossal interest in the field of contemporary metallo-supramolecular chemistry.[7–10] As a flexidentate coordinating ligand **tptz** shows various coordination modes with the metal centers (Scheme S1, ESI†). The predominant coordination mode of '**tptz**' is tridentate terpyridine like (Scheme S1d, ESI†). Moreover, it is also able to coordinate two metal centers in one terpyridine and one bipyridine like coordination mode (Scheme S1e, ESI†) or bind three metal centres *via* all bipyridine-like coordination modes, although the latter binding mode is quite rare (Scheme S1f, ESI†). Several mononuclear complexes of transition metal ions with the '**tptz**' ligand have been reported including Cr(II),[9] Mn(II),[9,11] Fe(III),[12] Co(II),[13] Ni(II),[10,14] Cu(II),[15] Ag(I),[16] *etc.* The '**tptz**' has also been used to separate trivalent lanthanides and actinides[17,18] from nitric acid media (>0.1 M) in which '**tptz**' is protonated as '**Htptz**$^+$'. For coordination chemists, '**tptz**' is a ligand of interest because of its multiple coordination sites, large π conjugation for stabilization and variable hapticities to be used for designing building blocks, that recognizes each other through direction specific supramolecular interactions to form extended architectures.[9,13]

The under-appreciation of anion···π interactions relied on the intuitive assumption of repulsive force between the anion and the electron rich π-system of an arene.[19] But in recent years, the

[a] *Department of Chemistry, Jadavpur University, Kolkata 700032, India. E-mail: ju_subrata@yahoo.co.in*
[b] *Department of Chemistry, Chandernagore College, Hooghly, West Bengal 712136, India. E-mail: kdaschem@yahoo.in*
[c] *Serveis Científico-Tècnics, Universitat de les IllesBalears, Crta. de Valldemossa km 7.5, Palma 07122, Baleares, Spain*
[d] *Departament de Química, Universitat de les IllesBalears, Crta. de Valldemossa km 7.5, Palma 07122, Baleares, Spain. E-mail: toni.frontera@uib.es*

† Electronic supplementary information (ESI) available. CCDC 2024203. For ESI and crystallographic data in CIF or other electronic format see DOI: 10.1039/d1nj01880a

anion···π interaction, *i.e.*, the non-covalent force between the electron deficient aromatic system and anions has been recognized as a potential non-covalent bonding interaction.[20,21] From the crystallographic database, it was evident that the interplay between anion···π and π···π or anion···π and hydrogen bonding interactions plays a significant role in a synergistic manner to stabilize the crystal structure in the solid state. But the challenging task was to ensure both anion···π and π···π interactions simultaneously because for the former, electron deficient π systems and for the latter, electron rich π systems are required. When the heterocycle ring is coordinated to the metal centre, the ring becomes electron deficient, but not to such an extent that it can be utilized to ensure a strong anion···π interaction, but this interaction becomes a significant one if the aromatic ring moiety is protonated.[22]

Keeping all these factors in mind, we strategically protonate one peripheral pyridine ring (to restrict coordination of the second metal centre as shown in Scheme S1e, ESI†) of '**tptz**' to ensure not only NNN tridentate terpyridine-like major coordination sites are active, leaving moderate and minor coordination sites inactive in the coordination game towards the metal centre (Scheme S2a and b, ESI†) but also to make the triazine ring sufficiently electron deficient to encourage it to participate in strong anion···π interaction.

We have succeeded in synthesizing a Ni(II) complex of the protonated ligand (**Htptz$^+$**) that is characterized by single crystal X-ray analysis. As anticipated the electron deficient triazine ring (one nitrogen of the triazine ring is coordinated to the metal Ni(II) and one peripheral substituted pyridine ring is protonated) participates in anion···π interaction, and the substituted non-protonated pyridine rings are engaged in π···π and π$^+$···π interactions (using one protonated pyridine ring) along with several hydrogen bonding interactions (classical O–H···O, O–H···Cl, N–H···Cl and non-classical C–H···Cl type) to construct different networks of varying dimensionalities. Finally, the present work uses DFT calculations and several computational tools (QTAIM and NCIPlot) to rationalize the noncovalent interactions and their decisive role in forming the solid-state architecture of complex **1**.

Experimental section

Materials and measurements

All chemicals were of reagent grade, purchased from commercial sources and used without further purification. 2,4,6-Tris(2-pyridyl)-1,3,5-triazine (**tptz**) and ethanol were purchased from Aldrich Chemical Company, USA and used without further purification. All reactions were carried out under aerobic conditions and in an ethanol–water medium (Scheme S3, ESI†). During the whole experiment, freshly boiled, doubly distilled water was used. The PerkinElmer RXI FT-IR spectrophotometer was used to record the IR spectrum in the range of 4000–400 cm^{-1} and an elemental analysis (carbon, hydrogen and nitrogen) of the metal complex was determined with a PerkinElmer CHN analyzer (2400). UV-Visible spectrum was recorded on a UV-Visible spectrophotometer (Hitachi UH 4150). Thermogravimetric analysis (TGA) data were collected with an SDT 2960 thermoanalyzer under nitrogen (50° to 850 °C) at a heating rate of 10 °C per minute for **1**. The room temperature magnetic moment of the complex was taken from the magnetic susceptibility balance MK1 Sherwood.

Synthesis

Synthesis of protonated ligand (Htptz$^+$). Protonated '**Htptz$^+$**' [2,4,6-tris(2-pyridyl)-1,3,5-triazine] was synthesized by following a reported procedure.[17]

Synthesis of [Ni(Htptz$^+$)Cl(H_2O)$_2$]2Cl·2H_2O (complex 1)

The protonated ligand, **Htptz$^+$** (0.376 g, 1.2 mmol) was dissolved in ethanol (15 mL) and dropwise an aqueous ethanolic solution of $NiCl_2$, $6H_2O$ (0.284 g, 1.2 mmol) was added under constant stirring that continued for 4 hours. Then the solution was filtered, and the filtrate was left for slow evaporation. After one-week, brownish green X-ray quality crystals of **1** were isolated. (Yield: 73%). Anal. calc. for $C_{18}H_{21}NiN_6O_4Cl_3$: C, 39.21; H, 3.81; N, 15.26. Found: C, 38.98; H, 3.83; N, 15.28%. Main FT-IR absorptions, (KBr, cm^{-1}): 3407 (m), 3260 (m), 3047 (s), 3027 (s), 1730 (s), 1577 (s), 1561 (s), 1547 (s), 1473 (s), 1439 (s), 1377 (s) (Fig. S1, ESI†). $\lambda_{max/nm}$ = 233, 311 and 379 (Fig. S2, ESI†). Room temperature magnetic moment (μ_{eff}) = 2.79 B.M.

X-ray crystallographic analysis

Data collection was made using a Bruker SMART APEX II CCD area detector equipped with a graphite monochromated Mo Kα radiation (λ = 0.71073 Å) source in the φ and ω scan mode at 150(2) K for **1**. Cell parameters refinement and data reduction were carried out using Bruker SMART and Bruker SAINT software.[23] The structure of the complex was solved by conventional direct methods with the SHELXS-97 program[24] and refined by full-matrix least squares on F^2 by using the SHELXL-97 program.[24] The structure of the complex was solved by conventional direct methods and refined by full-matrix least squares methods using F^2 data. SHELXS-97 and SHELXL-97 programs[24] were used for the solution and refinement of the structure of the complex, respectively. CCDC 2024203 (**1**) includes additional crystallographic information. Selected crystallographic features for **1** are given in Table S1 (ESI†) and selected geometrical parameters of the complex are shown in Table S2 (ESI†).

Theoretical methods

The calculation of the interaction energies was carried out using Gaussian-16[25] and the PBE0-D3/def2-TZVP level of theory and using the crystallographic coordinates. Grimme's D3 dispersion correction has been used in the calculations because it is important to evaluate anion···π interactions properly.[26] This procedure and level of theory have been successfully used to evaluate similar interactions.[27–30] The interaction energies were computed by calculating the difference between the energies of the isolated monomers and their assembly and they have been BSSE corrected.[31] The QTAIM[32] and NCIPlot calculations[33] have been performed at the same level of theory and using the AIMAll program.

Results and discussion

Single-crystal X-ray structural analysis confirms that the asymmetric unit of the title complex (**1**) consists of one protonated heterocyclic ligand (**Htptz**$^+$) [**tptz** = 2,4,6-tris(2-pyridyl)-1,3,5-triazine] moiety with Ni(II), chloride ions and solvent water molecules. In this complex, the protonated ligand acts as a monopositive tridentate NNN donor, meridionally coordinated to form two five membered chelate rings around the central metal ion. Two non-coordinated chloride ions and two water molecules are there to complete the asymmetric unit of **1**. The molecular representation with an atom numbering scheme (only selected atom numbering was done for maintaining the clarity of the picture) of the complex is shown in Fig. 1.

Structural description of complex 1

The perspective view of the molecular structure of complex **1** with the selected atom numbering scheme is shown in Fig. 1 whereas selected bond lengths (Å) and bond angles (°) are listed in Table S2 (ESI†). Complex **1** crystallizes in the space group $P2_1/n$ and its unit cell is comprised of four molecules. Complex **1** is a distorted octahedron where the title ligand '**tptz**' in its protonated form (**Htptz**$^+$) spans in the meridional position [N1–Ni1–N2 = 76.62(4)°, N2–Ni1–N3 = 75.96(5)° and N1–Ni1–N3 = 152.56(5)°] as a monopositive [due to the protonation of third pendant pyridine ring nitrogen (N6)] NNN donor *via* two pyridyl nitrogen atoms (N1 and N3) and one triazine ring nitrogen (N2). In association with the ligand (**Htptz**$^+$), two oxygen atoms (O1 and O2) from two different water molecules and one chlorine atom (Cl1) complete the octahedral geometry.

The dipositive charge of the heteroleptic complex is taken care of by two non-coordinated chloride ions (Cl2 and Cl3) present outside the metal coordination sphere. Besides coordinating water molecules, two non-coordinated water molecules are also present in **1**. Among the three trans angles, two [O1–Ni1–O2 = 172.51(5)° and N2–Ni1–Cl1 = 176.55(4)°] are close to ideal trans angle 180°, while the third one [N1–Ni1–N3 = 152.56(5)°] is deviated more probably due to small bite angles (forming two five-membered chelate rings towards the central metal ion) of the title ligand [N1–Ni1–N2 = 76.62(4)°, N2–Ni1–N3 = 75.96(5)°] that may induce a distortion in the *trans* angle in the entire octahedral geometry (Table S2, ESI†). The average Ni–N and Ni–O bond lengths are 2.107 Å [Ni1–N1 = 2.1486(12) Å, Ni1–N2 = 2.0010(11) Å and Ni1–N3 = 2.1721(12) Å] and 2.077 Å [Ni1–O1 = 2.0726(13) Å and Ni1–O2 = 2.0822(12) Å], and these are consistent with the reported six coordinated Ni(II) complexes available in the Cambridge Crystallographic database.[7,10,14,34,35]

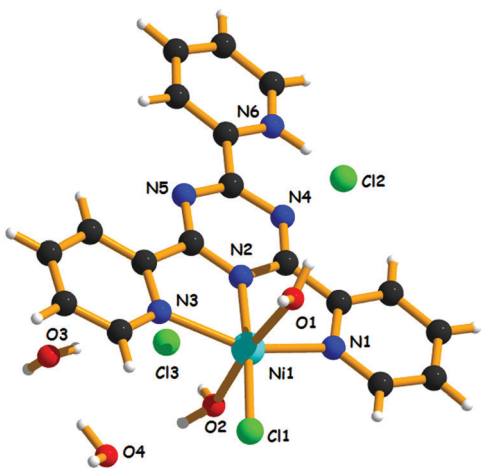

Fig. 1 Asymmetric unit of complex **1**.

The Ni–$N_{triazine}$ (Ni1–N2) bond length is, to some extent, shorter than those of Ni–$N_{pyridyl}$ (Ni1–N1 and Ni1–N3), which may be due to the stronger π-accepting properties of the triazine ring or due to the constricted coordination geometry imposed by the triazine ligand.[10] The dihedral angles of the ring C1C2C3C4C5N1, C14C15C16C17C18N3 and C8C9C10C11C12N6 with the triazine ring N2C6N4C7N5C13 are 2.88°, 1.28° and 4.22°, respectively. This shows that the coordinated pyridyl rings are almost coplanar and the uncoordinated, protonated pyridyl ring is slightly nonplanar with respect to the triazine ring. The pendant protonated pyridine ring makes an angle 6.34° with the equatorial plane (N1N2N3Cl1), displaying the maximum degree of twisting. The central Ni atom is placed almost in the equatorial plane constituted by N1N2N3Cl1.

In the present structure, both coordinated and non-coordinated chloride ions participate in several hydrogen bonding interactions. According to Jeffrey's categorization based on donor–acceptor distances of hydrogen bonds, they are found to be moderately and weakly electrostatic.[36] Though C–H···Cl hydrogen bonding is comparatively less frequent, it has been well appreciated in recent years.[7,37–40] When the heterocyclic ring bears a donor atom that is capable of reducing the electron density in the ring sufficiently, it produces non-classical C–H···Cl hydrogen bonding interactions. For better C–H···Cl interaction, the H···Cl distance should be less than the sum of their van der Waals radii (2.95 Å).[41] We find in our work that this distance ranges from 2.60 to 2.82 Å (Table S3, ESI†). Both the coordinated and one non-coordinated chloride ions (Cl1 and Cl2, respectively) engaged in these C–H···Cl type non-classical hydrogen bonding interactions (C3–H3···Cl1, C2–H2···Cl2 and C4–H4···Cl2), leading to the generation of $R_3^2(11)$ synthons. An additional electrostatic attraction enables N6–H5 in hydrogen bonding interaction only to the chloride ion (non-coordinated Cl2) and not to either coordinated or non-coordinated water molecules. The N–H···Cl distance is short (2.32 Å) because the hydrogen bonding occurs through non-coordinated ionic chloride (Table S3, ESI†) that is expected to be stronger compared to the chloride attached to the metal ion. The N–H···Cl interaction along with C4–H4···Cl2 constitutes $R_2^1(10)$ synthons. These $R_3^2(11)$ and $R_2^1(10)$ synthons propagate to generate a 1D tape (Fig. 2).

This 1D arrangement is further stabilized by intermolecular π···π and π^+···π interactions between the six membered coordinated pyridine ring [Cg(3)centroid] of one layer with the six membered coordinated pyridine ring [Cg(5) centroid] and another six membered non-coordinated, protonated pyridine ring [Cg(6) centroid] from two different (almost parallel) layers with the shortest centroid–centroid distances 3.6757(9) Å and 3.8936(10) Å, respectively (Table S4, ESI†). These π···π and π^+···π stacking

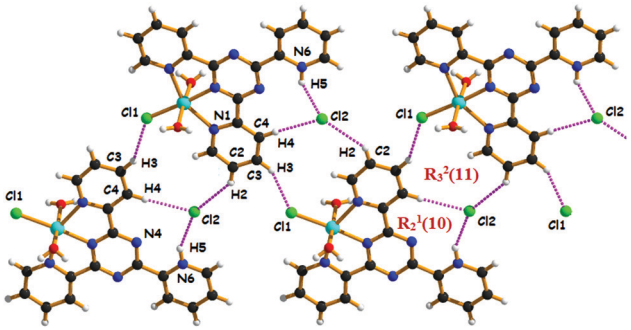

Fig. 2 1D tape formed by various hydrogen bonding interactions incorporating both coordinated (Cl1) and non-coordinated ionic chloride (Cl2) ions along the *c* axis.

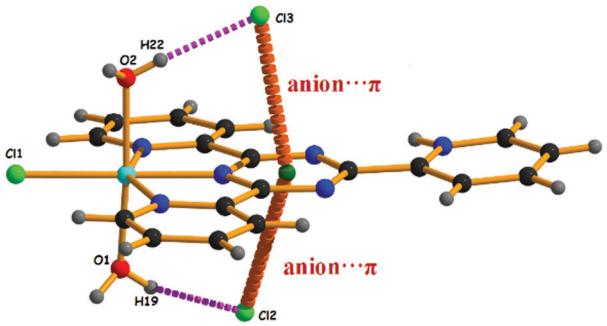

Fig. 4 Anion···π interactions in association with hydrogen bonding interactions in complex **1**.

interactions increase the dimensionality of the tape from 1D (Fig. 2) to 2D (Fig. 3).

Here, the triazine ring is trisubstituted by three pyridyl groups among which one pyridine ring is protonated. One triazine nitrogen (N2) and two pyridyl nitrogen atoms (N1 and N3) are directly coordinated to the Ni(II) center. From the database, it was evident that simple metal coordination will not provide sufficient polarization to produce strong anion···π interaction. But *ab initio* calculation has provided evidence that these weak interactions can afford a significant degree of stability if the aromatic moiety is protonated.[22,42]

In structure **1**, two non-coordinated chloride ions (Cl2 and Cl3) are located above and below the electron deficient triazene ring to form effective anion···π interactions in association with a hydrogen bonding interaction with the hydrogen atoms of axially coordinated water molecules [O1–H19···Cl2 and O2–H22···Cl3] available in proximity (Fig. 4).

In **1**, there is a dimeric distribution as shown in Fig. 5 that is formed by anion···π and hydrogen bonding involving coordinated water along with two different hydrogen bonding interactions involving N–H···Cl (N6–H5···Cl2) and C–H···Cl (C4–H4···Cl2). Hence the combined effect mutually strengthens each other.

Non-coordinated water molecules are also susceptible to form several hydrogen bonding interactions with coordinated as well as non-coordinated chloride ions [O1–H20···Cl1, O3–H23···Cl3, O4–H26···Cl3 and O3–H24···Cl2]. In the solid state, complex **1** forms an infinite chain through O2–H21···O4, O2–H22···Cl3, O4–H25···O3 and O3–H23···Cl3 classical hydrogen bonding interactions that are responsible to form $R_4^3(8)$ synthons and are interconnected through O4–H26···Cl3 to form a 1D chain.

These 1D chains are interconnected through symmetric $R_2^2(8)$ synthons and generate a 2D layer structure through intermolecular hydrogen bonding interactions of O1–H20···Cl1. In association with anion···π interactions, the non-coordinating Cl2 atom further strengthens the stability of the 2D layer as it introduces strong O3–H24···Cl2 and O1–H19···Cl2 interactions (Fig. 6).

We have also compared the structure reported herein with other Ni(II) complexes reported in the literature involving the **tptz** ligand (compounds **2**–**10**), as shown in Table 1. The presence and structure guiding role of the anion···π interactions were unnoticed by the original authors because in most cases, the X-ray analysis was used to confirm the composition of the compound. In some instances, the description of the solid state structure was limited to π···π and hydrogen bonding interactions.[14,43,44] The potential versatility of the **tptz** ligand in Ni(II) coordination chemistry was initially explored by Barclay *et al.*[43] In 1977, this group studied a Ni(II) complex (**7** in Table 1) of **tptz** in its protonated form (**Htptz**$^+$).[43] In this example, the tricationic complex was counter-balanced by three bromide ions. Similarly to compound **1**,

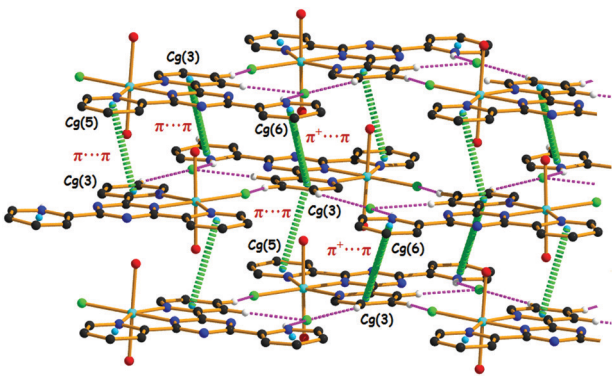

Fig. 3 2D layer formed by hydrogen bonding, π···π and π$^+$···π stacking interactions (H-atoms not involved in hydrogen bonding have been omitted for clarity).

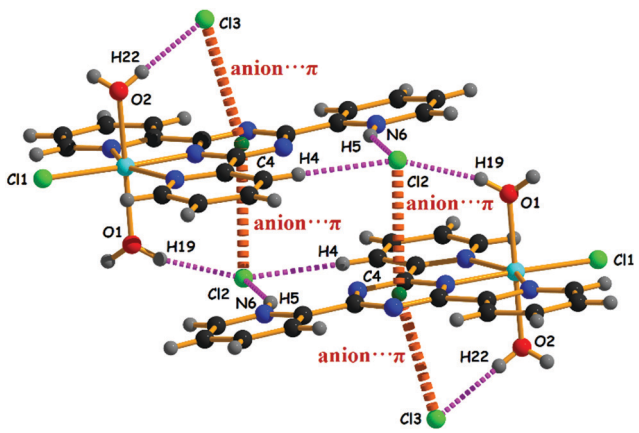

Fig. 5 Dimeric distribution of **1** using anion···π and different hydrogen bonding interactions.

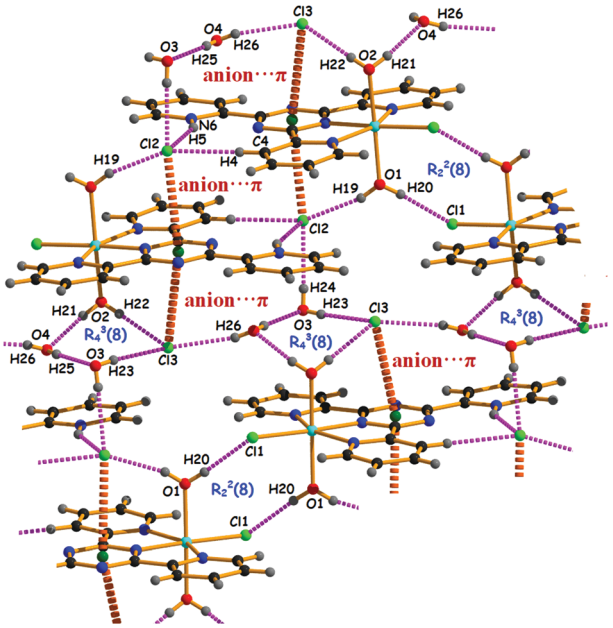

Fig. 6 2D network generated by the anion···π, several hydrogen bonding interactions and $R_4^3(8)$ and $R_2^2(8)$ synthons.

this complex exhibits an anion···π interaction where the bromide is located over the central triazine ring.

In 2005, Zibaseresht *et al.*[44] reported several Ni(II) complexes (complexes **3**, **4**, **5**, **8**, **9** and **10** as mentioned in Table 1) derived from **tptz** (either non-protonated or protonated). All of them exhibit short anion···π interactions with non-coordinated chloride, nitrate or perchlorate anions. It should be emphasized that complex **5** has the same molecular formula and coordination geometry as the complex reported herein but exhibits different cell parameters. In fact, one of the anion···π distances differs significantly (3.951 Å in **5** *vs.* 3.549 in **1**). Moreover, the original authors did not describe the anion···π interactions in complex **5**. Complex **4** is actually a mixture of two different crystallographic units of Ni(II), exhibiting a quite long anion···π interaction with the triazine ring (3.879 Å). In complex **8**, the oxygen atoms of perchlorate were actively engaged in anion···π interactions with the central triazine ring with short distances (3.109 and 3.016 Å). In complexes **9** and **10**, the oxygen atoms of non-coordinated nitrate ions participate in anion···π interactions above and below the central triazine ring.

Table 1 Comparison of anion···π interactions in 2,4,6 tris-(2-pyridyl)-1,3,5 triazine derived Ni(II) complexes **1**–**10**

Complex	X	X···Cg(triazine)	Ref.
$[Ni(tptz)(H_2O)Cl_2]H_2O$ (**2**)	Cl	3.393	14
$[Ni(tptz)(H_2O)_3]Cl_2{\cdot}2H_2O$ (**3**)	Cl	3.307	44
$[Ni(tptz)Cl(H_2O)_2]Cl{\cdot}[Ni(tptz)(H_2O)Cl_2]{\cdot}4H_2O$ (**4**)	Cl	3.879	44
$[Ni(Htptz^+)(H_2O)_2Cl]Cl_2{\cdot}H_2O$ (**5**)	Cl	3.951 & 3.513	44
$[Ni(tptz)(H_2O)_3Cl_2][Ni(tptz)(H_2O)Cl]Cl{\cdot}5H_2O$ (**6**)	Cl	3.204 & 3.506	—[a]
$[Ni(Htptz^+)(H_2O)_3]Br_3{\cdot}H_2O$ (**7**)	Br	3.729	43
$[Ni(tptz)_2](ClO_4)_2$ (**8**)	O	3.109 & 3.016	44
$[Ni(tptz)(H_2O)_3](NO_3)_2$ (**9**)	O	3.470 & 3.485	44
$[Ni_2(tptz)(EtOH)_2(NO_3)_3(H_2O)]NO_3$ (**10**)	O	2.944 & 3.114	44
$[Ni(Htptz^+)(H_2O)_2Cl]Cl_2{\cdot}H_2O$ (**1**)	Cl	3.549 & 3.527	—[b]

[a] No associated publication, CSD ref. code EREWEF. [b] This work.

In 2017, Yagci *et al.*[14] reported the Ni(II) complex (**2**) where the octahedral geometry around the central Ni(II) was constituted by one **tptz** ligand, one water and two chloride ions. Here, the equatorially coordinated chloride (that is placed *trans* with respect to the triazine coordinating nitrogen atom) ion is engaged in a short anion···π interaction (3.393 Å) with the central triazine ring. From the data of Table 1, it is clear that Cg(triazine)···Cl, Br (complexes **1**–**7**) distances are longer than the Cg···O distances (from nitrate or perchlorate anions, complexes **8**–**10**) in line with the van der Waals radii of these elements (1.75 Å for Cl, 1.85 Å for Br and 1.52 for O), and theoretical predictions.[45] The fact that all structures of Table 1 present anion···π interaction in the solid state strongly highlights their structural and functional significance.

Theoretical study

The theoretical study is focused on the analysis and rationalization of both types of anion···π interactions that are observed in the solid state of the Ni-complex **1**. The dication $[Ni(\mathbf{Htptz})(H_2O)_2Cl]^{2+}$ interacts with the chloride counterions by means of collaborative H-bonds and anion···π interactions, as represented in Fig. 7a. The O–H···Cl distances are similar (2.26 and 2.27 Å) along with the anion···π distances (measured from the anion to the triazine ring centroid). The top view of the complex (Fig. 7b) illustrates the difference of both anion···π interactions; in one case (Cl3), the anion is located approximately over the center of the ring, slightly displaced toward the coordinated N-atom. In the other case (Cl2), the anion is located approximately over one C-atom of the triazine ring.

First, we have computed the molecular electrostatic potential (MEP) surface of the hypothetical $[Ni(\mathbf{tptz})(H_2O)_2Cl]{\cdot}(Cl)$ compound

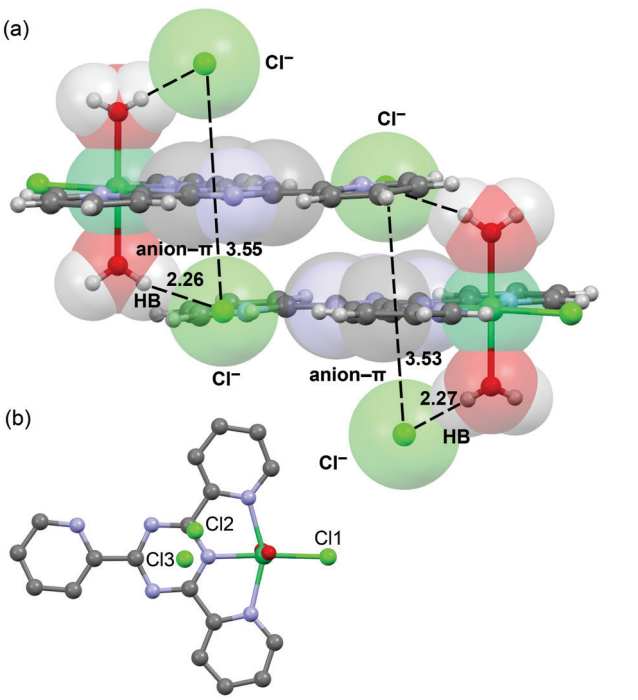

Fig. 7 (a) Partial view of the X-ray structure of **1** with indication of the anion···π and O–H···Cl interactions. (b) Top view of the complex.

where the **tptz** ligand has been considered de-protonated in order to visualize the most electrophilic parts of the molecule in a neutral system. The surface is represented in Fig. 8 and it can be observed that the MEP maximum is located at the H-atoms of the coordinated water molecules, due to the enhanced acidity of these protons due to the coordination of the O-atom to the Ni(II) metal centre. The MEP is also positive over the centre of the three aromatic rings coordinated to the Ni(II) ion. The MEP values over the pyridine ring (15–17 kcal mol^{-1}) are smaller than those over the triazine ring (+26 kcal mol^{-1}), thus revealing that the coordinated triazine ring is significantly more acidic than the pyridine ring. This explains the location of the non-coordinated chloride ions that are located above and below the triazine ring (see Fig. 7). The MEP minimum is located at the noncoordinated Cl^- atom (−55 kcal mol^{-1}) and that at the coordinated Cl-atom is −31 kcal mol^{-1}.

We have analysed the interaction energies associated with the H-bonds and anion···π interactions described above and studied the effect of the positive charge on one of the pyridine rings of the **tptz** ligand. Two different types of anion···π interactions are observed in the solid state of **1**, as represented in Fig. 9, which have been denoted as (anion–π)$_1$ and (anion–π)$_2$. In the former, the Cl anion is located approximately over the centre of the ring and in the latter, it is displaced toward one C-atom of the ring (see also Fig. 7b). Fig. 9 shows the binding energy of the interaction of the two possible cationic $\{[Ni(\mathbf{Htptz}^+)(H_2O)_2Cl]\cdot(Cl)\}^+$ moieties and chloride. It can be observed that both binding energies are very large (−100.3 kcal mol^{-1} and −97.9 kcal mol^{-1}) due to the strong electrostatic attraction between the counter ions. In an effort to estimate the energetic features of the anion···π and HBs in the absence of strong electrostatic effects, we have used the neutral $\{[Ni(\mathbf{tptz})(H_2O)_2Cl]\cdot(Cl)\}$ moieties shown in Fig. 9b, where the pyridine ring of the **tptz** ligand is not protonated. Consequently, the binding energies are significantly reduced to −43.1 and −40.9 kcal mol^{-1} for (anion–π)$_1$ and (anion–π)$_2$, respectively, that correspond to the contribution of both the H-bonds and anion···π interactions. These large interaction energies agree well with the strong electrophilicity of the complex, as shown by the MEP surface. The combination of interactions labelled as (anion–π)$_1$ and HB$_1$, where the chloride anion is located over the centre of the triazine, is stronger than the combination (anion–π)$_2$ and HB$_2$, where the chloride anion is located over one carbon atom of the triazine ring.

In order to analyse the relative importance of H-bond and anion···π interactions in complex **1**, we have used additional models where one of the water molecules has been eliminated (see Fig. 10), therefore only the anion···π interaction is evaluated. The results included in Fig. 10 reveal that (anion–π)$_1$ is around 4 kcal mol^{-1} stronger than (anion–π)$_2$. Moreover, the contributions of the HBs can be deduced by comparing the energies shown in Fig. 9b with those of Fig. 10, which are −13.8 and −15.5 kcal mol^{-1} for HB$_1$ and HB$_2$, respectively. This energetic analysis suggests that the anion···π interactions are stronger than the HBs.

Finally, we have performed a combined QTAIM/NCIplot analysis in both combination of interactions. Each HB is characterized by a bond critical point (CP, red sphere) and bond path interconnecting the H and Cl atoms (see Fig. 11).

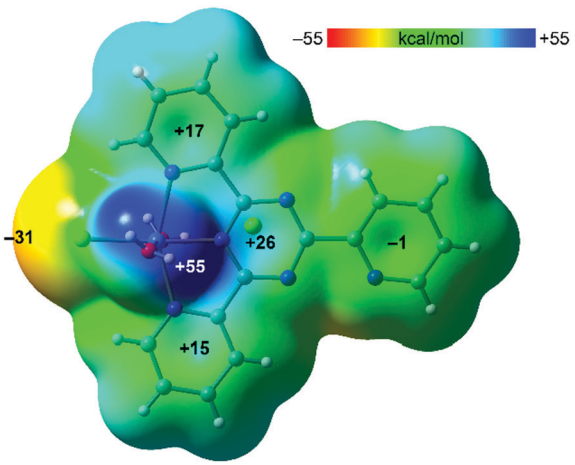

Fig. 8 MEP surface (isosurface 0.001 a.u.) of [Ni(**tptz**)$(H_2O)_2Cl]\cdot(Cl)$ at the PBE0-D3/def2-TZVP level of theory. The values at selected points of the surface are given in kcal mol^{-1}.

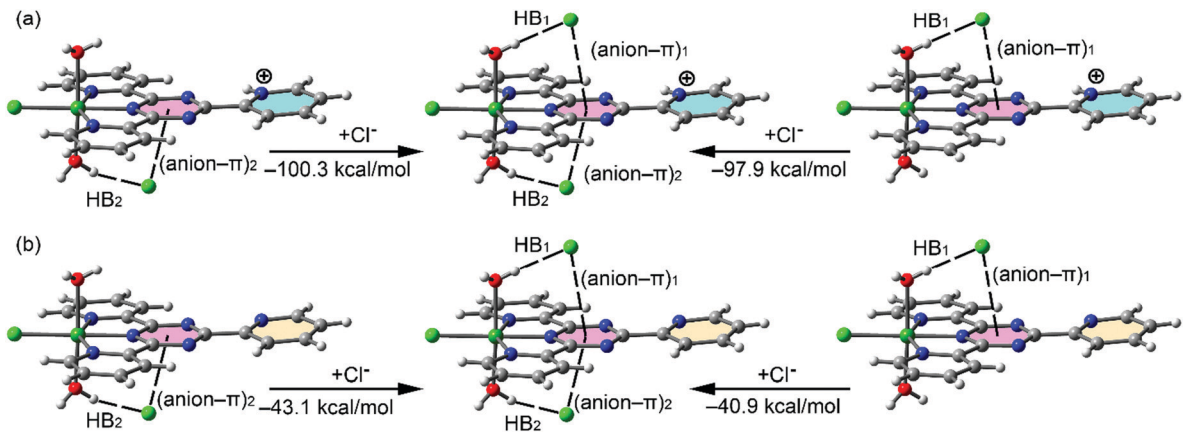

Fig. 9 Models used to evaluate the interaction energies for both combinations of anion···π and HB interactions by using charged (a) and neutral models (b) in complex **1**.

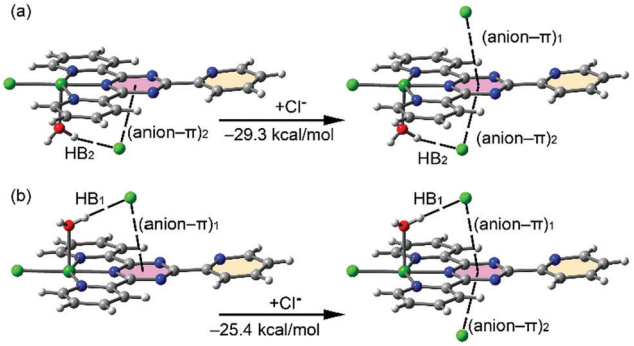

Fig. 10 Models used to evaluate the anion···π interaction in complex **1**.

Moreover, a small blue (strong interaction) NCIplot isosurface is also located between the Cl and H-atoms, which coincides with the position of the bond CP. The (anion–π)$_1$ binding mode is characterized by a bond CP connecting the Cl to the Ni(II) coordinated N-atom of the triazine ring.

Moreover, a large green NCIplot isosurface (attractive interaction) embracing the whole π-system is also observed that further corroborates the existence of the anion···π interaction. The (anion–π)$_2$ binding mode is characterized by a bond CP and bond path connecting the Cl to the closest C-atom of the triazine ring. The green NCIplot isosurface that characterizes the anion···π interaction is smaller compared to that of the (anion–π)$_1$ binding mode and displaced toward the C-atom, in good agreement with the smaller binding energy obtained for this interaction.

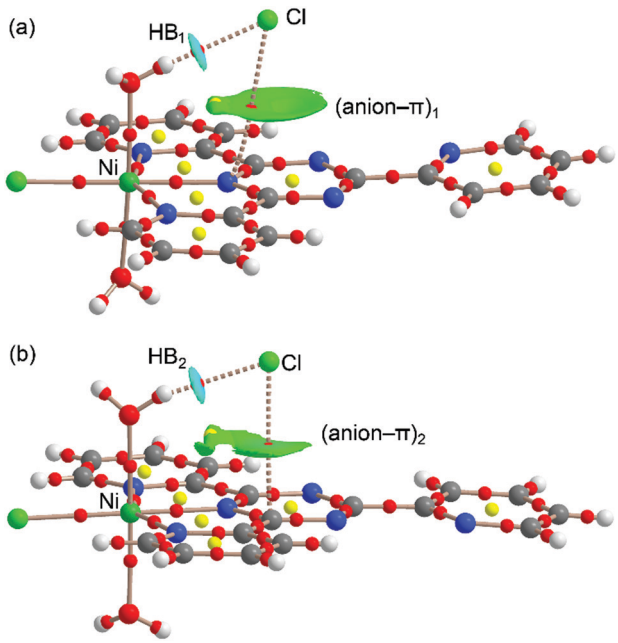

Fig. 11 Distribution of bond and ring CP (red and yellow spheres, respectively) and bond paths for both for (anion–π)$_1$ (a) and (anion–π)$_2$ (b) binding modes at the PBE0-D3/def2-TZVP level of theory. The overlapped NCIplot has been constructed using the 0.5 a.u. |RGD| isosurface and the sign(λ_2)ρ has been mapped using the ρ = 0.04 a.u. cut-off. For clarity, only the intermolecular isosurfaces have been plotted.

Thermal analysis

Thermal analysis was carried out to obtain an idea about the thermal stability of the complex. The TG curve for complex **1** is shown in Fig. S3 (ESI†). For **1**, it clearly shows that the complex is thermally stable up to 110 °C. In the temperature range 110 °C to 125 °C, complex **1** loses two non-coordinated water molecules (calculated mass loss 6.54%, found 6.4%). A second weight loss is observed in the temperature range 170 °C to 187 °C due to the decomposition of two coordinated water molecules (calculated mass loss 7%, found 6.8%). Then the complex is stable thermally up to 378 °C and finally **1** exhibits a consequent weight loss, indicating multistep decomposition above 400 °C.

Conclusions

We have successfully synthesized and crystallographically characterized a new metal–organic complex that possesses several functional groups responsible for giving rise to supramolecular architectures with the help of a heterocyclic ligand in its protonated form. The coordination environment of Ni(II) in **1** is a distorted octahedron built by the protonated '**tptz**' ligand (bound meridionally as a tridentate terpyridine like coordinating agent) along with one chloride and two water molecules. The protonated pyridine ring acts as a potential π^+ ring that ensures π^+···π interactions in conjugation with π···π interactions between π-enriched non-protonated pyridine moieties. Both coordinated and non-coordinated water molecules and chloride ions are actively engaged in forming various classical and non-classical hydrogen bonding interactions. Finally, we have demonstrated that there is an orchestrated interplay between anion···π and hydrogen bonding interactions. This can lead to a strong cooperative effect. Hence, the protonated ligand plays a dual role to interact with the metal as well as counter anions. A DFT study has been used to evaluate the cooperative influence of both types of anion···π and hydrogen bonding interaction quantitatively and demonstrating that the former is stronger. Finally, both interactions have been characterized using a combination of QTAIM and NCI plot tools, confirming the attractive nature of both interactions.

Conflicts of interest

There are no conflicts to declare.

Acknowledgements

We acknowledge the MCIU of Spain (project CTQ2017-85821-R, AEI/FEDER, UE funds) for financial support. Anowar Hossain thankfully acknowledges University Grans Commision (New Delhi) for a senior research fellowship).

Notes and references

1 N. H. Evan and P. D. Beer, *Angew. Chem., Int. Ed.*, 2014, **53**, 11716–11756.

2 J. L. Atwood, G. W. Gokel and L. J. Barbour, *Comprehensive supramolecular chemistry II*, Elsevier, 2017.
3 A. Mukherjee, *Cryst. Growth Des.*, 2015, **15**, 3076–3085.
4 O. V. Shishkin, R. I. Zubatyuk, S. V. Shishkina, V. V. Dyakonenko and V. V. Medviediev, *Phys. Chem. Chem. Phys.*, 2014, **16**, 6773–6786.
5 I. Alkorta, J. Elguero and A. Frontera, *Crystals*, 2020, **10**, 180.
6 S. Scheiner, *Non covalent forces*, Springer, Dordrecht, 2015.
7 P. Pal, K. Das, A. Hossain, A. Frontera and S. Mukhopadhyay, *New J. Chem.*, 2020, **44**, 7310–7318.
8 A. M. Maharramov, K. T. Mahmudov, M. N. Kopylovich and A. J. L. Pombeiro, *(Edn) Non-covalent interaction in the synthesis and design of new compounds*, John Wiley & Sons. Inc., Hoboken, NJ, 2016.
9 M. G. Alexandru, D. Visinescu, B. B. Cula, F. Lloret and M. Julve, *Eur. J. Inorg. Chem.*, 2018, 349–359.
10 H. Hadadzadeh, M. Maghami, J. Simpson, A. D. Khalaji and K. Abdi, *J. Chem. Crystallogr.*, 2012, **42**, 656–667.
11 K. N. Lazarou, I. Stamatopoulos, V. Psycharis, C. Duboc, C. P. Raptopou and Y. Sanaki, *Polyhedron*, 2018, **155**, 291–301.
12 A. Majumder, G. Pilet, M. S. El. Fallah, J. Ribas and S. Mitra, *Inorg. Chim. Acta*, 2007, **360**, 2307–2312.
13 A. Das, C. Marschner, J. Cano, J. Baumgartner, J. Ribas, M. S. El. Fallah and S. Mitra, *Polyhedron*, 2009, **28**, 2436–2442.
14 N. K. Yagci, K. Guven and G. D. Yildiz, *Z. Kristallogr. - New Cryst. Struct.*, 2017, **232**(3), 485–487.
15 K. Abdi, H. Hadadzadeh, M. Salimi, J. Simpson and A. D. Khalaji, *Polyhedron*, 2012, **44**, 101–112.
16 L. Zhang, X.-Q. Lu, Q. Zhang, C. L. Chen and B. S. Kang, *Trans. Met. Chem.*, 2005, **30**, 76–81.
17 P. Byers, G. Y. S. Chan, M. G. B. Drew, M. J. Hudson and C. Madic, *Polyhedron*, 1996, **15**, 2845–2849.
18 R. Weitzke, M. Mazzanti, J. M. Latour and J. Picaut, *Inorg. Chem.*, 1999, **38**, 3581–3585.
19 M. Giese, M. Albrecht and K. Rissanen, *Chem. Commun.*, 2016, **52**, 1778–1795.
20 (*a*) A. Bauzá, T. J. Mooibroek and A. Frontera, *CrystEngComm*, 2016, **18**, 10–23; (*b*) A. Frontera, *Coord. Chem. Rev.*, 2013, **257**, 1716–1727.
21 A. Frontera, P. Gamez, M. Mascal, T. J. Mooibroek and J. Reedijk, *Angew. Chem., Int. Ed.*, 2011, **50**, 9564–9583.
22 (*a*) C. Biswas, M. G. B. Drew, D. Escudero, A. Frontera and A. Ghosh, *Eur. J. Inorg. Chem.*, 2009, 2238–2246; (*b*) A. Das, S. R. Choudhury, B. Dey, S. K. Yalamanchili, M. Helliwell, P. Gamez, S. Mukhopadhyay, C. Estarellas and A. Frontera, *J. Phys. Chem. B*, 2010, **114**, 4998–5009.
23 *Bruker, SMART v5.631*, Bruker AXS Inc., Madison, WI, USA, 2001.
24 G. M. Sheldrick, *SHELXS-97 and SHELXL-97*, University of Göttingen, Germany, 1997.
25 M. J. Frisch, G. W. Trucks, H. B. Schlegel, G. E. Scuseria, M. A. Robb, J. R. Cheeseman, G. Scalmani, V. Barone, B. Mennucci, G. A. Petersson, H. Nakatsuji, M. Caricato, X. Li, H. P. Hratchian, A. F. Izmaylov, J. Bloino, G. Zheng, J. L. Sonnenberg, M. Hada, M. Ehara, K. Toyota, R. Fukuda, J. Hasegawa, M. Ishida, T. Nakajima, Y. Honda, O. Kitao, H. Nakai, T. Vreven, J. A. Montgomery Jr., J. E. Peralta, F. Ogliaro, M. Bearpark, J. J. Heyd, E. Brothers, K. N. Kudin, V. N. Staroverov, R. Kobayashi, J. Normand, K. Raghavachari, A. Rendell, J. C. Burant, S. S. Iyengar, J. Tomasi, M. Cossi, N. Rega, J. M. Millam, M. Klene, J. E. Knox, J. B. Cross, V. Bakken, C. Adamo, J. Jaramillo, R. Gomperts, R. E. Stratmann, O. Yazyev, A. J. Austin, R. Cammi, C. Pomelli, J. W. Ochterski, R. L. Martin, K. Morokuma, V. G. Zakrzewski, G. A. Voth, P. Salvador, J. J. Dannenberg, S. Dapprich, A. D. Daniels, O. Farkas, J. B. Foresman, J. V. Ortiz, J. Cioslowski and D. J. Fox, *Gaussian 16*, Gaussian Inc., Wallingford CT, 2016.
26 S. Grimme, J. Antony, S. Ehrlich and H. Krieg, *J. Chem. Phys.*, 2010, **132**, 154104.
27 L. E. Zelenkov, D. M. Ivanov, E. K. Sadykov, N. A. Bokach, B. Galmes, A. Frontera and V. Yu. Kukushkin, *Cryst. Growth Des.*, 2020, **20**, 6956–6965.
28 L. Bofill, R. Prohens, R. Barbas and A. Frontera, *Cryst. Growth Des.*, 2020, **20**, 6691–6698.
29 C. Alvarez-Lorenzo, A. Castiñeiras, A. Frontera, I. Garcia-Santos, J. Gonzalez-Perez, J. Niclos-Gutierrez, I. Rodriguez-Gonzalez, E. Vilchez and J. K. Zareba, *CrystEngComm*, 2020, **22**, 6674–6689.
30 J. C. Belmont-Sánchez, M. E. García-Rubiño, A. Frontera, J. M. González-Pérez, A. Castiñeiras and J. Niclós-Gutiérrez, *Crystals*, 2021, **11**, 48.
31 S. F. Boys and F. Bernardi, *Mol. Phys.*, 1970, **19**, 553–566.
32 R. F. W. Bader, *Chem. Rev.*, 1991, **91**, 893–928.
33 J. Contreras-Garcia, E. R. Johnson, S. Keinan, R. Chaudret, J. P. Piquemal, D. N. Beratan and W. Yang, *J. Chem. Theory Comput.*, 2011, **7**, 625–632.
34 E. Freire, S. Baggio, C. J. Munoz and R. Baggio, *Acta Crystallogr.*, 2002, **C 58**, m221–m224.
35 M. E. Diazde Vivar, S. Baggio and R. Baggio, *Acta Crystallogr.*, 2006, **E 62**, m986–m988.
36 George A. Jeffrey, *An introduction to Hydrogen bonding*, Oxford University Press, New York, 1997.
37 L. M. Eytel, H. A. Fargher, M. M. Haley and D. W. Johnson, *Chem. Commun.*, 2019, **55**, 5195–5206.
38 Y. Liu, W. Zhao, C. H. Chen and A. H. Flood, *Science*, 2019, **365**, 159–161.
39 M. Maghami, F. Farzaneh, J. Simpson, M. Ghiasi and M. Azarkish, *J. Mol. Struct.*, 2015, **1093**, 24–32.
40 G. R. Desiraju and T. Steiner, *The weak hydrogen bond in structural chemistry and biology*, Oxford University Press Inc, New York, 1999.
41 G. Aullon, D. Bellamy, A. G. Orpen, L. Brammer and E. A. Bruton, *Chem. Commun.*, 1998, 653–654.
42 S. Scheiner, T. Kar and J. Pattanayak, *J. Am. Chem. Soc.*, 2002, **124**, 13257–13264.
43 G. A. Barclay, R. S. Vagg and E. C. Watton, *Acta Crystallogr., Sect. A: Cryst. Phys., Diffr., Theor. Gen. Crystallogr.*, 1977, **B33**, 3487–3491.
44 R. Zibaseresht and R. M. Hartshorn, *Aust. J. Chem.*, 2005, **58**, 345–353.
45 C. Garau, D. Quiñonero, A. Frontera, P. Ballester, A. Costa and P. M. Deyà, *Org. Lett.*, 2003, **5**, 2227–2229.

